THE INVESTIGATION OF SOME CHEMICAL PROBLEMS BY RAMAN SPECTROSCOPY

A Thesis submitted for the
Degree of Doctor of Philosophy
in the University of Oxford,

by

Howell G.M.Edwards, B.A., B.Sc.

BODLEIAN LIBRARY OXFORD
DEPOSITED
THESIS
28.iii.69

October 1968.

Jesus College,
Oxford.

ACKNOWLEDGEMENTS

The author is deeply indebted to Dr.L.A.Woodward, under whose stimulus and continuous, skilful guidance the present work was carried out.

He is particularly grateful to Mr.M.J.Gall, of the University of Southampton, for obtaining the Raman spectra of highly-coloured MX_4^{n-} species on the Cary Laser Spectrometer.

Gratitude is expressed to Dr.J.S.Rollett, Deputy Director of the Oxford Computing Laboratory, and to Dr.M.J.Bruton, B.O.A.C.Computer Research, Heathrow, London, for invaluable discussions on the computer and force-constant aspects of this work.

The author would also like to thank the Science Research Council for a Research Studentship, during the tenure of which this work was carried out.

ABSTRACT

The work described is concerned with the vibrational spectra of

(a) compounds containing phosphorus trifluoride and related ligands,

and

(b) highly-coloured halogen compounds of transition metals.

Despite extensive research into compounds of phosphorus trifluoride very little is known about the vibrational spectra of these compounds. To date, the only compound of phosphorus trifluoride to have its Raman spectrum characterised is tetrakistrifluorophosphinenickel°, $Ni(PF_3)_4$, studied in the Oxford Laboratory by L.A.Woodward and J.R.Hall. Infra-red work on similar compounds has been incomplete and normally only the phosphorus-fluorine stretching vibrations have been recorded. A testing of the predictions of much theoretical discussion on the bonding in such zerovalent metal-trifluorophosphines may be afforded by a spectroscopic examination of a series of $M(PF_3)_4$ compounds.

The series $M(PF_3)_4$, where M = Ni, Pd, Pt, was selected for investigation; the platinum and palladium compounds have only recently been prepared (Prof.Krück, Köln) and a preparative technique was developed in the present work

for the synthesis of these compounds. This involved the setting-up of a high-pressure bomb and attendant vacuum line for the isolation and purification of the metal-trifluorophosphines. The compounds were fairly stable, with the exception of the palladium compound, which was very unstable.

A discrepancy in the reported vibrational spectrum of PF_3 itself necessitated a re-investigation of the infra-red spectrum of PF_3 in the vapour state. The assignment of Wilson and Polo is confirmed, and that of Gutowsky (and also Yost) disproved. A reason for the discrepancy in the results of these workers is proposed. The complete infra-red spectrum of $Ni(PF_3)_4$ was then obtained, the preparation and purification of this compound being useful experience for the preparation of the precious-metal compounds later to be investigated. A revised assignment for the molecule is suggested in the light of the work on PF_3.

The complete vibrational spectrum of the analogous platinum compound, $Pt(PF_3)_4$, was obtained: the assignment was supported by Raman work on solid $Pt(PF_3)_4$, it being concluded that each F_2-species vibration, splitting into two bands for the solid, was indicative of a lowering of the molecular symmetry from point group T_d to C_{3v}.

The investigation of the palladium analogue was difficult on account of the great instability of the compound. The solid melts at -40°C and decomposition to palladium metal is noticed at -35°C. At -20°C decomposition is extensive. Raman spectra were obtained in solution in chloroform and from the solid at low temperatures. To enable the Raman spectra to be observed it was necessary to modify the spectrometer for the attainment of accurately-controlled low temperatures. The infra-red spectrum was obtained in the vapour state and as a solid, decomposition occurring above a certain pressure in the vapour state. The Raman spectrum of the pure liquid was obtained by accurate temperature control at just above the melting-point of solid $Pd(PF_3)_4$. The spectra were exceedingly complex, and were interpreted as indicating that monomeric $Pd(PF_3)_4$ molecules (confirmed by molecular weight measurements)existed only in the vapour at low pressures. It is thought that polymerisation occurs in the condensed phases. A tentative assignment of $Pd(PF_3)_4$ monomer is proposed.

In Chapter 7 detailed force-constant calculations on the A_1-species vibrations are described. The limitations of the SVFF field are pointed out. Some conclusions are drawn concerning the bonding in the $M(PF_3)_4$ series, with particular reference to the metal-phosphorus stretching

vibration. Although the latter is very much higher for platinum than for nickel in these PF_3-compounds, it was not possible to conclude anything definitely about the extent of π-bonding.

An extension of the work to the $M(PX_3)_4$ series was performed for M = nickel, X = halogen. The compound $Ni(PCl_3)_4$ was prepared and the Raman and infra-red spectra were obtained. Great difficulty was experienced in obtaining the Raman spectra from solutions of $Ni(PCl_3)_4$ in organic solvents, since such solutions were very unstable and were also pale yellow in colour. The formation of a turbidity in the solutions after a certain time had elapsed was delayed using a specially constructed device for moderate cooling of these solutions. Circa 150 g. of $Ni(PCl_3)_4$ were consumed in the obtaining of a vibrational assignment.

The work was further extended with a similar investigation of $Ni(PBr_3)_4$. An attempt was then made to synthesize the hitherto unknown $Ni(PI_3)_3$, an extreme member of the $Ni(PX_3)_4$ series. This compound might be expected to be the least stable member of the series from the work on the previous members. A very unstable black solid was isolated, analysing approximately as $Ni(PI_3)_4$, and the infra-red spectrum obtained. A possible assignment for

the compound is suggested, and, although the evidence does not definitely confirm the molecule to be $Ni(PI_3)_4$, the assignment is promising.

Force constant calculations were carried out for $Ni(PCl_3)_4$, and also the bromo-compound. Owing to extensive "mixing" of the vibrational modes in the A_1 species the SVFF was unstable. A detailed analysis of the force-constants and coordinate vectors revealed some useful information on the motions of atoms within the molecule. More sophisticated calculations are also recorded, involving the modification and use of the Bruton UBG1 computer programme.

The next chapter, Chapter 11, reports the extension of the high-pressure bomb method successfully applied to the synthesis of the new compounds $Ni(PMe_3)_4$ and $Pt(PMe_3)_4$. The vibrational spectra of these compounds are reported, although the greater instability of the platinum compound prevented the obtaining of a Raman spectrum in this case. A force-constant calculation on $Ni(PMe_3)_4$ follows, and a discussion on the effect of replacement of the highly electronegative halogen atoms with methyl-groups in the series $Ni(PF_3)_4 \rightarrow Ni(PCl_3)_4 \rightarrow Ni(PMe_3)_4$.

No such tetrakis-compounds are known for antimony ligands. From the reaction between nickel carbonyl and

antimony trichloride the compound $Ni(CO)_3SbCl_3$ was isolated. The vibrational spectrum of this compound is reported in Chapter 12.

In Chapter 13, work on the tetrahalo-complexes of transition metals is described. The species are highly-coloured and weak-scatterers in the Raman effect. Until recently the Raman spectra of these complexes were not observable. In this work, the Raman spectra of some of the complexes MX_4^{n-}, where M = Mn, Fe(III), Co, Ni and X = Cl, Br, I, are described. To confirm the Raman assignments, the observation of infra-red overtones and combination bands was conceived. Unfortunately, there seems to be a discrepancy in the assignment of the ν_1 vibration of $MnBr_4^{2-}$ (obtained by Davidson and confirmed by the combination band analysis of the present work); Goodgame, in a private communication, although agreeing with $MnCl_4^{2-}$ and MnI_4^{2-}, disagrees with the $MnBr_4^{2-}$ assignment.

Experiments were devised to investigate the source of this discrepancy and a possible explanation is suggested. The situation is not, however, finally resolved, although it seems as if the Goodgame assignment of ν_1 is the correct one for $MnBr_4^{2-}$.

CONTENTS

		Page
Chapter 1	The Theory of Molecular Vibrations	1
1(1)	The Raman Effect	1
1(2)	Molecular Vibrations	3
1(3)	Classical Treatment of Small Vibrations	5
1(4)	Molecular Symmetry	8
1(5)	Force Constants	12
1(6)	Selection Rules	14
1(7)	The Polarization Rule for Raman Scattering	19
1(8)	Predictions from the Selection Rules	20
Chapter 2	Instrumental Techniques	24
2(1)	Raman Spectroscopy	24
2(2)	The Cary 81 Raman Spectrophotometer	26
2(3)	Modifications to the Cary 81	30
2(4)	Pilot experiments with the Low-temperature Modifications	33
2(5)	The Helium Source	35
2(6)	Modifications to the Helium Source	46
2(7)	Laser-excited Raman Spectra	48
2(8)	Infra-red Spectrometers	48
2(9)	Infra-red Sample Cells	49
Chapter 3	Phosphorus trifluoride and Zerovalent Metal-Trifluorophosphines	52
3(1)	General Introduction	52
3(2)	Bonding in metal-trifluorophosphine compounds	55
3(3)	Spectroscopic Activity of $M(PF_3)_4$ vibrations	60
3(4)	Vibrational assignment of PF_3	64
3(5)	The Infra-Red Spectrum of PF_3	67

		Page
Chapter 4	Tetrakistrifluorophosphinenickel°	71
4(1)	The Preparation of metal-trifluorophosphines	71
4(2)	The Vacuum Line	74
4(3)	The Purification of the PF_3	75
4(4)	The Bomb	79
4(5)	The Isolation and Purification of the $M(PF_3)_4$ sample	82
4(6)	Molecular Weight Determination and Analysis	86
4(7)	The Infra-red spectrum of $Ni(PF_3)_4$	89
4(8)	Discussion	90
Chapter 5	Tetrakistrifluorophosphineplatinum°	98
5(1)	Preparation	98
5(2)	The Raman Spectrum of $Pt(PF_3)_4$	99
5(3)	The Infra-red Spectrum of $Pt(PF_3)_4$	102
5(4)	Discussion of the Assignment	103
Chapter 6	Tetrakistrifluorophosphinepalladium°	114
6(1)	Preparation	114
6(2)	The Raman Spectrum of tetrakistrifluoro-phosphinepalladium°	118
6(3)	Raman spectra of the palladium compound in the solid and liquid states	123
6(4)	Infra-red spectra	124
6(5)	Discussion	129
Chapter 7	Force-constant Calculations on $M(PF_3)_4$ Molecules	135
7(1)	General Introduction	135
7(2)	The Calculation of Force Constants from Frequencies	138
7(3)	Force-constant calculations on $M(PF_3)_4$ molecules	143
7(4)	Force constants of PF_3	148
7(5)	Discussion of Force Constants in $M(PF_3)_4$	154

		Page
Chapter 8	Tetrakistrichlorophosphinenickel°	162
8(1)	Introduction	162
8(2)	The Preparation of $Ni(PCl_3)_4$	163
8(3)	Solution Properties of $Ni(PCl_3)_4$	166
8(4)	The Raman Spectrum of $Ni(PCl_3)_4$	169
8(5)	The Infra-red Spectrum	174
8(6)	Discussion of the Assignment	174
8(7)	Some studies on the decomposition of $Ni(PCl_3)_4$ in solution	182
Chapter 9		
A	Tetrakistribromophosphinenickel°	184
9(1)	Preparation	184
9(2)	Properties	185
9(3)	Vibrational spectrum of $Ni(PBr_3)_4$	187
9(4)	Discussion of the assignment	189
B	Tetrakistriiodophosphinenickel	192
9(5)	The Preparation of $Ni(PI_3)_4$	193
9(6)	Properties	194
9(7)	Spectroscopic Investigations	196
Chapter 10	Force-constant Calculation on $Ni(PCl_3)_4$ and $Ni(PBr_3)_4$	200
10(1)	Preliminary calculations using a SVFF	200
10(2)	The Bruton Programme	204
10(3)	The Programme UBG1	208
10(4)	Application of UBG1 to $M(PF_3)_4$ molecules	211
10(5)	Application of UBG1 to $Ni(PCl_3)_4$	214
10(6)	Bonding in $Ni(PCl_3)_4$	220

		Page
Chapter 11	Tetrakistrimethylphosphine-nickel° and -platinum°	224
11(1)	Introduction	224
11(2)	Preparation of the ligand, PMe_3	226
11(3)	Preparation of the $M(PMe_3)_4$ compounds	230
11(4)	Characterisation of $Ni(PMe_3)_4$ and $Pt(PMe_3)_4$	232
11(5)	Vibrational Spectra of $Ni(PMe_3)_4$ and $Pt(PMe_3)_4$	233
11(6)	Discussion	239
11(7)	Extension of Procedure	243
11(8)	Force Constant Calculation	243
Chapter 12	Trichlorostibine-tricarbonmonoxide nickel	249
12(1)	General Introduction and Preparation	249
12(2)	Vibrational Spectra of $Ni(CO)_3SbCl_3$	252
12(3)	Discussion of the Assignment	254
12(4)	Conclusions	257
Chapter 13	Tetrahalo-complexes of Transition Metals	260
13(1)	Introduction	260
13(2)	Preparation	261
13(3)	Characterisation of the Compounds	264
13(4)	Raman Spectroscopy	266
13(5)	Infra-red Spectroscopy	271
13(6)	Force-constants of MX_4^{2-} Species	278
13(7)	Sequel	283
Appendix 1		
References		

LIST OF ILLUSTRATIONS

FIGURE		Following Page
1A	Tetrahedral XY_4 and Character Table	7
2A	Cary 81 Toronto-Arc Source	26
2B	The Nielsen Conditions	28
2C	Controlled Temperature Raman Cell	30
2D	Cold Cell Arrangement for Cary 81 Spectrometer	31
2E	Calibration Graph for ρ	35
2F	The Helium Source	37
2G	Filters and Photographic Plates in the Red	43
2H	Cooling Arrangement for Helium Source	46
2I	Infra-red cells	51
3A	PF_3 as Donor and Acceptor	57
3B	T_d Configuration of $M(PF_3)_4$	60
3C	Deformation Region in the Infra-red spectrum of PF_3 (Present Work)	68
4A	Vacuum Line for $M(PF_3)_4$ Compounds	74
4B	Bomb Attachment to Vacuum Line	80
4C	Infra-red spectrum of $Ni(PF_3)_4$ vapour	89
5A	$Pt(PF_3)_4$ Raman Samples	100
5B	Raman Sample Mounts	101
5C	Raman Spectrum of $Pt(PF_3)_4$ Liquid	102
5D	Raman Spectrum of $Pt(PF_3)_4$ Solid	102
5E	Infra-red Spectrum of $Pt(PF_3)_4$ Vapour	102
5F	Resolution of 216 cm^{-1} feature in the Raman Spectrum of $Pt(PF_3)_4$ liquid	105
5G	Correlation Diagram for $M(PF_3)_4$ and PF_3	113
6A	Preparation of a $CHCl_3$ solution of $Pd(PF_3)_4$	118
6B	Raman Spectrum of $Pd(PF_3)_4$ in $CHCl_3$ ($\sim$1M solution)	120
6C	$Pd(PF_3)_4$ Liquid Sample	123

/Cont.

		Following Page
6D	Raman Spectrum of $Pd(PF_3)_4$ liquid (-38°C)	124
6E	Raman Spectrum of $Pd(PF_3)_4$ solid (-90°C)	124
6F	Infra-red Spectrum of $Pd(PF_3)_4$ vapour	126
6G	Infra-red Spectrum of $Pd(PF_3)_4$ solid (-196°C)	129
7A	$M(PF_3)_4$ Internal Coordinates	144
8A	The Preparation of $Ni(PCl_3)_4$	164
8B	Apparatus for the making and filtering of Raman solutions of $Ni(PCl_3)_4$ in a dry, inert atmosphere	167
8C	Raman Spectrum of $Ni(PCl_3)_4$ solid	170
8D	Raman Spectrum of a CCl_4 solution of $Ni(PCl_3)_4$	171
8E	Raman Spectrum of a benzene solution of $Ni(PCl_3)_4$	173
8F	The Infra-red Spectrum of $Ni(PCl_3)_4$ solid	175
8G	Correlation Diagram for $Ni(PCl_3)_4$ and PCl_3	178
9A	The Raman Spectrum of $Ni(PBr_3)_4$ solid	187
9B	The Infra-red Spectrum of $Ni(PBr_3)_4$ solid	189
9C	$Ni(PX_3)_4$ Correlation Diagram	191
9D	The Infra-red Spectrum of $Ni(PI_3)_4$	196
9E	Ni-P Stretching for $Ni(PX_3)_4$ molecules	199
10A	Ligand Motions in $Ni(PX_3)_4$	203
10B	Flowchart, UBG1 Programme Logic	210
10C	$Pt(PF_3)_4$ RMS % Discrepancy for every Modification of Force Constants	214
11A	Generation of PMe_3 from the Silver Iodide Adduct	228
11B	Tetrakistrimethylphosphinenickel°	233
11C	Visible Absorption of $Ni(PMe_3)_4$	235
11D	The Raman Spectrum of $Ni(PMe_3)_4$ solid	235
11E	The Infra-red Spectrum of $Ni(PMe_3)_4$	236

		Following Page
12A	Character Table and Configuration of $Ni(CO)_3SbCl_3$	252
12B	Correlation Diagram for $Ni(CO)_3SbCl_3$	254
13A	Raman Spectrum of $MnCl_4^{2-}$	269
13B	Combination Bands in $MnCl_4^{2-}$	277
13C	Combination Bands in $MnBr_4^{2-}$, MnI_4^{2-}	277
13D	Force Constants of MX_4 Species	282

Abbreviations used in the Text

ν_i	vibrational frequency of the i^{th} mode
ν	stretching mode
δ	deformation
ρ	rocking mode or depolarisation ratio
τ	torsion

Band-intensities are estimated as:

vw	very weak
w	weak
mw	medium-weak
m	medium
ms	medium-strong
s	strong
vs	very strong

sh	shoulder	s,sym(m)	symmetric
br,bd	broad	as,asym(m)	asymmetric
depol.,dp	depolarised	def.	deformation
pol., p	polarised		

$\sim$ approximately

CHAPTER 1

Chapter 1

THE THEORY OF MOLECULAR VIBRATIONS

Although vibrational spectra are observed experimentally as infra-red or Raman spectra the physical origins of the two are different. Infra-red spectra originate from the transitions between two vibrational levels of the molecule in the electronic ground state, and are usually observed as absorption spectra in the infra-red region. Raman spectra, however, originate from the electronic polarisation caused by ultra-violet or visible light, the vibrational frequencies being observed as Raman shifts from the incident frequency.

1(1) The Raman Effect

When a beam of monochromatic light is passed through a homogeneous medium (solid, liquid or gaseous) which does not appreciably absorb the incident light, most of the light passes straight through, but a small fraction is scattered in all directions. Most of the scattered light is of unchanged frequency (Rayleigh scattering) but a closer examination of the spectrum reveals weaker lines symmetrically

positioned on either side of the Rayleigh line. This scattering with change of frequency was first discovered by Raman (1) in 1928 after a theoretical prediction by Smekal in 1923 (2). An interesting historical account of the investigations made into light scattering effects is given by Placzek (3). The effect is most easily observed in liquids, where the intensities of Rayleigh and Raman Scattering are of the order of 10^{-5} and 10^{-8} respectively of the incident light intensity.

The pattern of Raman lines is found to be characteristic of the scattering substance, the frequency shifts being independent of the exciting frequency. In all cases it is found that the lines lying on the lower-frequency side (Stokes lines) are of much greater intensity than the higher-frequency (anti-Stokes) lines.

The Raman lines are caused by the incident photons interacting with the vibrational and rotational motions of the scattering molecule, and the photons may gain or lose energy. A vibrational transition from the ground state to the first excited state, $0 \rightarrow 1$, occurs with absorption of energy $h\nu_{vib}$, where ν_{vib} is the fundamental frequency. If this transition is induced by a photon of energy $h\nu_o$ the scattered photon will have a depleted energy $h(\nu_o - \nu_{vib})$

and will appear on the Stokes side of the exciting line with frequency shift $\nu_{vib.}$. The corresponding vibrational transition $1 \rightarrow 0$ results in an increase in the energy of the scattered photon and will similarly produce a line on the anti-Stokes side of the exciting line, with identical frequency shift. The intensities of the Raman lines will depend on the population of the vibrational levels: thus since the population of the first vibrational level is considerably less than that of the ground state at room temperature (about one-tenth of the population of the ground state for a vibrational mode of 500 cm^{-1}), the anti-Stokes lines will be much weaker than the Stokes lines.

Transitions between rotational levels occur with too small a change in energy (except for the lightest molecules) to give rise to Raman lines which can be resolved from the accompanying vibrational Raman line.

1(2) Molecular Vibrations

The vibrational motion of a diatomic molecule is approximately simple harmonic, with both nuclei moving along the line of centres in phase and with identical frequencies. The motions are not independent and can be described by a single time-dependent variable Q, the normal coordinate of the molecule. Motion of the system along this normal coordinate is said to be a normal mode.

Polyatomic molecules will execute a much more complicated vibrational motion, but this motion can be represented as a superposition of a number of independent normal modes. Each normal mode will be described by a normal coordinate, which will be a complicated combination of atomic displacements. In terms of this coordinate, however, the vibrational motion of the system will be simply described, and a displacement of the system, according to the normal coordinate, will lead to a motion in which all the particles move with simple harmonic motion, in phase and with the same frequency. Every normal mode is separately quantised, thus giving rise to a set of vibrational energy levels for the molecule. The population of these levels is determined by the Boltzmann distribution, and transitions between them may be induced by electromagnetic radiation.

The motion of an N-atomic molecule can be described by 3N cartesian coordinates and if the vibrational motion is to be treated independently of rotation and translation, six conditions must be realised; three locate the origin of the coordinate system at the centre of mass, the other three ensure that the axes of the rotating coordinate system rotate with the molecule. This leaves (3N-6) degrees of vibrational freedom corresponding to the (3N-6) normal modes. For linear molecules there are (3N-5) degrees of vibrational freedom.

1(3) Classical Treatment of Small Vibrations

A good description of normal modes is given by a classical treatment of small vibrations (4,5). The cartesian displacement coordinates Δx_i, Δy_i, Δz_i of the i^{th} nucleus from its equilibrium position are replaced by a set of mass-weighted displacement coordinates q_i defined by

$$q_i = m_i^{\frac{1}{2}} \Delta x_i ; \quad q_j = m_i^{\frac{1}{2}} \Delta y_i ; \quad q_k = m_i^{\frac{1}{2}} \Delta z_i$$

The total kinetic energy T is then given by,

$$2T = \sum_{i=1}^{3N} \dot{q}_i^2$$

while for small displacements the potential energy V may be expressed as a Taylor series, approximately given by the quadratic form,

$$2V = 2V_o + 2 \sum_{i=1}^{3N} \left(\frac{\partial V}{\partial q_i}\right)_o q_i + \sum_{i,j=1}^{3N} \left(\frac{\partial^2 V}{\partial q_i \partial q_j}\right) q_i q_j$$

When $q_i = 0$, V is a minimum, thus $\left(\frac{\partial V}{\partial q_i}\right)_o = 0$ for all i, and by choosing the zero of energy so that $V_o = 0$, we get:

$$2V = \sum_{i,j=1}^{3N} \left(\frac{\partial^2 V}{\partial q_i \partial q_j}\right) q_i q_j = \sum_{i,j=1}^{3N} f_{ij} q_i q_j$$

where f_{ij} is the force constant of interaction for the i^{th} and j^{th} displacement coordinates. Lagrange's form of the Newton equation

$$\frac{d}{dt}\left(\frac{\partial T}{\partial \dot{q}_i}\right) + \left(\frac{\partial V}{\partial q_i}\right) = 0$$

may be applied to the above equations to give

$$\ddot{q}_j + \sum_{i=1}^{3N} f_{ij} q_i = 0, \quad j = 1,2,3,\ldots,3N \qquad \ldots(1)$$

This is a set of 3N simultaneous second-order differential equations, having a possible solution:

$$q_i = A_i \cos(\lambda^{\frac{1}{2}} t + \epsilon) \qquad \ldots(2)$$

where $\lambda = 4\pi^2 c^2 \nu_i^2$, ν_i being the vibrational frequency of the i^{th} normal mode. Substituting (2) into (1) gives:

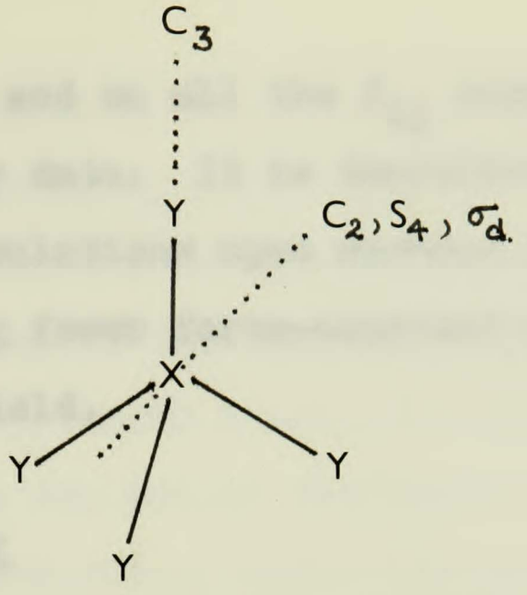
$$\sum_{i,j=1}^{3N} (f_{ij} - \delta_{ij}\lambda) A_i = 0$$

This set of simultaneous linear equations in the 3N amplitudes, A_i, only has non-vanishing solutions for special values of λ, namely those which satisfy the secular equation:

$$\begin{vmatrix} f_{11}-\lambda & f_{12} & f_{13} \cdots & f_{1,3N} \\ f_{21} & f_{22}-\lambda & f_{23} \cdots & f_{2,3N} \\ . & . & . & . \\ . & . & . & . \\ . & . & . & . \\ f_{3N,1} & f_{3N,2} & f_{3N,3} \cdots & f_{3N,3N}-\lambda \end{vmatrix} = 0$$

For each root, λ, there is a corresponding set of 3N amplitudes A_i. The secular equation is of the order 3N, but only (3N-6) roots describe genuine vibrations as there are six zero roots for rotation and translation. These genuine solutions correspond to the (3N-6) normal modes <u>each</u> of which has a motion described by an equation of type (2). This shows that all the nuclei vibrate with the same frequency, in phase, but with varying amplitudes. When two or more roots of the secular equation are identical, the normal modes have the same frequency and are said to be degenerate; they are not distinguished by spectroscopy.

The secular equation is very important in the study of molecular vibrations. Except for diatomic molecules, however, the number of force constants f_{ij} exceeds the number of



Tetrahedral XY_4 symmetry

(i)		(ii)				(iii)	(iv)
T_d	E	$8C_3$	$3C_2$	$6S_4$	$6\sigma_d$		
A_1	1	1	1	1	1		$(\alpha_{xx}+\alpha_{yy}+\alpha_{zz})$
A_2	1	1	1	-1	-1		
E	2	-1	2	0	0		$(\alpha_{xx}+\alpha_{yy}-2\alpha_{zz})$, $(\alpha_{xx}-\alpha_{yy})$
F_1	3	0	-1	1	-1	(R_x, R_y, R_z)	
F_2	3	0	-1	-1	1	(T_x, T_y, T_z)	$(\alpha_{xy}, \alpha_{yz}, \alpha_{xz})$

FIGURE 1A. Character Table for T_d point group

observable frequencies, and so all the f_{ij} cannot be evaluated from frequency data. It is therefore customary to base force-field calculations upon assumed simplified types of field involving fewer force-constant parameters than the general force-field.

1(4) Molecular Symmetry

It is not necessary to solve the secular equation to obtain information on the normal modes of a particular molecule. From considerations of molecular symmetry (6) it is possible to determine:

(a) the number of fundamental vibrations and their degeneracies

(b) the selection rules

(c) the polarisation properties of Raman-active modes.

In its equilibrium configuration a molecule may possess a number of symmetry elements, each of which is associated with a symmetry operation the performing of which produces a structure indistinguishable from the original configuration. The symmetry operations exist in sets, each of which constitutes a mathematical group; by determining what symmetry operations may be carried out on a molecule, it may be assigned to one of the forty-four symmetry point groups.

Consider as an example an XY_4 molecule, e.g. CH_4, belonging to the point group T_d (see Fig.1A). A <u>character table</u> for this point group can be drawn up giving a group-theoretical representation of the transformation properties of the internal vibrations which a molecule in that point group will undergo. The top row of the table lists all the distinct symmetry operations, while the symbols in the left-hand (i) column indicate the various possible symmetry species into one of which each normal mode will fall. (ii) gives the characters of the irreducible representations of the group. (iii) gives the symmetry species of rotational and translational motion, and (iv) shows to which representations the various components of the polarisability ellipsoid belong (from which one can determine the Raman activity of the modes).

One method of determining the number of normal modes in a given symmetry species would be to examine the effect of all the symmetry operations on the displacement vectors. This is tedious and unnecessary as group theory provides a simple method based on the character table.

The number of normal modes, n_r, within a given symmetry species depends on the character χ_j of the transformation of

the atomic coordinates in the molecule when a symmetry operation of type j is performed. χ_j is the sum of the diagonal elements in the transformation array. For atoms which are interchanged during the symmetry operation the diagonal element is zero, so that only unshifted atoms contribute to χ_j and hence to n_r. For each symmetry operation the contribution of each unshifted atomic χ_j^{atom} to the total character of the molecule χ_j can be calculated (4). Multiplication of χ_j^{atom} by the number of unshifted atoms then gives χ_j.

The number of vibrations in the symmetry species r can now be calculated by means of the expression:

$$n_r = \frac{1}{g} \sum_j g_j \chi_j^r \chi_j$$

where g_j is the number of symmetry operations of type j, g is the total number of symmetry operations and χ_j^r is the number listed in the character table under symmetry class r and symmetry operation j. The result of this analysis on the T_d model for an XY_4 molecule is shown in Table 1A.

TABLE 1A

Vibrational analysis of XY_4, T_d symmetry

Symmetry operation	E	C_3	C_2	S_4	σ_d
No.of unshifted atoms	5	2	1	1	3
χ_j^{atom}	3	0	-1	-1	1
χ_j	15	0	-1	-1	3
g_j	1	8	3	6	6

$$n_{A_1} = \frac{1}{24}(1\times1\times15 + 1\times0\times8 + 1\times3\times-1 + 1\times-1\times6 + 1\times3\times6) = 1$$

$$n_{A_2} = \frac{1}{24}(1\times1\times15 + 1\times0\times8 + 1\times3\times-1 + 6\times-1\times-1 + 6\times-1\times3) = 0$$

$$n_{E} = \frac{1}{24}(2\times1\times15 - 1\times0\times8 - 1\times3\times2 - 1\times6\times0 + 6\times3\times0) = 1$$

$$n_{F_1} = \frac{1}{24}(3\times1\times15 + 0\times0\times8 - 1\times-1\times3 + 1\times-1\times6 + 3\times6\times-1) = 1$$

$$n_{F_2} = \frac{1}{24}(3\times1\times15 + 0\times0\times8 - 1\times-1\times3 - 1\times-1\times6 + 3\times6\times1) = 3$$

Species	n	trans.	rot.	vibrations
A_1	1			1
A_2	0			0
E	1			1
F_1	1		1	0
F_2	3	1		2

Giving $\Gamma_{vib.} = 1A_1 + 1E + 2F_2$

Symmetry coordinates

If the positions of the nuclei are defined by a set of internal coordinates (bond lengths and interbond angles) it is possible, in a manner very similar to that outlined above, to select a set of symmetry coordinates as linear combinations of the internal coordinates, which belong to the symmetry species of the molecule. The normal coordinate for a given mode is a linear combination of the symmetry coordinates of the species to which that mode belongs. In cases where there is only one normal mode to a given species, its symmetry coordinate representation will be an exact description of the nuclear displacements. More often, however, more than one mode belongs to a particular species and then the description of each separately by a symmetry coordinate is no longer exact. Every normal mode mixes together the symmetry coordinates of its species, and this mixing depends on the reciprocal atomic masses (mechanical coupling) and on the molecular force field (electronic coupling).

1(5) Force constants

In order to obtain the force constants, f_{ij}, from the fundamental frequencies, ν_k, the secular equation [1(3)] must be solved. This is a polynomial of the $(3N-6)^{th}$ degree;

consequently computation is rather difficult, but considerable simplification can be achieved using the Wilson $\mathcal{FG}$ matrix method (4,7) which requires the solution of the matrix secular equation

$$\left| \mathcal{GF} - E\lambda \right| = 0$$

The $\mathcal{G}$ matrix is related to the kinetic energy of the system and depends on the molecular symmetry and masses of the atoms concerned. The $\mathcal{F}$ matrix is related to the potential energy of the system and contains the force constants of the modes involved. E is a unit matrix and λ is a diagonal matrix of the roots.

It is now possible to factorise the secular determinant into the product of a number of smaller determinants, one for each symmetry species. However, as noted in 1(3), even for molecules of high symmetry an insufficient number of observable frequencies dictates the assumption of approximate force-fields, and allowance for all the possible forms of intramolecular interaction cannot be made.

The bond-stretching force-constants are important mainly because of their relation to bond dissociation energies. If the potential energy V is expressed as a function of the nuclear displacements, q, then the force

constant is given by

$$f = \left(\frac{\partial^2 V}{\partial q^2}\right)_o$$

i.e. it is a measure of the curvature of the potential well at the equilibrium position. The dissociation energy, D_o, is the depth of this well. There is no necessary correlation between a deep well and one with a large curvature at the equilibrium position, but empirically a large force constant can be interpreted as indicating a strong bond.

The computation of force constants will be undertaken in later Chapters of this work and details of the approximations involved and the conclusions therefrom are included.

1(6) Selection Rules (8)

Having calculated the number of distinct frequencies of vibration of a molecule and an assignment into symmetry species made, it is necessary to determine which of the species absorb in the infra-red and those which are active in the Raman effect.

The vibrational selection rules for the Raman effect and for infra-red absorption, and the rule of polarisation

for vibrational Raman lines are all based solely upon symmetry considerations. For a molecule whose structure is known, application of the rules gives information as to the number of fundamental vibrational frequencies permitted in either type of spectrum and the number whose Raman lines will be polarised.

If a molecule is of unknown structure for which two (or more) models with different symmetries can be reasonably proposed, then predictions of the above kind can be made for each of them. In general, the predictions for the rival models will be different, so that by experimental observation of the actual spectra it will be possible in principle to discriminate between the proposed structures and to decide which is the correct one for the molecule.

It is important to note that this method, being based solely upon general symmetry theory, is quite independent of the special nature of the molecular force-field. For this reason it is a method of great power, since a complete description of the force-field is generally inaccessible. A brief account of the derivation of the selection rules will now be given; fundamentals are considered throughout, because, generally speaking, they are most easily observable. The

intensity of a transition is proportional to the square of the relevant transition moment, and so the condition that a transition be allowed is that the transition moment shall not vanish.

Infra-Red Absorption

For a fundamental transition (vibrational quantum number change from 0 to 1) the transition moment for infra-red absorption is given by

$$\mu_{01} = \int \psi_0 \mu \psi_1 \, dQ$$

where ψ_0, ψ_1 are respectively the wave-functions of the initial and final states, μ is the electric dipole moment of the molecule as a function of Q, the normal coordinate of the vibrational mode. The integral is to be extended over the whole coordinate range. The dipole moment, being a vector, has three components (μ_x, μ_y, μ_z in a Cartesian system), so that an integral of the above type applies separately to each of them.

The condition that the integral for the component μ_i (where i denotes either x, y or z) shall not vanish is that the integrand $\psi_0 \mu_i \psi_1$ shall be totally symmetric, i.e.

shall be transformed into itself by all the symmetry operations of the molecular point group. Since the ground vibrational state ψ_0 is known always to be totally symmetric, it follows that the product $\mu_i \psi_1$ must be totally symmetric. This is only the case provided that both factors belong to the same symmetry species. For the transition to be permitted it will suffice if this is so for at least one of the components of μ. It is also known that ψ_1 always belongs to the same symmetry species as the vibration itself, so the infra-red absorption selection rule can be stated as follows:

A fundamental is only permitted in infra-red absorption provided that its species is the same as that of at least one of the components of the electric dipole moment.

The species of the dipole-moment components are the same as those of the corresponding translations, and these are given in the point-group Character Table.

Raman Effect

In considering Raman scattering we are concerned with the dipole moment P induced in the molecule by the electric field E of the incident light. This is given by:

$$P = \alpha E$$

where α is the molecular polarisability.

If a vibration causes no change in α, the frequency of the induced dipole moment would always be the same as that of the incident radiation, and therefore, so would be the frequency of the scattered radiation (Rayleigh scattering). During a vibration a periodic change in the configuration of certain modes may cause a periodic change in α, and thus in P. These periodic changes in α are superimposed on the variations due to E, resulting in the frequency of the scattered radiation being modulated by the vibrational frequencies of the molecule.

For a fundamental Raman transition the transition moment is,

$$P_{01} = \int \psi_0 \alpha E \psi_1 \cdot dQ = E \int \psi_0 \alpha \psi_1 dQ$$

α is generally a <u>tensor</u>, representable by an array of nine components (α_{xx}, α_{yy}, etc.). However, because the tensor is a symmetric one $\alpha_{ij} = \alpha_{ji}$, and only six of the nine components are distinct. A transition moment integral of the above form applies separately to each component.

As in the case of infra-red absorption, the selection rule for Raman scattering can be stated as follows:

A fundamental is only permitted in Raman scattering provided that its species is the same as that of at least one of the components of the polarisability.

A component α_{ij} transforms in the same way as does the product of the translations T_i and T_j, and the species of the components of α (or in certain cases, linear combinations of them) are customarily given in the point-group Character Tables. It is therefore a routine matter to read the selection rules for vibrations of any species.

1(7) The Polarization Rule for Raman Scattering

For a fluid sample, when the incident light is natural (i.e. unpolarized) and the scattering is observed at right angles to the incident direction, the degree of depolarization ρ_n of a Raman fundamental is given by

$$\rho_n = \frac{6(\gamma_{01})^2}{45(\bar{\alpha}_{01})^2 + 7(\gamma_{01})^2}$$

where $\bar{\alpha}_{01}$ and γ_{01} are respectively the mean-value and anisotropy invariants of the transition tensor α_{01}. It follows that the line is only polarized (i.e. has $\rho_n < 6/7$) provided that $\bar{\alpha}_{01}$ does not vanish.

Now

$$\bar{\alpha}_{01} = \tfrac{1}{3}\left[(\alpha_{xx})_{01} + (\alpha_{yy})_{01} + (\alpha_{zz})_{01}\right]$$

$$= \int \psi_0 \bar{\alpha} \psi_1 \, dQ$$

where $\bar{\alpha}$ is the corresponding mean-value invariant of the molecular polarizability tensor α. It is known that $\bar{\alpha}$, being of the same symmetry as $T_x^2 + T_y^2 + T_z^2$, always belongs to the totally symmetric species. It follows that $\bar{\alpha}_{01}$ can only be different from zero provided that ψ_1 is also totally symmetric, i.e. provided that the vibration concerned belongs to this species.

The Raman polarization rule may thus be stated:

Only fundamentals of totally symmetric vibrations give polarized Raman lines ($\rho_n < 6/7$). The Raman lines of fundamentals belonging to all other species are depolarized i.e. have $\rho = 6/7$.

1(8) Predictions from the Selection Rules

For any proposed symmetry (i.e. point group) the symmetry species of the modes can be deduced. Where degenerate species are involved, pairs of modes (or sets of three) will be such that their members will necessarily have identically

the same frequency. In general, therefore, the number of distinct fundamental frequency-values will be less than the total number of normal modes (which is 3N-6, and is 3N-5 for linear molecules).

By using the selection and polarization rules it is possible, for any point-group, to make the following predictions:

(a) The number of fundamental frequencies which will be permitted in the infra-red absorption spectrum;

(b) The number of fundamental frequencies which will be permitted in the Raman spectrum;

(c) The number of coincidences i.e. the number which will be permitted in both types of spectrum; and

(d) The number of fundamentals in the Raman spectrum which will be polarized.

For different proposed models the sets of predictions will, in general, be different. This is the basis of the experimental method of determining which model is the correct one in any particular case.

As an example, it is useful to consider the tetrahedral XY_4 molecule of Figure 1A. The following information is deduced from the application of selection rules and vibrational analysis:

$\Gamma = A_1 + E + 2F_2$ (Table 1A)

Raman-active vibrations —— all 4

Infra-Red active vibrations —— 2 only, of f_2 species

Coincidences —— 2

Polarized in the Raman spectrum —— 1

For the square-planar XY_4 structure a different set of active vibrations is produced; a comparison of the tetrahedral and square-planar XY_4 is given below:

XY_4 Symmetry	Tetrahedral	Square-Planar
Point-group	T_d	D_{4h}
Total no.of vibrations	4	7
Raman-active	4	3
IR-active	2	3
Coincidences	2	0
Polarized in Raman	1	1
Inactive vibrations	0	1

From this information it should be possible to distinguish between the T_d and D_{4h} structures in the vibrational spectrum. It so happens that this case is

particularly favourable for structure elucidation, since the D_{4h}, XY_4 molecule has a centre of symmetry and therefore, according to the mutual exclusion rule, there should be no coincidences in the Raman and the Infra-red.

CHAPTER 2

Chapter 2

INSTRUMENTAL TECHNIQUES

In this Chapter the instruments used in the obtaining of the vibrational spectra in this work will be described. The emphasis is on Raman spectroscopy since the existing apparatus in the laboratory had to be modified to some extent. The modifications consist essentially of arrangements whereby samples are refrigerated; a necessity with some of the compounds studied, on account of their thermal decomposition under Raman excitation.

2(1) Raman Spectroscopy

The essential equipment for the observation of the Raman effect consists of,

(a) a high-intensity light source producing monochromatic light of a wavelength which is not absorbed by the sample being irradiated,

(b) a means of collecting the scattered light,

(c) a spectrograph which will resolve the scattered wavelengths,

(d) a convenient means of recording spectra.

During the course of the investigations pursued in the present work two Raman instruments were used, each satisfying the above criteria but differing in the nature of the light source and method of recording spectra. Because of the weakness of the Raman effect a source of high intensity is required. The ideal lamp would emit one strong line only, since other lamp lines obscure Raman lines and also give rise to their own Raman spectra. The lamp spectra should also be as free as possible from background continuum in the region where Raman lines may appear. The frequency of excitation should be chosen so that appreciable absorption by the sample does not occur: this would result in a decreased intensity of the scattered light and possibly photodecomposition of the sample. No source has yet been found which fulfils the necessary conditions for all samples, but for many purposes the low-pressure, D.C., mercury-vapour discharge lamp is useful.

In the present work two Raman instruments were used:

(a) The Cary 81 Raman spectrophotometer; a commercial instrument using a sealed, low-pressure, mercury source and sophisticated photoelectric recording designed to give a high signal-to-noise ratio.

(b) The Helium Source; built in 1960 and later modified, which uses a high-voltage discharge through helium at low pressure and records photographically.

2(2) The Cary 81 Raman Spectrophotometer

This is a precise, photoelectric-recording instrument consisting of a mercury source coupled with a highly-efficient optical train which selectively transmits the inherently-weak Raman scattering with little loss. The source is a 3-kilowatt, water-cooled mercury lamp consisting of two large mercury pools connected through seven coils of Corning 1720 glass of Toronto-arc design. This source, shown in Figure 2A, gives strong lines at 4046 Å, 4358 Å and 5461 Å, with relatively few weaker lines.

To start the lamp, the coils are heated and the mercury is volatilised in the pools by passing water at 80°C through the sealed-in fingers. A potential of 300 volts D.C. is applied across the lamp and a Tesla h.f.induction coil, developing 85,000 volts, is discharged near the mercury pools and coils. To assist the discharge from one pool to the other the coils have a graphite strip painted along their whole length, which also ensures that the high-voltage stress is distributed evenly over the evacuated lamp. After

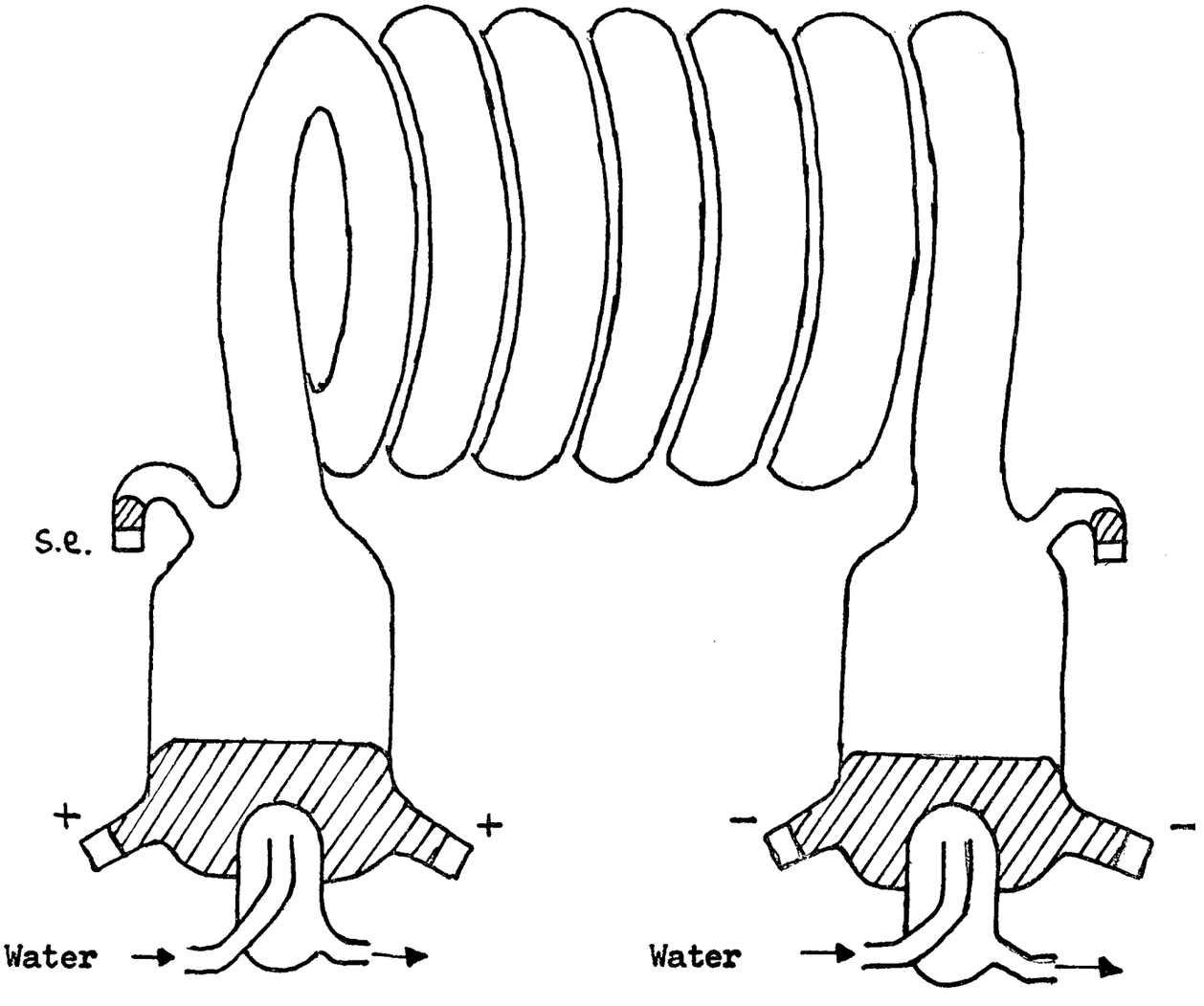


Figure 2A. Cary 81 Toronto-Arc Source.

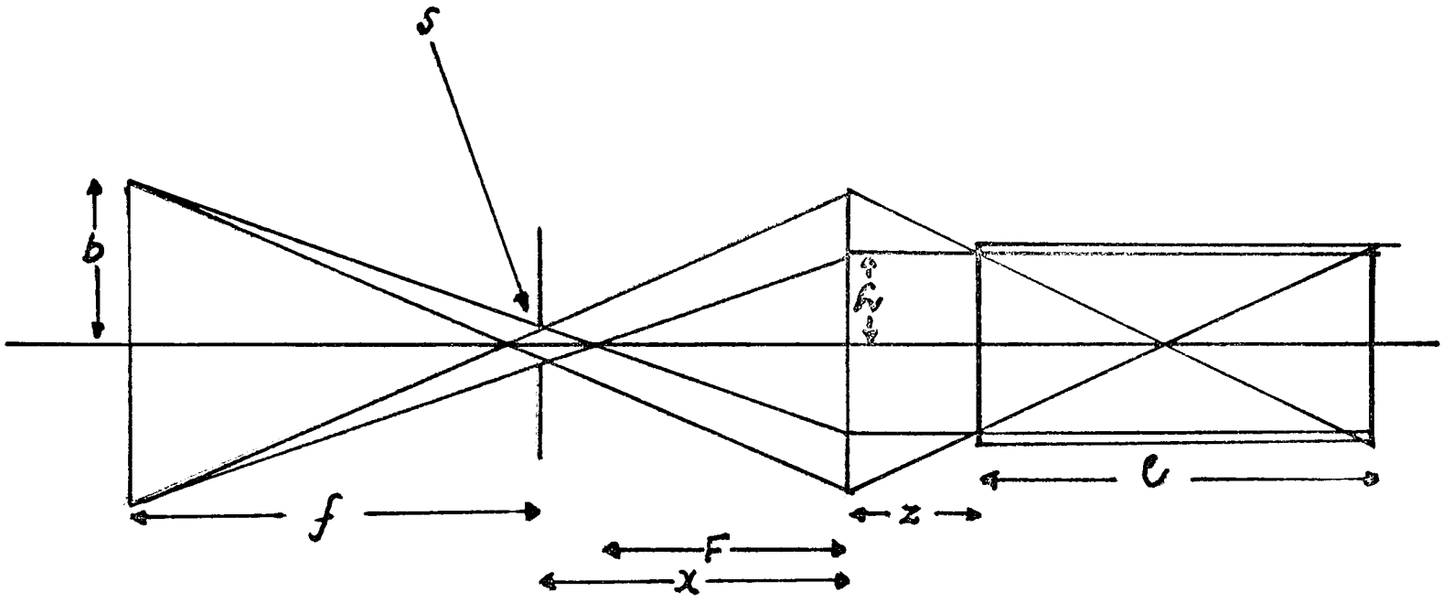
striking of the lamp, the running voltage drops to 190 volts D.C. at a current of 13 amps. The pools are now cooled to 27°C and cold air is blown over the coils, ensuring that the lamp continuum is reduced to a minimum by keeping just enough mercury vaporised to maintain the discharge. D.C. running conditions are better than A.C. on account of the very low background continuum in the region of 4358 Å. This intense line has a clear region of 2,400 cm^{-1} on the low-frequency (Stokes) side. The green 5461 Å line is sometimes of use with samples that absorb the blue, but its use is limited.

The mercury arc produces lines of higher frequency which could cause photodecomposition and might excite fluorescence, thereby obscuring the region of interest. To remove undesirable lines a pre-filter solution is placed between the lamp and the sample. The standard filter solution is ethyl violet in iso-propanol and o-nitrotoluene; the disadvantage of this filter is that the green line at 5461 Å is removed, so for the work on yellow compounds described later the filter solution was o-nitrotoluene in iso-propanol. The filter solution (volume circa 3 litres) deteriorates with the absorption of UV from the lamp, and needs regular replacement since the intensity of the 4358 Å line may be reduced by as much as 70%.

The optical system

In earlier instruments an optical system was required in which the maximum amount of scattered light from the sample was collected, while ensuring complete rejection of primary light scattered by the walls of sample tubes. To this end, an optical coupling arrangement of the type devised by Nielsen (9) is used, and is an integral part of the Helium Source to be described later. The geometry of the system is illustrated in Figure 2B: the convex coupling lens focusses the spectrograph slit at the top of the sample, and the image of the collimator lens appears at the bottom. The rectangular slit image occupies only a small fraction of the area of one end of the sample cell; only rays passing through this narrow area can reach the monochromator so that most of the light emerging from the cell window is lost.

In the Cary 81, however, the incorporation of image slicers between the sample cell and the entrance slit makes it possible to use rays from the entire end of the sample cell instead of only a narrow strip in the middle. The image of the cell-window is sliced into twenty strips which are superposed into two sets of ten strips each; the two images thus formed are now magnified to the exact size of the entrance slit.



$$F = hf/(b - s) \qquad l = h^2 f/sb$$

$$z = (f + x)\, h/b \qquad x = (h + s)f/(b - s)$$

Figure 2B. The Nielsen Conditions.

Slits are arranged in pairs, and the instrument is normally used on double-slits except when working near the exciting line when single-slit operation is advised. The double monochromators discriminate against Tyndall and Rayleigh scattering effects; one of the chief advantages of the attendant low stray light is that internal-reflection sample cells may be used. Thus, cells of small volume up to 5 ml. capacity can be used, e.g. the micro-cells containing 0.6 ml. liquid in a 25 cm. length. Also, Raman spectra may be obtained from crystalline solids despite the fact that the crystal faces are rough and effective light-scatterers. Useful general references for the optical arrangements described above are found in books on experimental spectroscopy (10, 11).

The recording of the Raman spectra is made photo-electrically. The optical system is connected to the photometric system via a chopper. The photo tube signals are amplified and compared with a reference signal which is obtained from a light pipe monitoring the lamp flux. The difference between reference and sample signals is converted into a d.c. voltage and used to drive a pen motor.

2(3) Modifications to the Cary 81

In order to obtain Raman spectra from some of the samples made in the present work, it was necessary to cool the samples. The reasons for this are considered in the relevant text, but generally cooling is advisable where samples are volatile or decompose thermally. Two distinct arrangements were used in such cases: one being suitable for solids and liquids at very low temperatures, the other arrangement involving only moderate cooling for solutions.

(a) Arrangement for the moderate cooling of a solution

This consists of a 5-ml. Raman tube encased in a Liebig-type jacket (shown in Figure 2C) which was devised by Clarke(12) for temperature control in quantitative Raman spectroscopy. Clarke initially used water as a coolant, but spurious features were observed in the resulting Raman spectrum which were ascribed to the internal reflections at the liquid-glass-liquid interfaces. Ellis (13) confirmed this conclusion by using carbon tetrachloride as a 'coolant' for a water sample and observing the Raman spectrum of carbon tetrachloride. Because of this, an air-cooling system was devised; air from a compressor, the speed of which is controlled by a Variac potentiometer, is cooled by passage through a copper coil

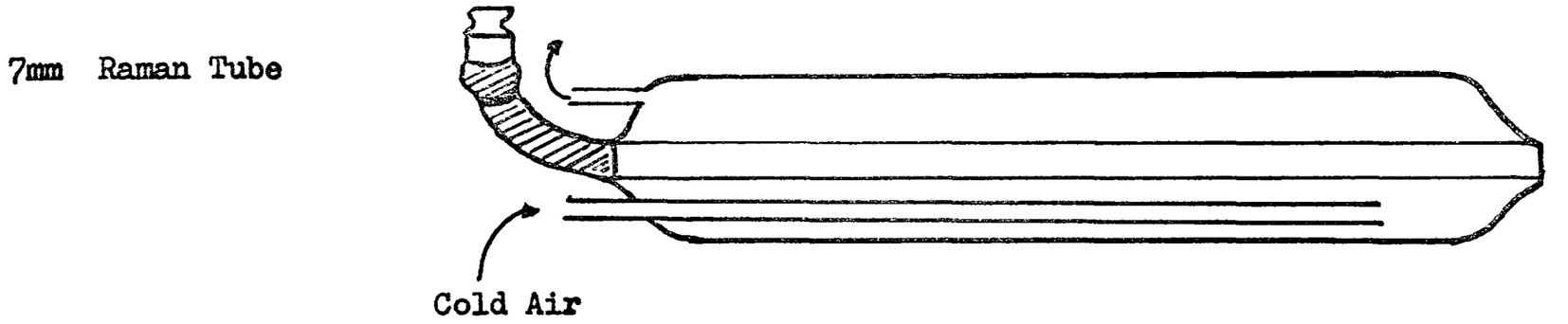


Figure 2C. Controlled Temperature Raman Cell.

immersed in an acetone-CO_2 bath at -78°C. To prevent condensation of ice in the copper coil two silica gel drying towers were incorporated into the system.

With the acetone bath at -78°C and a sample of carbon tetrachloride in the Raman tube (in which was immersed one end of a copper-constantan thermocouple), the Variac settings and resultant flow of air through the system could be calibrated against temperature. Only moderate cooling could be effected in this way, the limit being approx. 0°C. The normal operating temperature in the sample compartment of the Cary 81 spectrometer is 42°C.

Such an arrangement was used to obtain the Raman spectra of tetrakistrichlorophosphinenickel in carbon tetrachloride and benzene. The big advantage of this design is that samples can be changed quickly and temperature equilibration of new samples is rapid: both factors are essential where, as in the case cited above, unstable compounds in solution are being handled.

(b) Cold cell arrangement for very low temperatures

This arrangement is of more complicated design and is shown in Figure 2D. It was designed specifically for work on the volatile, unstable metal-trifluorophosphines described later. Using this cold cell it was possible to obtain the

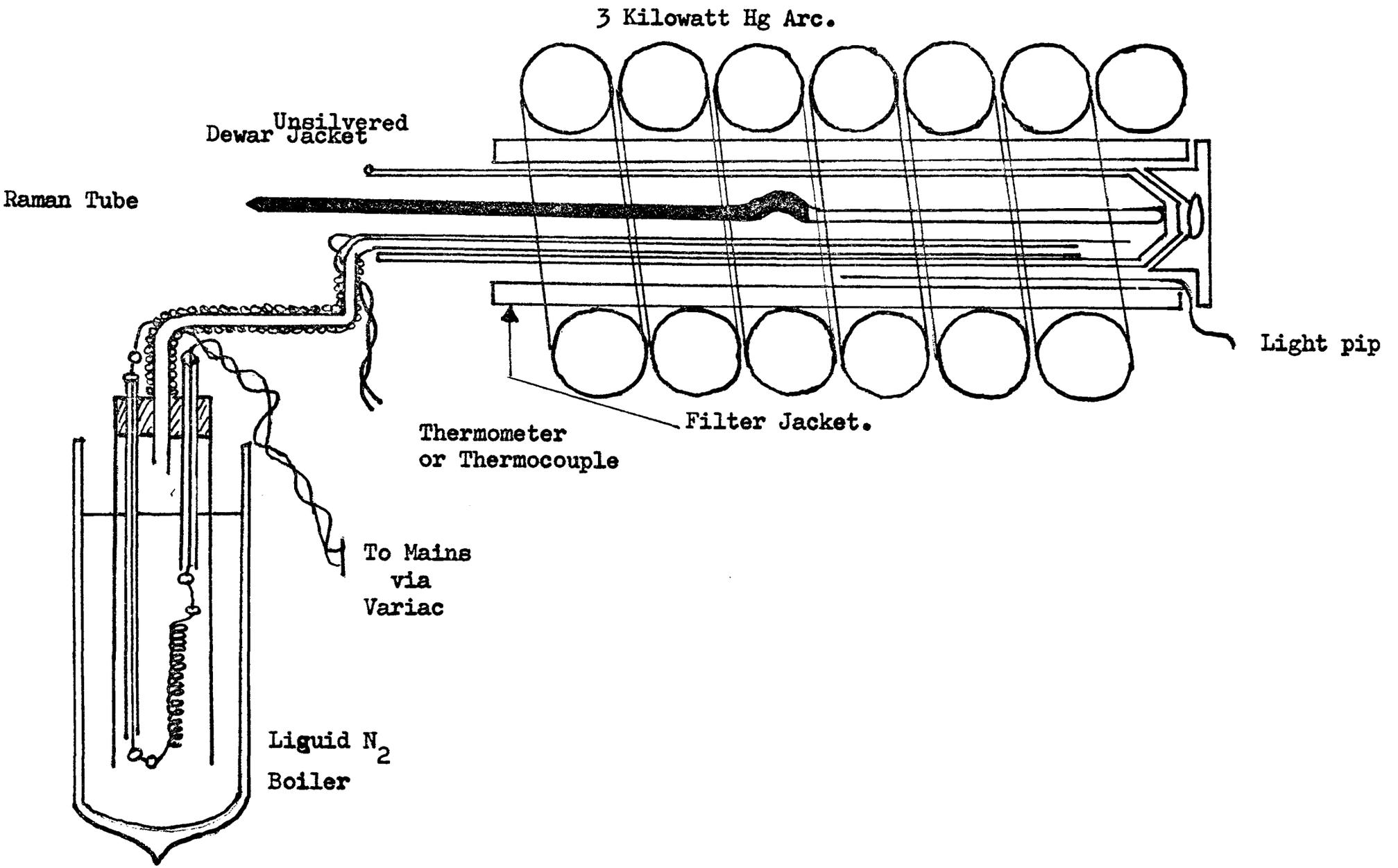


Figure 2D. Cold Cell Arrangement for Cary 81 Spectrometer.

Raman spectra of such compounds in the solid state at temperatures down to -100°C for direct comparison with the infra-red spectra in the same state.

The unsilvered Dewar jacket is 40 cm. long and can be clamped horizontally outside the lamp housing. The diameter was made such that minimal clearance of the reference light pipe was obtained, so giving the maximum amount of space inside the jacket, and allowing the use of diverse sample tubes (including solid cells of the conical type) within the cold cell. One end of the jacket consists of optically-plane windows, the other end being left open to the atmosphere. The sample tubes are mounted horizontally and may be of any size commensurate with their insertion in the jacket. The tube shown in position in Figure 2D is typical, the diameter of the tube and position of the 'kink' being quite arbitrary and dependent only on the volume of liquid available.

The refrigerant is cold nitrogen, boiled from liquid nitrogen by means of a heating coil, the current through which is controlled by a Variac potentiometer connected to the mains supply. The cold nitrogen passes through an asbestos-lagged inlet tube leading to the bottom of the jacket and issues freely at the open end. Temperatures are read from a

calibrated thermocouple or alcohol thermometer, and equilibration is effected after some ten minutes. Temperature adjustment is made by Variac control: it is possible to calibrate the Variac for temperature, but this is not advisable for accurate work since the characteristics of the heating coil change with age and time of immersion in the liquid nitrogen. The lowest temperature reached using this system was -110°C.

An inherent setback to be guarded against in low-temperature work is the frosting of the windows of the jacket or Raman tube due to the deposition of ice. In the arrangement above no 'iceing-up' was observed even after many hours at low temperatures. An explanation of this is that the refrigerant is dry (cold nitrogen from liquid nitrogen), and that the flow-rate is high enough to prevent back-diffusion of moist air into the cold jacket.

2(4) Pilot experiments with the low-temperature modifications

Aside from the qualitative experiments on cooling outlined above, the most important experiments initially carried out using this equipment involved the determination of depolarisation ratios, ρ; effectively, this was a calibration of sample tubes in the low-temperature set-ups under different conditions. The

smaller Cary 81 sample tubes rely on internal reflections for the enhancement of Raman scattering, but this introduces some degree of non-ideality in the measurement of ρ . For the accurate determination of ρ all light flux from the Raman source should enter the sample radially, and this is not achieved unless a complicated system of baffles is used to eliminate non-radial light. The intensity of illumination of the sample is thereby greatly diminished and such a modification is impractical for normal work.

Polarisation properties are determined using a double-exposure method of polarised incident light (14); in this method, polaroid cylinders with their directions of polarisation parallel (axial) and perpendicular (cross-axial) to the direction of observation are respectively placed around the Raman tube during successive exposures. Compensation for the non-ideality of the arrangement is essential for the determination of true ρ-values, and the best method involves the determination of experimental ρ-values under standard conditions for standard samples. True ρ-values have been measuredfor a variety of well-known liquidsby Cabannes (15).

In the present work the calibration was performed as

follows: the samples selected as standards were carbon tetrachloride, chloroform, and dimethyl sulphoxide, which have ρ-values in the range 0 to $^{6}/_{7}$. The vibrational band contours were scanned photoelectrically, and traces were obtained under standard instrument settings with the cylinders of axial and cross-axial polaroid around the samples. Areas were measured with an 'Albrit' planimeter, and the area ratio is then taken as the experimental ρ-value, $\rho_{observed}$. Results are tabulated in Table 2A and the calibration graphs for the 7 mm. diameter 'kinked' tube and for the 2 mm. diameter microtube are shown in Figure 2E. It is immediately noticed from Figure 2E that the 2mm. sample tube is far less ideal than the 7 mm. tube; this would be expected on account of the greater use of internal reflections in the former.

2(5) The Helium Source

The colour of many transition metal compounds forbids their study by conventional Raman spectroscopy involving mercury blue excitation. Considerable effort has been made to develop sources which are suitable for the study of such compounds by Raman spectroscopy. Sources using molten alkali metals have been described but one of the most successful sources for red-end spectroscopy uses a discharge through

TABLE 2A

ρ-value calibration of sample tubes

Sample	Band (cm^{-1})	ρ true	Ref.	ρ observed (pres.work)	
				7 mm.	2 mm.
CCl_4	214	0.83	16	1.23	-
	318	0.79	16	1.14	-
	460	0.01	17	0.31	0.52
$CHCl_3$	261	0.70	16,17	1.00	1.18
	365	0.18	16,17	0.45	0.66
	667	0.06	16	0.30	0.53
	759	0.68	16	-	1.22
	3020	0.32	16	0.52	0.69
Me_2SO	306	0.83	18,19	1.00	1.35
	334	0.83	18,19	0.94	1.25
	668	0.17	20	0.50	-
	698	0.65	18,19	0.88	-
	952	0.57	18,19	0.85	0.92
	1042	0.40	20	0.69	0.90

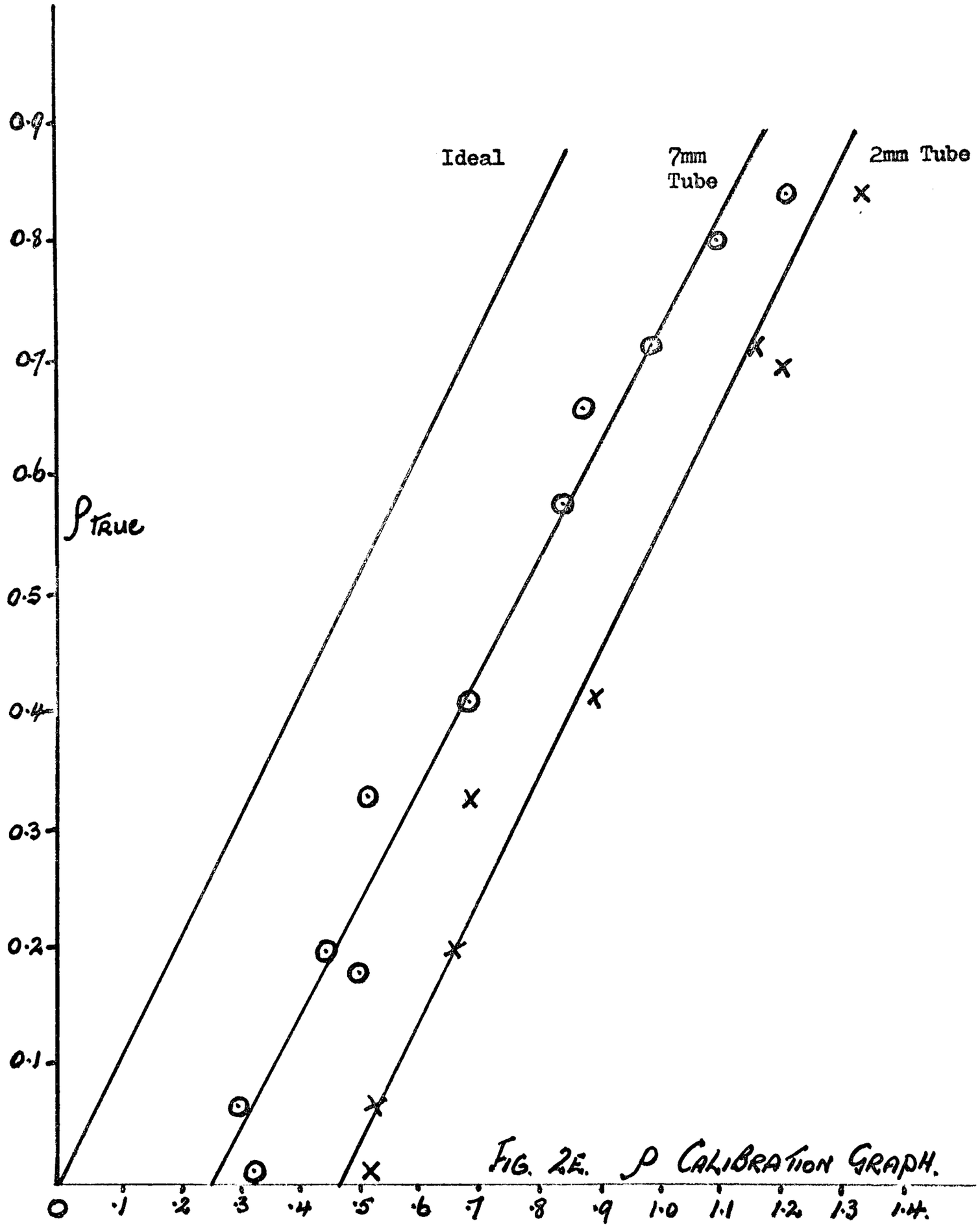


FIG. 2E. ρ CALIBRATION GRAPH.

helium gas. The helium discharge has suitable lines at 5876, 6678, and 7065 Å which may be employed for the excitation of Raman spectra. The difficulties of excitation in the red region of the spectrum may be summarised as follows:

(i) The dispersion and resolving power of a prism spectrograph falls off rapidly in the red region as compared with the blue.

(ii) Raman scattering is inversely proportional to the fourth power of the wavelength, so that a line excited by He 5876 Å will be 5½ times weaker than the same line excited by Hg 4358 Å for sources of similar power.

(iii) Photographic plates are slower in the red region.

(iv) The sample may absorb the exciting radiation.

A useful account of the practical difficulties of exciting Raman spectra in the red is given in papers by Stammreich (23, 24) on high-resolution Raman spectroscopy.

The helium lamp used in the present work was developed by Rendell (25) after the pattern briefly described by Stammreich (21, 22). It employs an 8 kv discharge through pure helium at 2 mm. pressure. The lamp envelope and sample housing are shown in Figure 2F. The electrodes

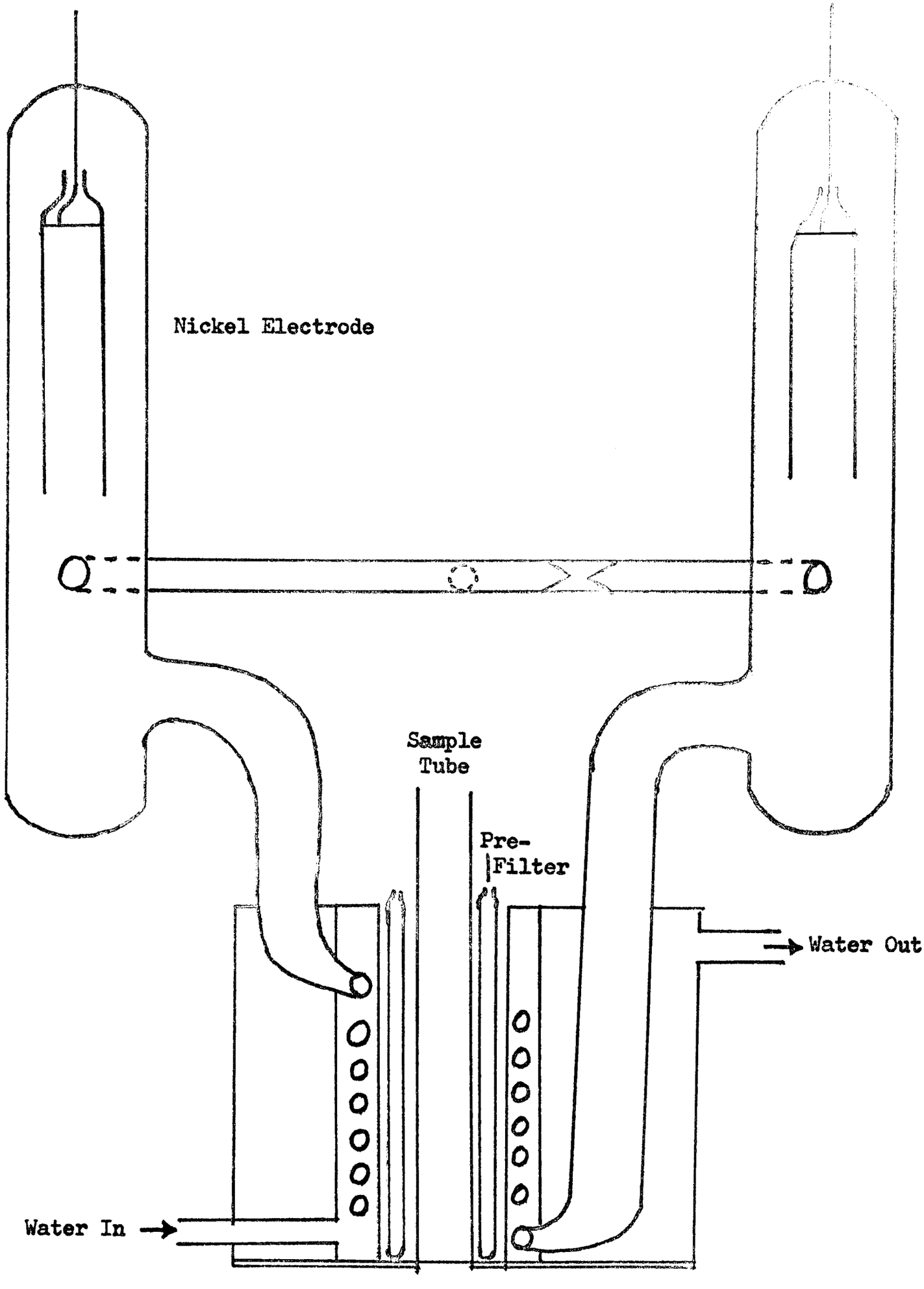


Figure 2F. The Helium Source.

are spot-welded cylinders of pure nickel foil, closed at one end and attached to a pyrex-tungsten seal. The lamp helix, which surrounds the sample, is totally immersed in an annular water tank whose inner wall is glass. Light losses are reduced by surrounding the helix with a reflector coated with water-resistant white paint. The helium used was 'Grade X' helium supplied in one-litre bulbs by the B.O.C. The level of trace impurities, chiefly hydrogen, was reduced by leaving the helium in contact with activated charcoal cooled in liquid nitrogen. The pressure of helium in the lamp falls with time and use, due to adsorption on the surface of sputtered nickel deposited on the walls, and to diffusion through the pyrex lamp envelope, which is slightly porous to helium when hot.

Power for the lamp is provided by an 8000 volt transformer rated at 0.5 amp secondary current, and to limit the current actually drawn by the lamp the 230 v primary windings are in series with a water-cooled ballast resistance.

Sample size is rather large, being about 15 ml. volume in a 15 mm. diameter tube. It will be seen later that for coloured compounds it is better to use a larger, more dilute solution than a smaller, more concentrated one.

In the early experiments using this helium lamp a serious disadvantage was found; the lamp spectrum contained weak band systems which were identified as arising from excited He_2 molecules (26). One such system extends from 5900-6200 Å, i.e. covering the Stokes region of the 5876 Å line from 200 cm^{-1} to 600 cm^{-1}. When weak Raman spectra are being studied this band system can obliterate a region of great interest. The transition to the ground state from the ^3S excited state of He at 19.77 eV is forbidden. Atoms in this excited state are therefore metastable and have a sufficient lifetime to associate, giving He_2 molecules. The formation of molecules may be suppressed by lessening the lifetime of the atoms in the ^3S state; this can be achieved by increasing the rate of collision between the atoms and a foreign substance such as the walls of the lamp envelope. Thus the surface area/volume ratio of the lamp envelope should be as large as possible.

This has been verified by Stammreich (27), who investigated helium discharge tubes of different diameters; the proportion of molecular bands decreases sharply as the diameter falls below 2 mm. For a Raman source of workable dimensions, however, the narrowness of bore is limited by

the voltage available for striking and maintaining the discharge. Ware (28) found an improvement in the quality of the lamp spectrum when the helix was changed from one of 3½ turns of 6 mm. i.d. tubing to one of 9½ turns of 3 mm. i.d. tubing. For the present work the helix was further reduced to 7½ turns of 2 mm. i.d. tubing. The disadvantage of such a narrow helix is that the initial outgassing process is slow. This is hastened by running the lamp at 6 mm. pressure of helium, causing heating of the electrodes and envelope, and then evacuating the lamp. The process is repeated until de-gassing is complete.

The pressure of helium normally employed in the lamp is 2.5 mm. Hg, the current at this pressure being 550 mA. The 'lifetime' of one charge of helium is approximately 12 hours, so evacuation and replenishment from the attendant vacuum line is necessary quite regularly. An electric fan was arranged to provide general lamp cooling in the neighbourhood of the electrodes, preventing overheating and loss of helium in this way.

Light scattered vertically downwards from the sample tube enters the optical box and is reflected by a silver mirror into the spectrograph. In the alignment of the source with

the spectrograph it is essential that primary scattering from the walls of the Raman tube should not enter the spectrograph; for this purpose an optical coupling arrangement of the Nielsen type is used.

The Grating Spectrograph

The luminosity of a spectrograph may be increased by using a camera of larger aperture. This entails a shorter focal length at the expense of dispersion at the photographic plate. In contrast to prism spectrographs, the dispersion of a diffraction grating increases with wavelength; and this ensures adequate dispersion even if a camera of large aperture is used. It is thus possible to construct a grating spectrograph for the red region, whose performance in dispersion and luminosity is equivalent to that achieved by a prism instrument in the blue. Such is the spectrograph constructed by Creighton (29) for use in conjunction with the helium source in this laboratory. It employs a plane echelette grating (Bausch and Lomb) blazed for 8000 Å. The camera is a Hilger E613 of aperture f/1.5. The spectrograph has a linear dispersion of 100 $cm^{-1}/mm.$ and a resolving power of 10^5. Greater dispersion could be achieved by using higher orders of the grating but only to the detriment of overall speed.

Optical filters

In any lamp spectrum the exciting line is usually accompanied by lines of shorter wavelength which may cause fluorescence, photochemical decomposition or give rise to Raman lines overlying the region of interest. The intensities of such lamp lines are reduced by an optical pre-filter annulus surrounding the sample tube. The following filter solutions were used in 1 cm. thickness,

He 5876 Å	Saturated aqueous	$K_2Cr_2O_7$
6678 Å	0.4M	Na_2PtBr_6 in 5M HBr

Low-lying Raman features can be observed with advantage if the intensity of the Rayleigh-scattered line is reduced; an optical post-filter with a sharp long-wavelength cut-off is required. Sharp absorption bands in the spectra of Nd^{3+} and Er^{3+} (30) coincide with the helium lines at 5876 Å and 6678 Å respectively. A saturated solution of erbium perchlorate in 1 cm. thickness is particularly suitable for removing He 6678 Å; by placing this solution in front of the spectrograph slit the quality of spectra is greatly improved. This is useful when long exposures are needed, as halation of the Rayleigh line on the photographic plate can obscure Raman features up to 200 $cm.^{-1}$ The neodymium

postfilter is less satisfactory since its absorption band in the region of 5876 Å is not so sharp as is the erbium for 6678 Å.

A Raman line at 100 cm^{-1} is transmitted to the extent of 70% while the 6678 Å exciting line is strongly absorbed by the erbium postfilter. For an analogous feature excited by 5876 Å, however, a quarter-saturated neodymium nitrate solution of 1 cm. thickness will transmit only 29% of the Raman line and 9% of the exciting line. For lines higher than 150 cm^{-1} the Nd^{3+} solution is satisfactory, but below 100 cm^{-1} its use is limited. Figure 2G illustrates the absorption characteristics of the filters discussed above.

Photographic plates

The photographic plates used in recording Raman spectra must have good reciprocity and should have as high a speed as possible consistent with fine grain. These requirements are adequately provided by the Kodak Oa series of special scientific plates of different colour sensitisings. In the present work the plates were Oa-F, sensitive out to 6850 Å, being very useful for 5876 Å, but of limited use only (out to 500 cm^{-1} shifts) for the 6678 Å helium line. V1034 plates are sensitive out to 8800 Å and are of use with 7065 Å

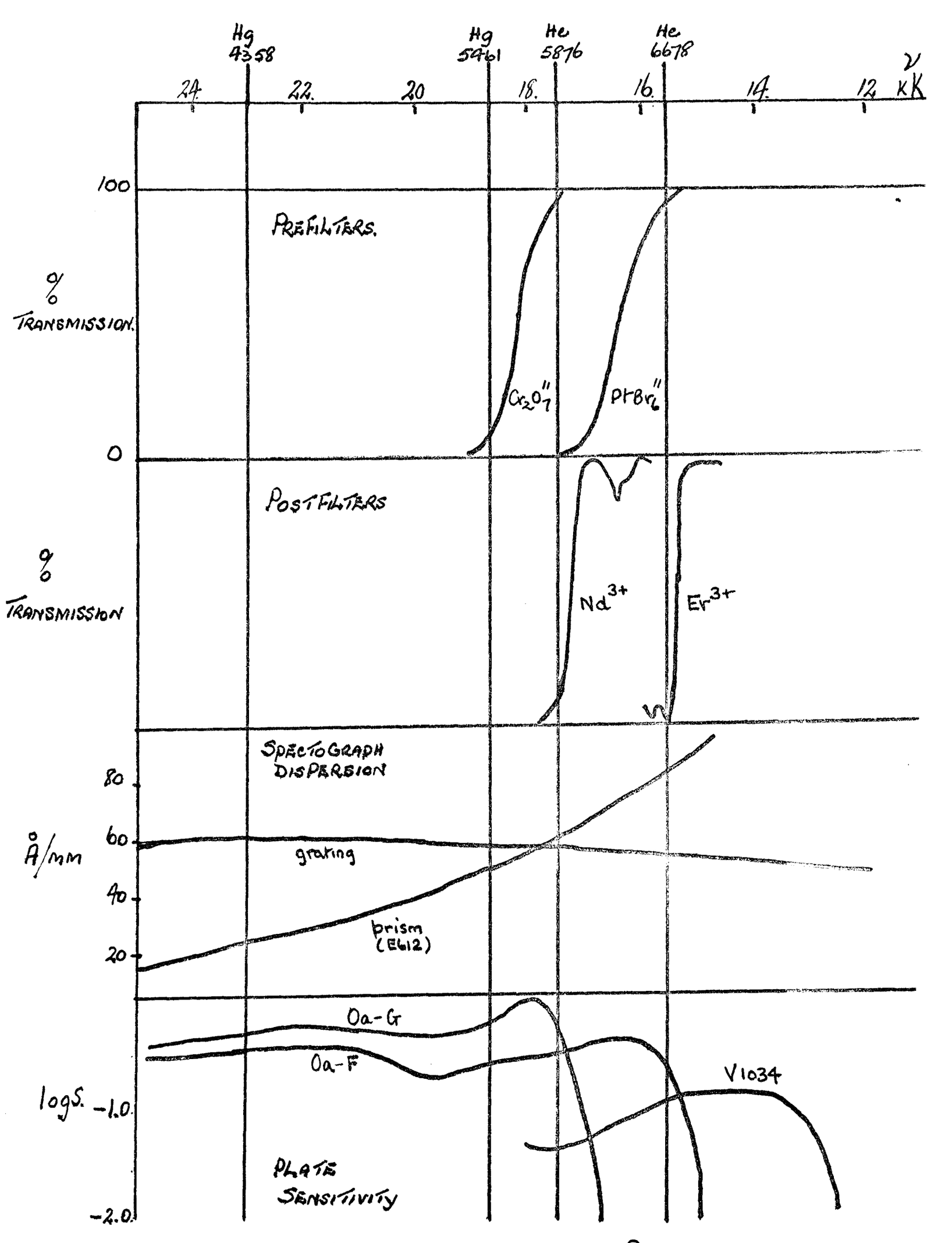


FIGURE 2 G. FILTERS AND PHOTOGRAPHIC PLATES IN THE RED.

excitation. A marked increase in the speed of the Oa-F plates is obtained by pre-exposure (1/50th sec. at f/4.5) to a tungsten lamp (29).

The plates are developed for 5 minutes at 20°c in Kodak D19b developer and fixed in an acid hypo bath containing chrome alum hardener. Loading and developing were performed in complete darkness.

Measurement of Raman frequencies

A preliminary series of exposures is taken under varying conditions of slit width and time. An over-exposed lamp spectrum is included so that any weak lamp lines or spectrograph 'ghosts' are identified. On each plate the emission spectrum of a suitable element is included for calibration purposes; arc spectra are chosen which have a large number of sharp well-characterised lines in the desired spectral region. A neon bulb is suitable for He 5876 Å, whereas Xenon is better for the 6678 Å region.

The grating spectrograph gives a dispersion on the plate that is nearly linear in wavelength and a Raman line may be measured with sufficient accuracy by linear interpolation between two bracketing calibration arc lines. Raman frequencies are accurate to $\pm$ 2 cm^{-1} for all except weak or diffuse features where the error may be $\pm$ 5 $cm.^{-1}$

Coloured samples

Even with a favourable choice of exciting line a given sample may absorb an appreciable proportion of the incident and scattered light. The scattered light flux is then no longer proportional to the concentration of scattering species. There is therefore an optimum concentration for observing the Raman spectrum. The problem has been considered theoretically and experimentally by Lippincott (31) and Creighton (29), whose modified equation is used in the present work. The optimum concentration, C_{opt}, is given by

$$C_{opt} = \frac{ct}{D'L} \log_{10} \left(1 + \frac{2D'L}{\pi DR}\right)$$

where C = concentration of test solution.

D,D' are the optical densities of a t cm. thickness of solution at the exciting and Raman wavelengths respectively.

R,L are the radius and length of sample in the Raman source.

By this means it is possible to determine the feasibility of an attempted Raman investigation. It is difficult to record Raman spectra at concentrations less than 0.1M, and Creighton showed that the Raman flux emitted

at the optimum concentration increases with the sample size; it is therefore better to work with larger, more dilute solutions when the limits of practicability are approached.

2(6) Modifications to the Helium Source

The premier modification facilitated the examination of cooled samples. This was necessary for the work, described later, on solutions of tetrakistrichlorophosphine-nickel in chloroform and benzene. Such solutions were thermally unstable at the normal operating temperature of the source, 30°C. The arrangement for cooling is shown in Figure 2H. Owing to the limitations on space within the glass annulus surrounded by the lamp helix, the annular jacket containing the filter solution was removed to accommodate the bulky Dewar jacket. A gelatin cylinder (Kodak Master Wratten filter) was now inserted in the Dewar jacket to act as pre-filter. The absorption characteristics of Wratten filters Nos.22 and 29 respectively match the filter solutions used for the 5876 and 6678 Å lines.

The Raman tube was held in position in the jacket by split corks. Cold nitrogen from a liquid-nitrogen boiler was passed through a lagged tube, over the sample, emerging finally from the space between the jacket and the glass

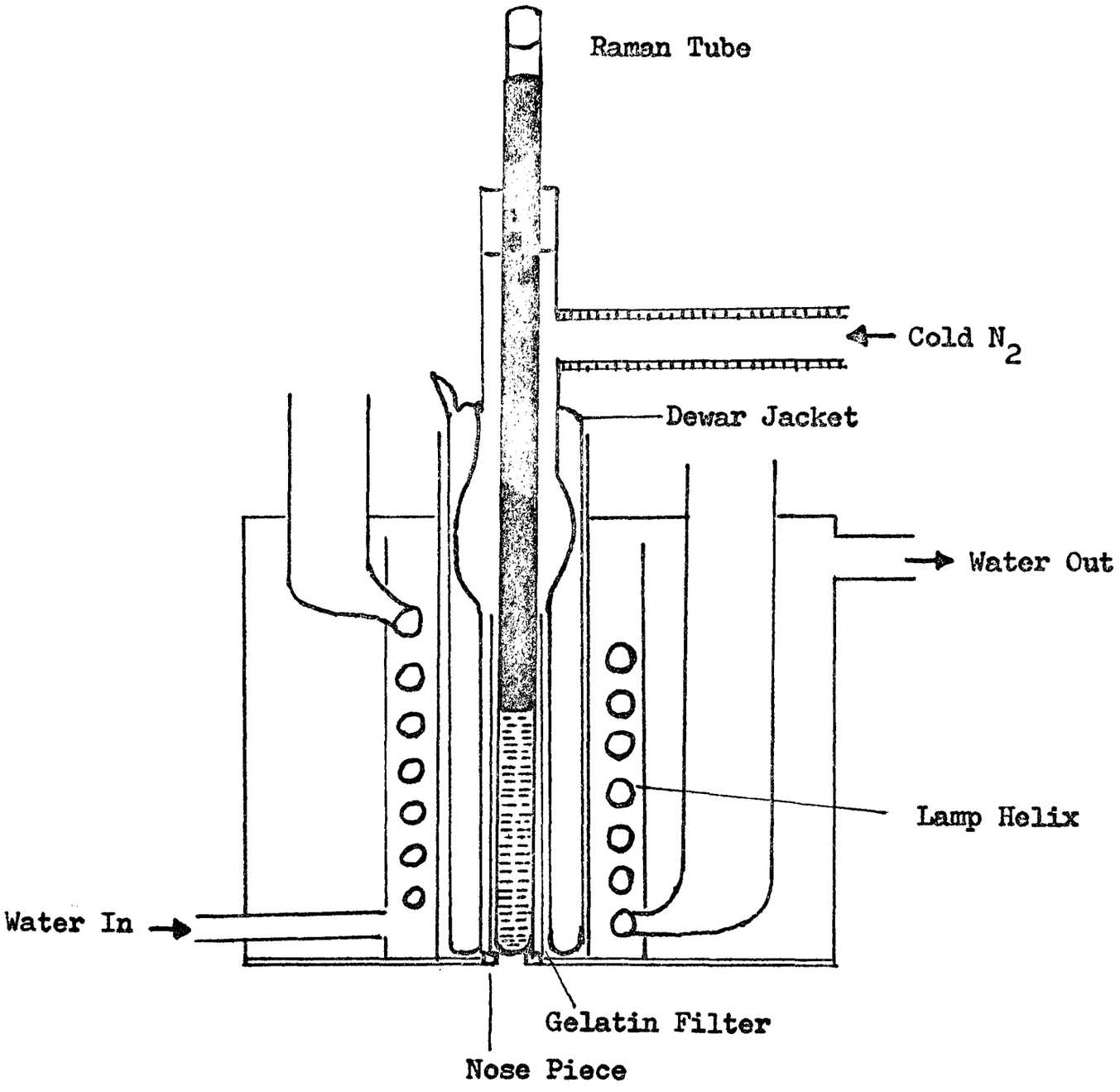


Figure 2H. Cooling Arrangement for Helium Source.

annulus of the lamp helix. To allow for the outlet of this nitrogen the Dewar jacket was positioned on a cork 'tripod'. The liquid nitrogen boiler is identical in design to that used in the cooling arrangement of the Cary 81 spectrometer in 2(3). Calibration and recording of the temperatures was effected in precisely the same fashion. The lowest temperature attained in practice was -60°C, for a solution of $Ni(PCl_3)_4$ in chloroform.

Another modification that was made to the helium source in course of the present investigations was the adjustment of the source optics to accommodate smaller samples. This is sometimes advantageous where only small quantities of a strongly scattering species are available. Smaller tubes of volume 5 ml. were used, the length of sample exposed to the lamp flux being kept the same as for the 15 ml. sample tube. The necessary adjustments were calculated from the Nielsen formulae; the slit height being decreased to allow the slit image to fall within the window of the Raman tube. Re-alignment to the Nielsen conditions then involves movement of the condensing lens along its optic axis until the image of the collimator was sharply focussed at the window of the Raman tube. Final adjustment was made to the mirror in the optical box to ensure that the cone of reflected light is vertical.

With such modifications and adjustments, the helium source is quite versatile. Liquids and solutions give good results when care is taken in their preparation to exclude dust and small particles which could give rise to Tyndall scattering. Primary scattering from solid surfaces is too great, however, and solid samples cannot be investigated with the helium source and grating spectrograph.

2(7) Laser-excited Raman spectra

The Raman spectra of some coloured transition-metal species were obtained on the Cary 81 Laser Spectrometer at Southampton University by M.J.Gall, Esq. This instrument uses a He/Ne gas laser of 50 mw power (80 mw when tuned); the exciting line being the 6328 Å Ne line.

2(8) Infra-red spectrometers

Two instruments were used to obtain spectra in the infra-red region. The Perkin-Elmer 225 grating infra-red spectrometer covered the region 5000-200 cm^{-1}, and the Beckman IR11 was used to investigate the 800-33 cm^{-1} region. A very large majority of stretching and deformation frequencies of the compounds under investigation fell into the latter region, so most of the infra-red work was accomplished on the IR11.

The IR11 employs a mercury lamp in a quartz envelope as a source of radiation. Energy fluctuations in the radiant source are eliminated in the final trace by using the instrument on 'double beam'. After passing through the sample, the radiation falls on a diamond-windowed Golay detector. To remove traces of atmospheric water vapour, which strongly absorbs in the far infra-red, the instrument and sample compartment are purged continuously with clean, dry air from a compressor. As the spectrometer scans from 33 cm^{-1} to 800 cm^{-1} the slit width is programmed to ensure that the energy falling on the detector per spectral slit-width is constant. The scanning region is served by four diffraction gratings and eight filters which are manually operated at the appropriate time. The high signal-to-noise ratio of the instrument is useful when recording weak absorption features, such as overtones, which were investigated in later chapters of this work.

2(9) Infra-red sample cells

Solids were investigated as mulls with an involatile oil, such as nujol and hexachlorobutadiene. The mull is pressed into a thin, uniform layer between polished alkali-halide or polythene plates in a copper cell-holder. The

plates are 32 mm. in diameter and were selected for various regions as follows:

4000-140 cm^{-1}. Caesium iodide, polished with rouge and methanol/water. Readily attacked by halide ions and water.

650-33 cm^{-1}. Polythene discs of $^{40}/_{1000}$ th inch thickness. Unreactive, but main disadvantage is a tendency to deform and distort under vacuum or in a hot sample compartment.

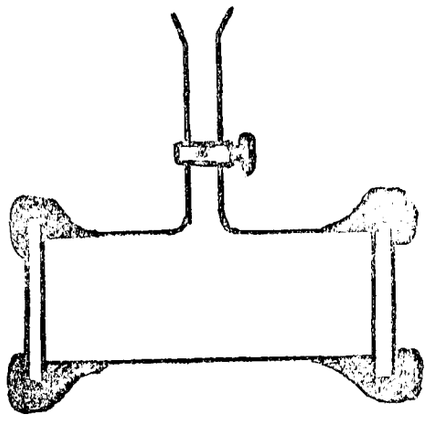
The 'overlap' region of these two window materials is a useful one.

Vapours were investigated using two gas cells that were specially constructed with polythene and caesium iodide windows, so that the region 5000-33 $cm.^{-1}$ was accessible to observation. The polythene windows were $^{1}/_{10}$ th inch in thickness to provide resistance to distortion when the cell is evacuated. The windows were sealed onto the glass flanges of the cell with molten black-wax, large quantities of which were used to provide a vacuum-tight seal. A cell was judged to be air-tight when it held 'black vacuum' for periods up to 48 hours. The polythene plates were slightly porous to air but the leak was negligible over a period of two days.

The testing, evacuation and sampling procedures for vapour infra-red cells are described later in the text.

The infra-red spectra of solids from compounds which are vapours at room temperature were obtained using a special cell. The window material was again either polythene or caesium iodide. The vapour concerned was sprayed onto another window cooled to -196°C by a supply of liquid nitrogen.

Both vapour and condensed-vapour infra-red cells are illustrated in Figure 2I.



Vapour Cell with CsI or Polythene Windows.

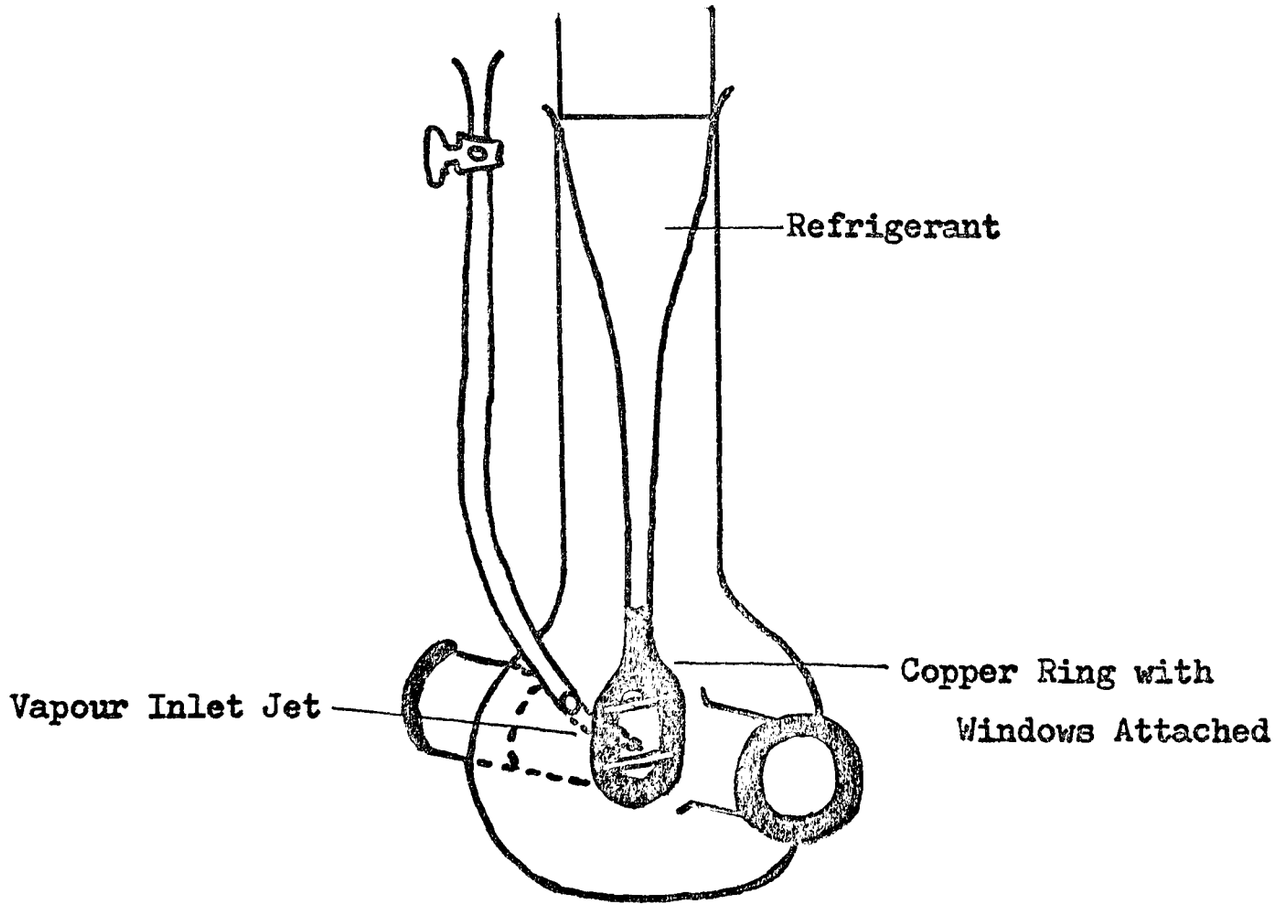


Figure 21. Infra-Red Cells.

CHAPTER 3

Chapter 3

PHOSPHORUS TRIFLUORIDE AND ZEROVALENT METAL-TRIFLUOROPHOSPHINES

3(1) General Introduction

For a long time the metal carbonyls occupied a special position in co-ordination chemistry by virtue of their stoichiometry and their chemical properties. Until 1951 the only compounds of metals in the zerovalent oxidation state were carbonyls. In that year, however, Wilkinson (32, 33) prepared tetrakistrichlorophosphinenickel and the analogous trifluorophosphine complex; these compounds contain nickel in the zerovalent state.

Tetrakistrichlorophosphinenickel was prepared as a yellow solid by the substitution of all the carbon monoxide in nickel carbonyl with phosphorus trichloride. The trifluorophosphine analogue was made by heating the $Ni(PCl_3)_4$ with PF_3 in a Carius tube at 100°C for 24 hours. The volatile product, $Ni(PF_3)_4$, is more stable than the tetracarbonyl.

It is, perhaps, necessary here to consider the meaning of 'stability'; a compound is said to be stable when it resists chemical change, which may consist of heat, hydrolysis, oxidation, reduction or any other process. A

useful criterion of the stability of a zerovalent metal compound is resistance to oxidation. Thermal stability is then a secondary consideration, and it is sometimes found that many complexes of metals in low-valent states are not very resistant to heat, but have a moderately good hydrolytic stability (e.g. metal carbonyls).

In the ensuing years, 1951-1964, there was much research into the substituted phosphines of nickel° using $Ni(CO)_4$ and $Ni(PCl_3)_4$ as starting materials. The preparation of $Ni(PBr_3)_4$ was achieved (33) but all attempts failed to extend the field to complexes of nickel with ligands other than phosphorus donors. Only partially substituted products of nickel carbonyl could be obtained, for example $Ni(CO)_3SbCl_3$ and the work by Bigorgne (34,35) on $Ni(CO)_3AsEt_3$. It was discovered that only in the case of phosphorus trichloride did the substitution reaction with nickel carbonyl go to completion, giving $Ni(PX_3)_4$. All other analogous reactions either did not go far enough, giving partially-substituted products, or gave extremely unstable, unisolable products. A good example of the former is provided by the reaction between nickel carbonyl and trimethylphosphine; all three substitution products up to $Ni(CO)(PMe_3)_3$ could be obtained (36,37) quite smoothly, but no inducement to the trisubstituted product would result

in the formation of $Ni(PMe_3)_4$. Unlike the antimony case, from the reaction between arsenic trichloride and nickel carbonyl no isolable product could be obtained apart from nickel metal, formed presumably by the decomposition of the very unstable partially-substituted carbonyls (42).

The complexes $Ni(CO)_x(PF_3)_{4-x}$, x being 0 → 4, are known, as are the PCl_3 analogues (though the latter are not so well characterised (38,39)). Similar complexes containing metals other than nickel have been made (34-37), notably molybdenum. More recently, the synthesis of new organo-halophosphines (40) has provided more ligands for reaction with nickel carbonyl, but only $\emptyset PCl_2$ reacts as does PCl_3 to give the fully-substituted product.

The main disadvantage of phosphorus trifluoride as a ligand seems to be its very low boiling-point (-100°C). The expansion of the preparative chemistry of metal-trifluorophosphine compounds was made possible only in 1964 by the development of a special high-pressure technique(41). By this means, the fully phosphinated compounds of many transition metals in the zeroth oxidation state have been obtained.

Spectroscopic work on these zerovalent metal-phosphines is sparse. Wilkinson gave no vibrational data for any of his compounds, whereas Bigorgne mainly studied the carbonyl

stretching region in some substituted nickel and molybdenum carbonyls (34-37). The first compound of zerovalent nickel, other than nickel carbonyl, to be studied spectroscopically was $Ni(PF_3)_4$, whose Raman spectrum was reported by Woodward(43) in 1958. Seel et al.(44) quote limited infra-red data for $Ni(PF_3)_4$ and fluoro-chlorophosphine complexes of nickel°. Kruck, who was responsible for the high-pressure techniques that gave impetus to the studies in this field, investigated only the phosphorus-fluorine stretching region in the infra-red (45,46).

In the present work an investigation of the vibrational spectra of the tetrakis-compounds $M(PF_3)_4$ was made, where M is nickel, palladium, platinum. Similar investigations were carried out on $Ni(PX_3)_4$ compounds, where X = chlorine, bromine. From a comparison of the vibrational spectra in such a series it is sometimes possible to make conclusions regarding the bonding in such molecules, and to consider the effects of substitution in $Ni(PX_3)_4$, where X = F, Cl, Br, on the nickel-phosphorus bond.

3(2) Bonding in metal-trifluorophosphine compounds

It was recognized that an important condition for the stability of complexes $M°L_n$ is the possibility of formation

of double bonds between the central transition metal atom M and the ligand L. That this ability should be confined to unsaturated carbon compounds seems unlikely, as is shown by the existence of nitrosyl complexes and of carbonyl complexes containing organo-substituted or chloro-substituted ligands of trivalent phosphorus. A neutral inorganic molecule would have to satisfy the following further requirements if stabilisation of the zerovalent state of transition metals is to be achieved:

(a) The molecule L must possess a lone pair in order to form a co-ordinate L $\rightarrow$ M sigma, σ, bond, i.e. a donor function.

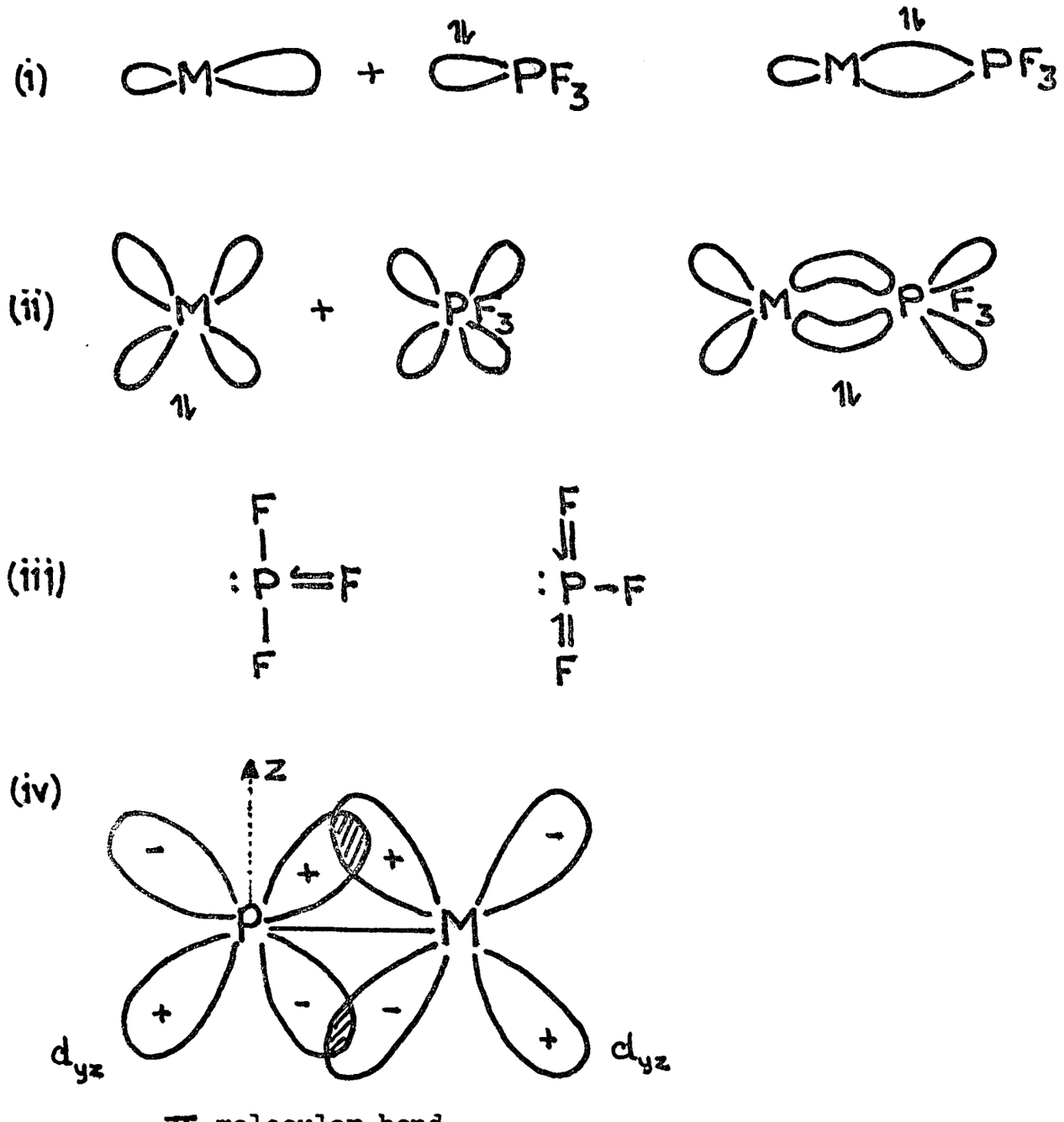
(b) The molecule must also have available unoccupied π-orbitals of suitable energy and symmetry to accept the electronic back-donation (M $\leftrightarrow$ L) which relieves the metal of the negative charge placed on it by the σ-bond, i.e. an acceptor function.

(c) Its steric structure must favour the establishment of a Coordination number, n, that satisfies the 'inert gas rule'.

It seems, then, that the simultaneous donor and acceptor properties of a ligand could affect its ability

to form complexes. The extreme of pure donor ability, exemplified by amines NR_3, has been extensively studied; such ligands stabilise medium, positive oxidation states. The other extreme, that of pure acceptor ability, has not been studied, but carbon monoxide, whose donor and acceptor properties are almost equal, forms complexes with transition metals in the zerovalent and negative oxidation states.

Trivalent phosphorus is an electronegative carrier of a lone pair of electrons and also has acceptor properties in the form of vacant 3d orbitals. The introduction of fluorine atoms onto the phosphorus atom modifies the situation slightly, enhancing the acceptor properties of the 3d orbitals but weakening the donor ability of the phosphorus. In the coordinate bonding of phosphorus trifluoride to a transition metal atom therefore, the doubly occupied sp^3 orbital of the phosphorus and the 3d π orbitals are of decisive importance. Overlap of the doubly occupied sp^3 orbital of the phosphorus with suitably directed free hybrid orbitals of the metal leads initially to a weak donor σ-bond, Figure 3A(i). Such donor function of PF_3 is manifest (47) in the adduct $F_3P\text{-}BH_3$ (cf.$OC\text{-}BH_3$). In boron trifluoride, however, the electrophilic action of



π-molecular bond

Figure 3 A. PF_3 as Donor and Acceptor.

the p_z orbital of boron is no longer sufficient for the co-ordinate bonding of the very weak Lewis base PF_3, although bonding is effected with the stronger donor PCl_3 to give a rather unstable adduct.

The high electronegativity of the fluorine atoms in PF_3 strengthens the acceptor function of the phosphorus atom by lowering the energy of the 3d orbitals of the phosphorus (Figure 3A(ii)). The overall result would be a synergic effect, but the situation is rendered more complex by the double-bond character of the PF_3 itself. The superposition of a π-bond on the P-F σ-bond results from the overlap of occupied 2p orbitals of fluorine with the 3d orbitals of the phosphorus, so that limiting structures such as those shown in Figure 3A(iii) make a contribution to the bonding in PF_3. Chemical evidence for the importance of such bonding in phosphorus trifluoride is provided by the stability towards hydrolysis in comparison with the other phosphorus trihalides.

Thus, when PF_3 is linked to a metal in the zeroth oxidation state the donor σ-bond leads to a decrease in electron density on the phosphorus which necessarily leads to an increase in the π-bond order of the P-F bonds. This effect must be weak since it is distributed over

the three P-F bonds and is opposed by the simultaneous metal-phosphorus back-donation. A formal negative charge on the metal, such as would be provided by the introduction of another donor D, would be absorbed by the metal-phosphorus π-bond with an increase in the electron density on the phosphorus and a resulting decrease in the π-componeht of the P-F bonds. A π-type molecular bond, formed by the overlap of d_{yz} orbitals on the metal and phosphorus atoms is illustrated in Figure 3(iv). The stability conferred on a molecule by such π-type molecular bonding is well illustrated in the comparison of PF_3 and NF_3, the latter having no d-orbitals with which the π-bond may be formed (48).

Support for the above discussion on bonding is givenby Kruck (49), Chatt (48,50) and Booth (51), but Venanzi (52,53) holds the opinion that π-bonding is of little importance in square-planar complexes of divalent transition metals, although it may well be important in the stabilisation of the zeroth state. The very existence of the tetrakistrifluorophosphine metal° compounds also refutes the view of Nyholm (54), that ligands which rely on strong π back-donation are less suitable for the stabilisation of the zeroth oxidation state of a metal than negatively-charged ions such as acetylide or cyanide.

3(3) Spectroscopic activity of $M(PF_3)_4$ vibrations

By group theoretical methods which utilise the character tables it is possible to deduce the activity of the vibrational modes of $M(PF_3)_4$ in the infra-red and in the Raman spectrum. The procedure has been illustrated for a simple XY_4 molecule in Chapter 1. In the $M(PF_3)_4$ model various arrangements of the PF_3 groups around the central atom M are possible, including a square planar structure for the MP_4 skeleton, which approximates to D_{4h} symmetry for freely-rotating PF_3 groups. A likely structure for $M(PF_3)_4$ is shown in Figure 3B, in which the configuration of the PF_3 groups is important for the possession of all symmetry elements of the T_d point group. Woodward and Hall(43) investigated the Raman spectrum of $Ni(PF_3)_4$, the only compound of this type to be studied in this way, and their results imply that the molecule obeys the selection rules of the T_d point group. A later infra-red study by Seel (44) confirms the conclusions of Woodward and Hall of tetrahedral symmetry for the molecule.

The spectroscopic activity of the vibrational modes for the $M(PF_3)_4$ molecule of the T_d symmetry is deduced in Table 3A. There will be fourteen Raman-active modes (three polarised), of which seven will occur in the infra-red. The A_2 and F_1 species are inactive in both the Raman and the infra-red.

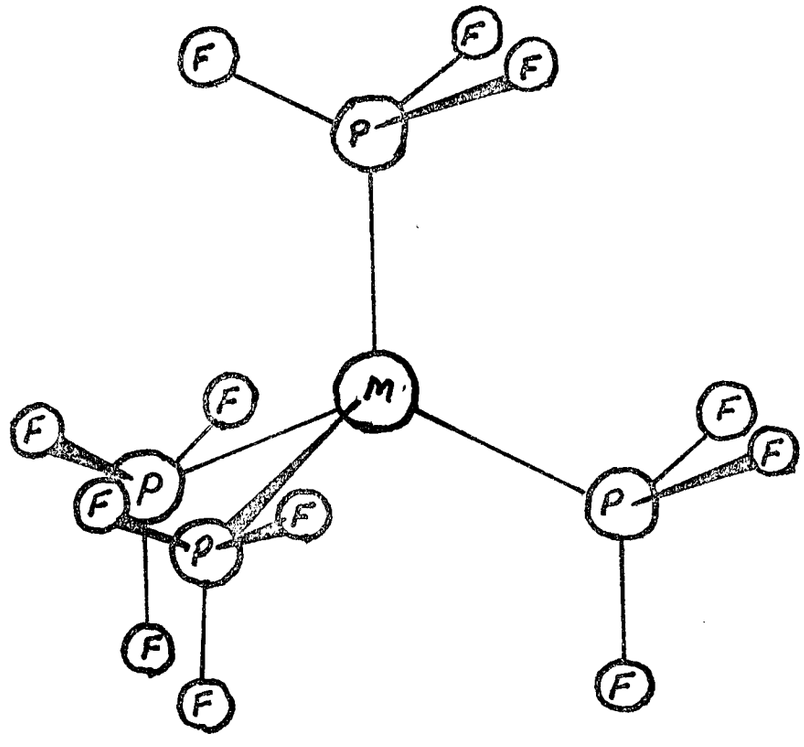


Figure 3B. T_d Configuration of $M(PF_3)_4$.

TABLE 3A

Spectroscopic Activity of $M(PF_3)_4$ vibrations

Symmetry operations	E	C_3	C_2	S_4	σ_d
Unshifted atoms	17	2	1	1	5
χ_j^{atom}	3	0	-1	-1	1
χ_j	51	0	-1	-1	5
g_j	1	8	3	6	6

Species	n	T	R	Number of vibrations
A_1	3			3
A_2	1			1
E	4			4
F_1	5		1	4
F_2	8	1		7

$$\Gamma = 3A_1 + 1A_2 + 4E + 4F_1 + 7F_2$$

Raman active	✓		✓	✓
Infra-red active				✓

Coincidences: 7

Polarised in Raman: 3

Infra-red spectra frequently contain features attributable to overtones and combination bands of the fundamental vibrations. The overtones and combinations are also subject to symmetry selection rules, and their activity in the infra-red will occur only if the symmetry species of the combination band contains the necessary infra-red active elements. In the case of a binary combination band the symmetry species is not necessarily that of the fundamentals of which it is composed. Multiple excitation of a single, degenerate vibration results in overtones, the symmetry species of which are not easily calculated, although simplification results from the use of tables compiled by Tisza (55). Application of the methods of Herzberg (5) yields Table 3B. Here the rows and columns signify vibrations of the symmetry species indicated; the overtones and combinations will be active in the infra-red only if they contain the F_2 species in their overall symmetry class. Active binary combinations are ringed thus $\square$. Ternary combinations, such as the combination $(2\nu_3 + \nu_4)$, may be analysed in a like manner, and in this table activity in the infra-red is indicated by a ✓.

Mere possession of the correct overall symmetry species for activity of the overtone or combination does not imply

TABLE 3B

Symmetry species of overtones and combinations

Binary combinations

	A_1	A_2	E	F_1	F_2
A_1	A_1	A_2	E	F_1	$\boxed{F_2}$
A_2		A_1	E	$\boxed{F_2}$	F_1
E			$A_1 + E$	$\boxed{F_1 + F_2}$	$\boxed{F_1 + F_2}$
F_1				$\boxed{A_1 + E + F_2}$	$\boxed{A_2 + E + F_1 + F_2}$
F_2					$\boxed{A_1 + E + F_2}$

Ternary combinations

	A_1	$(A_1)^2$	A_2	$(A_2)^2$	E	$(E)^2$	F_1	$(F_1)^2$	F_2	$(F_2)^2$
A_1								✓	✓	✓
$(A_1)^2$								✓	✓	✓
A_2							✓	✓		
$(A_2)^2$								✓	✓	✓
E							✓	✓	✓	✓
$(E)^2$							✓	✓	✓	✓
F_1							✓	✓	✓	✓
$(F_1)^2$								✓	✓	✓
F_2									✓	✓
$(F_2)^2$										✓

that such an activity is actually observable. Overtones and combinations are much weaker than the corresponding fundamentals; in addition, a combination band can be a 'sum' tone or a 'difference' tone, the latter being so much weaker in intensity relative to the former that they are never observed unless the corresponding 'sum' tone is also manifest.

3(4) Vibrational assignment of phosphorus trifluoride

An assignment of the vibrational modes of the $M(PF_3)_4$ molecule is assisted by reference to the free ligand PF_3. The vibrational spectrum of PF_3 has been reported by various authors. The only Raman work is that of Yost and Anderson (56) in 1934, when spectra, without polarisation data, were obtained in the gaseous and liquid states. For C_{3v} symmetry in PF_3, group theory predicts four fundamental vibrations, all active and coincident in the Raman and infra-red:

$$\Gamma = 2A_1 + 2E$$

The infra-red spectrum of PF_3 has been observed by Gutowsky (57) and by Wilson and Polo (58); there is disagreement between these workers in the assignment of the two deformation frequencies (a_1 and e). The conflicting

evidence is presented in Table 3C, and it is seen that there is a discrepancy not only in the assignments, but also in the frequency-values.

The failure of Gutowsky to observe the feature at 344 cm^{-1} reported by Wilson and Polo may be attributed to the KBr-optics of the instrument used by the former, since this limits the observation of bands in the infra-red above 400 cm^{-1} only. Gutowsky does, however, agree with the Raman evidence of Yost in reporting a feature at 532 cm^{-1} which is absent in the Wilson spectrum. The published spectra of both Gutowsky and Wilson show band contours, and Gutowsky attempted to use the additional information that can be given by band contour analysis to assign the deformations. The 532 cm^{-1} feature is reported as a perpendicular band, and the 487 cm^{-1} feature a parallel band. An inspection of the spectrum confirms the prominent Q branch in the 487 cm^{-1} feature, but the 532 cm^{-1} band is less easily described as it occurs as a weaker shoulder on the R branch of the strong 487 cm^{-1} feature.

Wilson's spectrum indicates clearly the Q branch in the 487 cm^{-1} band, but also reveals an equally prominent Q feature in the 344 cm^{-1} band envelope. That both of these

TABLE 3C

Assignment of PF_3 vibrations

Vibration	IR/R	State	ν_{P-F}	ν_{P-F}	δ_{PF_3}	δ_{PF_3}
Species			a_1	e	a_1	e
Yost, Anderson	R	Liquid	890	840	531	486
	R	Gas	893	851	-	486
Gutowsky, Liehr	IR	Gas	892	848	532	487
Wilson, Polo	IR	Gas	892	860	487	344
*Present work	IR	Gas	892	860	485	344

bands exhibit prominent Q branches, and the general similarity of the spectrum to CHF_3, is in agreement with the behaviour of symmetric top molecules. Band contour analysis was of some assistance in the assignment of the stretching vibrations. For the deformations, however, it is useful to consider the work of Meal and Polo (59) on vibration-rotation interaction in polyatomic molecules. Briefly, it was shown that Coriolis coupling in a symmetric top molecule would confer a P, Q, R type structure on the asymmetric vibrations in a molecule such as PF_3.

This may be a reasonable explanation of the prominent Q branch in the 344 cm^{-1} band envelope in the infra-red spectrum of PF_3 reported by Wilson and Polo. However, the assignment problem is still not solved, since whereas Gutowsky agrees with Yost, Wilson does not. It thus became necessary in this present work to repeat the infra-red work and to confirm either Wilson or Gutowsky.

3(5) The Infra-red spectrum of PF_3

In this investigation the infra-red vapour sampling apparatus described in the next Chapter was used. Phosphorus trifluoride, a commercial sample, was purified in a vacuum line (as described in Chapter 4) and was admitted to a

caesium iodide-windowed infra-red cell to a pressure of 7.5 cms Hg. The infra-red spectrum was obtained on a Perkin-Elmer 225 operating on double-beam, an evacuated cell being inserted into the reference beam to compensate for water absorption in the purged sample compartment. The deformation region of interest is illustrated in Figure 3C. Immediately apparent from the spectrum are

(a) the absence of any feature at 532 cm^{-1},

(b) the presence of the band with a prominent Q branch at 344 cm^{-1}.

The observed spectrum obtained in the present work is exactly similar to that of Wilson and Polo, and is appended to Table 3C. This result makes the Raman data of Yost and Anderson even more perplexing. A possible explanation of the 'absence' of the lower deformation in Yost's spectrum could be high background-scattering; bearing in mind the early year and instrumentation, and the difficulty of holding PF_3 in the liquid state.

The 532 cm^{-1} feature reported by Gutowsky, absent in this present work and from Wilson's spectrum, must surely be spurious. It is interesting that both Yost and Gutowsky prepared their PF_3 samples from the reaction of arsenic trifluoride with phosphorus trichloride. The P-Cl stretching

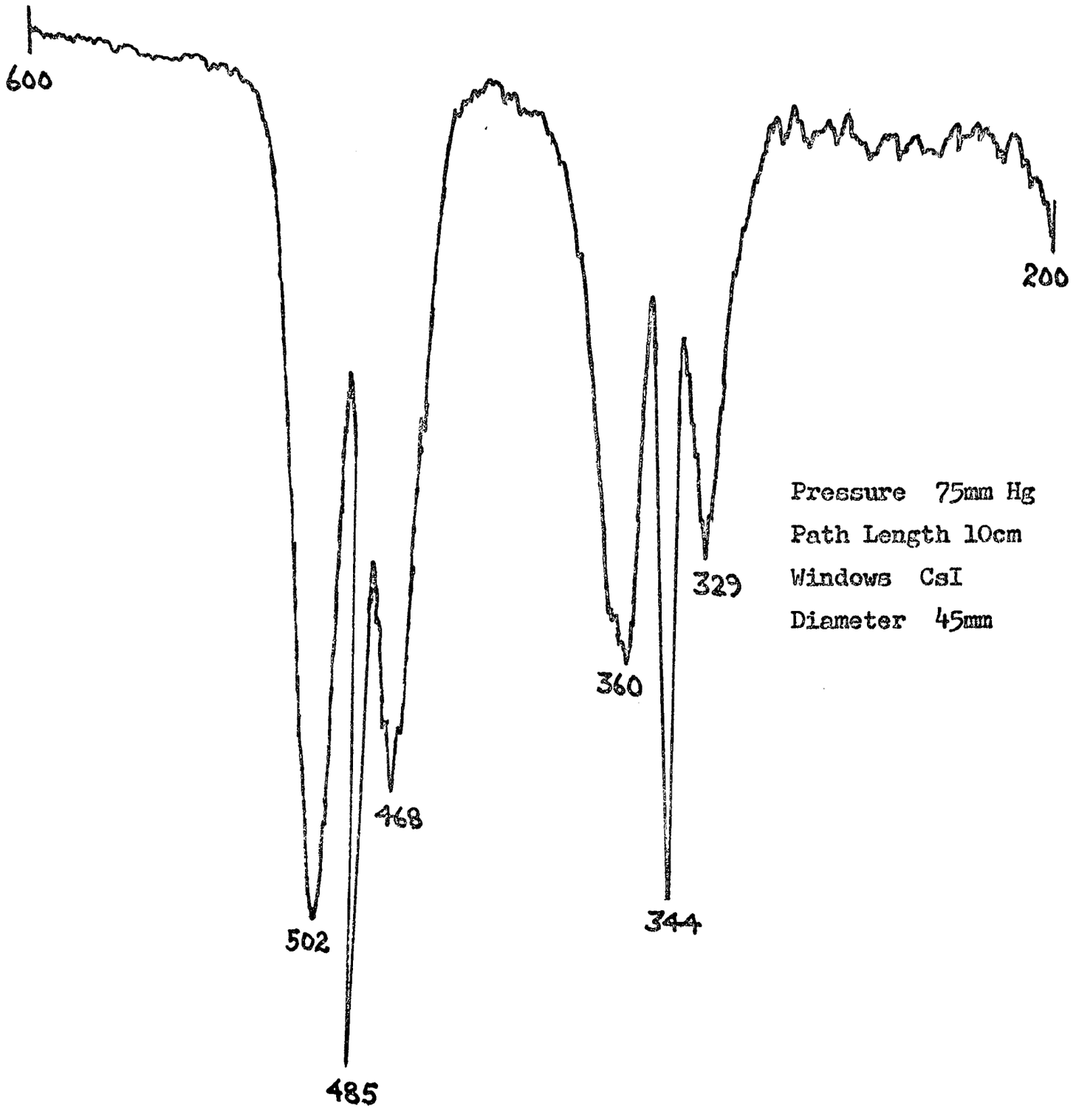


Figure 3C. Deformation Region in the Infra-Red Spectrum of PF_3. (Present Work).

frequency in PCl_3 is at 511 cm^{-1}, but could well be in the region of 530 cm^{-1} for a fluorochlorophosphine of the type PCl_xF_{3-x}, where x is 1 or 2. Also, a P-F deformation in PF_5 occurs at 534 cm^{-1}. Wilson states that he especially purified the PF_3 used in his investigation, and in the present work the PF_3 was carefully purified on a vacuum line from a commercial supply made by reacting zinc fluoride with phosphorus trichloride. It is suggested therefore that the samples of both Yost and Gutowsky were contaminated with a compound of type PCl_xF_{3-x}, which would be fairly volatile, and that the 532 cm^{-1} band reported by these authors is the ν_{P-Cl} stretching frequency of this compound. Wilson suggests that the 531 cm^{-1} band of Yost and Gutowsky could be the (890 - 344)cm^{-1} difference tone, i.e. $(\nu_1 - \nu_4) = 546\ cm^{-1}$. The combination band $(\nu_1 + \nu_4)$ was assigned to a weak feature at 1238 cm^{-1}, which was very close to the calculated combination of 1236 cm^{-1}.

It is relevant here to note that Delwaulle (60) has obtained the Raman spectrum of trifluorophosphine oxide, PoF_3. Two depolarised features at 476 and 387 cm^{-1} are quoted, and these would admirably fit the two PF_3 deformations in frequency-value, although one should be polarised.

Delwaulle assigned the 387 cm^{-1} band to a PF_3 rocking mode, and 476 cm^{-1} to a deformation (the other deformation, it was assumed, being unobservable). Delwaulle's assignment must be regarded as anomalous if one accepts the Wilson data for PF_3 and the findings of the present work, since the PF_3 rocking mode is then assigned <u>higher</u> in frequency than the corresponding deformation.

In the next Chapter, recourse will again be made to these findings when the Woodward-Hall assignment for $Ni(PF_3)_4$, for which the Gutowsky PF_3 assignment was used at that time, and the partial infra-red assignment of Seel will be discussed.

CHAPTER 4

Chapter 4

TETRAKISTRIFLUOROPHOSPHINENICKEL°

4(1) The preparation of metal-trifluorophosphines

Tetrakistrifluorophosphinenickel was first prepared by Wilkinson (33) using the method of halogen exchange on the chloro-analogue (32),

$$Ni(PCl_3)_4 \xrightarrow[SbF_3/SbCl_5]{} Ni(PF_3)_4$$

The perfluorination of the chloro-compound has also been achieved (44) with potassium fluorosulphinate, KSO_2F. As general methods of preparation of metal trifluorophosphines, however, these syntheses are of limited application only since the PCl_3 analogues of other metals are not known.

A more general method of preparation was hence sought; Chatt (61) and Wilkinson (33) investigated the reaction of metal powders with PF_3 under various conditions of temperature and pressure. This is a standard procedure in the analogous field of carbonyl synthesis but all attempts at extending it to the trifluorophosphines failed. It is only very recently that Kruck (45) reported the successful synthesis of $Ni(PF_3)_4$ by this method; the criterion was in preparation of a very finely-divided form of nickel (from the

thermal decomposition of nickel oxalate), and under fairly mild conditions (100°C, 70 atmospheres of PF_3) the reaction proceeds smoothly. This, however, is the only example of the direct synthesis of a metal-trifluorophosphine known.

A method of wider application involves the displacement reactions of suitably coordinated complexes (46). The method uses ligand exchange under high pressures of PF_3 and was first demonstrated (62) by the synthesis of $M(PF_3)_6$ compounds, M = Cr, Mo:

$$M(C_6H_6)_2 + 6PF_3 \xrightarrow[200\ at.]{100\text{-}200°C} M(PF_3)_6 + 2C_6H_6$$

The synthesis of $Ni(PF_3)_4$ by this means was successful when $Ni(PCl_3)_4$ or $Ni(CO)_4$ were used as starting materials:

$$NiL_4 + 4PF_3 \xrightarrow{80\text{-}300\ at.} Ni(PF_3)_4 + 4L$$

Wilkinson was successful earlier (32) in reacting $Ni(PCl_3)_4$ with PF_3 in a Carius tube, obtaining $Ni(PF_3)_4$. Chatt (61), however, found only di- and tri-substituted nickel carbonyls produced by the reaction of PF_3 with nickel carbonyl. Clark and Brimm (63) used elevated temperatures and improved the yields reported by Wilkinson; in a reaction with nickel carbonyl, a 90% yield of $Ni(PF_3)_4$ was obtained, under a

PF_3-pressure of only twenty atmospheres. Kruck (46,62) used rather higher pressures in his successful preparations.

Nixon (64) and Kruck (65) realised that organometallic compounds of nickel in the zeroth oxidation state may be induced to react with phosphorus trifluoride under pressure. Both workers used nickelocene as a reactant, and very smooth cleavage in high yield, producing $Ni(PF_3)_4$, was reported under mild conditions. A disadvantage of this otherwise very neat reaction is the rather lengthy synthesis and purification of the starting material (66).

It seems that nickel carbonyl is unique in reacting completely with PF_3 to form the completely-substituted product. Other metal carbonyls do not react analogously under PF_3-pressure alone. Clark *et al.* (67,68) report that the UV-irradiation of the products $Fe(CO)_{5-x}(PF_3)_x$ of reaction between PF_3 and $Fe(CO)_5$ in the presence of PF_3 does, in fact, result in complete substitution of carbonyl, producing $Fe(PF_3)_5$. Kruck, in an excellent review (49), is of the opinion that this could well be of general synthetic application.

The most important method of synthesis of the trifluorophosphine-metals has been devised and exploited by Kruck, is widely applicable and is extremely simple in

choice of starting materials. The method involves the 'reductive fluorophosphination' of metal salts and is a high-pressure method (41). The anhydrous metal halide is reduced in an autoclave by a halogen-accepting metal (generally copper or zinc), and simultaneously under high pressures of the phosphine the addition of PF_3 to the liberated metal takes place. The temperature and pressure required for reaction depend on the metal but generally are 100-150°C and 100-300 atmospheres. In some cases a secondary metal is not essential since PF_3 itself can act as a halogen-acceptor. Other reactants, such as hydrogen, may be incorporated to give the trifluorophosphine metal hydrides.

This is the only general synthetic method and forms the basis of the synthesis of the $M(PF_3)_4$ compounds in the present work.

4(2) The Vacuum Line

The experimental procedure used in this work for the preparation of $M(PF_3)_4$ compounds, where M = Ni, Pd, Pt, is essentially similar for all. The vacuum line illustrated in Figure 4A was developed to this final state after preliminary experiments and manipulations with $Ni(PF_3)_4$, which was selected, on ecenomic grounds, as a suitable

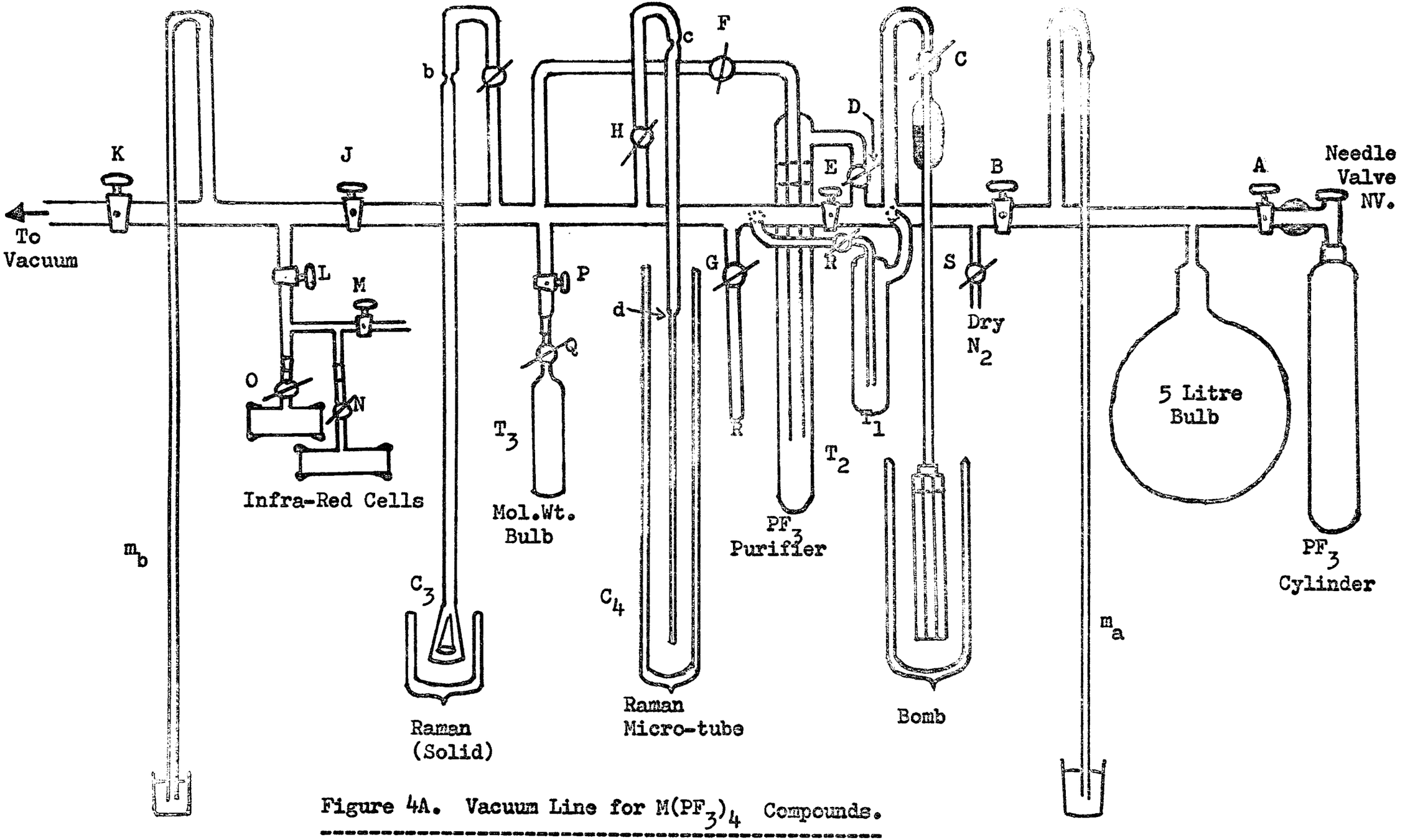


Figure 4A. Vacuum Line for $M(PF_3)_4$ Compounds.

compound for test runs before the platinum compound was investigated.

The purpose of the vacuum line is to enable the requisite charge of PF_3 to be placed in the bomb, and to facilitate the handling of the trifluorophosphine-metal that has been formed in the reaction. The metal-trifluorophosphines of nickel, palladium and platinum have all been reported by Kruck(49,69-71), and are volatile liquids which, although water stable, are sensitive to oxygen and temperature. In the apparatus shown in Figure 4A the crude metal-trifluorophosphine is extracted from the bomb, purified by trap-to-trap distillation, and stored as a solid at -196°C to minimise thermal decomposition. The remainder of the vacuum line consists of sampling apparatus whereby the infra-red and Raman spectra, molecular weight, and analytical samples could be obtained.

4(3) The Purification of the PF_3

Phosphorus trifluoride is a gas (m.pt. -152°C, b.pt. -102°C) which is slowly hydrolysed by water. The preparation of PF_3 can be effected by fluorinating PCl_3; Kruck (49) and Clark (67) favoured anhydrous zinc fluoride as a mild fluorinating agent, whereas earlier workers (56)

used arsenic trifluoride. In the present work the PF_3 was obtained commercially from the "K and K" Company, New York, being stored in a steel cylinder under pressure (this pressure was not stated, but from the cylinder volume and the weight of PF_3 therein, the pressure was estimated as 40 atmospheres).

The vacuum line was evacuated up to the needle valve NV using a good rotary pump and a mercury diffusion pump. The apparatus was tested for pinholes and leaks using a Tesla high-frequency induction coil; a potential of 88,000 volts is applied to the 'evacuated' apparatus and any residual air or gas becomes ionised and glows - the colour and intensity of the glow discharge is dependent on the gas pressure in the system. For example, water and mercury vapours have sky-blue discharges, air is pink-purple, whereas the metal-trifluorophosphines have a brilliant orange glow discharge. Thus, the Tesla coil may also give an indication of the sort of gas in the apparatus.

It should be possible with the rotary-diffusion pump combination to reach pressures of 10^{-6} mm. Hg or less, the time taken to reach this low pressure is dependent on the bore of the tubing and the total volume of the vacuum line. In this vacuum line 9 mm. tubing (Pyrex) was used for the

main line and 3-7 mm. tubing for the attachments. All taps were high-vacuum taps of 4 mm. bore and were lubricated with general purpose Apiezon 'L'. Initially, it was thought that the phosphine might attack this hydrocarbon grease, so a fluorocarbon lubricant (Fluorube A, I.C.I.) was used. PF_3, however, does not attack the Apiezon grease over the duration of the experiments, and this made unnecessary the use of the rather unpleasant Fluorube.

With all taps open the line is evacuated, and during this process 'degassing' of the glass surfaces will occur. Continuous pumping and warming of the glass is performed to assist this de-gassing process, until the apparatus can hold a good vacuum over long periods. At pressures lower than 10^{-6} mm. Hg the Tesla coil will not induce a discharge, and the state known as "black vacuum" has been reached. This is the condition or "hardness" of vacuum that is desired in practice. Having evacuated the system, tap B was closed and needle valve NV was opened to admit PF_3 into the 5-litre bulb. The pressure of PF_3 in the bulb was registered by the fall of mercury manometer m_a. The volume of the bulb and system between taps A and B was previously determined as 5.6 litres; application of Avogadro's Law then gives 0.3 gm.PF_3

equivalent to a 1 cm. pressure in the bulb, which makes it possible to calculate the weights of phosphine being transferred in operations on the vacuum line.

The needle valve NV was then closed and small trap T_1 cooled in liquid nitrogen. On closing J and opening B the PF_3 should rapidly condense in T_1 as a white solid. It was found, however, that this condensation process was only partially successful and some 5 cms. pressure only of PF_3 would condense in T_1. There was obviously some defect which prevented the condensation of phosphine in T_1, and it was realised, after trial-and-error, that any incondensible impurity in the PF_3 would form a vapour lock in the liquid nitrogen trap and prevent the condensation of phosphine beyond a certain limit. To test this hypothesis, the large trap T_2 was incorporated into the system and a known pressure of PF_3 was held in the bulb. By closing taps R, E and F, and opening D and B, the phosphorus trifluoride is condensed in T_2, the process stopping when 12 cm. pressure still remained in the bulb. B was then closed and evacuation of the cooled T_2 commenced. A purple discharge was obtained on applying a Tesla coil to the trap, indicating the presence of an incondensible gas. The procedure was repeated until all the PF_3 in B had been condensed in T_2.

Trap T_2 was then immersed in an acetone-CO_2 bath at -78°C and the PF_3 allowed to volatilise into the bulb. From the difference between initial and final PF_3-pressures, i.e. 'crude' and purified PF_3 pressures, the amount of the incondensible impurity was found to be 12%.

The impurity, it is thought, could well have been nitrogen gas (which is not condensed by liquid nitrogen traps), and its presence in the commercial PF_3 would be accounted for if, in the preparation of the PF_3, a stream of dry nitrogen was used to keep an inert atmosphere and to sweep the phosphine into a storage receiver. It was then verified that the purified PF_3 could be distilled and condensed in any quantity easily in any part of the apparatus.

4(4) The Bomb

Kruck and Prasch (41), in the development of their high-pressure technique, used an electrically-heated rotary autoclave for the synthesis of metal-trifluorophosphines. Such an autoclave was not available in the Oxford Laboratory, so the following arrangement was adopted. The bomb is hexagonal and had been machined from a single lump of stainless steel. The capacity of the bomb is 16 ml. A hexagonal head screws into the main body of the bomb, a

pressure-tight and vacuum-tight seal being effected by the use of a pliable copper gasket; a circular ridge on the bomb head forces the gasket into a runnel of similar dimensions in the body.

A similar device for the attachment of the bomb to the vacuum line is shown in Figure 4B. Connecting the bomb body to the vacuum line was a piece of copper tubing welded at one end to a heavy brass hexagonal head drilled to a bore of 3 mm. The other end of the copper tube was gripped in polythene, so providing a flexible copper-to-glass seal (which was black-waxed for protection). This flexible seal was necessary to eliminate any strain that was set up in the copper connections in the process of attaching the bomb to, or removing from, the vacuum line. The attachment of the bomb to the hexagonal head was accomplished using two heavy wrenches working in opposite directions to minimise torsional strain.

After attachment of the bomb to the vacuum line had been made, experiments were performed to test the behaviour of the joints under vacuum and under the experimental conditions. The high-pressure limit of the bomb was said to be 400 atmospheres, but it was deemed wise to test the bomb in a pilot run, using the sort of pressures that were

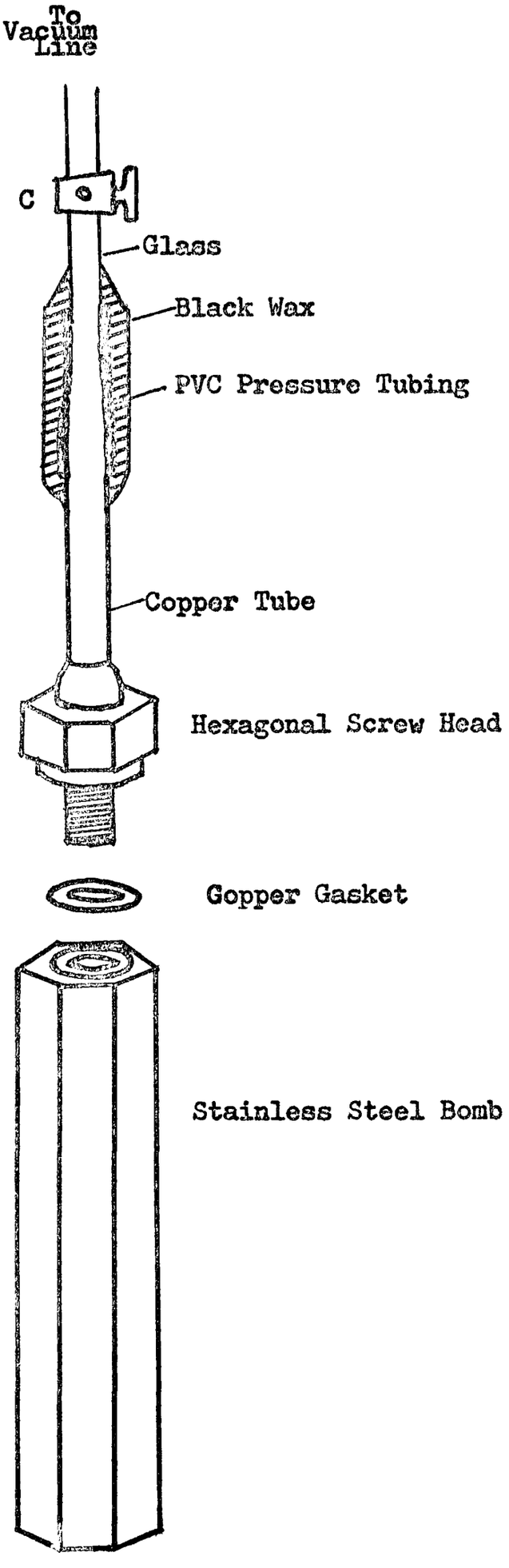


Figure 4B. Bomb Attachment to Vacuum Line.

to be encountered in the subsequent experiments. After evacuation, purified PF_3 was condensed in the bomb cooled in liquid nitrogen. During this process care was taken to keep the bomb-head joint warm to avoid condensation of PF_3 in the narrow bore of the head, and consequent blockage of the system. Two hot-air blowers were directed onto this joint, maintaining this part of the apparatus at $\sim$0°C, whilst the rest of the bomb was at -196°C. The requisite charge of PF_3, which would give a pressure of 200 atmospheres in the bomb at 100°C (amounting to some 10 gm. PF_3), was then condensed in the bomb.

Tap B was then closed, S opened, and dry white-spot nitrogen was admitted to bring the apparatus to atmospheric pressure. The joint still being kept warm, the bomb was unscrewed from the vacuum line; a warm joint was essential here to avoid the possibility of shearing the cold threads at liquid-nitrogen temperatures. The hexagonal bomb-head nut was quickly screwed into the detached bomb and hammered home, the refrigerated bomb being held in a vice for this last procedure. On attaining room temperature, the pressure developed in the bomb was 150 atmospheres, and leaks could be detected by ear or by immersing the bomb in a dish of liquid. Such leaks, occurring in later experiments, were normally traced to defective gaskets.

After heating the bomb for 24 hours in an oven at 100°C, the above procedure was reversed, the bomb again attached to the line and the PF_3 restored to the bulb. The actual preparation and isolation of a sample of a metal-trifluorophosphine was similar to the above procedure, except that the bomb initially contained the requisite stoichiometric charges of metal halide and copper powder. The metal halide and very finely-divided copper dust were dried at 80°C and were then intimately mixed in an agate pestle and mortar in the stoichiometry copper/metal halide = 2 : 1. The introduction of this charge to the bomb diminished the bomb capacity for PF_3, the volume decrease being 1 ml. per 3 gm. of charge. The result was a higher pressure of PF_3 amounting to 6 atmospheres per 100 atmospheres per ml. decrease in volume in bomb capacity from 16 ml. Allowance was made for this "excess" pressure in later experiments, especially where large pressures of PF_3 were used.

4(5) The Isolation and Purification of the $M(PF_3)_4$ sample

The charged bomb was removed from the oven after 24 hours heating, was cooled, attached to the vacuum line and evacuated as described above. The next step involved the separation of

the excess PF_3 from the $M(PF_3)_4$ compound. Phosphorus trifluoride is expensive and poisonous (33), reacting with blood to form haemoglobin-PF_3, so recovery of the excess PF_3 was carried out as follows.

Taps R, E and D were closed and C, B opened. The liquid nitrogen Dewar was removed from the bomb and replaced with an acetone-CO_2 bath at -78°C. At this temperature PF_3 is a gas, whereas the trifluorophosphine-metal compound is a solid; hence, the PF_3 expanded into the bulb to a pressure registered by manometer m_a. When m_a had ceased to fall, tap B was closed, E, R opened and the line re-evacuated.

Isolation of the $M(PF_3)_4$ remaining is hampered by its tendency to decompose under its own vapour pressure into PF_3 and metal M. This instability increases with temperature:

	M.pt.	Decomp.Temp.	B.pt.
$Ni(PF_3)_4$	-55°C	155°C	71°C
$Pd(PF_3)_4$	-41	-20	?
$Pt(PF_3)_4$	-15	90	86

There is normally extensive decomposition at temperatures far below the stated decomposition temperatures. Professor Kruck (72) reports that, whereas the nickel and platinum compounds are conveniently handled in glass apparatus without

much visible sign of decomposition, the palladium compound decomposes to form a film of palladium metal in the vacuum line. This metallic film then catalyses the decomposition of further quantities of $Pd(PF_3)_4$. Thus, in the present work, the purification of the $M(PF_3)_4$ compounds consisted of the standard trap-to-trap distillation technique, with the added difficulty of performing such distillations rapidly to minimise contact of the vapour with the vacuum line at room temperature.

The technique employed was as follows: trap T_1 was cooled in liquid nitrogen, taps B, D, E and R were closed and taps C, J, K opened. The acetone-CO_2 bath cooling the bomb (after removal of the excess PF_3) was removed and the bomb was allowed to warm up slowly to room temperature (a process which occurred slowly, naturally, since the specific heat of the steel bomb is large). Tap R was then opened fractionally, so that as soon as the solid $M(PF_3)_4$ melted in the bomb the vapour was quickly drawn into T_1 with the assistance of the vacuum pumps. It should be noted that T_1 was connected to the line in "reverse order", so the vapour emanating from the bomb was presented with a large, cold surface area for condensation.

When the white solid $M(PF_3)_4$ had been collected in T_1,

tap G was closed and the system evacuated. Taps C and J were then closed, and the cold-finger reservoir R refrigerated with liquid nitrogen while T_1 was immersed in an acetone bath at -20°C. The tetrakistrifluorophosphine metal was collected in reservoir R, around which was placed a large storage Dewar containing two days supply of liquid nitrogen.

It was found useful to examine the vacuum line with a Tesla coil from time to time to see how the distillations were progressing, as the $M(PF_3)_4$ compounds have a characteristic bright orange glow discharge. This should be done sparingly, however, since the high-voltage discharge disrupts the metal-phosphine bond, and causes the liberation of metal on the glass surfaces of the apparatus.

The yields of pure $M(PF_3)_4$ obtained in syntheses using the procedure outlined above were ca. 20-30% of the theoretical based on the weight of metal halide. These yields are much lower than those reported by Kruck (who gives 80-100% for the same compounds). It is suggested that the main factor contributing to the diminution of yield in the preparations in the present work is the lack of a rotary autoclave. Kruck, during the whole 24 hour period of heating, was able to expose freshly-reduced metal surfaces to the PF_3. The bomb used in the present preparations had to be manually shaken at

intervals, which could not possibly be as effective as a continually rotating bomb. Support for this conclusion was given by an examination of the solid residue in the bomb after the $M(PF_3)_4$ had been extracted; a rather lumpy, granular solid remained, consisting of metal M, copper, and cuprous halide. In the case of Pt and Pd, all bomb residues were preserved and could be re-converted to the dihalides if necessary.

4(6) Molecular Weight Determination and Analysis

A description of the procedures used to obtain the molecular weight and analytical figures follows, with reference to the case of $Ni(PF_3)_4$. In the reaction,

$$NiX_2 + 2Cu + 4PF_3 \longrightarrow Ni(PF_3)_4 + 2CuX$$

X was iodine, and the pressure of PF_3 used was 135 atmospheres (45). 1 gm. of anhydrous NiI_2 (dried at 80°C) and 1 gm. copper dust were intimately mixed and heated at 100°C for 24 hours with 6.0 gm. PF_3 (corresponding to a pressure of 20 cm. in the 5.6 litre bulb). The stoichiometric quantity of PF_3 required was 1.2 gm., so excess PF_3 was present. Yield of pure $Ni(PF_3)_4$ was 0.2 ml. in reservoir R.

Kruck, in his work on the $M(PF_3)_4$ compounds, gives no information on the molecular weights, and assumes in his

vapour infra-red work that the gases are monomeric. The basis of the molecular weight determination is the weighing of a known volume of the vapour at known pressure and temperature, whereupon the application of Avogadro's Law gives a reasonably accurate value of the molecular weight of the gaseous phase. The actual procedure used in the present work was as follows:

The bulb T_3 was evacuated to 'black vacuum', taps P and Q closed and the bulb weighed. The volume of the bulb was determined by two methods,

(a) tap Q was opened in air and the temperature and atmospheric pressure recorded. The bulb was weighed in air, and consultation of critical tables (73) yields the volume of the bulb.

(b) the bulb was filled to the base of the tap bore with distilled water at known temperature. The weight was recorded and reference to the density of water at that temperature gives the volume of the bulb.

In this way the bulb volume was estimated as:

Method (a) V = 52.5 ml.

(b) V = 52.7 ml.

Mean = 52.6 ml. at 291°K

The bulb was re-evacuated on the vacuum line, the liquid nitrogen removed from reservoir R and the $M(PF_3)_4$ allowed to melt. The pressure in the apparatus was recorded on manometer M_b, and taps Q and P were closed when a suitable pressure reading had been taken. For the case of $Ni(PF_3)_4$ the following data,

Temperature 291°K, Pressure of vapour 5.35 cm.Hg

Weight of vapour 0.00585 gm.

gave an observed molecular weight of 405.6. The calculated value is 410.6.

Analysis

The sample was analysed for metal as follows:

Trap T_3 was evacuated and cooled in liquid nitrogen; a sample of the $M(PF_3)_4$ compound was then allowed to condense in T_3. The weight of the sample was recorded. The decomposition of the sample may be effected in one of two ways,

(a) by the addition of nitric acid and hydrogen peroxide,

(b) by the action of caustic soda solution.

To the cold $Ni(PF_3)_4$ liquid a strong nitric acid-hydrogen peroxide solution was added. A green solution containing Ni^{2+} was formed; the metal was estimated as $Ni(DMG)_2$ by precipitation from a faintly ammoniacal solution, after removal of nitric acid by fuming with hydrochloric acid.

0.1129 gm. $Ni(PF_3)_4$ gave 0.0787 gm. $Ni(DMG)_2$.
Observed % Ni = 14.17%, calculated = 14.29%.

4(7) The Infra-red spectrum of $Ni(PF_3)_4$

The infra-red sampling arrangement is shown in Figure 4A, the cells themselves being described in Chapter 2. The cells were kept evacuated in a large desiccator over silica gel to preserve their dryness, and when being kept in the laboratory for any length of time, the windows were protected from moisture by enclosing the cell in a stout polythene bag containing silica gel.

The cells were evacuated and tested for leaks with a Tesla coil; then with tap K closed and J open, the $M(PF_3)_4$ vapour was admitted to the cells to a pressure indicated by m_b. The advantage of this design is that both cells may be filled to the same pressure of vapour. The infra-red spectrum was obtained from 2000 cm^{-1} to 33 cm^{-1} at pressures of 1, 5, 10, 20 and 70 mm. Hg, the latter being the vapour pressure of $Ni(PF_3)_4$ at the temperature of the room.

The infra-red spectrum of $Ni(PF_3)_4$ is shown in Figure 4C; the figure consists of the superimposed spectra from the caesium iodide and the polythene cells. The lower region was obtained at a pressure of 5 mm. mercury, while the rather stronger

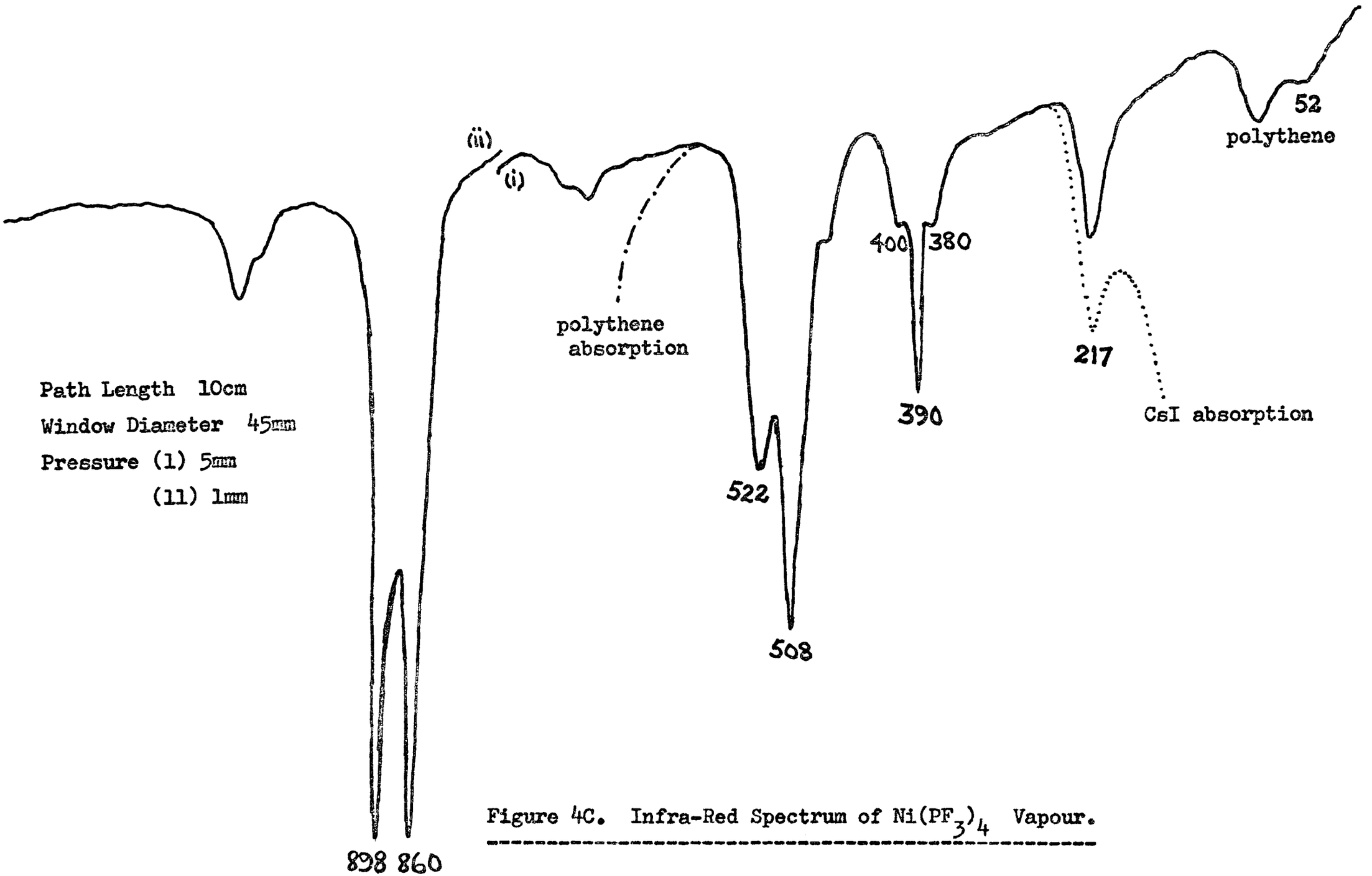


Figure 4C. Infra-Red Spectrum of $Ni(PF_3)_4$ Vapour.

P-F stretching features in the upper region were investigated at the lower pressure of 1 mm.

The assignment of frequency-values is shown in Table 4A, and in Table 4B the evidence of the present investigation is compared with the previous work of Seel (44), Kruck (69), and the Raman work of Woodward (43).

4(8) Discussion

In Table 4A the fundamentals and possible combination bands are listed. It is to be noted that some fundamentals, although themselves inactive in the infra-red, have active combinations. These latter were deduced in Chapter 3, and in Table 4A the combination activity of ν_3 and ν_2, of a_1 species, is seen. Frequency values of the fundamentals that were inactive in the infra-red were taken from the Raman paper of Woodward and Hall (43).

The assignment in Table 4A was based on the revised assignment of PF_3 (Wilson and Polo (58), and present work), and the discrepancy between this assignment and that of Woodward and Hall is seen in Table 4B. The Woodward-Hall assignment was made with the assistance of the erroneous Gutowsky assignment (57) for PF_3. If the Wilson assignment of PF_3 is applied to the Raman data for $Ni(PF_3)_4$ then the following modification to the Woodward assignment is made:

TABLE 4A

Assignment of the infra-red spectrum of $Ni(PF_3)_4$

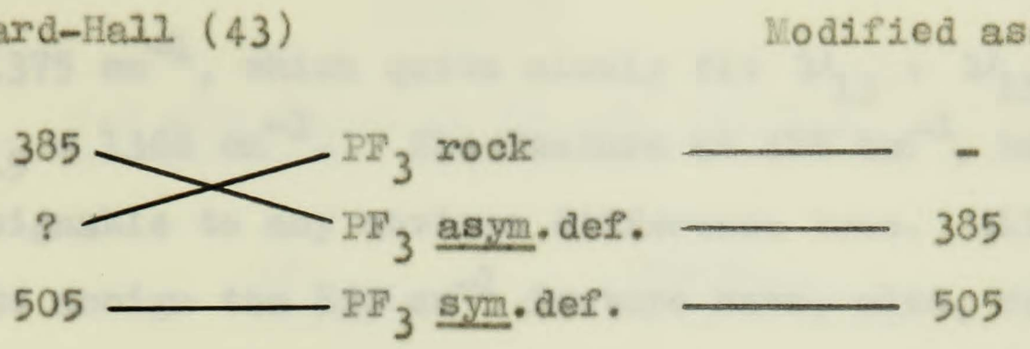
F_2 Species

cm^{-1}		Assignment of mode	
52m, bd	ν_{19}	NiP_4 deformation	
217 ms	ν_{18}	Ni-P asymmetric stretch	
242 vw	$\nu_3+\nu_{19}=247$		ν_3 of species a_1 = 195
287 w	$\nu_{15}-\nu_{18}=291$		
380 P)			
390 s Q)	ν_{16}	PF_3 asymmetric deformation	
400 R)			
488			
508 s	ν_{15}	PF_3 symmetric deformation	
522			
562 vw	$\nu_{15}+\nu_{19}=560$		
593 vvw	$\nu_3+\nu_{16}=585$		ν_3 of species a_1 = 195
724 w	$\nu_{15}+\nu_{18}=725$		
749 mw	$\nu_2+\nu_{18}=751$		ν_2 of species a_1 = 534
785 w	$2\nu_{16}=780$		
860 vs	ν_{14}	P-F asymmetric stretch	
898 vs	ν_{13}	P-F symmetric stretch	
990 w, sh			
1022 mw	$2\nu_{15}=1016$		
1097 w	$\nu_3+\nu_{13}=1093$		ν_3 of species a_1 = 195

TABLE 4B

Assignment of F_2-species fundamentals in $Ni(PF_3)_4$

I.R.	I.R.	I.R.	I.R.	Raman		Mode
PF_3	$Ni(PF_3)_4$	$Ni(PF_3)_4$	$Ni(PF_3)_4$	$Ni(PF_3)_4$		
Wilson(58)		Seel(44)	Kruck(69)	Woodward(43)		
Present work	Present work					
Vapour	Vapour	Vapour	-	liquid		
	52	-	-	54	ν_{19}	δ_{NiP_4}
	217	-	-	219	ν_{18}	$\nu_{NiP\ as}$
	-	-	-	385	ν_{17}	ρ_{PF_3}
344	390	386	-	505(ν_{15})	ν_{16}	$\delta_{PF_3\ as}$
487	508	503	-	- (ν_{16})	ν_{15}	$\delta_{PF_3\ s}$
860	860	859	864	883	ν_{14}	$\nu_{P-F\ as}$
892	898	898	904		ν_{13}	$\nu_{P-F\ s}$



There is now very good frequency-value agreement with the infra-red data.

An interesting feature of the infra-red spectrum shown in Figure 4C is the band contour of the ν_{16} deformation. A P, Q, R structure is seen, with a prominent Q branch, and a P-R separation of 20 cm^{-1}. This is the only feature to show partial fine structure, and the presence of the prominent Q branch is in agreement with theory. At first, it seems as though the other PF_3 deformation, ν_{15}, also manifests P, Q, and R branches, the prominent Q branch being at 508 cm^{-1}. Closer inspection, however, reveals that, not only does the P-R separation of 34 cm^{-1} differ from the case discussed previously, but the splittings, P-Q and Q-R within the band envelope are unequal.

If one cannot assign the 522, 508, 488 cm^{-1} complex to a P, Q, R structure, then, taking the 508 cm^{-1} band as the genuine ν_{15} deformation, the satellites must be combination features. Inspection of the upper region of the spectrum yields two prominent bands of medium-weak intensity at

1410 and 1375 cm^{-1}, which quite nicely fit $\nu_{13} + \nu_{15} = 1406$, $\nu_{14} + \nu_{15} = 1368$ cm^{-1}. The feature at 488 cm^{-1}, however, is not assignable to any obvious difference tone. All such attempts to assign the 522 cm^{-1} feature have, also, resulted in failure. Because of this, the possibility that the band at 522 cm^{-1} is a fundamental cannot be rigorously excluded from the discussion. An assignment that would fit the infra-red data, and also would agree with Woodward and Hall's assignment is given below:

PF_3 symmetric deformation	522 cm^{-1}
PF_3 asymmetric deformation	508 cm^{-1}
PF_3 rock	385 cm^{-1}

Raman polarisation data cannot clarify the dispute, since all modes under consideration belong to the F_2 species. A comparison of the stretching and bending frequencies of $Ni(PF_3)_4$ and PF_3, however, is quite illuminating (Table 4C). By analogy with the f_2-species stretches, which have been slightly affected by coordination into $Ni(PF_3)_4$ from the free PF_3 itself, one would sensibly choose the 508, 385 cm^{-1} pair for the f_2-species deformations as these are quite close in frequency to the deformations, at 487, 344 cm^{-1}, in PF_3 itself.

In a later Chapter, force-constant calculations are

TABLE 4C

P-F vibrations in PF_3 and $Ni(PF_3)_4$

	PF_3 (58)	$Ni(PF_3)_4$ (43)	
		954	
ν_{P-F} a_1	892		
ν_{P-F} e	860	851	
ν_{P-F} f_2	-	898,860	
		534	
δ_{PF_3} a_1	487	505	
δ_{PF_3} e	344		
δ_{PF_3} f_2	-	522	or 508 (present work)
		508	385

performed on the $Ni(PF_3)_4$ molecule and it is shown that the ν_2 frequency, a PF_3 deformation, is 'impure' and contains a lot of mixing from the ν_1 (P-F stretching) and ν_3 (Ni-P stretching) modes. Such mixing will be discussed later, but it is well to note here that considerable contribution from ν_1 and ν_3 could shift ν_2 to a higher frequency than would be expected if ν_2 were a 'pure' deformation mode. If this were so, then the assignment of the deformations to 522 and 508 cm^{-1} is again perfectly plausible. The assignment of the latter pair of frequencies to the deformations now leaves the 390 cm^{-1} band in the infra-red, which would well fit the PF_3 rocking mode.

In passing, it should be realised that the coincidences in the infra-red and Raman spectra observed, and assignable to the F_2-species vibrational modes, provides further conclusive support for the selection of the T_d point group for the $Ni(PF_3)_4$ molecule.

The final outcome of this discussion is the doubt cast on the Woodward-Hall assignment of $Ni(PF_3)_4$, although the revised assignment postulated itself suffers from an inability to explain the satellite at 522 cm^{-1}. A re-iteration of the evidence favouring either assignment is given below,

(a) Woodward-Hall assignment (43)

An assignment of the 522 cm^{-1} feature in the infra-red to the f_2-species symmetric PF_3 deformation seems reasonable. However, one must then explain why no Raman-coincidence was observed at 522 cm^{-1}. Inspection of the Raman spectrum (43) is inconclusive, since any feature at 522 cm^{-1} would probably be hidden under the more intense 505-534 cm^{-1} features due to other PF_3 deformations of e,f_2 and a_1 species respectively. Later force-constant calculations show that the PF_3 deformation in the a_1 species is 'impure', but whether the extent of mixing is great enough to justify such a change in the frequency of the deformations relative to PF_3 itself is a question for argument.

(b) The revised assignment of this present work

Support for this assignment is the revised assignment for PF_3 itself. The PF_3 deformation frequency-values are rather similar, like their stretching counterparts, to the frequencies in PF_3 itself. Also, the Woodward-Hall assignment suggests that the 385 cm^{-1} feature in the Raman spectrum is a PF_3 rocking mode, which is greater in frequency than a PF_3 deformation in PF_3 itself (at 344 cm^{-1}). This state of affairs is most unsatisfactory, and the PF_3 rock would be

expected to be lower in frequency than 344 cm^{-1}. Although the rocking mode has not been found in the present investigation of the infra-red spectrum of $Ni(PF_3)_4$, there is good reason to believe that the weak feature at 287 cm^{-1} in the infra-red could be this mode. In the vibrational spectra of $Pt(PF_3)_4$ discussed in the next Chapter, a weak feature at 283 cm^{-1} (Raman), 281 cm^{-1} (Infra-red) was assigned to the rocking mode (e, f_2 species).

In the present work the revised assignment of $Ni(PF_3)_4$ was adopted as the basis for the assignment of the other $M(PF_3)_4$ molecules to be studied in later Chapters.

CHAPTER 5

Chapter 5

TETRAKISTRIFLUOROPHOSPHINEPLATINUM°

5(1) Preparation

The preparation of tetrakistrifluorophosphineplatinum, $Pt(PF_3)_4$, has been described by Kruck (71), who used the high-pressure reductive phosphorylation method. As starting materials $PtCl_4$ or $PtCl_2$ are considered best (71,72).

Platinous chloride, used in the present work, was obtained from the Johnson Matthey Company. It was dried and intimately ground with 100% excess over the stoichiometric weight of copper dust required by the equation,

$$\underset{266}{PtCl_2} + \underset{352}{4PF_3} + \underset{128}{2Cu} \longrightarrow \underset{547}{Pt(PF_3)_4} + 2CuCl$$

The mixture contained approximately one gm. of copper per gm. of $PtCl_2$ used. A pressure of 100 atmospheres will be generated at 100°C by 6.3 gm. PF_3, which also provides some 400% excess. 1 gm. of $PtCl_2$ was taken, the total volume of solids in the bomb being 1.7 ml., and the preparation was carried out exactly as for the synthesis of $Ni(PF_3)_4$ in Chapter 4.

The purified product was collected in reservoir R of the vacuum line (Figure 4A), and subjected to a molecular

weight determination and a chemical analysis. The results were as follows:

Temperature of bulb = 291°K

Pressure of vapour = 6.55 cm.Hg, Weight of vapour = 0.10210 gm.

giving the molecular weight as 538.6; the theoretical molecular weight for $Pt(PF_3)_4$ = 547.2.

Analysis was accomplished by decomposing a known weight of $Pt(PF_3)_4$ in the bulb with strong caustic soda solution. The platinum is deposited as metal and may be filtered and weighed directly.

0.2456 gm. $Pt(PF_3)_4$ gave 0.0860 gm. Pt metal

Observed % Pt = 35.07%, theoretical = 35.65% Pt.

5(2) The Raman spectrum of $Pt(PF_3)_4$

A small sample of this compound was sent by Professor Th.Kruck of Cologne; the sample had decomposed somewhat and was a yellow liquid, with suspended particles of platinum. About 0.3 ml. of pure, colourless $Pt(PF_3)_4$ was obtained when this impure liquid was purified under vacuum. Preliminary spectra were obtained from this sample, but it was found necessary to make larger quantities by the method described

above. The spectra obtained from the Kruck sample and from the samples prepared in this work were identical in all respects. Yields in the preparation were again much lower than those reported by Kruck (30%, compared with 70-80% obtained by Kruck).

The Raman spectrum was obtained from a 0.3 ml. sample contained in a 15 cm. length of 2 mm. diameter thin-walled tubing (Raman micro-tube C_4 in Figure 4A). The fragile micro-tube was handled with care and was sealed off in vacuum. By use of internal reflections which amplify the Raman scattering, the resultant intensity of Raman scattering from a sample in such a tube is almost equal to that obtained from a 19 mm. diameter tube (65 ml. capacity), which does not employ internal reflections.

The part of the vacuum line used to isolate samples of $Pt(PF_3)_4$, for the investigation of the Raman spectrum in the solid and in the liquid states is illustrated in Figure 5A. The $Pt(PF_3)_4$ was condensed in the wider part of C_4, which was cooled in liquid nitrogen held in a specially-constructed long Dewar vessel which has an unsilvered strip running down its length to facilitate observation of the cooled tube. The Dewar was then removed and the solid $Pt(PF_3)_4$ allowed to melt and collect in the micro-tube as a liquid. The sample

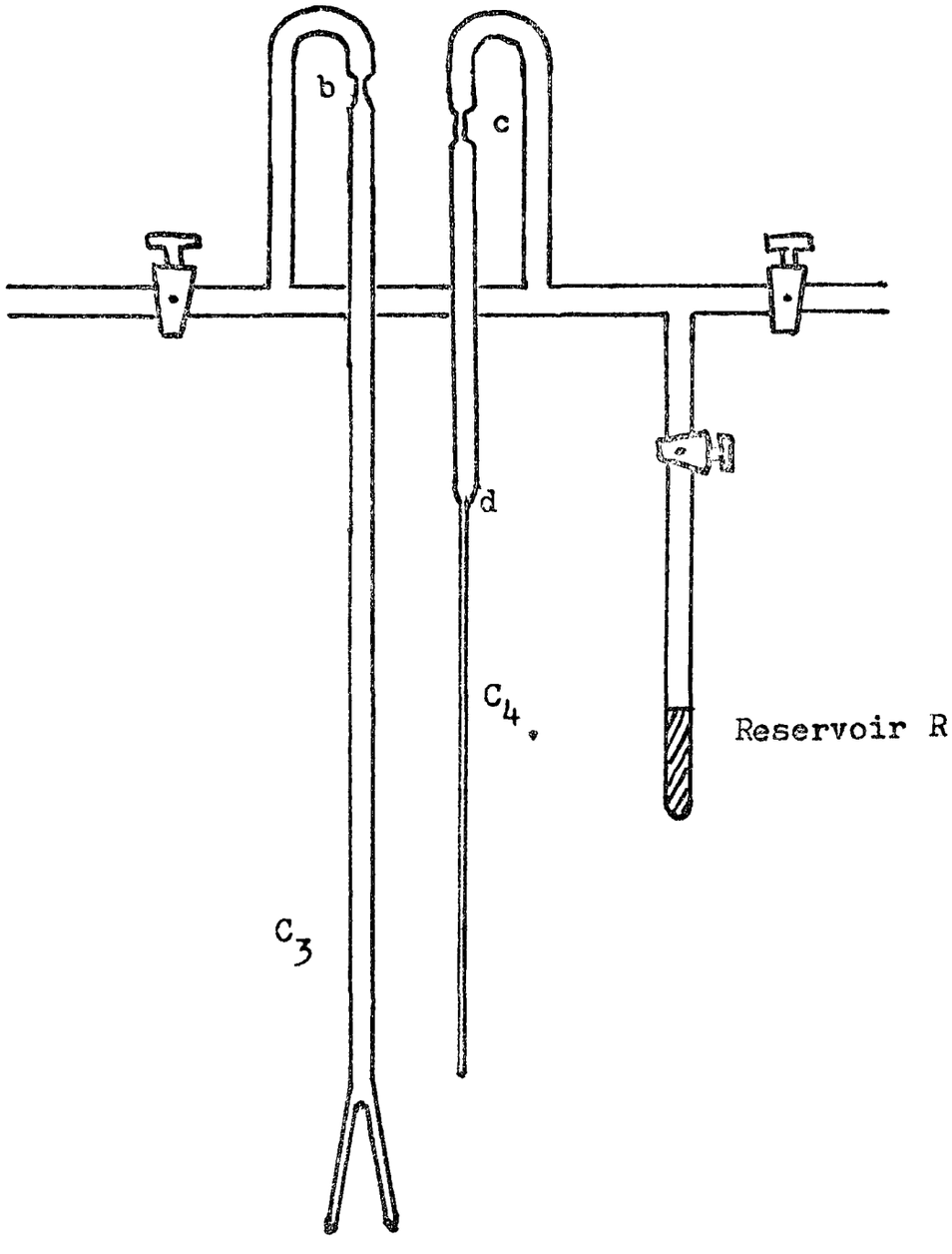
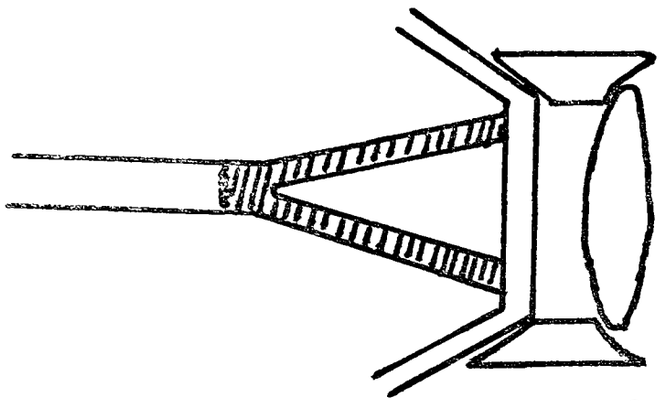


Figure 5A. $Pt(PF_3)_4$ Raman Samples.

was sealed under vacuum at point d (Figure 5A), which gave a sample some 15-20 cm. in length. The mounting of the tube in the optics of the Cary 81 spectrometer is shown in Figure 5B; the round end of the micro-tube was placed against a hemispherical lens which was bathed in glycerol. In this way, the Rayleigh and Raman scattering was focussed onto the image-slicer of the spectrometer.

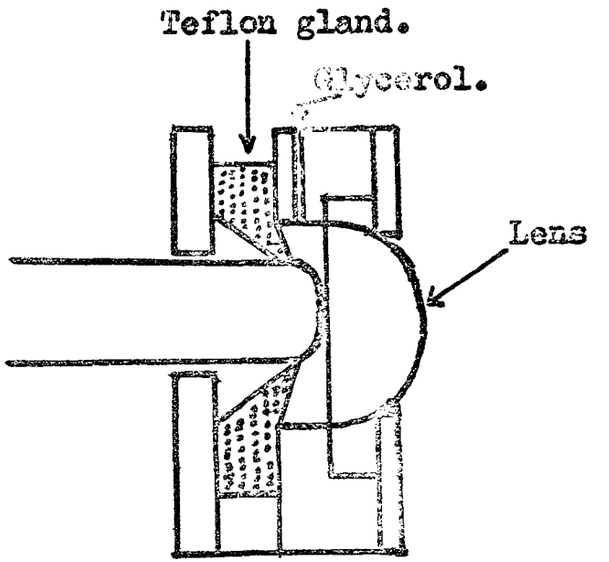
The liquid $Pt(PF_3)_4$ was found to be stable under the ordinary operating temperature of the Raman source, so obviating the need for any special cooling arrangement. Polarisation data were obtained, as outlined in Chapter 2, by the double-exposure method using cylindrical sheets of axial and cross-axial polaroid.

The Raman spectrum of solid $Pt(PF_3)_4$ was obtained using the conical cell C_3 in Figure 5A. The sample was condensed as a solid at liquid-nitrogen temperatures in the wider parts of this cell, which was then sealed off under vacuum at constriction b. Allowing the sample to melt and re-solidify, whilst rotating the cell rapidly at 45° to the vertical in a liquid-nitrogen bath, it was possible to spread the liquid evenly over the conical surface and solidify it there. The low-temperature arrangement designed for the Cary 81 spectrometer and described in



Cary 81
Spectrometer.
2mm Optics.

Cooled Solid Sample.



2mm Sample Tube for Liquids

Figure 5B. Raman Sample Mounts.

Chapter 2 (illustrated in Figure 2D) was utilised to maintain the $Pt(PF_3)_4$ in the solid state for the duration of the investigation. The sample cell was aligned horizontally with the condensing lens of the optics, as depicted in Figure 5B.

The Raman spectra of $Pt(PF_3)_4$ in both the liquid and the solid states are shown in Figures 5C and 5D. The instrumental operating conditions are stated in each figure, and the temperature at which the solid state spectrum was obtained was -70°C. An assignment of $Pt(PF_3)_4$ from the liquid-state spectrum is given, along with the Woodward-Hall assignment for $Ni(PF_3)_4$ in a similar state, in Table 5A. The solid-state spectrum of $Pt(PF_3)_4$ is rather more complex and will be discussed later.

5(3) The infra-red spectrum of $Pt(PF_3)_4$

The infra-red cells and sampling techniques used were exactly the same as those used in the investigation of the nickel analogue in Chapter 4. Spectra at similar pressures (1 mm. - 70 mm. Hg) were obtained, and a typical spectrum is shown in Figure 5E; an assignment is given in Table 5B.

Unlike the nickel analogue, the band-contour resolution for the $Pt(PF_3)_4$ case is ill-defined for the 384 cm^{-1} feature (390 cm^{-1} for $Ni(PF_3)_4$).

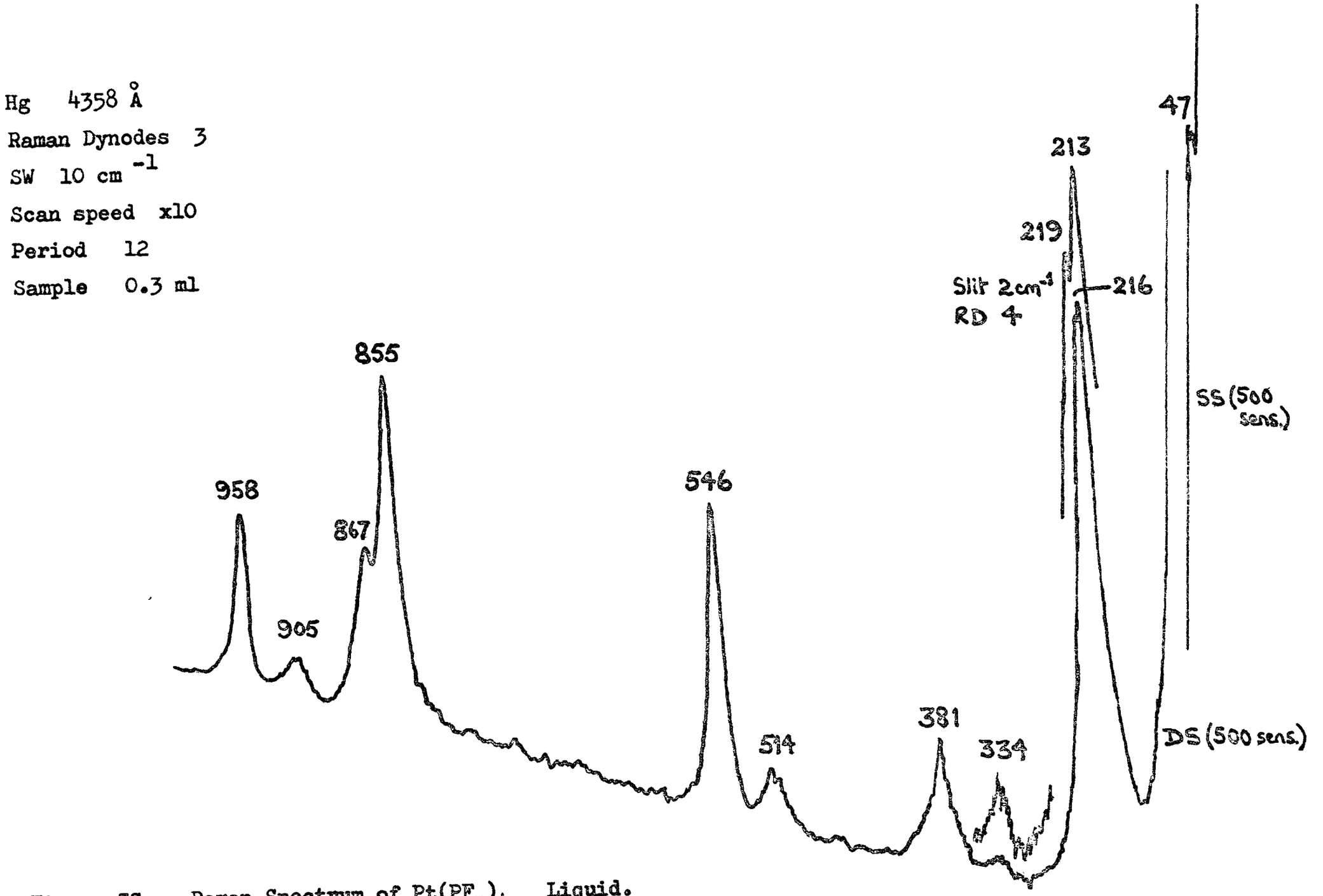


Figure 5C. Raman Spectrum of $Pt(PF_3)_4$ Liquid.

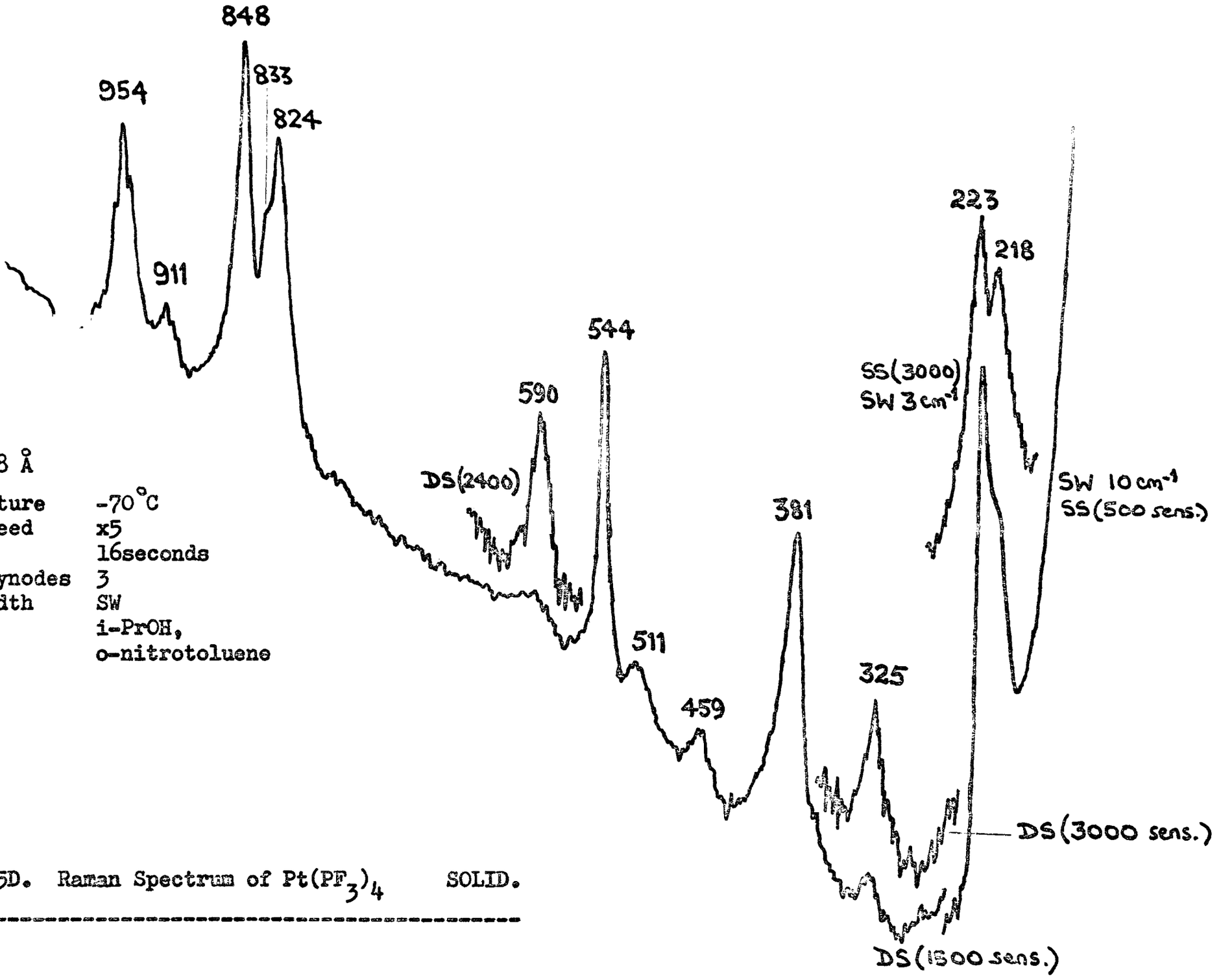


Figure 5D. Raman Spectrum of $Pt(PF_3)_4$ SOLID.

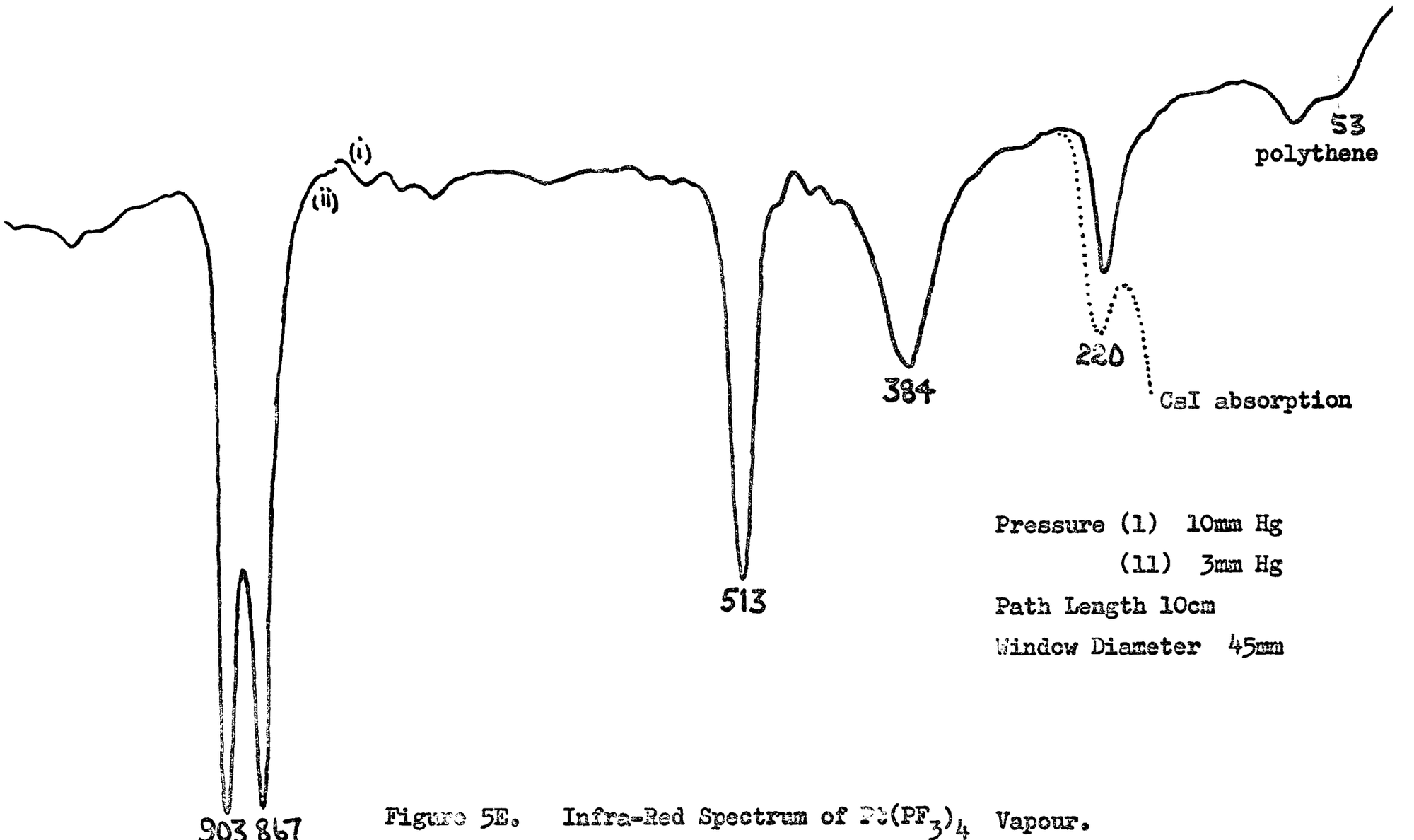


Figure 5E. Infra-Red Spectrum of $Pt(PF_3)_4$ Vapour.

TABLE 5A

Raman spectra of $Pt(PF_3)_4$ and $Ni(PF_3)_4$

Class	ν	Assignment of mode $M(PF_3)_4$	$Pt(PF_3)_4$ LIQUID	$Ni(PF_3)_4$ LIQUID (Ref.43) revised
A_1	ν_1	P-F symm.stretch	958 s,pol.	954 ms,pol.
	ν_2	PF_3 symm.def.	546 s,pol.	534 s,pol.
	ν_3	M-P symm.stretch	213 vs,pol.	195 vs,pol.
A_2	ν_4	PF_3 torsion	inactive	inactive
E	ν_5	P-F asymm.stretch	855 vs,depol.	851 vs,depol.
	ν_6	PF_3 asymm.def.	382 m,depol.	385 m,br,depol.
	ν_7	PF_3 rock	-	-
	ν_8	MP_4 deformation	47 m	54 s,br,depol.
F_1	ν_9	P-F asymm.stretch	inactive	inactive
	ν_{10}	PF_3 asymm.def.		
	ν_{11}	PF_3 rock		
	ν_{12}	PF_3 torsion		
F_2	ν_{13}	P-F symm.stretch	905 mw	883 m,depol.
	ν_{14}	P-F asymm.stretch	867 mw	
	ν_{15}	PF_3 symm.def.	514 m,depol.	505 m,depol.
	ν_{16}	PF_3 asymm.def.	382 m,depol.	385 m,br,depol.
	ν_{17}	PF_3 rock	-	-
	ν_{18}	M-P asymm.stretch	219 vs,depol.	219 vs,depol.
	ν_{19}	MP_4 def.	47 m	54 s,br,depol.

5(4) Discussion of the assignment

Reference to Table 5A, which compares the Raman spectra of $Pt(PF_3)_4$ and $Ni(PF_3)_4$ in the liquid state, shows a great similarity in the Raman spectrum of these compounds. Like the nickel analogue, polarisation measurements indicated that three features in the Raman spectrum of the platinum compound were polarised. One of these features, however, the intense 216 cm^{-1} band, was only partially polarised, and was thus suspected of containing both the symmetric and the asymmetric metal-phosphorus stretching modes within its envelope. In $Ni(PF_3)_4$, these metal-phosphorus modes were found as the polarised-depolarised pair at 195 cm^{-1} and 219 cm^{-1}, respectively. The former was highly polarised, as would be expected for the completely symmetrical skeletal stretching mode of a tetrahedral molecule.

A change of instrumental operating conditions, which involved a reduction of slit-width and an increase in sensitivity, produced a resolution of the feature at 216 cm^{-1} in the spectrum of liquid $Pt(PF_3)_4$. Subsequent polarisation measurements gave the information illustrated in Figure 5F. In this investigation of the 216 cm^{-1} feature, observed intensity ratios were referred to the calibration graph

TABLE 5B

Assignment of the infra-red spectrum of $Pt(PF_3)_4$

F_2 species

Kruck (71)	cm^{-1}	ν	Description of mode
	53 m	ν_{19}	PtP_4 deformation
	220 ms	ν_{18}	Pt-P asymmetric stretch
	281 mw	$\nu_{18} + \nu_{19} = 273$	
	327 vw	$\nu_{16} - \nu_{19} = 331$	
	384 s	ν_{16}	PF_3 asymmetric def.
	434 mw	$\nu_{16} + \nu_{19} = 437$	
		$2\nu_{18} = 440$	
	457 w	$\nu_{15} - \nu_{19} = 460$	
	513 s	ν_{15}	PF_3 symmetric def.
	553 w		
	568 mw	$\nu_{15} + \nu_{19} = 566$	
	602 vw	$\nu_{16} + \nu_{18} = 604$	
	642 w	$\nu_{14} - \nu_{18} = 647$	
	745 w	$\nu_{15} + \nu_{18} = 733$	
	768 w	$2\nu_{16} = 768$	
867 vs	867 vs	ν_{14}	P-F asymm.stretch
906 vs	903 vs	ν_{13}	P-F symm.stretch
	950 w	$\nu_{13} + \nu_{19} = 956$	
	1023 mw	$2\nu_{15} = 1026$	
	1090 w	$\nu_{14} + \nu_{18} = 1087$	
	1130 w	$\nu_{13} + \nu_{18} = 1123$	

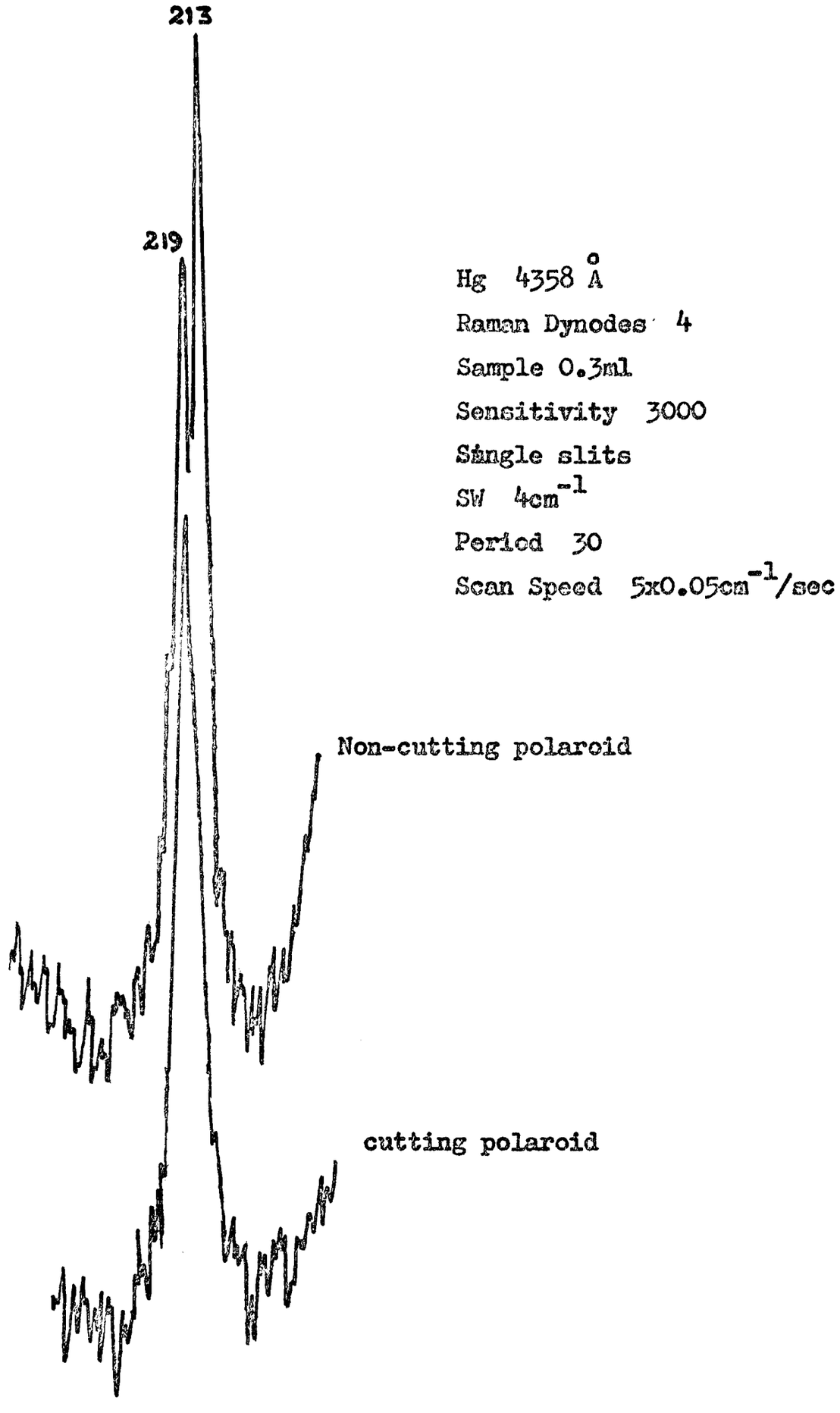


Figure 5F. Resolution of 216cm^{-1} feature in Raman Spectrum of $Pt(PF_3)_4$ Liquid.

in Chapter 2 for samples in 2 mm. micro-tubes, so obtaining corrected ρ-values for the bands, which allowed for the non-ideality of the tubes. The results are summarised below, for the 216 cm^{-1} feature, and for the bands at 213 and 219 cm^{-1} into which it was resolved:

Band	Observed ρ	Corrected ρ
216 cm^{-1} (unresolved)	0.74	0.28
219 cm^{-1}	1.13	0.70 depolarised
213 cm^{-1}	0.51	0.03 polarised

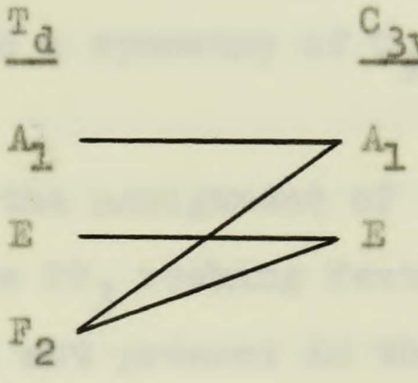
The Raman spectrum of <u>solid</u> $Pt(PF_3)_4$ at -70°C shows some anomalies when compared with that obtained from the liquid sample. The Raman spectra obtained from both states are given in Table 5C. It is immediately noticed that, whereas some fundamentals are reproduced to a close frequency agreement in both the liquid- and the solid-state spectra, other features manifest some degree of duplication in the solid-state spectrum, especially in the P-F stretching region. Consideration of the symmetry species of each mode yields further the information that the f_2-species modes are involved in this "duplication". Now, $Pt(PF_3)_4$ is spherically symmetric, or could reasonably be expected to be so in the vapour state; in the solid state, however, some breakdown in symmetry could

TABLE 5C

Raman spectrum of $Pt(PF_3)_4$

LIQUID	SOLID	Assignment	Class
958 s	954 s	ν_1	a_1
	911 mw, bd		
905 mw		ν_{13}	f_2
867 mw		ν_{14}	f_2
855 vs		ν_5	e
	848 s		
	833 m, sh		
	824 s		
	590 mw		
568 w, sh		$\nu_{15} + \nu_{19} = 561$	
546 vs	544 s	ν_2	a_1
514 m	511 m	ν_{15}	f_2
	459 w		
382 ms	381 ms	ν_{16}	f_2
334 w	325 w	ν_6 ?	e
283 w	280 w	ν_7, ν_{17} ?	e, f_2
219 vs	223 s	ν_{18}	f_2
213 vs	218 s	ν_3	a_1
47 m	-	ν_8, ν_{19}	e, f_2

occur, lowering the symmetry of the condensed $Pt(PF_3)_4$ and resulting in a partial removal of the degeneracy of the symmetry species. A correlation table relating the symmetry species in the T_d and C_{3v} point groups is shown below:



The F_2-degeneracy is partially lifted, and an f_2-mode will appear as <u>two</u> features, of a_1 and e symmetry respectively; the a_1- and e-species modes are unaffected by the change of symmetry from T_d to C_{3v}.

Such a breakdown in the tetrahedral symmetry of $Pt(PF_3)_4$ to C_{3v} would result from perturbation of one of the PF_3 groups; this could be achieved by the nearness of neighbouring molecules in the solid state. Why only <u>one</u> of the four PF_3 groups should appear to be affected in this way, to give a C_{3v} symmetry overall for the molecule, cannot be explained - but if more than one PF_3 group were so perturbed the resulting molecular symmetry would be only C_{2v} or C_1. The breakdown

of symmetry in the latter case would be so great that all degeneracy would be lifted and some (3N-6) modes become active in the Raman spectrum i.e. 45 vibrational modes for the $Pt(PF_3)_4$ molecule. The Raman spectrum of $Pt(PF_3)_4$ in the solid state is not vastly different from that in the liquid state, so a symmetry of C_{3v} in this state seems likely.

Absent in the assignment of the Raman spectrum of $Pt(PF_3)_4$ are the PF_3 rocking features, e- and f_2-species, which were also not present in the revised assignment of $Ni(PF_3)_4$. One would reasonably expect such rocking modes to lie lower than the deformations in cm^{-1} value. The Raman spectrum of liquid $Pt(PF_3)_4$ shows a weak feature at 334 cm^{-1}, and another at 283 cm^{-1}, which have counterparts at 325 and 280 cm^{-1} in the solid-state Raman spectrum. Both these modes are also weakly manifest in the infra-red spectrum of $Pt(PF_3)_4$ vapour. The weak features could be combination bands and have been assigned as such in Table 5B. However, the features could also be weak fundamentals and the following situations pertain:

(i) The band at 334 cm^{-1} in the Raman spectrum of liquid $Pt(PF_3)_4$ is the f_2- species rocking mode, ν_{17}, which has a coincidence in the infra-red at 327 cm^{-1}.

(ii) The 334 cm^{-1} feature is the Raman-active e-deformation, ν_6, and 283 cm^{-1} is the f_2-rocking mode. The infra-red band at 327 cm^{-1} is, thus, truly a combination rather than a fundamental, whereas the infra-red rocking coincidence (ν_{17}) is then given at 281 cm^{-1}.

The 281 cm^{-1} feature appears in the infra-red spectrum of the $Pt(PF_3)_4$ vapour at all pressures ranging from 3-60 mm. pressure and is weak to medium-weak in intensity, and assignment to the ν_{17} f_2-species PF_3 rock is favoured by a re-perusal of the $Ni(PF_3)_4$ infra-red spectrum in Table 4B. In the latter, a band of weak intensity at 287 cm^{-1} had been assigned to the difference tone, $\nu_{15} - \nu_{18}$. There was no feature at all in the neighbourhood of $\sim$330 cm^{-1} in the infra-red spectrum of $Ni(PF_3)_4$. This evidence, in conjunction with the conclusions drawn from the $Pt(PF_3)_4$ infra-red spectrum, suggests most strongly that the feature at 287 cm^{-1}, 281 cm^{-1} in the infra-red of $Ni(PF_3)_4$, $Pt(PF_3)_4$ respectively, is the PF_3 rocking-mode, ν_{17}, of each molecule.

It thus seems reasonable to assign the ν_{17} rock to the weak feature at 283 cm^{-1} in liquid $Pt(PF_3)_4$, leaving the 334 cm^{-1} band for assignment to the e-species PF_3 deformation. Reference to the Raman work (96) on liquid $Ni(PF_3)_4$ revealed that a weak feature at 332 cm^{-1} had been observed. This was

the properties of $Pd(PF_3)_4$ described in the next Chapter.

The final assignment and IR/Raman correlations in $Pt(PF_3)_4$ is given in Table 5D. The F_2-species assignment is omitted in the case of solid $Pt(PF_3)_4$, on account of the lifting of the degeneracy consequent from a breakdown in symmetry. The vibrational spectra support the assignment of $Pt(PF_3)_4$ to the T_d point-group. The remarkable similarity between the vibrational spectrum of $Ni(PF_3)_4$ and that of $Pt(PF_3)_4$ suggests that the bonding in both compounds is of similar nature. The correlation diagram for both molecules and PF_3 is given in Figure 5G. Bonding will be discussed at greater length when the results of force-constant calculations are later analysed.

ascribed to a PF_3-rocking mode, but in the light of the present work with $Pt(PF_3)_4$ it is perhaps better assigned to the e-species PF_3 deformation [which occurs at 334 cm^{-1} in $Pt(PF_3)_4$]. In the solid-state Raman spectrum of $Pt(PF_3)_4$, a weak feature at 280 cm^{-1} was found; if this were an f_2-mode then it should exhibit 'duplication' in common with the other f_2-species vibrations in the spectrum. The splitting resulting from a lifting of the degeneracy may well be small in this case; alternatively, one member of the 'split' feature' could be extremely weak and defy observation.

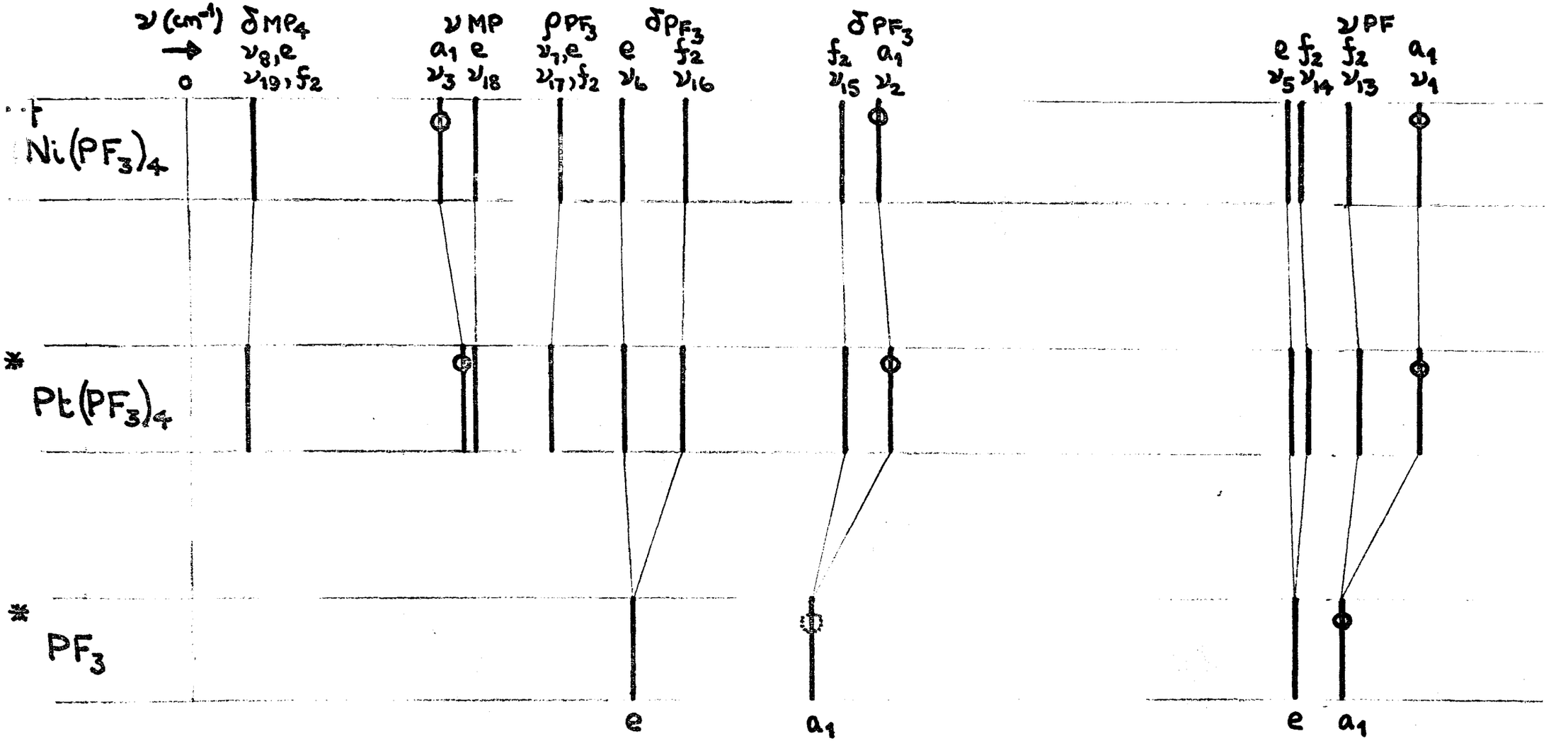
It should also be noted that band-contour resolution was <u>not</u> achieved in the vapour-state infra-red spectrum of $Pt(PF_3)_4$. This is consistent with theory; the P-Q-R separation of the bands would be much smaller in the case of $Pt(PF_3)_4$ than in the case of $Ni(PF_3)_4$, where resolution was achieved in the case of the PF_3 asymmetric deformation (band centre at 390 cm^{-1}).

The infra-red work of Kruck (71) was confined to the P-F stretching region, in which he observed two bands, at 867, 906 cm^{-1} vs. 867, 903 cm^{-1} in the present work (Table 5B). The vapour of $Pt(PF_3)_4$ seemed to be stable in the infra-red beam at all pressures investigated - in marked contrast to

TABLE 5D

Assignment and ir/R correlation ($Pt(PF_3)_4$)

Class	ν	Mode	Raman		Infra-red (vapour)
			C_{3v} Solid	Td liquid	Td
A_1	ν_1	ν P-F sym.	954	958	inactive
	ν_2	δ PF_3 sym.	544	546	
	ν_3	ν Pt-P sym.	218	213	
A_2	ν_4	τ PF_3	inactive	inactive	inactive
E	ν_5	ν P-F asym.	848	855	inactive
	ν_6	δ PF_3 asym.	325	334	
	ν_7	ρ PF_3	280	283	
	ν_8	δ PtP_4	-	47	
F_1	ν_9	ν P-F asym.	inactive	inactive	inactive
	ν_{10}	δ PF_3 asym.			
	ν_{11}	ρ PF_3			
	ν_{12}	τ PF_3			
F_2	ν_{13}	ν P-F sym.		905	903
	ν_{14}	ν P-F asym.		867	867
	ν_{15}	δ PF_3 sym.		514	513
	ν_{16}	δ PF_3 asym.		382	384
	ν_{17}	ρ PF_3		283	281
	ν_{18}	ν Pt-P asym.		219	220
	ν_{19}	δ PtP_4		47	53



Φ Polarised Band. * Present Work. † Ref. 43. ν Stretching. δ Deformation. ρ Rocking.

Figure 5G. Correlation Diagram for $M(PF_3)_4$ and PF_3

CHAPTER 6

Chapter 6

TETRAKISTRIFLUOROPHOSPHINEPALLADIUM°

6(1) Preparation

The stoichiometries are given by the equation:

$$PdCl_2 + 4PF_3 + 2Cu \longrightarrow Pd(PF_3)_4 + 2CuCl$$

213	352		459
1	1.7		2.2

Palladous chloride, obtained from the Johnson Matthey Company Ltd., was powdered and intimately mixed with twice the stoichiometric amount of copper powder. The pressure of PF_3 required in the bomb was rather larger for this preparation, compared with the analogous preparations of the platinum and nickel compounds, and amounted to some 300 atmospheres at 100°C.

After 24 hours heating in an oven at 100°C, the reaction products were extracted from the bomb as described previously for the nickel and platinum compounds. In the present case, however, the palladium compound is very much less stable than the other analogues of this series (72); extra precaution must therefore be taken to minimise the formation of a metallic palladium film by decomposition, which has a catalytic influence on the decomposition of further quantities

of $Pd(PF_3)_4$.

The vacuum-line arrangement was precisely that of Figure 4A, but now trap T_1 assumed a new importance by removing the reaction product from the bomb as quickly as possible as the cold bomb warmed up to room temperature. This latter is normally a slow process, and the consequent removal of palladium compound would be slow, affording much time and possibility for decomposition during the extraction of vapours from the bomb. Application of continuous pumping through tap R quickly condensed the volatile palladium compound in trap T_1 cooled by liquid nitrogen. In the further purification process, whereby the sample was collected in the cold-finger reservoir, the distillation is effected in a sealed system and cannot be hurried. This distillation, from T_1 cooled in acetone-CO_2 at -35°C into the reservoir cooled in liquid nitrogen, was in itself fairly rapid, however, and little deposition of palladium metal on the walls of the vacuum line occurred.

It need hardly be stressed that use of the Tesla coil is ill-advised as rapid decomposition of the palladium compound resulted.

On account of certain matters arising from the investigations of the vibrational spectra of this palladium compound, it became necessary to examine the spectra of this

compound in a number of physical states, for which rather a lot of compound was desired. Many bomb reactions were thus performed, and during the course of time various parts of the vacuum line had to be cut off and re-constructed owing to the appearance of palladium metal on the glass surfaces. All reaction product samples were collected in the cold-finger reservoir until enough compound had been isolated for the desired projects. From time to time it became essential to remove parts of the apparatus in the neighbourhood of the reservoir and to clear them with aqua regia. It is estimated that the whole vacuum line was renewed some two or three times (and some portions up to twice this amount) during the subsequent investigations with the unstable palladium compound. After renewal of any portion of the line, that part necessitated careful flaming and evacuation so the whole line again became of "black vacuum" standard.

It was found that the bomb, too, contained a film of palladium metal from decomposition of the trifluoro-phosphinemetal. This was removed after each preparation by dissolving in aqua regia. Much care had to be taken during this process to avoid attack of the acid on the steel bomb surface, but more important, on the steel screw threads of the bomb head.

In preliminary tests it was discovered that the vapour of

the trifluorophosphinepalladium compound under low pressure was much more stable than when under its own vapour pressure of 7-8 cms mercury at room temperature. Molecular weight determinations were thus performed at rather lower pressures than for the corresponding nickel and platinum compounds. A typical result of a molecular weight determination for a sample of the reaction product was:

Temperature 292°K

Weight of vapour = .02933 gm. Pressure = 2.40 cm.Hg

giving a molecular weight of 460.1, compared with a value of 458.6 calculated for $Pd(PF_3)_4$.

It seems, then, that the vapour of this volatile trifluorophosphinepalladium is monomeric and corresponds well to the molecular weight expected for $Pd(PF_3)_4$. This result will be of great significance in the later interpretation of the vibrational spectra of this compound.

The analytical procedure was precisely that used for the platinum analogue, but the alternative method of determining the palladium as $Pd(DMG)_2$ is also available.

.0932 gm. compound yielded .0214 gm. Pd metal, giving observed % Pd = 23.00%; theoretical % Pd for $Pd(PF_3)_4$ = 23.26%.

Unlike the nickel and platinum analogues, which are stable in the liquid state at room temperature, the palladium compound, which melted at -40°C, was extensively decomposed at -20°C and decomposition was complete at 0°C. Special measures were therefore taken in the obtaining of the vibrational spectra of this compound.

6(2) The Raman spectrum of tetrakistrifluorophosphinepalladium°

Because of the unstable nature of this compound it was thought to be impossible to obtain the Raman spectrum of the liquid; melting occurs at -40°C, and decomposition is noticed in the liquid at -30°C. Therefore, it was decided to make a sample in solution in chloroform, when temperatures near -40° could be used in an attempt at the obtaining of the Raman spectrum. Chloroform was selected as a suitable solvent since its Raman spectrum is simple, and because the freezing point is -63°C.

The vacuum-line modification of Figure 6A was designed for the preparation of a solution of $Pd(PF_3)_4$ in chloroform for Raman spectroscopy. The Raman tube was a 20 cm. length of 3 mm. i.d. pyrex tubing with a round bottom, connected to a 250 ml. bulb. The blackened-off kink was necessary to retain the solution in the Raman tube when the latter was

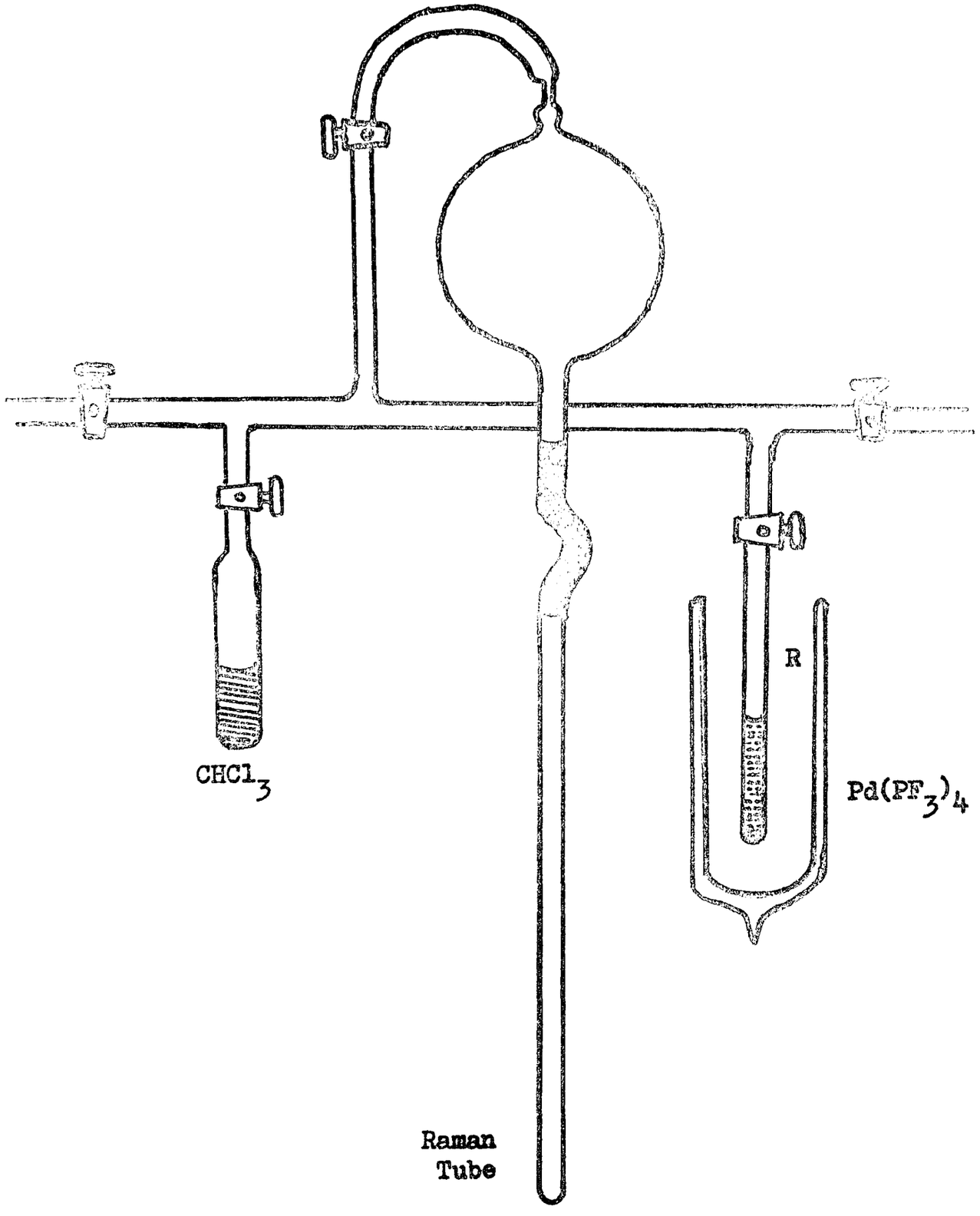


Figure 6A. Preparation of a $CHCl_3$ Solution of $Pd(PF_3)_4$.

mounted horizontally in the cold-cell arrangement of the Cary 81 spectrometer. The volume of the Raman tube was 2 ml., so a solution of approximately 0.3 ml. of $Pd(PF_3)_4$ in 1.7 ml. chloroform would be $\sim$ 1 Molar. The purpose of the bulb was to minimise the pressure build-up in the Raman tube if decomposition of the palladium compound occurs; the maximum pressure that could be attained if all the $Pd(PF_3)_4$ decomposed would be provided by 75 ml. of PF_3 (from 0.3 ml. compound) at 1 atmosphere pressure - which corresponds to a pressure of $\frac{1}{3}$ atmosphere in the Raman tube.

The Raman cold-cell arrangement described in Chapter 2 was used and was equilibrated at -35°C. Chloroform was distilled into the Raman tube, cooled in liquid nitrogen contained in a specially-constructed long Dewar, and then the 0.3 ml. sample of $Pd(PF_3)_4$ was quickly allowed to condense in the tube. More chloroform was condensed in the Raman tube until, on immersing the tube in an acetone bath at -35° to -40°C and allowing the contents to melt, the meniscus of the solution was obscured by the blackened kink in the tube. This ensured that, when the tube was finally inserted horizontally into the spectrometer, enough solution was present and that there would be no primary scattering from the meniscus of the sample.

The tube was sealed-off under vacuum at the constriction and mounted horizontally in the Cary instrument in such a way

that the rounded bottom was in contact with the optically-flat end of the cooling jacket. To prevent the condensation of water on the cold surface of the Raman tube prior to its insertion in the cold cell, the tube was washed with cold acetone immediately before mounting in the source.

The spectrum obtained is depicted in Figure 6B. It is seen that, after identification of the Raman bands due to chloroform, the remaining features are far too numerous to be assigned to the simple molecule $Pd(PF_3)_4$ alone. Discussion will be devoted to this later, but at present it looks as if the chloroform had 'reacted' with or partially decomposed the palladium compound. The solution remained perfectly clear throughout the Raman investigation, so decomposition to palladium metal under the 3 kilowatt radiation of the arc did not occur at -35°C.

Another explanation of the remarkably complex Raman spectrum in chloroform solution would be forthcoming if the compound initially isolated from the high-pressure bomb reaction was not $Pd(PF_3)_4$, but rather a mixture of palladium-PF_3 compounds such as bridged species. It has already been shown that the molecular weight of the <u>vapour</u> of the volatile product of reaction between $PdCl_2$ and PF_3 in the bomb is that of $Pd(PF_3)_4$ monomer. At this point an investigation was carried

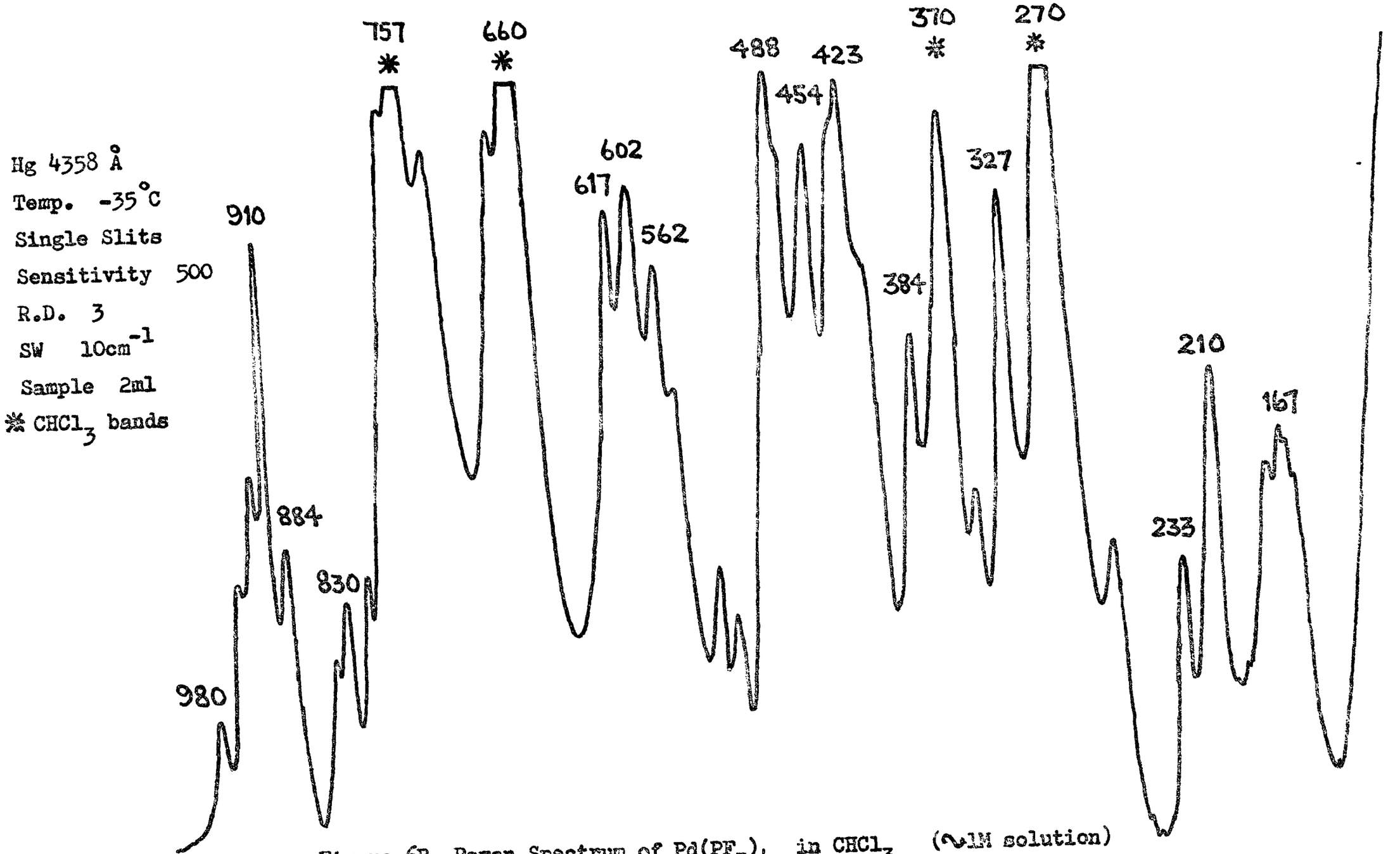


Figure 6B. Raman Spectrum of $Pd(PF_3)_4$ in $CHCl_3$ (~1M solution)

out to determine the molecular weights of the vapours from various samples, which were prepared under different conditions of temperature and pressure of PF_3. The range of experimental conditions varied from 150 atmospheres of PF_3 at 100°C for 12 hours, to 400 atmospheres PF_3 at 150°C for 72 hours. Six new preparations and isolation of the volatile palladium compound were performed at these, and intermediate pressures and temperatures, varying also the Cu:$PdCl_2$ weight above the requirements of the equation for the reaction.

Each sample was isolated as described in 6(1), and a determination of the molecular weight was made. In all cases, the value of the molecular weight obtained was not sensibly different from the theoretically calculated 458.6 for $Pd(PF_3)_4$; the extreme values for the molecular weight were found to be 449.7 and 463.2. For each sample, a portion was decomposed with caustic soda, and, after acidification with nitric acid, tested with silver nitrate solution. Qualitatively, thus, the absence of halogen was demonstrated; proving that no compounds of the intermediate substitution type containing chlorine contaminated the volatile reaction product.

It seems, then, that the volatile reaction product from the bomb contains palladium and phosphorus trifluoride only. That the vapour is monomeric $Pd(PF_3)_4$ has been shown by the molecular weight determinations, but the existence of dimers, trimers and other higher polymers of formula $[Pd(PF_3)_4]_x$ in the liquid state has not been disproved. To test for the presence of such polymers in a sample of the volatile reaction product, a molecular weight determination of the vapour and of the vaporised liquid-fraction remaining were made. Both determinations gave similar results for the molecular weight (456.9 and 460.0 respectively). Any polymers that may exist in the liquid reaction product must thus dissociate completely to the monomer form on passing into the vapour state.

The source of the anomalous spectrum of the chloroform solution may, thus, be due either to a reaction between $Pd(PF_3)_4$ and chloroform, or to the presence of compounds $[Pd(PF_3)_4]_x$ in the liquid "$Pd(PF_3)_4$" reaction product. It was therefore desirable to investigate the Raman spectrum of pure "$Pd(PF_3)_4$" in the solid state, and to attempt to obtain the Raman spectrum in the liquid state at -35°C.

6(3) Raman spectra of the palladium compound in the solid and liquid states

The procedure was exactly that which was used in the preparation of Raman samples of the platinum compound, except that more care was necessary in the manipulations of the liquid samples on account of the instability of the palladium compound. The apparatus used was similar to that of Figure 5A. The solid sample was maintained at -90°C in a conical cell. The obtaining of a sample in the liquid state proved more difficult; the $Pd(PF_3)_4$ vapour was firstly condensed as a white solid S on the walls of a 7 mm. i.d. tube to which was attached a 2 mm. diameter Raman micro-tube, the whole being cooled in liquid nitrogen contained in a long Dewar. Figure 6C illustrates the design of the apparatus. After sealing off the tube at constriction e, the liquid nitrogen refrigerant was replaced by an acetone-CO_2 bath at exactly -38°C, and the cold-cell arrangement of the Cary 81 spectrometer was accurately equilibrated at -35 to -38°C for the duration of the Raman investigation of liquid "$Pd(PF_3)_4$".

After many hours of Raman work the samples were found not to have deteriorated either through thermal effects or by irradiation from the mercury arc lamp. The spectra

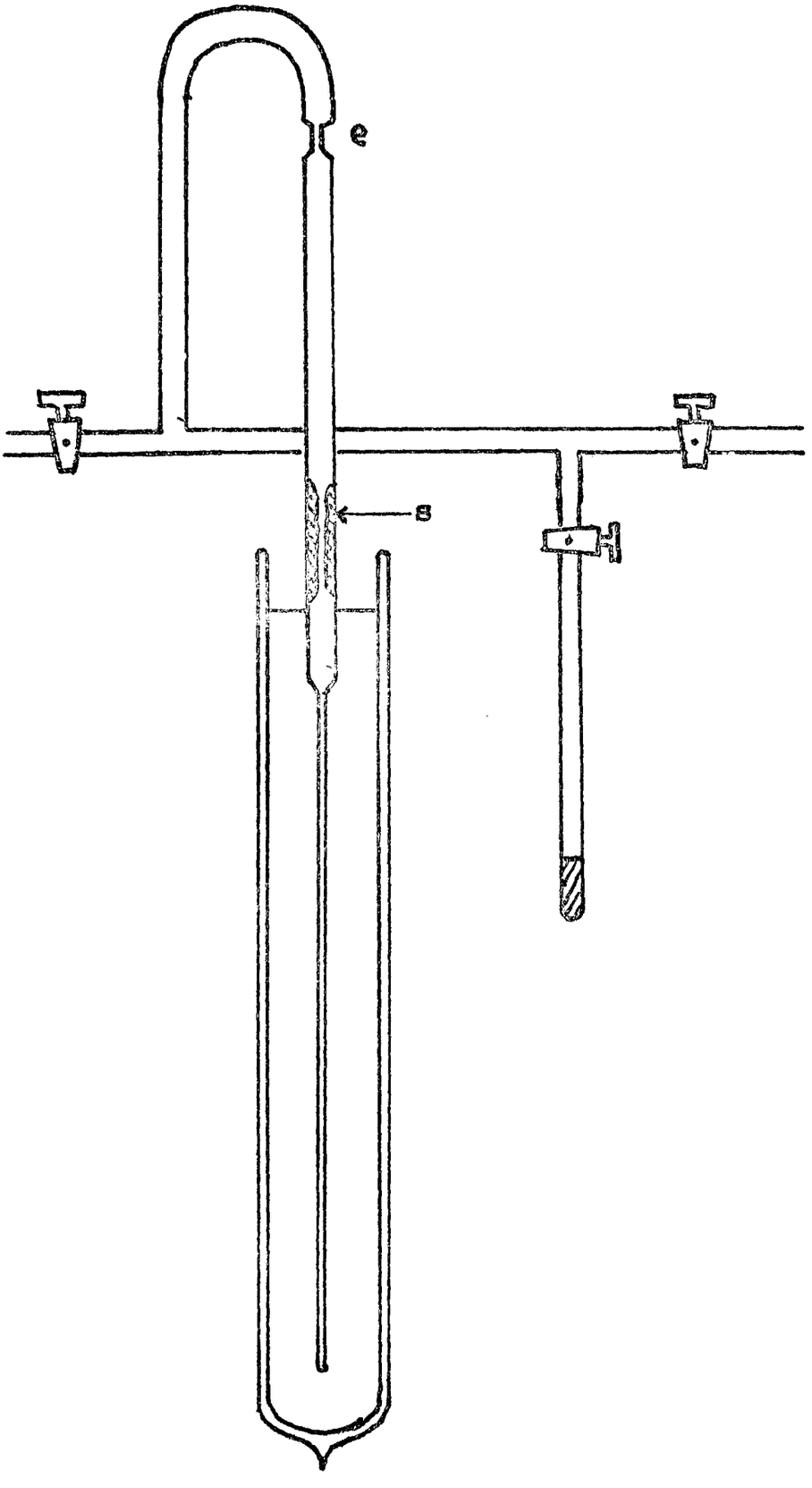


Figure. 6 C. $Pd(PF_3)_4$ Liquid Sample.

obtained from the liquid and solid samples of the trifluorophosphinepalladium compound are shown in Figures 6D and 6E respectively. The data are presented in Table 6A, with the inclusion of the Raman data from the chloroform solution for ease of comparison.

6(4) Infra-red spectra

The infra-red spectrum of $Pd(PF_3)_4$ was obtained in the vapour phase using caesium iodide and polythene-windowed cells. It was found that decomposition of the vapour at higher pressures in the infra-red beam proved troublesome. This was not experienced with the nickel and platinum analogues, but was only to be expected in this case where much care had to be taken to prevent decomposition of the $Pd(PF_3)_4$ vapour in the vacuum-line work. At pressures of 4 cm. Hg or lower the vapour seemed to be stable at room temperature in the infra-red cell, although reaction with the caesium-iodide plates occurred after a few hours standing, resulting in deposition of palladium metal on the windows. At pressures of circa 10 cm. Hg the vapour decomposed on the windows and cell walls within minutes. Especially prone to surface damage were the caesium iodide windows, which had to be removed from the cell, re-polished, and re-assembled on the cell after cleaning.

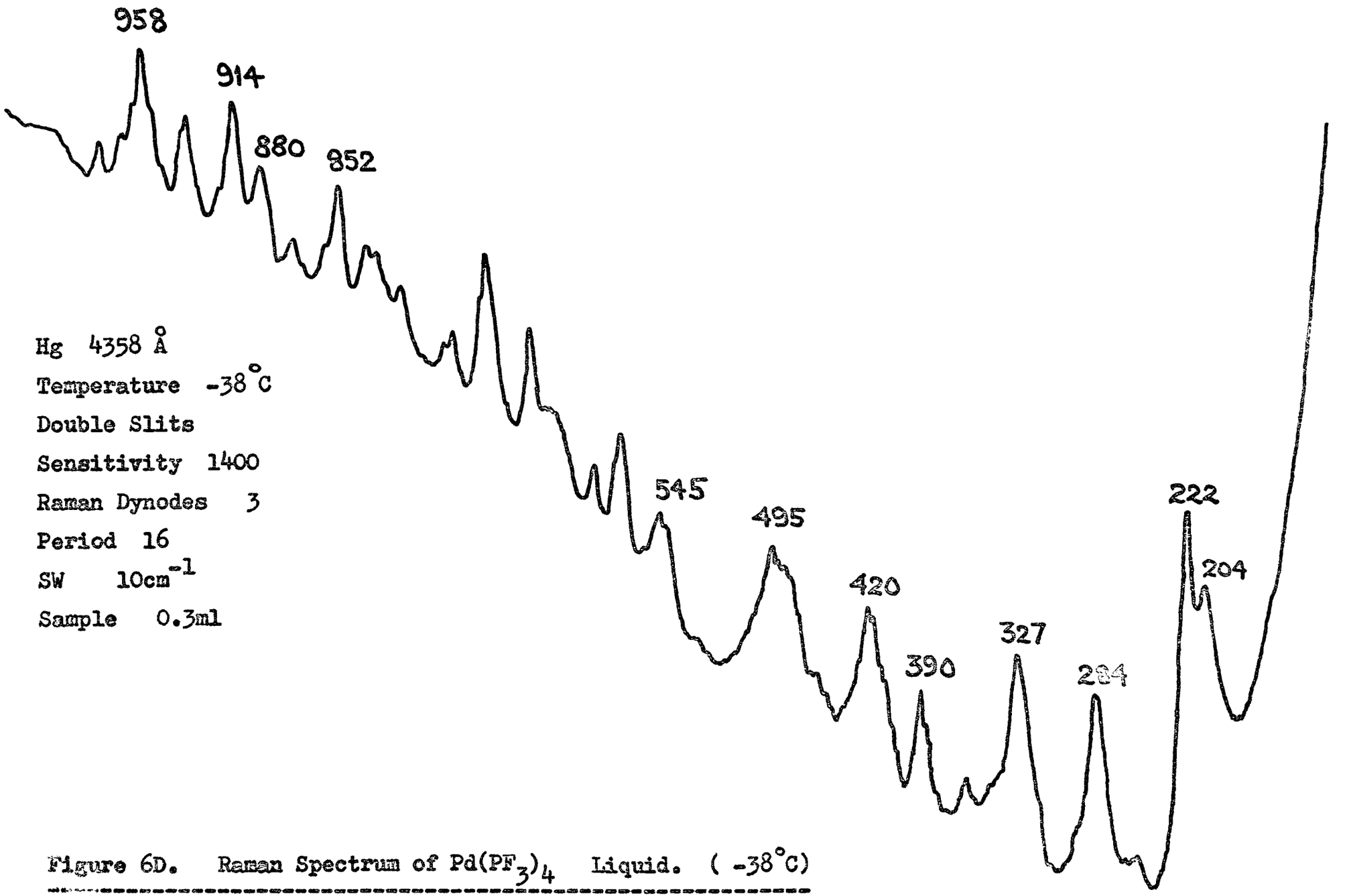
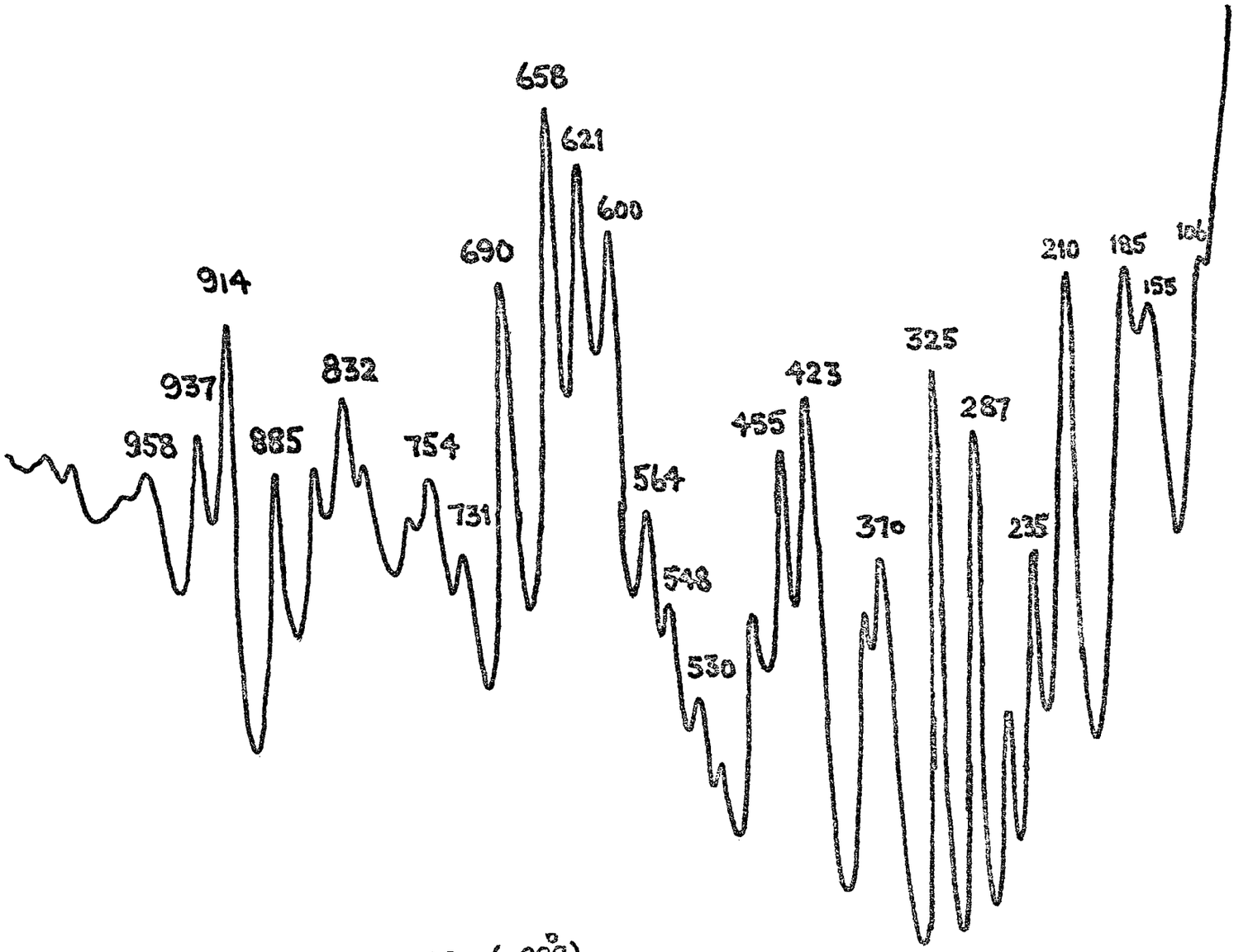


Figure 6D. Raman Spectrum of $Pd(PF_3)_4$ Liquid. (-38°C)



Hg 4358 Å
Temperature -90°C
Single Slits
Sensitivity 1000
SW 10cm^{-1}
Raman Dynodes 3

Figure 6E. Raman Spectrum of $Pd(PF_3)_4$ Solid (-90°C)

TABLE 6A

Raman spectrum of $Pd(PF_3)_4$

SOLID	1M SOLUTION IN $CHCl_3$	LIQUID
-90°C	-35°C	-38°C
106 mw, sh		
155 ms	167 ms	
185 ms	180 ms, sh	
210 ms	210 s	204 m
235 m	233 ms	222 ms
256 mw	256 mw	259 w
287 ms	*270 vs	284 m
325 ms	327 ms	327 m
349 vw	348 w	348 w
370 m	*370 s	368 w
386 m, sh	384 mw	390 m
423 ms	413 w, sh	
	423 s	420 m
455 ms	454 s	454 mw
475 m	470 m, sh	471 w
490 m	488 s	495 m
520 w	518 w	518 mw, sh
530 w	527 w	
548 mw	546 m	545 m
564 mw	562 mw	568 vw
600 ms	602 s	600 w, sh
621 ms	617 s	619 mw
658 s	*660 vs	660 mw
690 ms	687 ms, sh	690 mw
731 mw	728 m	726 w
754 m	*757 s	757 mw
780 m	778 m, sh	780 mw
809 w	808 mw	
832 ms	830 ms	829 mw
845 mw	843 w	852 m
		868 w
885 m	884 m	880 m
914 ms	910 ms	914 ms
937 m	934 m, sh	937 mw
958 m	955 mw	958 m
980 mw	980 w	980 w

* $CHCl_3$ bands

A partially-decomposed sample was also investigated in the caesium-iodide windowed cell. No features could be ascribed to polymers and the only new bands obtained were assignable to PF_3 itself, palladium metal having been formed on the walls of the cell.

In Figure 6F is shown a typical vapour-phase infra-red spectrum of $Pd(PF_3)_4$. The spectrum is remarkably similar to that of $Ni(PF_3)_4$, and of course $Pt(PF_3)_4$. The conclusion must therefore be that "$Pd(PF_3)_4$" exists as such, as the monomer, in the vapour state under the pressures at which the infra-red spectra were obtained. In Table 6B the vapour infra-red spectrum is given, along with the two bands, ν_{13}, ν_{14}, quoted by Kruck (71)for $Pd(PF_3)_4$. Some of the possible combination bands have been assigned by analogy with $Ni(PF_3)_4$, and calculated values of certain inactive or 'missing' frequencies have been tentatively tabulated. These frequency-values seem reasonable in the light of an assignment of monomeric $Pd(PF_3)_4$ which is later to be made. An assignment of the modes in the F_2 species of $Pd(PF_3)_4$ is made in Table 6C, which also contains a similar assignment of $Pt(PF_3)_4$ for comparison purposes.

The infra-red spectrum of the palladium compound in the solid state at -196°C was also obtained, using the cell

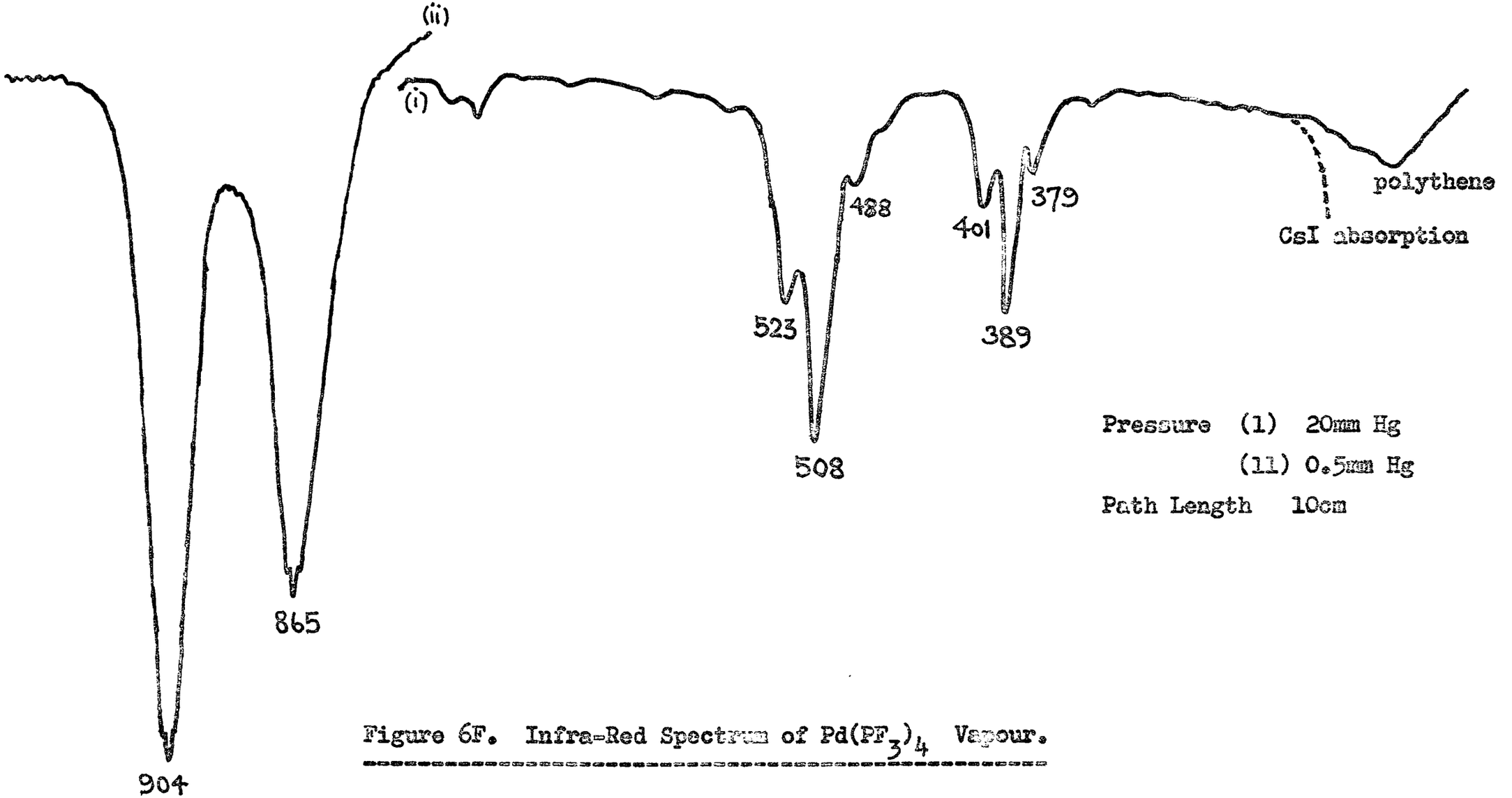


Figure 6F. Infra-Red Spectrum of $Pd(PF_3)_4$ Vapour.

TABLE 6B

The infra-red spectrum of $Pd(PF_3)_4$ vapour

Vapour state (ordinary temps.) Pressures: 20 - 80 mm. mercury

Kruck(71)	Present work ν (cm^{-1})		assignment
	379	P	
	389 ms	Q	ν_{16}
	401	R	
	473 mw		
	488 mw, sh		
	508 s		ν_{15}
	523 m, sh		
	596 w		$\nu_{16}(f_2) + \nu_3(a_1)$ gives ν_3 = 207 cm^{-1}
	616 w		$\nu_{16}(f_2) + \nu_{18}(f_2)$ gives ν_{18} = 227 cm^{-1}
	719 mw		$\nu_{15}(f_2) + \nu_3(a_1)$ gives ν_3 = 211 cm^{-1}
	728 m		$\nu_{15}(f_2) + \nu_{18}(f_2)$ gives ν_{18} = 220 cm^{-1}
	739 vw		
	765 vw		
	776 w		$2\nu_{16}$ = 778
	834 w		
860 vs	865 vs		ν_{14}
910 vs	904 vs		ν_{13}
	990 vw		
	1025 mw		$2\nu_{15}$ = 1016
	1289 w		$\nu_{13} + \nu_{16}$ = 1293
	1372 vw		
	1410 mw		$\nu_{13} + \nu_{15}$ = 1412
	1725 w		$2\nu_{14}$ = 1730
	1760 w		$\nu_{13} + \nu_{14}$ = 1769
	1815 w		$2\nu_{13}$ = 1808

TABLE 6C

F_2 class assignment for $Pd(PF_3)_4$

ν	Mode	Vapour $Pd(PF_3)_4$	Vapour $Pt(PF_3)_4$ (Chap.5)
ν_{13}	P-F symmetric stretch	904	903
ν_{14}	P-F asymmetric stretch	865	867
ν_{15}	PF_3 symmetric def.	508	513
ν_{16}	PF_3 asymmetric def.	389	384
ν_{17}	PF_3 rock	n.o.	281
ν_{18}	M-P stretch	n.o.	220
ν_{19}	MP_4 deformation	n.o.	53

n.o. = not observed

described in Chapter 2. The $Pd(PF_3)_4$ vapour at various pressures was led onto a caesium-iodide plate, refrigerated in liquid nitrogen, contained in a 10 cm. path length cell with caesium iodide windows. A fine jet leads the vapour to within close proximity of the cooled caesium-iodide surface, and condensed films of $Pd(PF_3)_4$ of varying thickness were obtained using different initial pressures of vapour. A typical spectrum is shown in Figure 6G, and the data presented in Table 6D.

6(5) Discussion

Consideration of the vibrational spectra in various states reveals that, whereas the vapour-state infra-red spectrum conforms nicely to that expected for monomeric, tetrahedral $Pd(PF_3)_4$, the complexity of the condensed phase spectra requires some explanation.

Some distortion from perfect tetrahedral symmetry is to be expected in the solid state by analogy with $Pt(PF_3)_4$; unlike the platinum case, however, no definite conclusions can be drawn from a study of the solid-state infra-red spectrum of $Pd(PF_3)_4$. Reference to Table 6A shows that there is good agreement in band frequencies in the Raman spectrum of the liquid and the solid, and indeed, with the

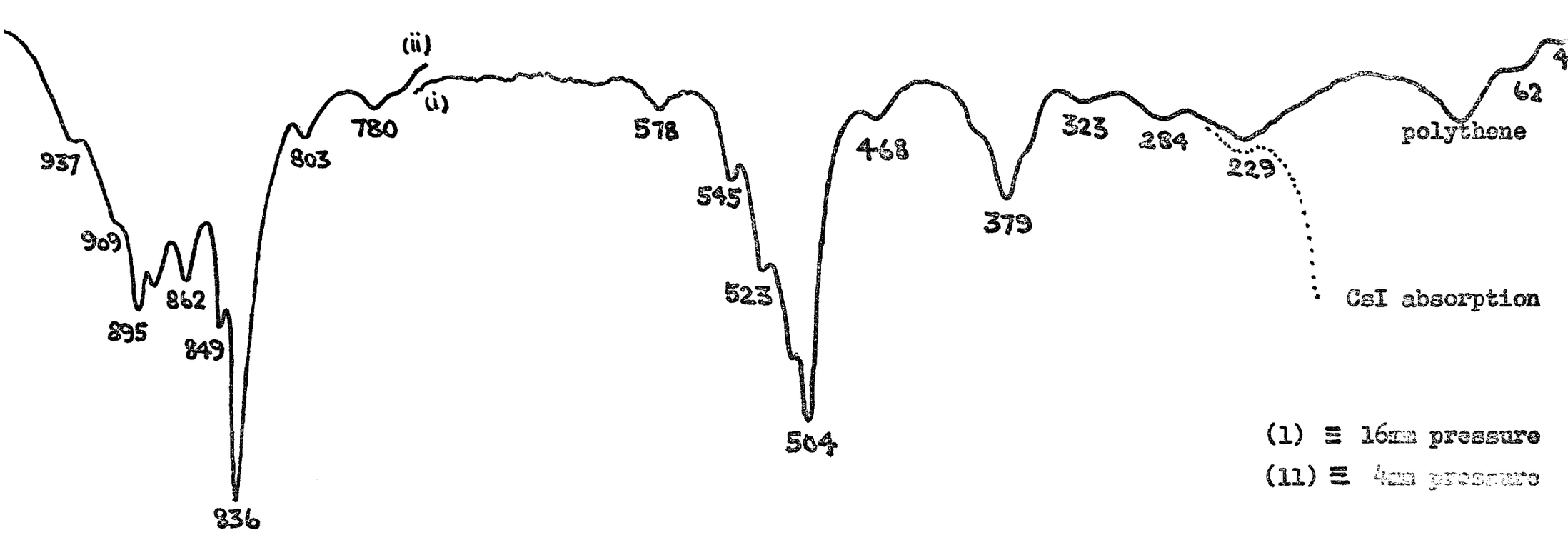


Figure 6G. Infra-Red Spectrum of $Pd(PF_3)_4$ Solid. (-196°C)

TABLE 6D

Infra-red spectrum of $Pd(PF_3)_4$ in the Solid State

Initial pressure of vapour before condensation = p_{mm}

p =	16 mm	4 mm	2 mm
	40 mw		
	62 mw		
	229 m,bd		
	284 mw		
	323 w		
	379 ms, bd	380 mw	
	468 mw		
	504 s	504 ms	502 mw
	523 m, sh	523 mw	525 w
	545 m	548 w	550 vw
	572 w		
	578 mw		
	609 vw		
	734 vw		
	750 w		
	767 w	770 vw	
	781 mw	780 w	
	803 mw	803 w	803 vw
	832	836 vs	834 w
	↓	849 m, sh	847 vw
	vs	862 m	
		883 m	
		895 ms	
	918	909 m, sh	908 mw
	936 ms, sh	937 m, sh	936 mw bd
	955 mw, sh		

1M solution of the liquid palladium compound in chloroform. The solid-state infra-red spectrum has rather fewer features than the corresponding Raman spectrum, but some of the strong Raman bands occur as weak features in the infra-red.

It was impossible to attempt a study of the breakdown of the polymers in the liquid state with increase in temperature, on account of the instability of the liquid over a small temperature range. Likewise, it was not feasible to study the vapour-state infra-red spectrum at high pressures, since above a pressure of 80 mm. Hg decomposition of the sample in the instrument was observed. At the highest pressure attainable with stability in the infra-red beam (circa 80 mm. Hg), the spectrum was essentially identical to those obtained at much lower pressures as regards the strongest features, although some weaker features, attributed to overtones and combinations, appeared in the higher-pressure spectra.

In the vapour-phase infra-red spectrum, the vapour conforms well to monomeric $Pd(PF_3)_4$, but the palladium-phosphorus stretching mode (ν_{18}) expected at $\sim$ 220 cm^{-1} was not observed. This feature appears at 229 cm^{-1} in the solid-state infra-red spectrum but is weaker than would be expected from a comparison with the $Pt(PF_3)_4$ analogue. A

direct comparison of the infra-red spectrum of the monomer with the vibrational spectra of the condensed-phase $Pd(PF_3)_4$, yields some useful information; perhaps the most important outcome of such a comparison is, that the P-F stretching region and to a lesser extent the PF_3-deformation region, are greatly broadened in the solid-state infra-red spectrum relative to the vapour-state spectrum. This would be a consequence of polymer-formation of the bridged-PF_3 type, $[Pd(PF_3)_4]_x$, of various chain-lengths (e.g. x = 2,3...). It is also possible to identify monomer features in the condensed-phase spectra, and by using the infra-red monomer and polymer spectra as templates, probable monomer features were extracted from the complexity of the condensed-phase Raman spectra.

In such a way the assignment of monomer $Pd(PF_3)_4$ given in Table 6E was constructed; it is emphasised that this assignment is tentative and is based on intuition and comparison with the other $M(PF_3)_4$ molecules. In the assignment, the a_1 modes were easily selected from the Raman spectrum by analogy with $Pt(PF_3)_4$; a possible frequency-value for the f_2-species rock, ν_{17}, was immediately suggested from such an analogy - being the band at 284 cm^{-1} in the infra-red (284, 287 cm^{-1} in the Raman spectrum of liquid, solid respectively).

TABLE 6E

Tentative Assignment for $Pd(PF_3)_4$ monomer

Class	ν	Mode	Raman	Infra-red
A_1	ν_1	ν P-F symmetric	958	inactive
	ν_2	δ PF_3 symmetric	545	
	ν_3	ν Pd-P symmetric	204	
A_2	ν_4	τ PF_3	inactive	inactive
E	ν_5	ν P-F asymmetric	852	inactive
	ν_6	δ PF_3 asymmetric	327/420	
	ν_7	ρ PF_3	-	
	ν_8	δ PdP_4	-	
F_1	ν_9	ν P-F asymmetric	inactive	inactive
	ν_{10}	δ PF_3 asymmetric		
	ν_{11}	ρ PF_3		
	ν_{12}	τ PF_3		
F_2	ν_{13}	ν P-F symmetric	914	904
	ν_{14}	ν P-F asymmetric	880	865
	ν_{15}	δ PF_3 symmetric	495/518	508
	ν_{16}	δ PF_3 asymmetric	390	389
	ν_{17}	ρ PF_3	284	284
	ν_{18}	ν Pd-P	222	229
	ν_{19}	δ PdP_4	-	-

Ware (75) has worked on $HCo(PF_3)_4$, which has C_{3v} symmetry, and reports finding PF_3 deformations up to 650 cm^{-1} in frequency. The appearance of features in the Raman spectrum of "$Pd(PF_3)_4$" in this region supports the conclusion that polymers of lower symmetry than T_d are formed in the condensed state.

This completes the experimental work on $M(PF_3)_4$ compounds. In the next Chapter some force-constant computation is described to determine how the metal-phosphorus bond-strength changes in the series Ni - Pd - Pt.

CHAPTER 7

Chapter 7

FORCE-CONSTANT CALCULATIONS ON $M(PF_3)_4$ MOLECULES

7(1) General Introduction

The traditional force-field problem is to solve for force-constants in a postulated quadratic force-field, given a set of vibrational frequencies corresponding to the normal modes of a molecule of a given molecular geometry. It is possible to calculate frequencies from any given set of force-constants, but the opposite process has always been a lengthy and unsystematic matter of trial and error. The number of force-constants in the approximate field is normally chosen to be less than the number of experimental frequencies, and so no exact solution will exist. Partly for this reason, and also because of the computational problems of solving simultaneous equations of different orders, no direct method is available for proceeding from frequencies to force constants. Trial values of the force-constants are thus, normally, used to calculate frequencies and then trial processes are applied to refine the frequencies so obtained to make them as close as possible to the experimental values.

By far the most generally useful data available for

the calculation of force constants are the normal vibration frequencies determined directly from Raman and/or Infra-red spectroscopy. Assignment of observed frequencies to the appropriate normal mode is often difficult, although group theory is of great help where some symmetry is present in the molecule.

The central task in the study of molecular vibrations is the determination of the potential energy function. This is a considerable problem, and the most general method of solution is to take the quadratic terms of a Taylor expansion in the coordinates chosen; then, using as many data as can be obtained for the molecule under consideration, it is possible to solve for the unknowns in the harmonic potential function. This process has been used by Mills (76) for CH_3F, where 20 pieces of information were used to solve for the 12 force constants in the symmetry co-ordinate representation. In practice, workers adopting this approach are severely restricted to dealing with small molecules of high symmetry; such molecules must normally contain hydrogen atoms, so isotopic substitution data may be used in the calculations. The resulting force constants are difficult to visualise as they are expressed in terms of symmetry coordinates and not in terms of the simpler valency coordinates.

The most common approach to the problem of the potential function is to accept that there are insufficient data to solve for the general harmonic functions, and then to try to find physically satisfying models involving fewer force constants. The simplest postulates are those of the simple valency and central force-fields (SVFF and CFF respectively). The SVFF is often remarkably successful and sometimes enables frequencies to be predicted to within 5% of their true values. The forces postulated for this field are simply those resisting stretching of the bonds and deformations of the interbond angles. The CFF postulates forces acting only along lines drawn between atoms of the system; this approximation is not very satisfactory and fails, for example, to account for the bending frequency in linear molecules. In the Urey-Bradley Force Field (UBFF), the above two force fields are combined successfully and allows for the steric effects of non-bonded atoms. Considerable improvements in the description of vibration frequencies may be obtained by the introduction of valency interaction terms (cross terms) of the stretch-stretch, stretch-bend type into the simple valency F matrix. Terms which are known to be large in one molecule are likely to figure in related molecules and it seems reasonable to transfer such terms in these cases.

7(2) The Calculation of Force Constants from Frequencies

Consider a molecule made up of N mass points which may be defined by the 3N coordinates, q. Of these, 3N-6 coordinates will be concerned with internal motions only, and they are defined as the internal coordinates. The most commonly used internal coordinates are changes of bond angles and bond lengths.

The potential energy is given by

$$2V = \sum f_{ij} q_i q_j$$

and in matrix form this becomes $2V = \tilde{R}FR$, where F is the matrix of force constants f_{ij}, and R is the matrix of the q's. The kinetic energy of the system is written as

$$2T = \dot{\tilde{R}} G^{-1} \dot{R}$$

where G is Wilson's G matrix.

It was shown in Chapter 1 that the equation

$$\sum_{j}^{3N-M} (f_{ij} - \delta_{ij}\lambda)A_j = 0, \quad i = 1,2,3\ldots(3N-6)$$

described a set of homogeneous linear equations in the (3N-6) unknown amplitudes A_j. An essential condition for these equations to have a meaningful solution is that the determinant of the coefficients of the A_j's shall vanish,

otherwise the solution is the trivial one, $A_j = 0$, corresponding to no vibrations. The determinant will only be zero for certain values of λ, λ_1, $\lambda_2 \ldots \lambda_{3N-6}$. These λ's are the latent roots of the matrix GF, and correspond to the normal vibration frequencies, given by $\lambda = 4\pi^2\nu^2$, where ν is a normal frequency of the molecular system.

Thus, knowing F and G, we are in a position to compute the normal frequencies of vibration for any molecular system. However, for a molecule of any size, F and G tend to be very large and the computation of roots is space-wasting and inefficient. Symmetry considerations can be used to overcome this problem; by choosing a suitable change of co-ordinate basis, it is possible to factor the secular determinant into a series of non-mixing blocks along the diagonal. Each block represents a secular equation of lower order and may be treated separately from the others. The new coordinates are symmetry coordinates and are defined by,

$$S = UR$$

If U is chosen correctly it is possible to obtain a degree of maximum simplification of the problem. The U matrix is set up according to standard procedures based upon Group Theory (4). Using symmetry coordinates as a basis the theory

of molecular vibrations is precisely similar to that for internal coordinates. We define new $\mathcal{G}, \mathcal{F}$ matrices as follows:

$$2T = \dot{\tilde{S}} \mathcal{G}^{-1} \dot{S} \quad \text{and} \quad 2V = \tilde{S} \mathcal{F} S$$

and $\mathcal{G} = UG\tilde{U}$, $\mathcal{F} = UF\tilde{U}$.

The secular equation now has the form

$$| \mathcal{G}\mathcal{F} - E\lambda | = 0.$$

In the above relationship it is convenient to use the following units in the computations. $\mathcal{G}$ is expressed in inverse atomic weights and λ is taken as $\nu^2/10^6$. We can therefore write

$$| \mathcal{G}\mathcal{F}z - E\lambda | = 0$$

where z is given by

$$z = 1/4\pi^2c^2.10^6.m_H = 1.69765 \times 10^{-5}$$

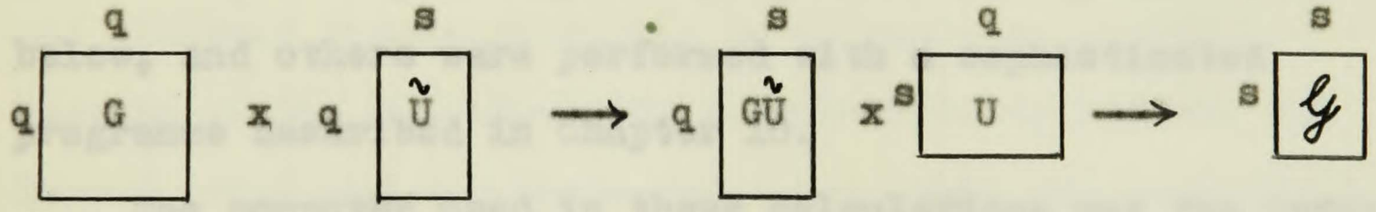
The force constants are expressed in "z-units" for insertion into the calculation, and to convert them to dynes/cm it is necessary to multiply the force constants by 1/z.

In all force-field calculations carried out in the course of the present study, the secular equations were set up in terms of a symmetry coordinate basis.

Construction of $\mathcal{G}$

The G matrix is first set up from the internal coordinates, q; this is a tedious task, especially for large unsymmetrical molecules. The fatigue factor in working up the G matrix results in errors, and the necessity for re-checking many times is called for. There are, fortunately, only a limited number of internal-coordinate types and Decius has tabulated (77,4) lists of G-matrix elements in terms of variable bond-parameters (Δ r change in length, $\Delta\alpha$ in angle) and atomic masses.

The U matrix is constructed and the following transformations are performed by hand:



Redundancy

This problem arises when the (3N-6) internal coordinates are in excess of the number required. Redunancies are removed from the final $\mathcal{G}$ and $\mathcal{F}$ matrices by application of redundancy conditions (4), which are calculated from symmetry coordinate relationships.

The $\mathcal{F}$ matrix

This is constructed in precisely the same way as is the $\mathcal{G}$, from the F matrix. On a SVFF basis, the final $\mathcal{F}$ matrix

has non-zero entries along the diagonal only ("diagonal field"), the force constants appearing with unit coefficients.

The Machine Computation of Force Constants

Before the advent of high-speed digital computers, force constant calculations were a laborious task, especially where the degree of the factored equations could not be reduced to three or less. Using a good electric desk calculator, the extraction of the roots of a 3 x 3 matrix takes about 2 to 3 hours. In the present work some calculations were accomplished using a 'Marchant' calculator, some using a simple computer programme briefly described below, and others were performed with a sophisticated programme described in Chapter 10.

The computer used in these calculations was the Oxford University, English Electric KDF9, and the language was Extended Mercury Autocode. The programme and numerical data were input on five-hole paper tape. The general routine for calculating roots and vectors of a matrix consists of a matrix iteration technique; a standard routine was already available, written by Dr.J.S.Rollett for Mercury, based on Given's process for extraction of roots and vectors from a real, symmetric matrix. The programme multiplied G and F, and symmetrised GF. Roots and vectors were

produced after minutes of computer time (circa 2 minutes for a 7 x 7 matrix).

Suitable modification of the force-constant values and re-insertion into the computer gave, after some 6-12 cycles, a final "best-fit" on frequency-values. Since the number of force-constants is normally much greater than the number of available frequencies, an approximation involving the selection of certain force-constants (those on the $\mathfrak{F}$ diagonal in a SVFF calculation) must be made. This means that no value of the constants will, in general, fit the frequencies exactly. The criterion of "best fit" is required, for which the root mean square (RMS) deviation between calculated and observed frequency-values is as small as possible. Because of the non-linearity in relationship between the latent roots and the force-constants it is not possible to obtain the "best fit" with only one modification to the initial force-constant set. Successive modifications were thus necessary with gradual convergence to the "best fit".

7(3) Force-constant calculations on $M(PF_3)_4$ compounds

The internal co-ordinates are arranged in sets as follows,

Number	Symbol	Type
4	ΔR	M-P stretch
12	Δr	P-F stretch
6	$\Delta \theta$	P-M-P bend
12	$\Delta \alpha$	F-P-F bend
12	$\Delta \beta$	F-P-M bend
4	$\Delta \gamma$	F-P-M torsion
50		

(3N-6) gives 45 vibrational modes, therefore there are 5 redundancies. These are accounted for by the 5 tetrahedral groupings of angles, i.e. 4 at the P atom and 1 at the M atom. The redundancy conditions then are,

$$\sum\Delta(\alpha+\beta) = 0, \quad \sum\Delta\theta = 0$$

The $M(PF_3)_4$ molecule and the internal coordinates are shown in Figure 7A.

The G matrix is a 50 x 50 block, symmetrical about the diagonal, and is too large to reproduce here. The γ coordinate may be omitted as the PF_3 torsional vibration is inactive in the infra-red and in the Raman. In the present calculation, the A_1 species vibrations only will be considered, these being,

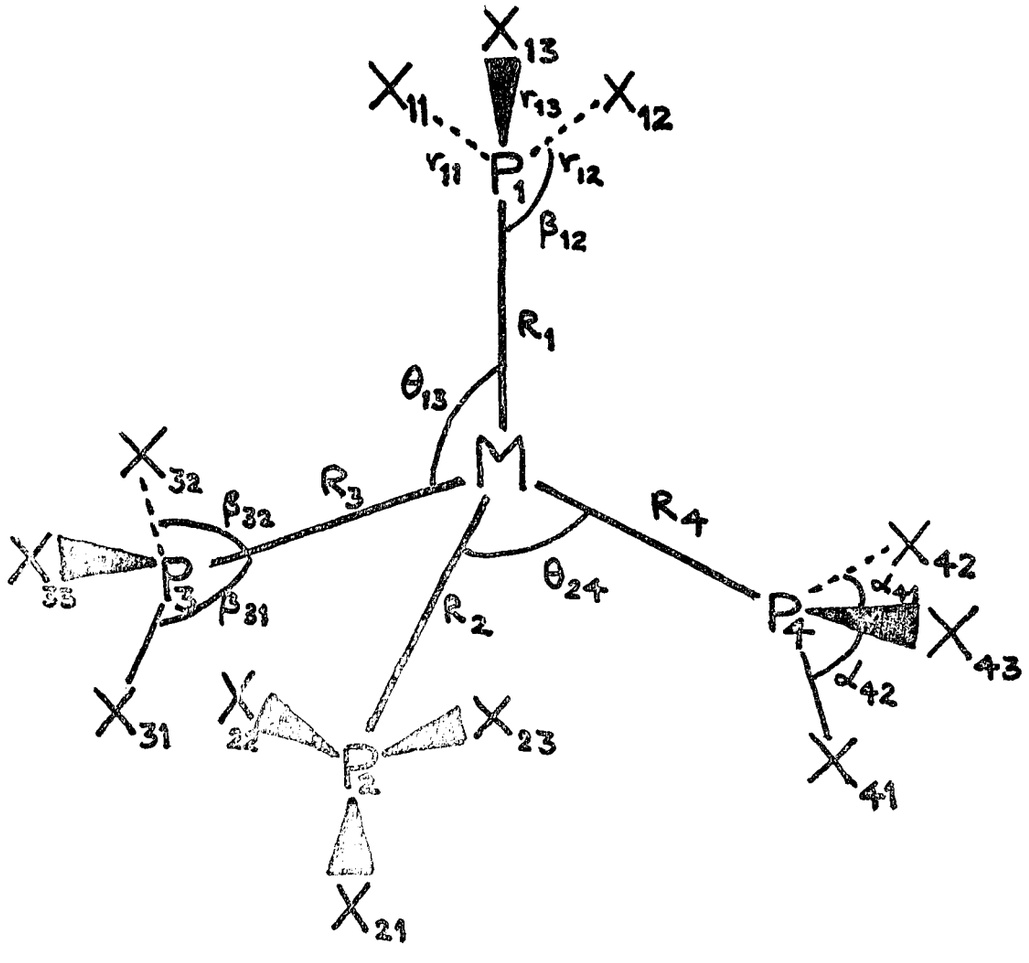


Figure 7A. $M(PF_3)_4$ Internal Coordinates.

ν_1 P-F symmetric stretching

ν_2 PF_3 symmetric deformation

and ν_3 M-P symmetric stretching

The symmetry coordinates for the A_1 block are,

$$S_1 = \frac{\Delta}{\sqrt{12}} (r_{11} + r_{12} + r_{13} + r_{21} + r_{22} + r_{23} + r_{31} + r_{32} + r_{33} + r_{41} + r_{42} + r_{43})$$

$$S_2 = \frac{\Delta r}{\sqrt{24}} (\alpha_{11} + \alpha_{12} + \alpha_{13} + \alpha_{21} + \alpha_{22} + \alpha_{23} + \alpha_{31} + \alpha_{32} + \alpha_{33} + \alpha_{41} + \alpha_{42} + \alpha_{43} - \beta_{11} - \beta_{12} - \beta_{13} - \beta_{21} - \beta_{22} - \beta_{23} - \beta_{31} - \beta_{32} - \beta_{33} - \beta_{41} - \beta_{42} - \beta_{43})$$

$$S_3 = \frac{\Delta}{2} (R_1 + R_2 + R_3 + R_4)$$

From the redundancy conditions $S_\gamma = 0$, and the S_2 is compounded as follows,

$$S_\alpha = \frac{1}{\sqrt{12}} \sum \Delta r\alpha$$

$$S_\beta = \frac{1}{\sqrt{12}} \sum \Delta r\beta$$

and $S_\alpha + S_\beta = 0$

$$S_{\alpha\beta} = S_2 = \frac{1}{\sqrt{2}} (S_\alpha - S_\beta) = \frac{\Delta r}{24} (\sum \alpha - \sum \beta)$$

These symmetry coordinates agree with those given for the analogous molecules CMe_4 and $SiMe_4$ by Murata (78,79). In the Woodward-Hall paper (43) on $Ni(PF_3)_4$, there seems to be a mis-print, as the S_2 is not properly normalised, containing a $1/\sqrt{12}$ factor instead of $1/\sqrt{2}.1/\sqrt{12}$.

The U matrix is thus a 50 x 3, which leaves the final $\mathcal{G}$, a 3 x 3 matrix, shown in Table 7A. In this reduction process the G elements are represented by symbols, which are later evaluated in terms of the Decius expressions. Likewise, the F matrix is a 50 x 50 which reduces to a 3 x 3 by an analogous procedure. Neglecting off-diagonal terms in the $\mathcal{F}$ matrix, we get the final $\mathcal{F}$ shown in Table 7A.

The $\mathcal{G}$ matrix agrees with that quoted by Murata for CMe_4, and also with Long et al.(80) for CMe_4. The $\mathcal{F}$ matrix, of course, depends on the force-field selected and the interaction constants (if any) considered.

Computation

The matrix, containing terms in μ_p, μ_F only, is identical for all three molecules $Ni(PF_3)_4$, $Pd(PF_3)_4$ and $Pt(PF_3)_4$. The $\mathcal{F}$ matrix elements were selected from the work of Woodward and Hall (43) on $Ni(PF_3)_4$. To test the computer programme, the force-constant values of Woodward and Hall were used; the frequency-values for $Ni(PF_3)_4$ were obtained.

TABLE 7A.

$\mathcal{G}$ and $\mathcal{F}$ matrices for $M(PF_3)_4$

$\mathcal{G}_{A_1}$	S_1	S_2	S_3
S_1	$1/3\,\mu_P + \mu_F$	$-4/3\,\mu_P$	$-1/\sqrt{3}\,\mu_P$
S_2	$-4/3\,\mu_P$	$2\mu_F + 16/3\,\mu_P$	$4/\sqrt{3}\,\mu_P$
S_3	$-1/\sqrt{3}\,\mu_P$	$4/\sqrt{3}\,\mu_P$	μ_P

$\mathcal{F}_{A_1}$	S_1	S_2	S_3
S_1	f_{11}		
S_2		f_{22}	
S_3			f_{33}

In Table 7B the results are tabulated. For all three molecules a very good "best fit" was obtained. Before an attempt is made to analyse the results of Table 7B, the force-constants of the free ligand PF_3 should be obtained. Earlier work on these lines used the erroneous assignment of PF_3, and the next few pages are devoted to the calculation of the force constants of PF_3 using the correct vibrational assignment.

7(4) Force constants of PF_3

In an early normal co-ordinate analysis of PF_3, Venkateswarlu (81) used the erroneous assignment of Yost and Anderson. A later analysis by Mirri et al. (82) used the correct assignment, but there is a discrepancy between the $\mathcal{F}$ matrix elements (off-diagonal terms) quoted by these two groups of workers. Later work by van der Kelen (83) on $AsMe_3$ and $AsCl_3$ agrees in the $\mathcal{F}$ matrix elements with Mirri.

To settle the question it was decided to set up the $\mathcal{F}$ matrix from first principles and calculate the force constants of PF_3. The C_{3v} character table gives four vibrations for PF_3 (Chapter 3), 2 of species a_1 and 2 of species e. The four symmetry coordinates selected were:

TABLE 7B.

Force-constants of $M(PF_3)_4$

	Initial f.c.set (z units)			Final f.c.set (z units)			No.of mods.	Calc. Frequencies			Obs. Frequencies		
	f_1	f_2	f_3	f_1	f_2	f_3		ν_1	ν_2	ν_3	ν_1	ν_2	ν_3
$Ni(PF_3)_4$	13.5131	1.2205	3.3452	13.1198	0.9157	4.5923	9	954	534	195	954	534	195
$Pd(PF_3)_4$	12.9943	0.7742	6.3299	13.1258	0.8944	5.3750	7	958	543	204	958	545	204
$Pt(PF_3)_4$	13.1748	0.9345	5.0162	13.0102	0.8188	6.4817	10	958	546	213	958	546	213

$$a_1 \quad \begin{cases} S_1 = \dfrac{\Delta}{\sqrt{3}} (R_1 + R_2 + R_3) \\ S_2 = \dfrac{\Delta R}{\sqrt{3}} (\theta_{12} + \theta_{23} + \theta_{31}) \end{cases}$$

$$e \quad \begin{cases} S_{3a} = \dfrac{\Delta}{\sqrt{6}} (2R_1 - R_2 - R_3) \\ S_{4a} = \dfrac{\Delta R}{\sqrt{6}} (2\theta_{23} - \theta_{12} - \theta_{31}) \end{cases}$$

All are properly <u>oriented</u> (4) with respect to the symmetry operations of the point group C_{3v}. The 6 x 6 G matrix of internal coordinates is symmetrised to a 4 x 4 $\mathcal{G}$ matrix, and a similar process with the F matrix yields a 4 x 4 $\mathcal{F}$. Both $\mathcal{G}$ and $\mathcal{F}$ matrices are shown in Table 7C. It should be noted that the 4 x 4 final matrix factorises into two 2 x 2 blocks, corresponding to the a_1 and e species vibrations.

The $\mathcal{F}$ matrix is identical with that used by Mirri, and by van der Kelen. It should be noted that, in this case, there are 6 force constants in the $\mathcal{F}$ matrix but we only have 4 vibrational frequencies. Two of the force constants must, therefore, be discarded and, in the present work, the off-diagonal $k_{R\theta}$ terms were neglected. The $\mathcal{F}$ matrix now contains the following:

$$k_R, \; k_{RR}, \; k_\theta, \; k_{\theta\theta}$$

in a SVFF diagonal array.

TABLE 7C

$\mathcal{G}$ and $\mathcal{K}$ matrices for PF_3

$\mathcal{G}$

$\mu_F + \frac{1}{3}\mu_P$	$-\sqrt{8}/3\,\mu_P$
$-\sqrt{8}/3\,\mu_P$	$\mu_F + \frac{8}{3}\mu_P$

$\mu_F + \frac{4}{3}\mu_P$	$\frac{4}{3}\sqrt{2}\,\mu_P$
$\frac{4}{3}\sqrt{2}\,\mu_P$	$\frac{5}{2}\mu_F + \frac{8}{3}\mu_P$

$\mathcal{K}$

$k_R + 2k_{RR}$	$k_{R\theta} + 2k'_{R\theta}$
$k_{R\theta} + 2k'_{R\theta}$	$k_\theta + 2k_{\theta\theta}$

$k_R - k_{RR}$	$k_{R\theta} - k'_{R\theta}$
$k_{R\theta} - k'_{R\theta}$	$k_\theta - k_{\theta\theta}$

The extraction of the roots from the $\mathcal{GF}$ matrix is easily accomplished as follows:

If λ_1, λ_2 are the roots of the a_1 block, and λ_3, λ_4 the roots of the e block, we can write

$$G_{11}F_{11} + G_{22}F_{22} + 2F_{12}G_{12} = \lambda_1 + \lambda_2$$

and $(F_{11}F_{22} - F_{12}^2)(G_{11}G_{22} - G_{12}^2) = \lambda_1 \lambda_2$,

$$G_{33}F_{33} + G_{44}F_{44} + 2F_{34}G_{34} = \lambda_3 + \lambda_4$$

and $(F_{33}F_{44} - F_{34}^2)(G_{33}G_{44} - G_{34}^2) = \lambda_3 \lambda_4$.

Substituting the known G-element values and λ-values (from the vibrational frequencies), the F-elements can be deduced.

Table 7D gives the results of the present investigation and other work on the force constants of PF_3. It is immediately apparent, from the results of Mirri and Venkateswarlu in Table 7D, that the revised assignment has had quite a profound effect on the magnitude of the force constants of PF_3; the new force constants should hence be considered in any discussion of the force constants of $M(PF_3)_4$ compounds.

TABLE 7D.

Force Constants of PF_3

	k_R	k_{RR}	k_θ	$k_{\theta\theta}$	$k_{R\theta}$	$k'_{R\theta}$
Venkateswarlu (81)	4.590	0.382	1.005	0.182	-	-0.119
Mirri et al. (82)	5.342	0.266	1.518	0.400	0.207	-0.470
Present work	5.170	0.811	0.799	0.195	-	-

7(5) Discussion of Force Constants in $M(PF_3)_4$

The final "best fit" force constant values given in Table 7B are there expressed in 'z'-units; in dynes/cm these become,

	$Ni(PF_3)_4$	$Pd(PF_3)_4$	$Pt(PF_3)_4$	
k_{P-F}	7.73	7.73	7.66	$\times 10^5$ dynes/cm
$k_\delta/r^2_{PF_3}$	0.53	0.53	0.48	$\times 10^5$
k_{M-P}	2.71	3.17	3.82	$\times 10^5$

Force constants for typical double-bond vibrations, such as C=C< and >C=O, average about 10×10^5 dynes/cm, which is well above the values quoted for the zerovalent meta-phosphorus stretching force constants in the above table. A study of the values of the force constants corresponding to accepted single and double bonds merely suggests that the metal-phosphorus bonds, in the $M(PF_3)_4$ compounds investigated above, are single.

When a ligand L donates a pair of electrons to a metal or an electron-accepting group M, the resulting formal positive charge on L would mean a greater attraction for the atom Y, where Y-L is a bond within the ligand and Y is more electronegative than L (e.g. M-P-F situation in the trifluorophosphine metals). This increased attraction would be reflected in a shorter bond length for Y-L than in the free ligand, and a <u>higher</u> force constant. Because of

uncertainty in the importance of interaction terms, a small change in the force constant for a bond in the free and bound ligand cannot be accepted as greatly significant. For example, in the case of borine carbonyl, $BH_3.CO$, regarded as a fair subject for the above mechanism, two independent calculations (84,85) produced values for k_{C-O} equal to 18.97×10^5 dynes/cm and 17.98×10^5 dynes/cm. These values are to be compared with 18.55×10^5 dynes/cm for carbon monoxide (86). In the case of borine carbonyl, one would expect the k_{C-O} to increase relative to the free CO ligand, but the unaffected C-O bond length (87) indicates only minor changes to the C-O group on coordination.

If like coordination were responsible for the bonding in $Ni(CO)_4$ only a small effect on k_{C-O} would be expected. In fact, the k_{C-O} force constant in nickel carbonyl is much less than that of the free ligand, being 16.01, 15.89×10^5 dynes/cm (44,88) respectively. In this case, however, π-bonding between the nickel and carbon is possible only if a p-orbital of carbon is released from π-bonding with oxygen. This results in a lowering of the C-O bond order and the force constant of C-O in nickel carbonyl approximates to that of k_{C-O} in CO_2 (ref.5), the latter being 15.5×10^5 dynes/cm.

In the case of the PF_3 ligand, as discussed in Chapter 3, there is evidence that the donor properties are weak towards acceptors where only simple σ-bond formation is possible. This has been accounted for by the electronegativity of the fluorine atoms, which affect the availability of the lone pair on the phosphorus for coordinate-bond formation. It seemed likely that the stability of the $M(PF_3)_4$ compounds was due to π-bonding between the metal and phosphorus atoms. There is no evidence against this view, but the force constants k_{M-P} for the $M(PF_3)_4$ series while not denying the existence of such bonding, do little to confirm this hypothesis.

With CO as ligand, the bond-formation to the metal (such as nickel) is accompanied by a lowering of k_{C-O} as explained above. With PF_3 however, the effect upon k_{P-F} is surprising. Formation of the dative σ-bond Ni$\leftarrow$P should result in an increase in k_{P-F} above that for PF_3 alone, since the electronegative fluorine atoms are faced with a formal positive charge on the P atom and this would result in a shortening of the P-F bond. Formation of the π-bond Ni$\rightarrow$P should, however, decrease k_{P-F} by the reverse effect. Reference to borine carbonyl, suggests that the former of these two effects is likely to be small; and on these grounds one would reasonably expect that the overall result of

π-bond formation between nickel and phosphorus would be a k_{P-F} which was <u>less</u> than the P-F stretching force constant in PF_3. In fact, as is seen from the results in this Chapter, in <u>all</u> the $M(PF_3)_4$ cases the k_{P-F} is 7.7×10^5 dynes/cm, which is much <u>higher</u> than the P-F force constant in PF_3 itself.

This fact remains inexplicable, although a possible key to solution is given in Table 7D. The interaction constants of the stretch-stretch and stretch-bend type are quite large in free PF_3, and could they not be even larger in a molecule such as $Ni(PF_3)_4$, where there are four PF_3 groups in close proximity and bonded to the same metal? In such a case, it might be expected that non-bonded interactions of the Urey-Bradley type might be important.

A similar situation could also apply to the PF_3 deformation force constant in $M(PF_3)_4$ molecules, which is <u>lower</u> than that of PF_3 itself. Here, however, the comparison is further complicated by the fact that we are trying to compare dissimilar force constants. The deformation force constant (k_δ/l^2) in free PF_3 consists of a k_α term, with a $k_{\alpha\alpha}$ type interaction constant; whereas in the $M(PF_3)_4$ compounds the k_δ/l^2 for the PF^3 deformation is a <u>compound</u> force constant, consisting of k_α and k_β terms, plus interaction constants i.e.

the deformation involves the force constant, k_β, for Ni-P-F bending.

Examination of the vectors associated with each symmetry coordinate for each force constant gives a measure of the "purity" of each mode. In Table 7E these vectors for the A_1 group modes are given for the two extreme members of the $M(PF_3)_4$ series, $Ni(PF_3)_4$ and $Pt(PF_3)_4$. In both cases there is no outstanding vector contributing to S_2, the symmetry coordinate for PF_3 deformation. Whereas the P-F stretching and M-P stretching modes are quite pure, the PF_3 deformation mode is extensively mixed. Effectively, the vectors indicate that there is little true deformation in the S_2 coordinate, and that the k_{P-F} and k_{M-P} force constants control the vibration. In the SVFF method the assumption is that k_i steers ν_i and has no effect on $\nu_j, \ldots \nu_k$ etc., where all ν's are frequencies of modes of the same symmetry species. In the case of $M(PF_3)_4$, however, the interaction of k_1 and k_3 with k_2 (the 'deformation' mode) is very large - so large, as to make the assignment of the ν_2 frequency, corresponding to the S_2 coordinate, as a 'deformation' a questionable one. It would perhaps be more correct to term the ν_2 frequency a "breathing mode" of the PF_3, involving much metal-phosphorus participation. This point will occur again in Chapter 10 in connection with $Ni(PCl_3)_4$.

TABLE 7E.

$M(PF_3)_4$ Vectors

	A_1 species		
	S_1 P-F stretching	S_2 PF_3 deformn.	S_3 Metal-P stretching
(a) $Ni(PF_3)_4$	3.387233	-0.256991	-0.495952
	-1.270520	-0.756629	-1.082441
	-0.170978	0.531196	-1.781756
(b) $Pt(PF_3)_4$	3.327882	-0.234317	-0.727718
	-1.382576	-0.631488	-1.540336
	-0.154404	0.604253	-1.891957

The discussion must rest at this point, with the hypothesis that interaction force constants in the $M(PF_3)_4$ compounds might well account for the surprising force-constants of the PF_3 modes. The proven "impurity" of the deformation mode makes nonsense of the idea of Miller (114) that the low deformation force-constant in these compounds might be due to a change in the "umbrella-angle" of the PF_3 group.

Whereas the P-F stretching force constant remains practically constant along the series from nickel to platinum, the metal-phosphorus force constant increases steadily, but attains only the value of 3.8 dynes/cm ($\times 10^5$), which is still in the region of single-bond force constants. The frequency change of the PF_3 modes along the series again provides evidence for the conclusions drawn above, concerning the deformation mode. On comparing $Ni(PF_3)_4$ and $Pt(PF_3)_4$, the following is noted:

	$Ni(PF_3)_4$	$Pt(PF_3)_4$	$\Delta\nu$	
$\nu_1(cm^{-1})$	954	958	+4	(0.4%)
$\nu_2(cm^{-1})$	534	546	+12	(2.4%)

Despite the small increase in ν_1 of 0.4%, ν_2 is affected by 2.4% in going along the series from nickel to platinum. This furnishes evidence of the participation in the deformation

mode, of metal-phosphorus stretching; the increase noted above, in sign if not in magnitude, would be expected since the k_{Pt-P} is some 40% greater than k_{Ni-P}.

CHAPTER 8

Chapter 8

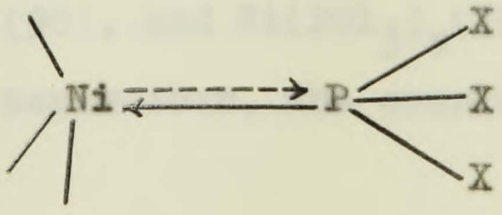
TETRAKISTRICHLOROPHOSPHINENICKEL°

$Ni(PCl_3)_4$

8(1) Introduction

Tetrakistrichlorophosphinenickel° was the earliest member of the $M(PX_3)_4$ type compounds to have been prepared (33). Ten years elapsed before the vibrational spectrum was investigated; the infra-red in the phosphorus-chlorine stretching region was reported by Seel et al.(44). No Raman data have been reported, probably for reasons which will be seen later.

In this work it was decided to investigate the vibrational spectra of $Ni(PX_3)_4$ molecules, where X is halogen, and attempt to relate the effects of the substitution of X = Cl, Br, on the nickel-phosphorus bond strength. As in the $M(PF_3)_4$ molecules, the bonding situation can be considered in terms of the electro-negativity of the halogen atom concerned, and the possibility of back-donation from the nickel atom to the phosphorus atoms. For example, in



the nickel-phosphorus bond is strengthened by back-donation, which decreases the P-X strength. However, the nature and electronegativity of atom X will affect the lone-pair available for donation to form the P-Ni bond. Thus, PCl_3 is a better donor than PF_3 (cf. Chapter 3), but since Cl < F in electronegativity the phosphorus will be less inclined to accept the back-donation from nickel.

A study of the $Ni(PX_3)_4$ series could illustrate these opposing effects with change of X, by the calculation of force constants from the observed vibrational spectra. Wilkinson (89) considered the stabilities of the compounds:

$$Ni(PF_3)_4 > Ni(PCl_3)_4 > Ni(PBr_3)_4$$

and considered that the highly-electronegative fluorine atoms made the vacant acceptor orbitals on the phosphorus more available for back-donation from the nickel 3d-orbitals.

8(2) The Preparation of $Ni(PCl_3)_4$

The compound was prepared by Irvine and Wilkinson in 1951 (32) by the reaction of nickel carbonyl with phosphorus trichloride. The substitution of nickel carbonyl by PCl_3 has been studied (90), and $Ni(PCl_3)_x(CO)_{4-x}$ have been prepared (39) by Meriwether, who concluded from a study of

the properties of such compounds that σ-bonding is more important than π-bonding for the Ni-P bond.

In an attempted synthesis of $Ni(PCl_3)_4$, whereby $Ni(CO)_4$ was heated with PCl_3 in a sealed tube, very little product was obtained since the CO was not allowed to escape (32).

$$Ni(CO)_4 + 4PCl_3 \rightleftharpoons Ni(PCl_3)_4 + 4CO$$

The reaction proceeds to completion in the liquid phase and in the present work the following method was adopted (32,91):

13 ml. of nickel carbonyl (17 gm., density 1.32 gm./ml.) was syringed into a 100 ml. flask cooled in ice-water. Care should be taken during this operation since nickel carbonyl is very toxic, decomposing in the lungs to give nickel metal and releasing carbon monoxide into the bloodstream. The apparatus in Figure 8A was set up in a fume cupboard, and excess PCl_3 (circa 35 ml.) added to the carbonyl. The flask was quickly attached to the two condensers 'in tandem', the exit tube leading to the air valve of a Bunsen burner.

The reaction mixture evolved carbon monoxide in the cold; there was no rise in temperature and evolution of CO decreased with time. The carbon monoxide and nickel carbonyl vapours are burned in the Bunsen flame.

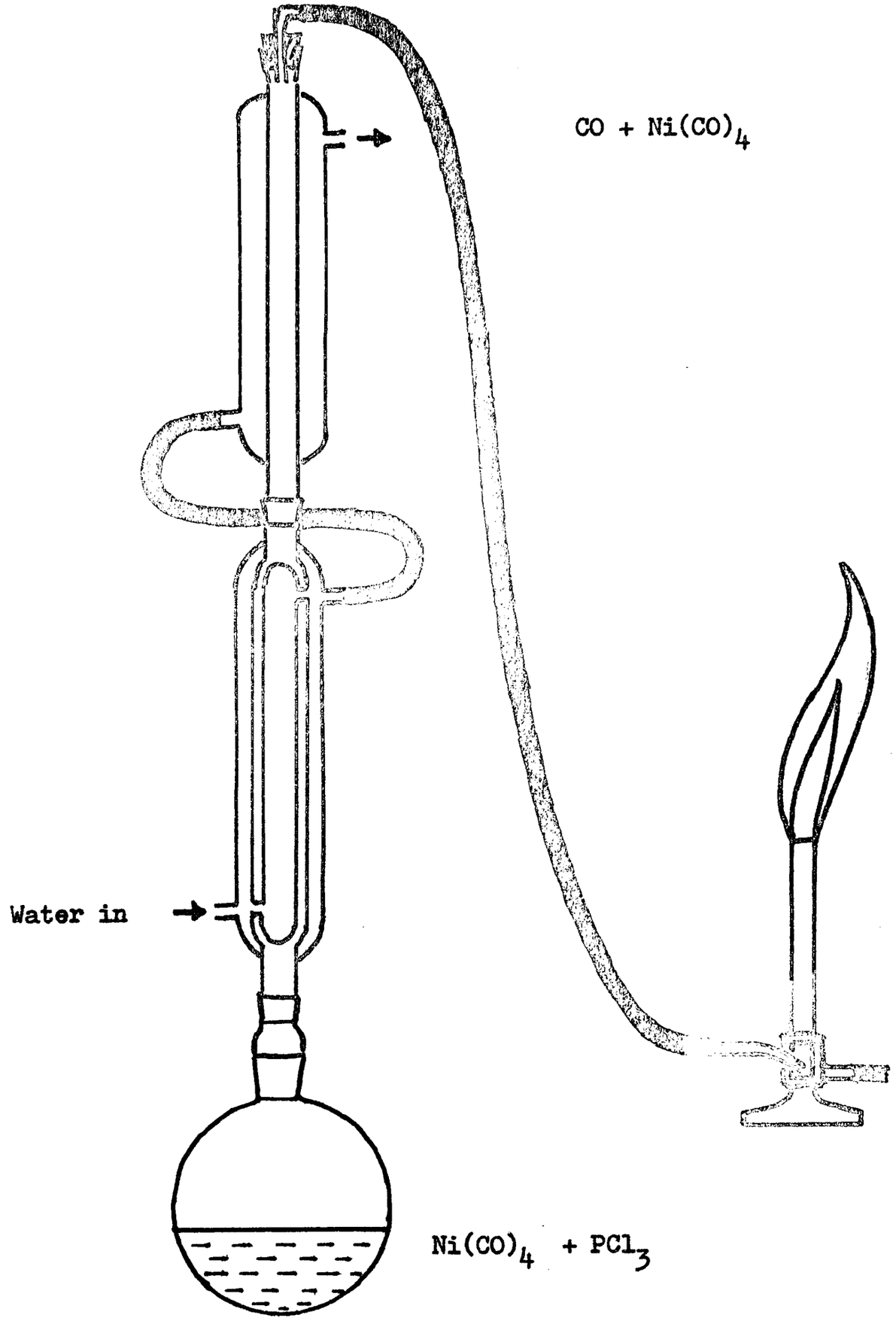


Figure 8 A. The Preparation of $Ni(PCl_3)_4$

After standing for two hours at room temperature, the reaction was completed by raising the temperature gently. The solution was refluxed at 60°C for one hour; when nickel begins to appear on the walls of the flask further heating is unprofitable. On cooling, the orange solution becomes a solid yellow mass, which was recrystallised from a large quantity of pentane (400 ml.) at acetone/CO_2 temperatures (-80°C). The last traces of PCl_3 and pentane were removed by pumping on the crystals, which were stored in a vacuum desiccator or a sealed tube. Yields are 86%-90% of theoretical (61 gm.).

Analysis was performed for nickel, phosphorus, and chlorine by standard procedures. By dissolving $Ni(PCl_3)_4$ in HNO_3/H_2O_2 the analysis for nickel and phosphate can be carried out; nickel is precipitated as the dimethylglyoxime complex, and phosphorus as magnesium ammonium phosphate. Chlorine is determined by reacting the compound with NaOH, and precipitating as the silver salt.

Result

	Found%	Calculated for $Ni(PCl_3)_4$
Nickel	9.69	9.65
Phosphorus	20.13	20.38
Chlorine	69.62	69.97

8(3) Solution properties of $Ni(PCl_3)_4$

Tetrakistrichlorophosphinenickel° is a pale yellow, thermochroic, crystalline solid which becomes white at -30°C. The crystals are stable to air and also to water, are non-volatile, and are thermally stable below 120°C, when PCl_3 is evolved.

Solutions can be made in benzene, carbon tetrachloride, pentane, cyclohexane - but all are unstable and decompose slowly at room temperature (rapidly on warming, depositing metallic nickel). In oxygenated solvents, such as alcohol or acetone, rapid decomposition occurs and a green solution is produced. Carbon disulphide reacts very rapidly to give nickel metal.

A molecular weight measurement in benzene indicates that $Ni(PCl_3)_4$ is monomeric in this solvent (40). The behaviour of its solutions in various solvents is illustrated below:-

* CCl_4	f.soluble	unstable
* $CHCl_3$	soluble	unstable
* C_6H_6	soluble	f.stable
Cyclohexane	soluble	unstable
CS_2	soluble	v.v.unstable
DMF	soluble	v.v.unstable
$MeNO_2$, MeCN	insoluble	
Decalin	v.soluble	f.stable

* possible Raman solutions; f = fairly; v = very.

The instability of the solutions is manifest in the formation of a turbidity, which develops in a matter of minutes only at room temperature. Before any Raman work was possible the question and extent of this turbidity had to be investigated.

Although the crystalline $Ni(PCl_3)_4$ itself is unaffected by water, it was thought at first that perhaps a trace of water in the solvents would react with the solution. This theory was soon disproved by the observation of turbidity in solutions of the crystals in vacuum-distilled solvents. Another possibility, that moist air could be the cause of the decomposition, was investigated by the construction of the apparatus in Figure 8B, for the preparation of Raman solutions of $Ni(PCl_3)_4$ in an air-free, dry, atmosphere.

Before use the whole apparatus was dried in an oven and allowed to cool in a desiccator. The selected solvent, e.g. decalin, was dried over P_2O_5 or sodium under vacuum and purged with nitrogen. With all taps open, solid $Ni(PCl_3)_4$ was introduced onto the sinter, and the whole apparatus purged with O_2-free nitrogen, dried by bubbling through sulphuric acid and finally passed through a copper coil refrigerated in an acetone/CO_2 bath. The de-oxygenated solvent was syringed through a rubber serum cap onto the

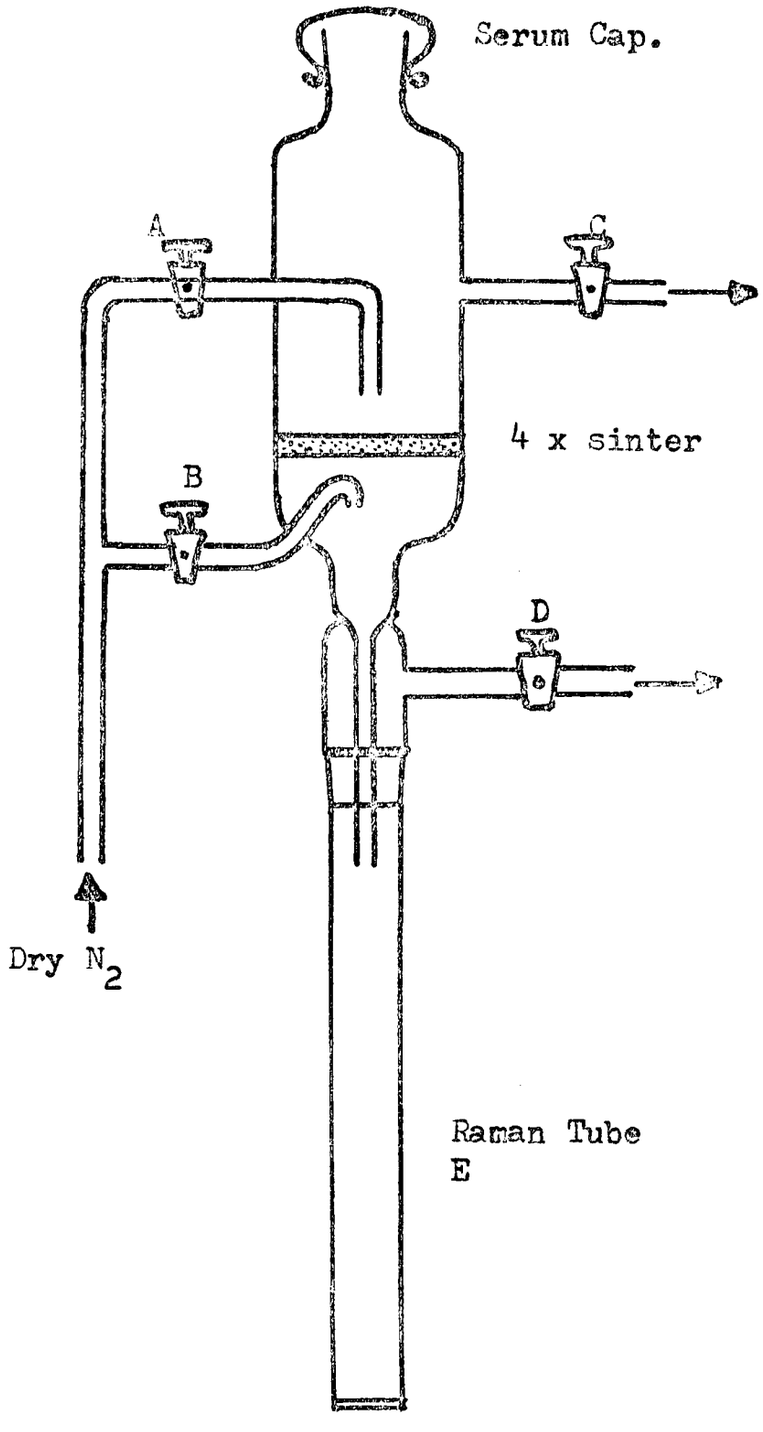


Figure 8 B. Apparatus for the making and filtering of Raman solutions of $Ni(PCl_3)_4$ in a dry, inert atmosphere.

$Ni(PCl_3)_4$; taps B and D were then closed and the solution blown through the 4 x sinter into the Raman tube E.

Turbidity was soon observed, after the elapse of only one or two minutes at room temperature for all solvents used. A pronounced delay in the formation of turbidity was noted when the Raman tube E was cooled before receiving the solution, indicating that the decomposition could be caused by temperature and/or a chemical reaction with the solvent. The extent of cooling, of course, varied with the solvents used - decalin being the most suitable on these grounds since it formed a <u>glass</u> with $Ni(PCl_3)_4$ at -78°C, and no precipitation of compound occurs. Unfortunately, decalin does not fulfil the requirements for Raman work, having a very complex spectrum: the crucial 150-600 cm^{-1} region is completely obscured. Qualitative experiments on cooling yielded the following results on selected solutions which were suitable for Raman work:

	Clear solution time	T°C
C_6H_6 solution (0.4M)	4 minutes	10°C
CCl_4 solution (0.2M)	2 minutes	-15°C

It is interesting to consider the possible products of such thermal decomposition. On allowing, say, a solution of $Ni(PCl_3)_4$ in CCl_4, to stand for a few days in a stoppered

vessel theyellow colour fades and a brownish-yellow precipitate was obtained. The filtrate fumed in air, fumes of HCl and PCl_3 being detectable. The fact that such a solution was unstable even under anaerobic conditions still lacks a detailed explanation. Schmutzler (40,44) et al. have examined the $CCl_4/Ni(PCl_3)_4$ system and have shown that the main reaction path resulted in the formation of C_2Cl_6 and Ni^{II}, while the coordinated PCl_3 is released (conferring fuming properties on the solution).

That a slightly different reaction path may be followed when oxygen and/or water were present was demonstrated by the lighter-coloured precipitates formed. It seems reasonable to postulate a hydrolysis-oxidation mechanism, giving nickel hydroxide, nickel phosphate, etc.

A spectroscopic investigation of the precipitate and solutions will later be described and compared with the vibrational spectrum of $Ni(PCl_3)_4$ itself.

8(4) The Raman spectrum of $Ni(PCl_3)_4$

The Raman spectrum of crystalline $Ni(PCl_3)_4$ was obtained using a conical cell described previously. The mercury 5461 Å (green) line was used as an exciting line since the yellow solid absorbs blue light. Kodak 'Wratten' filters

are available to remove the blue and ultra-violet mercury arc lines, which could cause photodecomposition of the sample; however, in this case the filters were unnecessary as the sample was stable to blue radiation. For larger crystals a round-bottomed tube was used. Spectra from both cells proved to be of excellent quality; the spectrum from the conical cell sample is reproduced in Figure 8C.

Spectra were obtained under different conditions of sensitivity and scan speed as a check on reproducibility and for confirmation of weak features. In using Hg 5461 Å as an exciting line, although the low-frequency region is clear of lamp features, weak lamp lines appear at 410 cm^{-1} and 590 cm^{-1}, in addition to the stronger feature at 290 cm^{-1}. A 'blank' of the lamp spectrum was obtained using cotton wool as scattering material, the relative intensities of the weak Raman lines can then be usefully compared with that of the 290 cm^{-1} features.

The interpretation of spectra obtained from the solid state must be carried out with reservation. Lattice vibrations occur in the low-frequency region, and lifting of the degeneracy of e- and f-modes often results in a splitting of these modes. Molecular symmetry may differ from the site symmetry of the crystal, and distortions in the crystal may lead to a breakdown in molecular symmetry

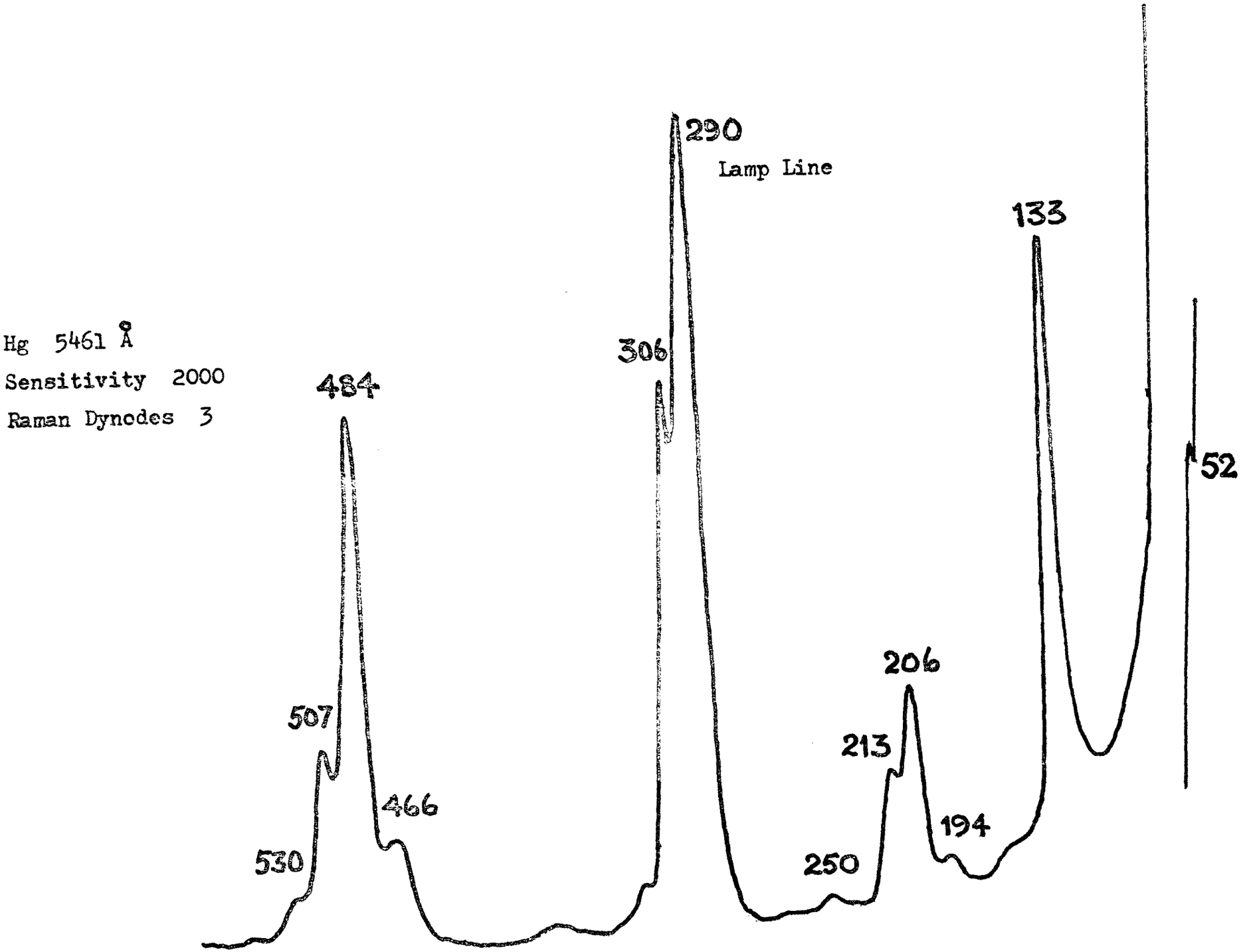


Figure 8 C. Raman Spectrum of $Ni(PCl_3)_4$ solid.

[as observed for $Pt(PF_3)_4$]. Thus, it is always advisable, wherever possible, to confirm conclusions reached from spectra obtained in the solid state by examining solution spectra. In the case of $Ni(PCl_3)_4$, the spectrum obtained from the solid state (Figure 8C) shows the prominent features one would expect for a molecule having the T_d point group.

The difficulties inherent in the preparation of Raman solutions of $Ni(PCl_3)_4$ have been discussed in 8(3). These, briefly, consist of the impossibility of maintaining the cooled solution for more than a few minutes at a time before turbidity occurs; and, of course, the yellow colour of the solution. The 'life' of the solutions of CCl_4 and benzene containing $Ni(PCl_3)_4$ in the mercury arc at 40°C was but 5 seconds only.

An air-cooled cell has been described in Chapter 2, which gives a temperature range of -5°C to 20°C for samples. Using this device the clear-solution lifetime of a benzene solution, or a CCl_4 solution, was increased to one minute. The Raman spectrum was thus scanned for one-minute periods, the solution replaced afresh, and the scanning continued. A fairly rapid scan speed was hence essential, and also rather a large quantity of $Ni(PCl_3)_4$ was needed. Each solution was circa 0.2 → 0.4M, volume 5 ml., for each

minute's scan, and the whole spectrum was repeated a few times at various sensitivities.

Due to the instability of the solutions, polarisation data were rather difficult to obtain, the procedure followed being: the filtered solution, saturated at room temperature, was cooled and the relevant polaroid cylinder placed around the cooling jacket. The time from filtration of sample to insertion in the Cary 81 was noted (average 10-15 seconds) and each band was examined individually as quickly as possible. Having scanned over one feature, the solution was removed and the procedure repeated with fresh solutions under identical, timed conditions. Finally, a "mixed series" was obtained, changing over the polaroid cylinders for successive scans over the same peak. By this means, some consistent meaningful polarisation data were obtained at the expense of approximately 150 gms. of $Ni(PCl_3)_4$.

The 'depolarisation ratio' measured in the above experiment does not give the correct ρ, due to non-idealities in design of instrument and the sample tube. A calibration curve for the 7 mm. tube was constructed (Figure 2E) in Chapter 2, and used to correct ρ-values for the features analysed in the above experiments.

The solution spectrum in CCl_4 is shown in Figure 8D, and confirms the solid-state spectrum. No polarisation data

a. Hg 5461 Å

b. Hg 4358 Å

* CCl_4 Bands

Temperature 0°C, 5°C.

Scan Speed x 20

Period 8

Sensitivity 3000

Raman Dynodes 3.

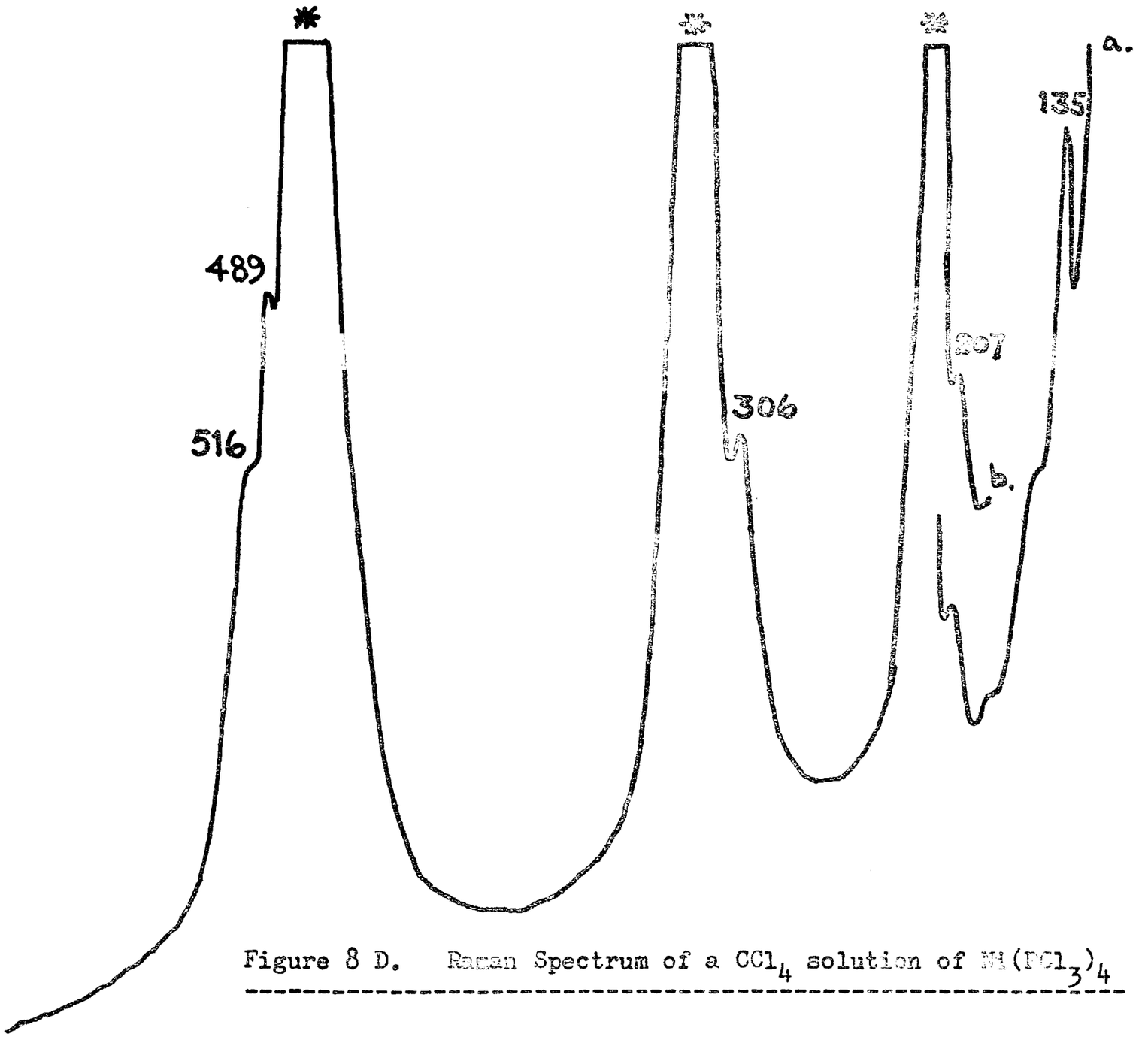


Figure 8 D. Raman Spectrum of a CCl_4 solution of $Ni(PCl_3)_4$

could be obtained since the solvent features interfere. The 135 cm^{-1} band was, unfortunately, too close to the broad exciting line for polarisation measurements to be made. The benzene solution spectrum is shown in Figure 8E. An interesting feature with the solution work was the transmission of both the benzene and the carbon tetrachloride solutions to Hg 4358 Å, despite their pale yellow colour. This was especially useful in the case of the 310 cm^{-1} band, which was partially obscured by the 290 cm^{-1} lamp line on Hg 5461 Å. In both Figures 8D and 8E, the spectra are shown for 'blue' excitation and green 5461 Å excitation.

An investigation of the Raman spectrum was also carried out using the modified Helium Source previously described. The exciting lines were He 5876 Å and He 6678 Å. In chloroform solutions the temperature was kept at -35°C, when the clear-solution time was approximately 4 minutes. The 15 ml. samples were interchanged every 2 minutes to give a required exposure by superimposing on the plate. Slit width was 100 μ and height 6 mm. Spectra were generally fairly poor, especially on the longer exposures (30 minutes); but the P-Cl stretching, PCl_3 deformation, and Ni-P stretching modes were observed. Background scattering on the plate was too heavy to permit polarisation measurements at longer exposures.

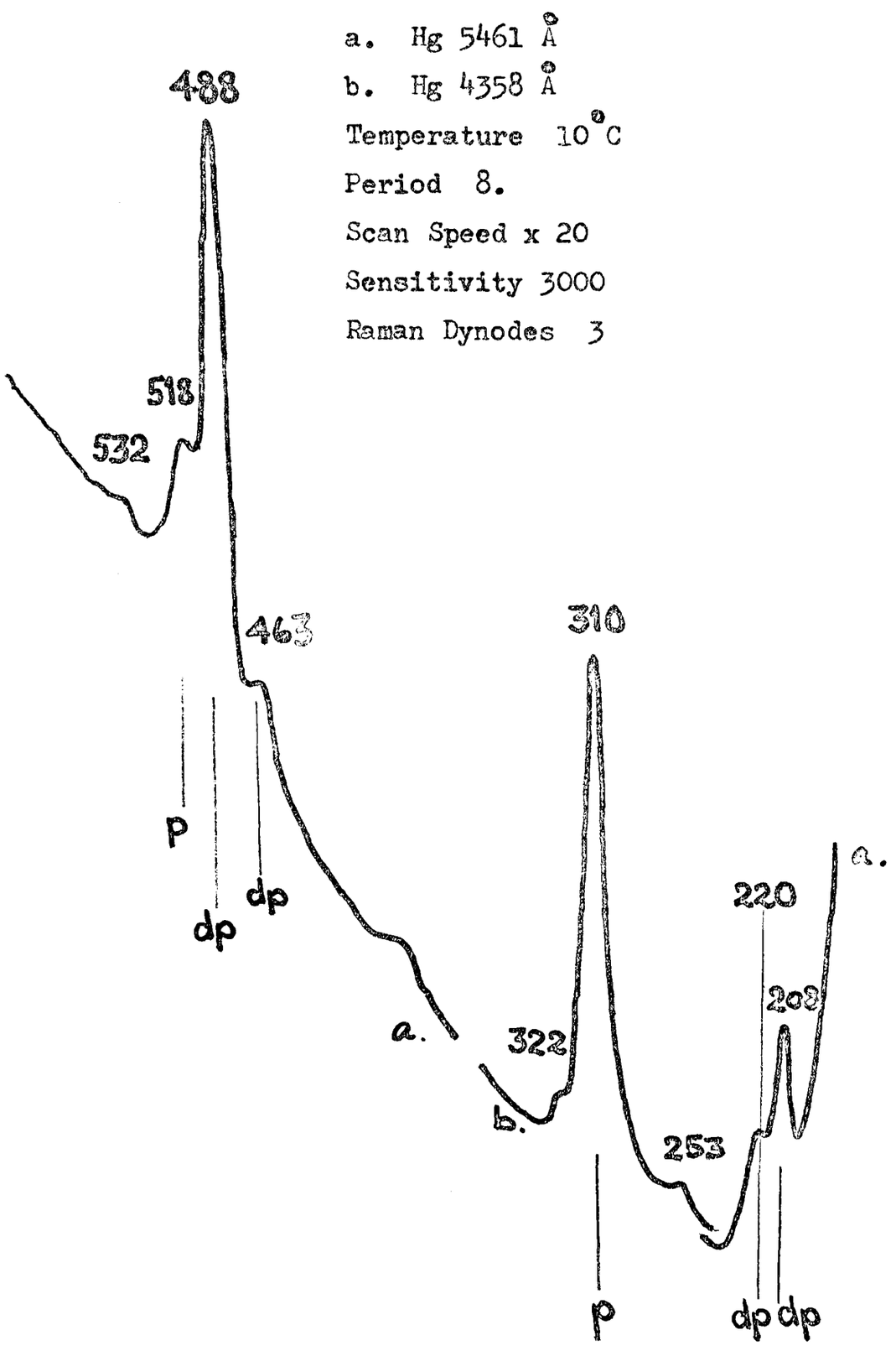


Figure 8 E. Raman Spectrum of a Benzene solution of $Ni(PCl_3)_4$

"Winging" of the exciting line, caused by rotational features, in the benzene solution prevented any attempt to observe the 135 cm^{-1} feature. Figure 8E illustrates a 'hybrid' spectrum, the high frequency region obtained on 5461 Å excitation, the 250-350 cm^{-1} region on 4358 Å, the low-frequency on 5461 Å. Table 8A gives the collected Raman solution data.

8(5) The Infra-red spectrum

The infra-red spectrum (Figure 8F) was obtained with nujol mulls between caesium iodide and polythene plates in the region 33-1100 cm^{-1}. The data and assignment of modes are given in Table 8B.

8(6) Discussion of the assignment

The complete vibrational assignment is given in Table 8C and a correlation diagram in Figure 8G.

For the T_d point group we should expect three strongly polarised lines in the Raman spectrum of $Ni(PCl_3)_4$. Only two polarised lines were, in fact, observed - no data could be obtained for the strong 135 cm^{-1} feature in solution. The intensity, position in the spectrum, and absence from the infra-red is strong evidence for the assignment of this

TABLE 8A

The Raman spectrum of $Ni(PCl_3)_4$

Solid (40°C) Hg 5461 Å	CCl_4 sol$^{n.}$ (0°C & 5°C) Hg 4358, 5461 Å	C_6H_6 sol$^{n.}$ (10°C) Hg 4358, 5461 Å
52 m	-	-
133 s	135 s	-
166 mw,sh	162 w	-
194 mw,sh	194 w	-
206 ms	207 ms,sh	208 ms,depol.
213 m,sh	-	220 mw,depol.
250 w	-	253 w
306 s	306 s,sh	310 s,pol.
324 w	-	322 w,sh
466 m,sh	-	463 mw,depol.
484 s	489 s,sh	488 s,depol.
507 ms,sh	516 m,sh	518 m,pol.
530 w	-	532 w

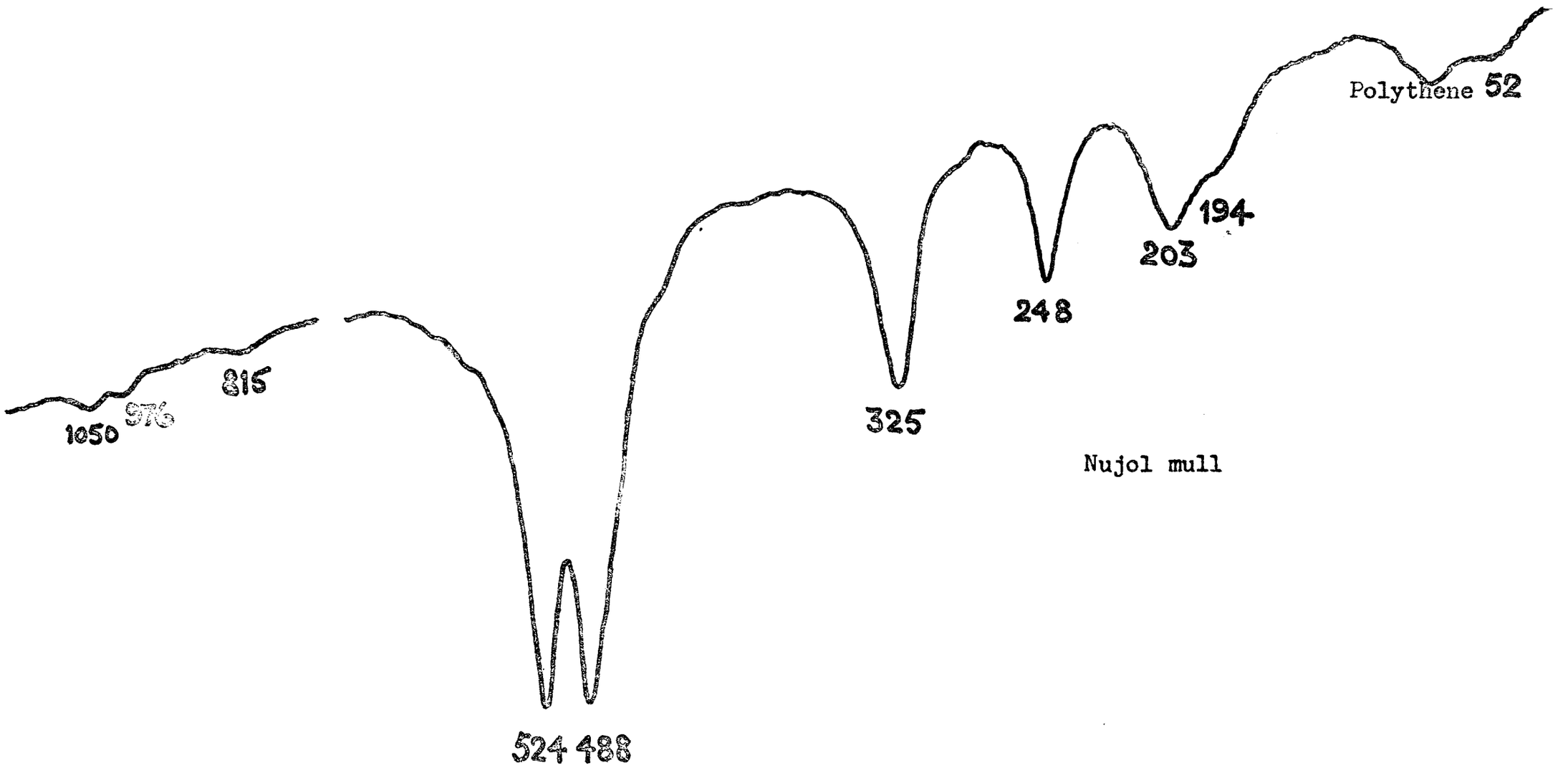


Figure 8F. The Infra-Red Spectrum of $Ni(PCl_3)_4$ solid.

TABLE 8B

The Infra-Red spectrum of $Ni(PCl_3)_4$

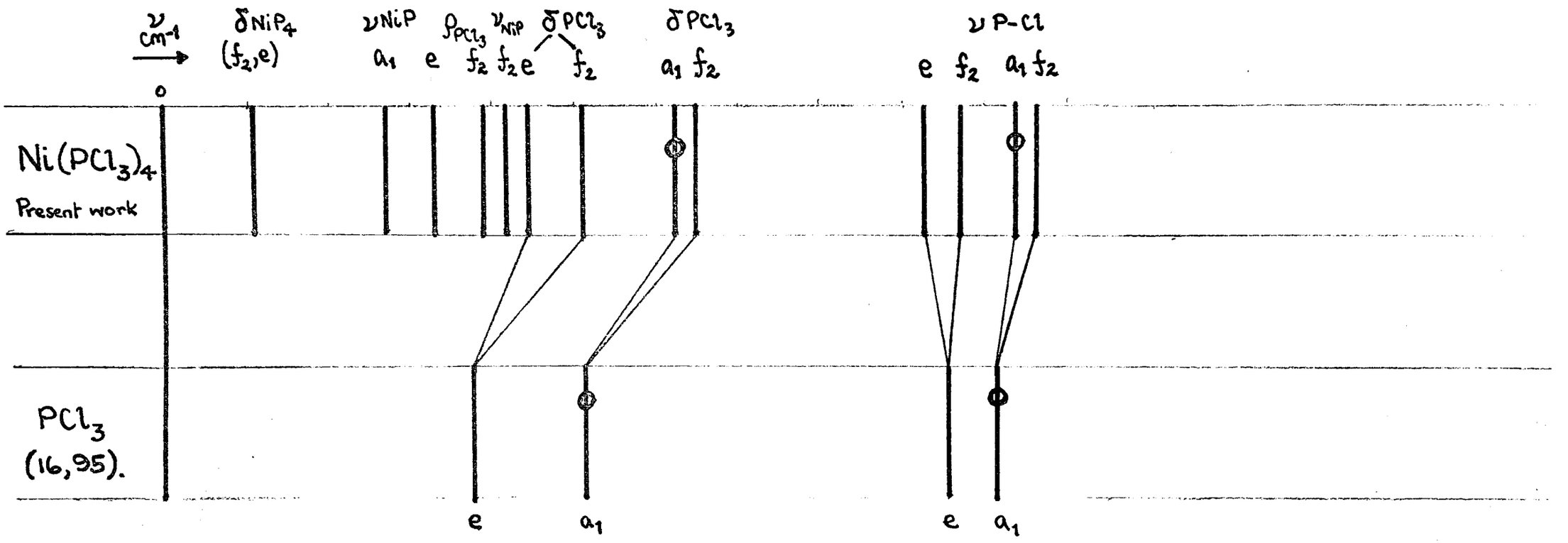
F_2 species

Seel (44)	Present work	ν	Assignment of mode
	52 mw,bd	ν_{19}	NiP_4 deformation
	123 vw		
	134 vvw		
	194 m,sh	ν_{18}	PCl_3 rock
	203 s	ν_{17}	NiP_4 asym.stretch
	248 s	ν_{16}	PCl_3 asym.def.
	278 vw		
	325 s	ν_{15}	PCl_3 sym.def.
	452 w	$\nu_{16} + \nu_{17} = 451$	
477 s	488 vs	ν_{14}	P-Cl asym.stretch
503 s	524 vs	ν_{13}	P-Cl sym.stretch
	570 w	$\nu_{15} + \nu_{16} = 573$	
	652 w	$2\nu_{15} = 650$	
	815 w	$\nu_{14} + \nu_{15} = 813$	
	855 vw	$\nu_{13} + \nu_{15} = 849$	
	976 mw	$2\nu_{14} = 976$	
	1050 mw	$2\nu_{13} = 1048$	

TABLE 8C

Assignment of $Ni(PCl_3)_4$

Symmetry species	ν	Description of mode	RAMAN		I.R.
			solution	solid	solid
A_1	ν_1	P-Cl stretch	518, m,pol.	507,ms,sh	inactive
	ν_2	P-Cl def.(sym)	310,s,pol.	306,s	inactive
	ν_3	Ni-P stretch	135,s,?	133,s	inactive
A_2	ν_4	PCl_3 torsion	inactive	inactive	inactive
E	ν_5	P-Cl asym.stretch	463 mw, dp	466 m	inactive
	ν_6	PCl_3 asym.def.	220 mw, dp	213 m	inactive
	ν_7	PCl_3 rock	162 w	166 mw	inactive
	ν_8	NiP_4 def.	-	52,m	inactive
F_1	ν_9	P-Cl asym.stretch	inactive	inactive	inactive
	ν_{10}	$P-Cl_3$ asym.def.	inactive	inactive	inactive
	ν_{11}	PCl_3 rock	inactive	inactive	inactive
	ν_{12}	PCl_3 torsion	inactive	inactive	inactive
F_2	ν_{13}	P-Cl sym.stretch	532 w	530 w	524 vs
	ν_{14}	P-Cl asym.stretch	488 s,dp	484 s	488 vs
	ν_{15}	PCl_3 sym.def.	322 w	324 w	325 s
	ν_{16}	PCl_3 asym.def.	253 w	250 w	248 s
	ν_{17}	NiP_4 asym.stretch	208 ms,dp	206 ms	203 s
	ν_{18}	PCl_3 rock	194 w	194 mw	194 m,sh
	ν_{19}	NiP_4 def.	-	52 m	52 mw, broad



Polarised Band. ν Stretching. δ Deformation. ρ Rocking.

Figure 8G. Correlation Diagram for $Ni(PCl_3)_4$ and PCl_3

TABLE 8D

Vibrational spectrum of PCl_3

	LIQUID			VAPOUR	
	Raman Cabannes (16)	Raman Yost (95)	I.R. Davis (93)	I.R. Lorenzelli (92)	Raman Neilsen (94)
$\nu_1(a_1)$	511	510	507	504	514
$\nu_2(a_1)$	258	257	260	252	256
$\nu_3(e)$	484	480	494	482	482
$\nu_4(e)$	190	190	189	198	184

band to the Ni-P symmetric stretch, ν_3; a rough value of ν_3 may be obtained by comparing $Ni(PF_3)_4$ and $Ni(PCl_3)_4$ on a point-mass basis, which gives ν_3 as being $\sim$150 cm^{-1} for $Ni(PCl_3)_4$.

The correlation diagram is useful in the assignment of ligand vibrations in conjunction with the vibrational spectrum (Table 8D) of PCl_3 itself.

Previous work on $Ni(PCl_3)_4$ amounts to an infra-red study by Seel et al.(44), who quote the two P-Cl stretching frequencies. There seems to be some discrepancy, see Table 8B, between the frequency values of Seel and those quoted in this work,; but Seel's spectra were obtained from a KBr pressed-disc containing $Ni(PCl_3)_4$, and are therefore not strictly comparable with the nujol mulls of this work. Good Raman-infrared coincidences in the F_2-species seem to confirm the assignment and frequency-values of the present work.

By analogy with phosphorus trichloride, where the P-Cl symmetric stretch is five times more intense than the anti-symmetric stretch (95), the 488 cm^{-1} feature in the benzene solution of $Ni(PCl_3)_4$ might be expected to be polarised. This feature is, however, definitely <u>depolarised</u> and must be an

antisymmetric P-Cl stretch. Also, the 488 cm^{-1} Raman-infra-red coincidence indicates that this is an f_2-species mode. The shoulder at 518 cm^{-1} in the Raman spectrum is <u>polarised</u> and is obviously the P-Cl a_1-mode, ν_1.

The assignment of ν_2, the a_1-deformation, to 310 cm^{-1} is unambiguous on polarisation data and absence from the infra-red spectrum. The corresponding mode in PCl_3 itself occurs at 260 cm^{-1}; thus, one might confidently predict that the P-Cl symmetric stretching frequency would likewise be greater than the value of 510 cm^{-1} in the free liquid.

Assignment of the Ni-P asymmetric stretch, ν_{17}, to 208 cm^{-1} in the Raman solution spectrum is convincing; evidence in support of this is the depolarisation ratio and the F_2-species coincidence in the infra-red spectrum. As will be remembered, in the analogous PF_3 molecules the assignment of the PF_3-rocking modes was in doubt, but a $\sim$ 280 cm^{-1} value was eventually considered reasonable for such vibrations. In the case of $Ni(PCl_3)_4$, however, the PCl_3 rocking mode has been identified in $POCl_3$ at 193 cm^{-1}(16). This is remarkably close to the PCl_3 rock, ν_{18}, assigned to a band at 194 cm^{-1} in both the infra-red and the Raman spectrum.

A query in the assignment of $Ni(PCl_3)_4$ given in Table 8C concerns the rocks and asymmetric deformations of the PCl_3

group. If one assigns the f_2-rocking mode to 248 cm^{-1} in the infra-red instead of 194 cm^{-1} as indicated in Table 8C, then 194 cm^{-1} is assignable to the asymmetric deformation. The e-rocking modes can now be assigned to the medium-weak intensity feature in the Raman at 220 cm^{-1} (solution), leaving the weak band at 162 cm^{-1} for the e-deformation. Either assignment could be likely, although the assignment of the 194 cm^{-1} to a f_2-rocking mode was favoured on account of the occurrence of a similar mode at 193 cm^{-1} in the $POCl_3$ molecule. Also, since the PF_3 rock in the $M(PF_3)_4$ analogues was assigned to a feature at $\sim$ 280-287 cm^{-1}, the occurrence of a PCl_3-rock at 248 cm^{-1} is rather too close in frequency for the PF_3-PCl_3 mass difference involved.

An interesting point emerging from a comparison of the assignments of $Ni(PF_3)_4$ and $Ni(PCl_3)_4$, concerns the identity of a weak feature observed (43) at 126 cm^{-1} in the $Ni(PF_3)_4$ Raman spectrum. This was polarised and was assigned to the first harmonic ($2\nu_4$) of the Raman-inactive ν_4 vibration, an a_2-mode. The frequency of this weak band is very close to that assigned to the Ni-P stretch (polarised), ν_3, in $Ni(PCl_3)_4$ at 135 cm^{-1}. The $Ni(PF_3)_4$ had been made from $Ni(PCl_3)_4$ and some difficulty in its purification was experienced (96). Could this feature be the Ni-P stretch of either:

(a) $Ni(PCl_3)_4$ impurity

or (b) Ni-(PCl_3) stretch of $Ni(PF_3)_x(PCl_3)_{4-x}$ impurity?

A volatile impurity, such as $Ni(PF_3)_3PCl_3$, would be a likely compound that could contribute to such a polarised P-Cl stretching at 126 cm^{-1}.

8(7) Some studies on the decomposition of $Ni(PCl_3)_4$ in solution

0.3M solutions of $Ni(PCl_3)_4$ in carbon tetrachloride and in chloroform were left to stand for a period of two weeks in sealed vessels. At the end of this time the precipitates and filtrates from each solution were collected in a dry, nitrogen-filled glove-box. Infra-red spectra were obtained for the filtrates in the region 200-2000 cm^{-1} using caesium iodide plates.

CCl_4 solution
- filtrate almost colourless (A)
- yellow-brown precipitate (A')

$CHCl_3$ solution
- filtrate slightly yellow (B)
- black-brown precipitate (B')

Both filtrates fume due to the presence of PCl_3, and qualitative tests on A' and B' indicate that A' is mainly $NiCl_2$ (anhydrous), whereas B' is mainly Ni metal (with some $NiCl_2$).

The infra-red spectra are very complex. The P-Cl stretching region is of great interest: in both filtrates the P-Cl stretches of $Ni(PCl_3)_4$ at 490 and 525 cm^{-1} occur strongly, but prominent shoulders at 510 and 478 cm^{-1} of medium intensity indicates that free PCl_3 is present. In infra-red spectra of the solids deposited from the above solutions, precipitate B' seemed to give features assignable to $Ni(PCl_3)_4$ alone; whereas A', in addition to these features, gave some new bands of medium intensity, chiefly at 450, 569, 626, 646, 682 and 691 cm^{-1}.

In the solution spectra some features attributable to hexachloroethane, C_2Cl_6, were identified; notably, prominent features at 980, 865 and 430 cm^{-1}.

The chloroform spectrum was more complex in the solution phase, which could be explained on the basis of formation of partially-substituted ethanes, such as $C_2H_2Cl_4$ and $C_2H_4Cl_2$.

CHAPTER 9

Chapter 9

TETRAKISTRIBROMOPHOSPHINENICKEL° AND TETRAKISTRIIODOPHOSPHINE-NICKEL°

A. Tetrakistribromophosphinenickel°

9(1) Preparation

Phosphorus tribromide reacts with nickel carbonyl in the liquid phase with loss of carbon monoxide and the formation of an orange solution. No compound of PBr_3 and nickel could, however, be isolated, presumably due to the ready decomposition of some intermediate. $Ni(PBr_3)_4$ has been made (33) by the action of PBr_3 on $Ni(PCl_3)_4$:

$$Ni(PCl_3)_4 + 4PBr_3 \rightleftharpoons Ni(PBr_3)_4 + 4PCl_3$$

In the present work 10 g. of $Ni(PCl_3)_4$, recrystallised from pentane at -80°C, was placed in a round-bottomed flask and excess PBr_3 added (20 ml., ρ = 2.85 gm./ml.). On warming gently to 70°C the yellow $Ni(PCl_3)_4$ dissolved to give a deep orange-red solution; temperature control is critical and even slight overheating resulted in extensive decomposition of the solution to nickel metal. Fumes of PCl_3 were evolved and pumped off using a rotary pump and two liquid-nitrogen traps.

The residual solution was now cooled to just above the melting point of PBr_3 (-38°C) and the orange-red crystals filtered at the pump. Excess PBr_3 was removed from the crystals by washing with cold pentane at -78°C. The solid was dried by pumping under vacuum at room temperature. The yield was 12 gm., i.e. 60% of theoretical.

9(2) Properties

Like $Ni(PCl_3)_4$, the crystals are thermochroic, having a deep orange colour at room temperature and very pale yellow at -38°C. $Ni(PBr_3)_4$ is stable to water and aqueous acid but is decomposed by caustic soda solution.

$Ni(PBr_3)_4$ is far less stable than the chloro-compound, and the solid darkens on exposure to air and light. When stored in a desiccator or sealed vessel, large amounts of PBr_3 are evolved and nickel is deposited on the surface of the crystals (in marked contrast with $Ni(PCl_3)_4$, which has very little PCl_3 overpressure). The crystals decompose thermally at 80°C.

Tetrakistribromophosphinenickel is soluble in the more non-polar organic solvents such as CCl_4, benzene, hexane. The deep yellow solutions formed are unstable, turbidity

being developed at room temperature within 5-10 seconds. The carbon tetrachloride solution is the most unstable and the benzene solution the least. The solutions were far too unstable for Raman work, which thus must be confined to the crystalline state.

The analysis of the crystals showed, qualitatively, the presence of chloride (97) - treatment with permanganate-acetone removed the bromine, leaving the chlorine content unaffected. It seems, then, that contamination with $Ni(PCl_3)_4$ or partially substituted $Ni(PBr_3)_x(PCl_3)_{4-x}$ is evident in the sample of $Ni(PBr_3)_4$ prepared above. Prolonged heating of the reaction mixture at 70°C for even a few minutes caused rapid deposition of nickel and nickel bromide; thus there was no way in which the reaction mixture could be 'refluxed' to ensure completeness of reaction.

After one recrystallisation from hot PBr_3 an infra-red spectrum was obtained in the P-Cl stretching region, 400-550 cm^{-1}. Medium-intensity features were noted at 514 and 484 cm^{-1}, which could be assigned to $Ni-PCl_3$ impurity, and also a weak band at $\sim$ 200 cm^{-1}, assignable to the Ni-P stretching mode of the chloro-compound.

The orange crystals were thus recrystallised three more times from PBr_3 and twice from pentane at -78°C. The crystals were then pumped on for about 10 minutes to remove PCl_3. A further recrystallisation from PBr_3 and drying under vacuum produced a sample of orange crystals that gave no features assignable to $Ni(PCl_3)_4$ impurity in the infra-red spectrum.
Quantitative analysis (as in the case of the chloro-compound) confirmed that a pure sample of $Ni(PBr_3)_4$ had been isolated:

	Found%	Theoretical%
Ni	5.08	5.14
P	10.63	10.84
Br	83.1	83.9

9(3) Vibrational spectrum of $Ni(PBr_3)_4$

The orange crystals were finely ground and the Raman spectrum was obtained using Hg 5461 Å excitation. The high sensitivities used indicate that the sample absorbed the green line to a certain extent. The Raman spectrum is shown in Figure 9A and Table 9A; an immediate point to note is the weakness of this spectrum relative to the chloro-analogue. No polarisation data were, of course, possible.

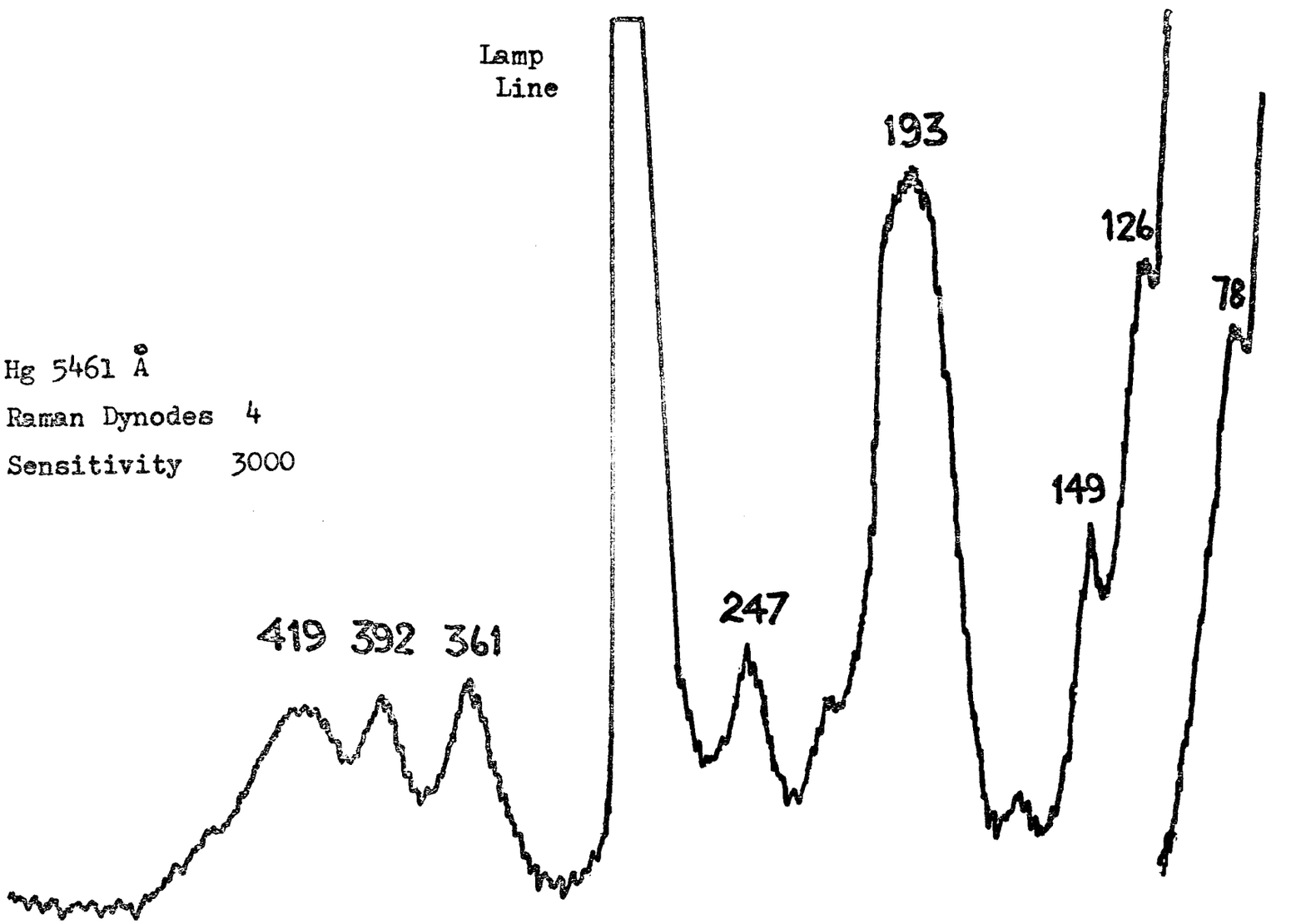


Figure 9A. The Raman Spectrum of $Ni(PBr_3)_4$ solid.

TABLE 9A

The Raman spectrum of $Ni(PBr_3)_4$ Crystals

Cary 81 spectrometer Hg 5461 Å excitation

ν cm^{-1}	
78	m, shoulder on exciting line
126	m "
149	m
168	w, broad
193	ms, broad
228	w, shoulder
247	mw
361	mw
392	mw
419	mw, broad
439	w, shoulder (?)

Infra-red spectra were obtained with nujol mulls in the polythene region (Figure 9B and Table 9B). The spectra are, again, rather weak compared to the $Ni(PCl_3)_4$ analogue, although there is no difficulty in assigning the features to the f_2-modes.

9(4) Discussion of the assignment

Owing to the lack of polarisation data in the Raman work the assignment of the F_2-species modes is the crux of the matter. Comparison with PBr_3 and $POBr_3$, as well as with the general pattern established by the work on $Ni(PF_3)_4$ and $Ni(PCl_3)_4$, indicates that $Ni(PBr_3)_4$ may again be assigned to the T_d point group. The coincidences between Raman- and i.r.-modes in the F_2-species are quite good, and the a_1-modes are assigned by analogy.

Table 9C gives the assignment; the three a_1 modes seem to be reasonably assigned in the absence of confirmatory polarisation data. It is seen that the ν_3, Ni-P symmetric stretch has decreased in frequency to 78 cm^{-1} relative to ν_3 in $Ni(PCl_3)_4$. Figure 9C is the correlation table for $Ni(PX_3)_4$ molecules where X = halogen. As the halogen increases in atomic weight F $\longrightarrow$ Cl $\longrightarrow$ Br the symmetric stretch Ni-P, ν_3, is seen to decrease markedly relative to the antisymmetric ν_{18} (ν_{17} for $Ni(PBr_3)_4$).

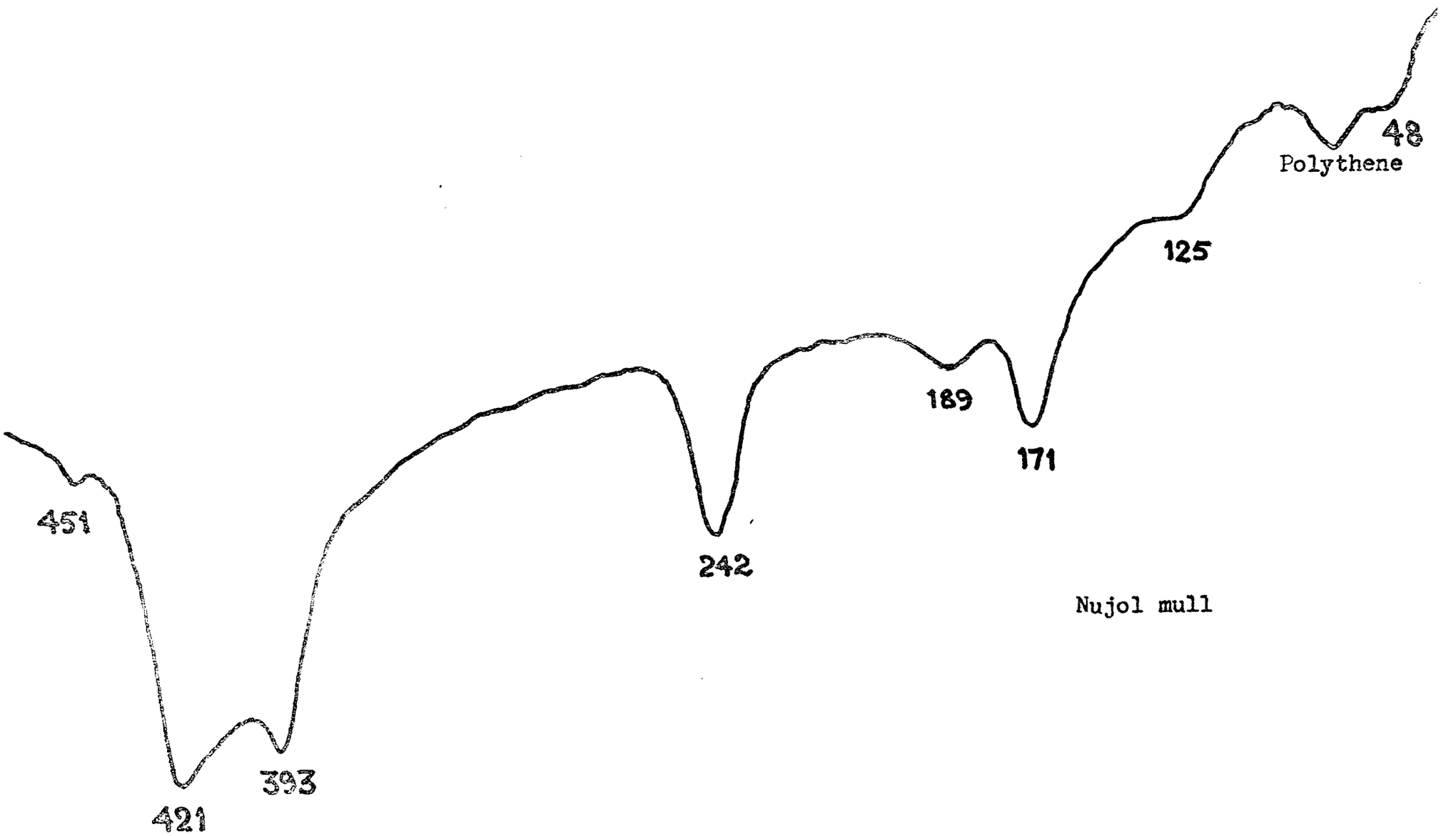


Figure 9B. The Infra-Red Spectrum of $Ni(PBr_3)_4$ solid.

TABLE 9B

Assignment of F_2 class from the i.r.

ν_{13}	P-Br asymmetric stretch	421 m
ν_{14}	P-Br symmetric stretch	393 m
ν_{15}	P-Br asymmetric def.	242 m
ν_{16}	NiP_4 asymmetric stretch	189 mw
ν_{17}	P-Br symmetric def.	171 m
ν_{18}	PBr_3 rock	125 w
ν_{19}	NiP_4 deformation	48 mw

Assignment made by analogy with $POBr_3$ and PBr_3

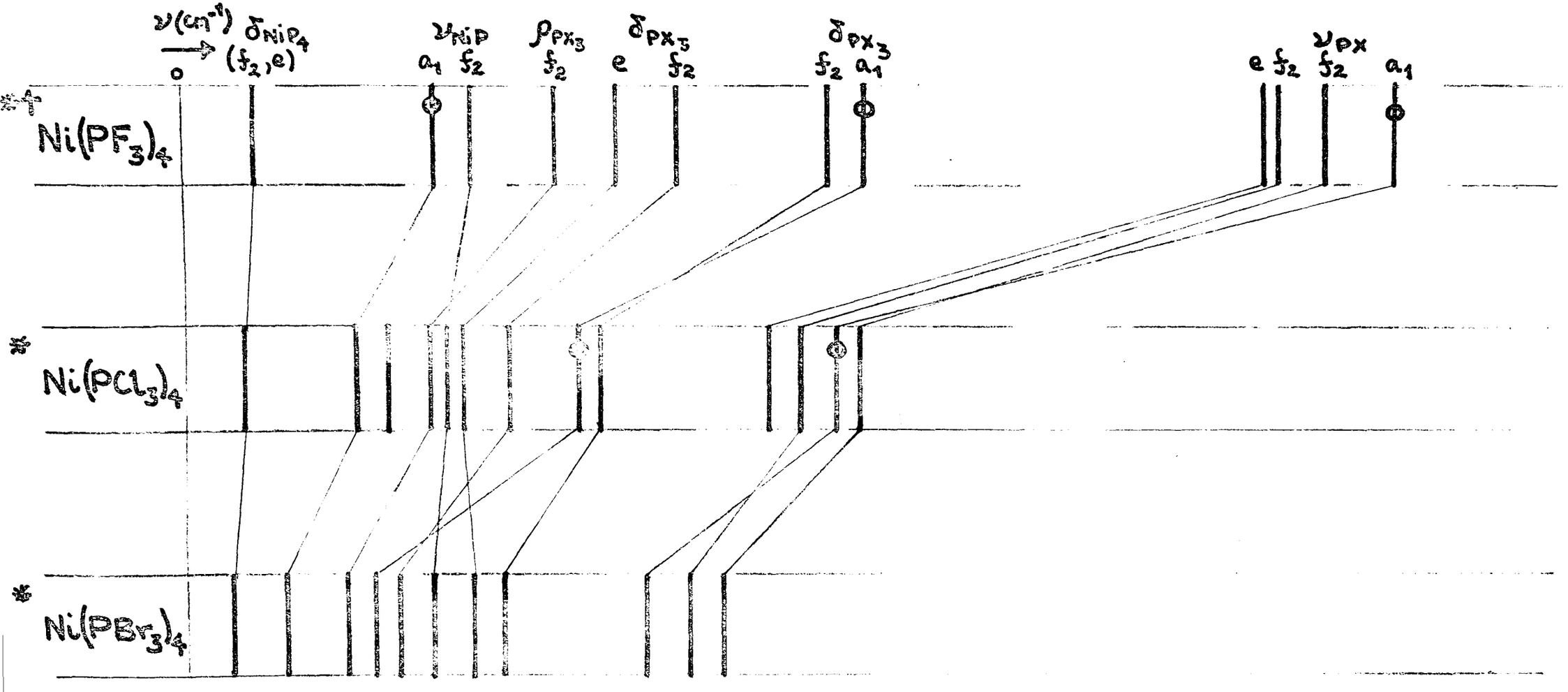
Note: inversion of defs. in $POBr_3$

	sym.def.	asym.def.
$POBr_3$	173	267
PBr_3	162	116
$Ni(PBr_3)_4$	171	242

TABLE 9C

Assignment of $Ni(PBr_3)_4$

Symmetry Class	ν	Mode	Raman (solid)	I.R. (solid)
A_1	ν_1	P-Br symmetric stretch	361, mw	inactive
	ν_2	PBr_3 symmetric def.	149, m	inactive
	ν_3	NiP symmetric stretch	78, m	inactive
A_2	ν_4	PBr_3 torsion	inactive	inactive
E	ν_5	P-Br asymmetric stretch	419, broad (439,?, shoulder)	inactive
	ν_6	PBr_3 asymmetric def.	228 w	inactive
	ν_7	PBr_3 rock	(126)	inactive
	ν_8	Ni-P def.	-	inactive
F_1	$\nu_9 \downarrow \nu_{12}$		inactive	inactive
F_2	ν_{13}	P-Br asymmetric stretch	419,mw,bd	421,m
	ν_{14}	P-Br symmetric stretch	392,mw	393,m
	ν_{15}	PBr_3 asym.def.	247,mw	242,m
	ν_{16}	PBr_3 sym.def.	168,w,bd	171,m
	ν_{17}	PBr_3 rock	126,m	125,w
	ν_{18}	Ni-P asym.stretch	193 ms,bd	189,mw
	ν_{19}	Ni-P def.	-	48 mw



Polarised Band. * Present Work. † Reference 43

ν Stretching δ Deformation ρ Rocking

Figure 9C. $Ni(PX_3)_4$ Correlation Diagram.

The deformation inversion in the PBr_3 compound resembles $POBr_3$ in having the sym./asym. deformations reversed compared with free PBr_3 itself. This 'reversed' deformation sequence is selected for $Ni(PBr_3)_4$ on an arbitrary basis, and here, again, polarisation data would help in the assignment. Some evidence supporting the 'reversed' deformations is provided by the existence of two Raman features, at 228 and 247 cm^{-1}, which have been assigned to the e- and f_2-asymmetric deformations respectively.

The remainder of this Chapter will be concerned with an investigation of $Ni(PI_3)_4$, the hitherto unknown last member of the halogen series $Ni(PX_3)_4$.

B. Tetrakistriiodophosphinenickel

There is no evidence in the literature of a synthesis of $Ni(PI_3)_4$, or indeed, of <u>any</u> nickel-triiodophosphine compound. Qualitatively, from the work on the other halogen compounds described previously, it would be reasonable to predict that $Ni(PI_3)_4$ would be much less stable than the bromo-compound.

Phosphorus triiodide itself is rather unstable; Stammreich et al.(98) reported turbidity in solutions of PI_3 in organic solvents, and extensive dissociation occurs at temperatures in the region of 61°C.

It was decided in this work to attempt the preparation of $Ni(PI_3)_4$, and, if possible, to examine its vibrational spectrum as a logical extension of the $Ni(PX_3)_4$ series.

9(5) The preparation of $Ni(PI_3)_4$.

An analogous method to the preparation of $Ni(PBr_3)_4$ was selected as the most promising for the synthesis of $Ni(PI_3)_4$.

$$\underset{608}{Ni(PCl_3)_4} + \underset{1647}{4PI_3} \rightleftharpoons \underset{1706}{Ni(PI_3)_4} + 4PCl_3$$

Phosphorus triiodide is a deep-red solid (m.pt.66°C) and may be prepared by refluxing the elements in carbon disulphide (98). PI_3 is, however, obtainable commercially from Harrington and Co. The solid fumes in moist air and reacts with oxygen, so the solvent for the reaction was degassed and sodium-dried before use.

A solvent is necessary since the above reactants are both solids: the solvent chosen was n-hexane (b.pt.67°C), in which both $Ni(PCl_3)_4$ and PI_3 are fairly soluble without extensive decomposition. 2g. of $Ni(PCl_3)_4$ were dissolved in the dried n-hexane and $\sim$8 g. PI_3 (60% excess) were similarly treated in a separate flask. The PI_3 dissolved rather reluctantly at first, but careful warming to 30°C

aided the process of solution. The two solutions were filtered from any undissolved material and immediately mixed. The bright orange solution of PI_3 slowly turned a very deep brown in colour and became almost black. The reaction mixture was warmed very slightly to assist reaction - the deposition of nickel metal is difficult to observe here, owing to the dark colour of the solution.

The solution was now attached to a rotary pump via two liquid-nitrogen traps, and the PCl_3 removed. On cooling the solution in an acetone/CO_2 bath at -78°C very deep violet-black crystals separated. This could be the desired product or nickel metal.

The presence of metallic Ni, or NiI_2, in the above sample was confirmed by re-dissolving in hexane and filtering off the black particles from the deep-brown solution. Low-temperature crystallisation yielded a black crystalline solid which was filtered on a 3X sinter and dried in a vacuum desiccator.

9(6) Properties

The crystals fume in moist air and darken with time (presumably due to nickel being deposited on the surface). A qualitative analysis on the green solution formed by

dissolving the crystals in concentrated HCl, demonstrated the presence of nickel, phosphorus and iodine. Quantitative analysis figures were not encouraging at first:

	Found %	Calculated for $Ni(PI_3)_4$ %
Ni	10.34	3.44
I	53.41	89.29

However, further recrystallisations and preparations from hexane containing PI_3 gave samples analysing typically as:

	Found %	Calculated for $Ni(PI_3)_4$ %
Ni	3.80	3.44
I	88.15	89.29

The analysis figures may be explained by partial decomposition to nickel metal and PI_3, and the possibility of $Ni(PI_3)_4$ having been isolated seems reasonable if not wholly definite.

The black solid dissolved in hydrocarbon solvents to give brownish-orange solutions which are turbid at the outset, so no Raman solution work was possible. The solid itself was too dark for Raman excitation. Spectroscopic investigations were thus limited to infra-red work.

9(7) Spectroscopic investigations

Stammreich has reported the Raman spectrum of PI_3 with polarisation data (98) using He 6678 Å excitation. The infra-red spectrum of the black crystals, prepared and analysed above, was obtained as a nujol mull between polythene plates in the region 33-500 cm^{-1}.

The sample proved to be unstable in the infra-red beam and decomposed after a few minutes. Spectra of fresh and decomposed samples are shown in Figure 9D, along with the spectrum of PI_3 itself. The broader features of the decomposed sample in spectrum (b) are consistent with spectrum (a) having spectrum (c), due to PI_3, superimposed upon it.

A tentative assignment of the modes in the F_2 species of the suspected $Ni(PI_3)_4$ may be made (Table 9D). The asymmetric Ni-P stretch, ν_{17}, seems quite prominent, as are the P-I stretching vibrations, ν_{13} and ν_{14}.

The PI_3 deformations are not, however, so evident; the one remaining feature in the spectrum is the medium-weak intensity band at 184 cm^{-1}. By analogy with the bromo-analogue, assuming the same reversal of symmetric and anti-symmetric deformations exists, this could reasonably be assigned to the asymmetric deformation. However, the

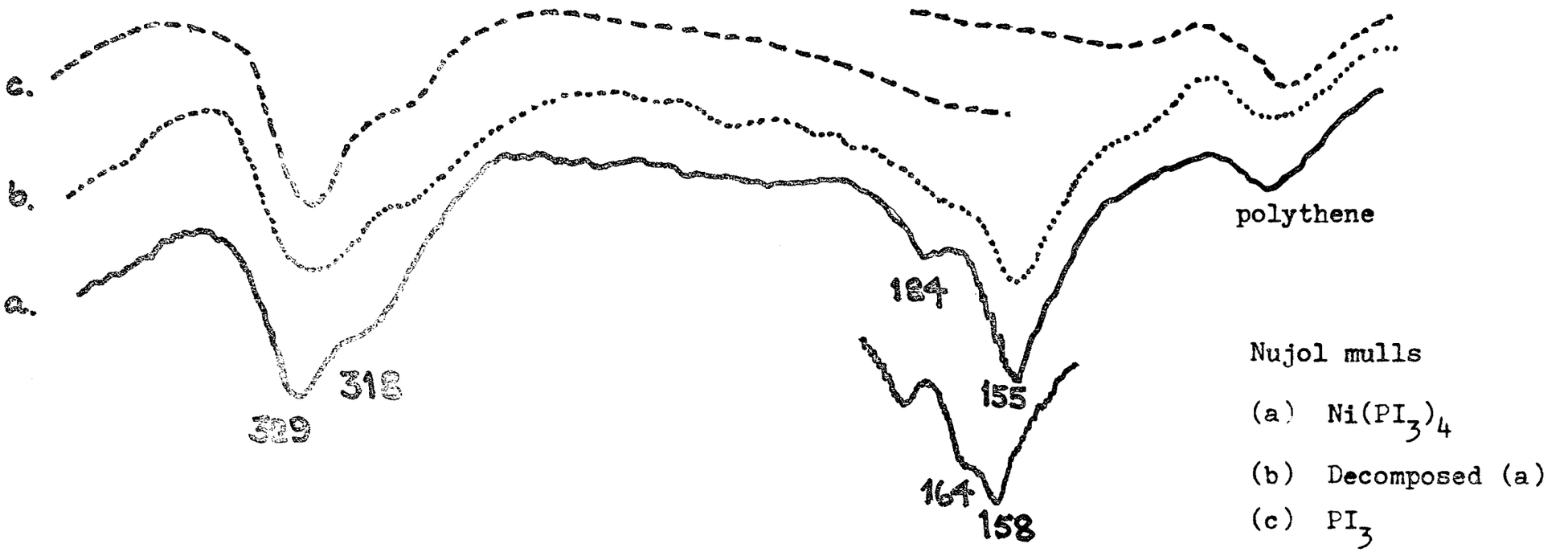


Figure 9D. The Infra-Red Spectrum of $Ni(PI_3)_4$

TABLE 9D

The Infra-red spectrum and tentative assignment of $Ni(PI_3)_4$

F_2-species

		cm^{-1}	PI_3 (98)
ν_{13}	P-I asymmetric stretch	329 m	325
ν_{14}	P-I symmetric stretch	318 m,sh	303
ν_{15}	PI_3 asymmetric def.	184 m	79
ν_{16}	PI_3 symmetric def.	-	111
ν_{17}	NiP asymmetric stretch	164 m,sh 155 m 158 m	
ν_{18}	PI_3 rock	-	
ν_{19}	NiP_4 def.	-	

feature at 155 cm^{-1} assigned to the ν_{17}, Ni-P stretch, would 'obscure' the symmetric PI_3 deformation.

There is, then, much doubt cast on the identification of this black solid as $Ni(PI_3)_4$ and possible alternative assignments of the 184 cm^{-1} and 155 cm^{-1} features are given below:-

(i) the 184 cm^{-1} band is the antisymmetric PI_3 deformation, and the 155 cm^{-1} is <u>either</u> the Ni-P stretch <u>or</u> the symmetric PI_3 deformation.

(ii) The 184 cm^{-1} band is the Ni-P stretch, leaving the 155 cm^{-1} feature to be assigned to the PI_3 antisymmetric deformation.

The situation could not be clarified further since the Raman data necessary were lacking. However, repeated infrared spectra of the 100-200 cm^{-1} region revealed that the rather broad 155 cm^{-1} feature did, in fact, consist of two features, at 165 and 158 cm^{-1} (see Figure 9D). This does not really clarify the situation since three alternative assignments are now possible:

	I	II	III
PI_3 def.asym.	164	184	184
PI_3 def.sym.	158	164	158
NiP stretch asym.	184	158	164

To assist in the assignment an estimated ν for the Ni P asymmetric stretch is given by plotting the ν_{Ni-P} against the atomic weight of X in the series $Ni(PX_3)_4$, (Figure 9E). The estimated ν_{Ni-P} asym. is given as 183 cm^{-1} for $Ni(PI_3)_4$. Also, a plot of ν versus the molecular weight of PX_3 gives a very similar result for ν_{Ni-P}. This result is fortuitously close to the band observed at 184 cm^{-1} above. Thus a <u>possible</u> partial assignment of $Ni(PI_3)_4$ is given below:

ν_{13}	P-I asym.str.	329 cm^{-1}
ν_{14}	P-I sym.str.	318 cm^{-1}
ν_{15}	Ni-P asym.str.	184 cm^{-1}
ν_{16}	P-I asym.def.	164 cm^{-1}
ν_{17}	P-I sym.def.	158 cm^{-1}

The whole situation, as seen above, is most unsatisfactory, and, in the absence of Raman data, is irresolvable. In view of this impasse it would be unjustifiable to assume that $Ni(PI_3)_4$ had been isolated, although the infra-red spectrum does give some promise that $Ni(PI_3)_4$ could well have been made.

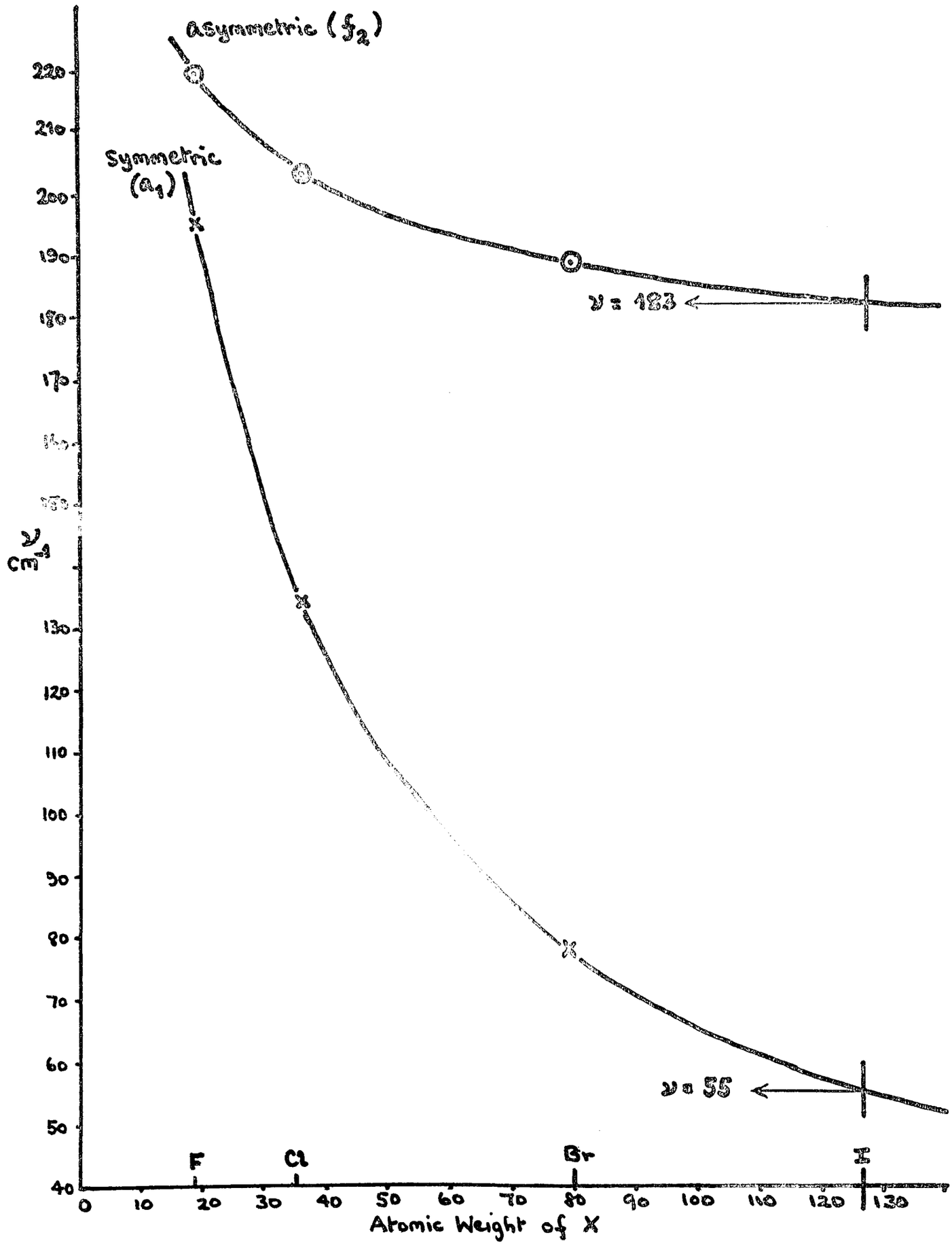


Figure 9E. Ni - P Stretching for $Ni(PX_3)_4$ molecules

CHAPTER 10

Chapter 10

FORCE CONSTANT CALCULATION ON $Ni(PCl_3)_4$ AND $Ni(PBr_3)_4$

10(1) Preliminary Calculations using a Simple Valence Force Field

In these calculations it was assumed that every mode was 'pure'; the force constants were calculated in an analogous manner to those which were obtained for the $M(PF_3)_4$ molecules in Chapter 7. In Chapter 7 it was pointed out that, while the P-F and M-P stretching modes were nicely described, that of the PF_3 deformation was extensively mixed. Exactly similar force constant calculations were carried out, using the simple computer programme (and also iterated manually), for the heavier molecules $Ni(PCl_3)_4$ and $Ni(PBr_3)_4$ on the A_1 block frequencies.

For $Ni(PCl_3)_4$, an initial trial set of force constants was selected using the force constants of PCl_3 (5, 82, 92). Iteration was accomplished and modifications were made to each force constant. These modifications are obtained by multiplying the calculated force constant by $\lambda_{observed}/\lambda_{cal.}$. In this way convergence to the "best fit" is normally

achieved, as, for example, in the case of the $M(PF_3)_4$ molecules. In the case of $Ni(PCl_3)_4$, however, convergence began to appear, and then further modification of the force constants resulted in a divergence from the observed λ values. Starting from slightly different initial sets of force constants, this divergence was found to occur at different points. The convergence-divergence is measured by the RMS deviation of the calculated ν's from the observed ν values.

Such a phenomenon is very perturbing and is normally indicative of a breakdown in the force-field applied to the calculations. Some illustrative data are reproduced in Table 10A for $Ni(PCl_3)_4$ and also for $Ni(PBr_3)_4$. The "best fit" in the case of the former is obtained with an RMS deviation of 4.92%, and in the latter case 11.82%. The symmetry coordinate vectors for each molecule at their respective "best fits" are given in Table 10B. It is seen that the extent of mixing of the three a_1 species in the case of $Ni(PCl_3)_4$ is greater than was experienced in the calculations on the fluoro-analogue. From these vectors it can be deduced that the nickel-phosphorus stretching mode is rightly described as such, but that the "PCl_3 deformation" is controlled by the P-Cl stretching

TABLE 10A

Convergence-divergence phenomenon

Molecule	Force Constant Set			Calc. ν's cm^{-1}			Observed ν's cm^{-1}			RMS deviation
	f_1	f_2	f_3	ν_1	ν_2	ν_3	ν_1	ν_2	ν_3	
$Ni(PCl_3)_4$	5.32769	0.68626	4.24413	605	341	137	518	310	135	11.32 %
	3.90562	0.56716	4.12105	555	301	130				4.92
	3.40222	0.60158	4.44414	559	288	134				6.15
	2.92140	0.69700	4.51071	569	274	135				8.77
	4.9232	0.3395	3.3953	527	299	108				11.76
	4.7502	0.3660	5.2633	569	316	121				8.32
	4.3712	0.3776	5.5455	570	310	123				7.73
	3.6159	0.3777	6.6906	584	294	126				8.82
	2.28472	0.4200	7.6518	603	269	134				12.16
	2.1014	0.5570	7.8194	619	237	148				18.48
	1.4703	0.7387	6.5206	609	204	154				23.65
$Ni(PBr_3)_4$	1.8000	0.3000	2.5000	397	141	66	362	155	78	11.00
	1.4975	0.3631	3.4542	441	132	75				18.35
	1.0069	0.4989	3.9725	480	122	83				21.80
	0.5725	0.9525	3.6566	550	102	80				34.71

TABLE 10B

Vectors for $Ni(PCl_3)_4$ and $Ni(PBr_3)_4$

A_1 block frequencies

A. $Ni(PCl_3)_4$

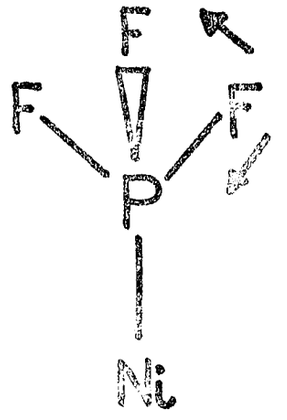
	S_1 P-Cl stretch	S_2 PCl_3 def.	S_3 Ni-P stretch
S_1	**1.057000**	-0.439775	**-1.239715**
S_2	**1.663548**	0.324538	0.660083
S_3	-0.144839	0.518106	**-1.465758**

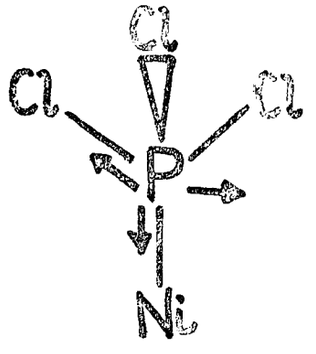
B. $Ni(PBr_3)_4$

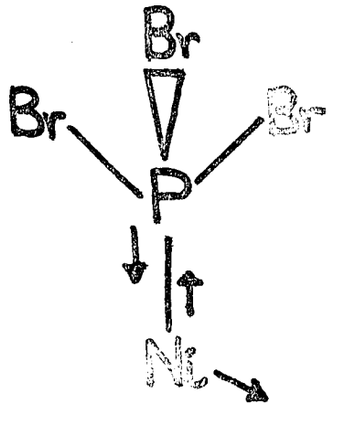
	S_1 P-Br stretch	S_2 PBr_3 def.	S_3 Ni-P stretch
S_1	0.107911	**-0.761094**	**-1.165481**
S_2	0.359581	0.579822	**-1.240996**
S_3	**0.656937**	-0.192351	**0.870719**

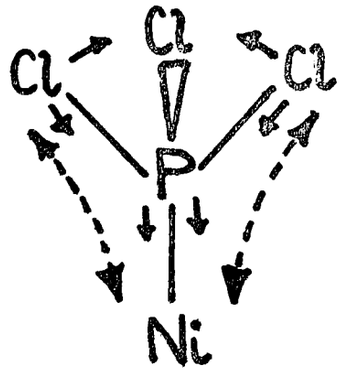
force constant. The "P-Cl stretching mode" contains a greater contribution from the nickel-phosphorus force constant than from its own phosphorus-chlorine force constant. The case of $Ni(PBr_3)_4$ is even more extreme, and here none of the modes is pure.

In the vibrational assignments of $Ni(PCl_3)_4$ and $Ni(PBr_3)_4$ it was observed that the a_1-species frequencies had 'moved' closer together relative to the fluoro-compound. This is expected as the mass of the ligand increased from PF_3 to PBr_3. If one considers the motion of the atoms in the ligand, a striking difference is noticed between the three molecules under investigation. Figure 10A shows a nickel atom bonded to PF_3, PCl_3 and PBr_3 respectively. On mass considerations, the mechanical motion of the fluorine atoms in a PF_3 group would involve but little motion of the phosphorus atom; therefore the vibrational modes may be fairly accurately termed PF_3-stretching or PF_3-deformation. On going over to PCl_3, however, chlorine exceeds phosphorus in atomic mass, so much more of the vibration is contributed to by the P atom. At the extreme, where a PBr_3 group is bonded to a nickel atom, both the P and Ni atoms are much lighter than bromine so virtually <u>all</u> the motion is dictated by the phosphorus atom. The nickel atom in $Ni(PBr_3)_4$ should move









PCl_3 Breathing

Atomic Weights.

Ni	58
P	31
F	19
Cl	36
Br	80

Figure 10 A. Ligand Motions in $Ni(PX_3)_4$

but little as it has four phosphorus atoms around it.

On these simple mechanical grounds, therefore, it is seen how we are highly idealising the situation by referring to modes as "P-X stretching" or "PX_3 deformation". It would, in the case of $Ni(PCl_3)_4$ especially, be more correct to refer to such vibrations as breathing motions of the PCl_3 group as a whole. Such a breathing motion of the PCl_3 group (to which the P atom contributes greatly) would involve nickel-phosphorus bond stretching - and affords an attractive mechanical model explaining the participation of the Ni-P force constant in the "PCl_3-modes", as given by the vectors in Table 10B. A graphic description of such a "breathing mode" is given at the foot of Figure 10A.

10(2) The Bruton Programme - a more sophisticated examination of force constants

Following the force-field work of M.J.Bruton (99), a computer programme existed which was quite versatile and suited admirably the problem of non-convergence in $Ni(PCl_3)_4$. The Programme, entitled the "Bruton UBG1" programme, had been written for the Ferranti "Mercury" computer, and was not directly applicable to the KDF9 computer presently available in Oxford. Some modifications had thus to be made, these being

(a) the replacement or erasure of 'machine instructions' which applied to the 'Mercury' computer, which would not be acceptable to KDF9. Such an instruction was 'HOOT', this being completely incomprehensible to KDF9. Gratitude is expressed to Dr.J.F.Rollett, Deputy Director of the Oxford Computing Laboratory, for advice on these computing matters.

(b) the substitution of two complete chapters in UBG1, involving GX multiplication and extraction of the roots and vectors, and their replacement with similar chapters specially written for KDF9 and available as a sub-routine, called Programme 517.

The final programme, the modified UBG1, consisted of 8 chapters and was printed on 5-hole paper tape. In view of the extensive modifications, described above, which had to be made to the original Programme UBG1, it was essential to test the modified programme in all its aspects to see if reproducibility of the original working operations occurred exactly. This will be described later; the logic of the UBG1 programme will now be outlined.

In the previous force constant calculations, trial values of the force constants were used to calculate frequencies, then trial and error processes were used to

refine the frequencies so obtained to make them as close as possible to the experimental values. In UBGl a systematic process of refinement based upon the Method of Least Squares was used (100). A trial set of force constants is fed to the computer together with other details necessary to define the force field and the geometry of the molecule. This initial set of force constants is used to calculate corresponding roots of the secular equation and also a Jacobian matrix of variations in the roots with variations in the force constant values. Using this matrix and suitably-weighted deviations between the calculated and observed roots, a set of modifications (δP) is derived; and these modifications, suitably scaled, are applied to the initial force constant values.

The whole process is repeated until, eventually, the calculated δP values converge to zero. At this point, the calculated frequencies correspond to a "best fit" set of force constant values, defined so that the weighted sum of squares of discrepancies in the λ values is a minimum. The δP vectors needed to be scaled if convergence is to take place, due to the unsatisfactory expectation that the linear relationship between $\delta\lambda$ and δP applies over the range of P values involved.

Mathematically,

$$\delta\lambda = R\,\delta P$$

where R is the Jacobian matrix $[\delta\lambda_i/\delta P_j]$, determined at an initially chosen set of P_k values. An optimum set of δP values is given by

$$\delta P = [R^T W R]^{-1} R^T W\,\delta\lambda$$

where W is a diagonal matrix of chosen weights, and $\delta\lambda$ the difference between experimentally observed values and those calculated from the set of force constants P_k.

The resulting P set will be the "best fit", where

$$\sum_i W_i(\delta\bar{\lambda}_i - \delta\lambda_i)^2 \text{ is a minimum.}$$

$\delta\lambda_i$ are the calculated changes in the roots, and $\delta\lambda_i$ the actual discrepancies.

In UBGl, W is taken as $[1/\lambda^2_{obs.}]$, and the best fit is based on a %age in ν i.e. $\sum(\delta\nu_i/\nu_i)^2$ = minimum.

Since the relationship between $\delta\lambda$ and δP is only approximately linear, then the new roots calculated from the new P values will <u>not</u> be those expected from the linear approximation. Therefore, although the best set of P values will not be obtained by one modification only from the initial set, the new frequencies should be an improvement on the

initial set. The process is repeated, until eventually the δP values will become very small, and a satisfactory degree of convergence has been attained.

10(3) The Programme UBG1

The basic requirement is to read in details of the molecule under investigation together with a trial force constant set. Input data required are,

$\mathcal{G}$ matrix, or matrices, if more than one symmetry species is being investigated,

U matrix of symmetry coordinates

F matrix

P set of trial force constant values

ν set of experimental frequencies

W the diagonal weight-matrix, to give a best fit on a %age basis

Y matrix relating $\mathfrak{F}$-entries to individual force constants

x scaling factor(s)

y specified number of modifications (i.e. "cycles")

An advantage of the programme is its flexibility. Force constants of the SVFF and UBFF type are read in separately. If a complete vibrational assignment is not known, the missing

frequency (or frequencies) can be calculated for by putting the relevant entry in the W-matrix equal to zero. The Jacobian R is calculated at each modification, the δP adjustments obtained and the cycle is repeated for a specified number of times or until convergence has been reached.

After the final modification of P has occurred, in addition to the frequencies, force-constants, % deviation of frequencies and RMS% which are printed at each stage in the process, other pieces of information are given. These include the $\mathcal{L}$ matrix of vectors, $\mathcal{G}$, Y which act as a check on the correctness of reading-in of data to the computer. The end-routine checks minimise the danger, ever present in computing-work, of spurious results being produced due to mis-calculation or mis-reading of data. For example, the $\mathcal{L}$ matrix is printed, and so is $\mathcal{L}^T$. Multiplication of $\mathcal{L}\mathcal{L}^T = \mathcal{G}$, and if this relationship holds the λ -values found are the correct roots of $\mathcal{G}\mathcal{F}$. Failures are found if, say, the F matrix is not symmetrical, or if an error in the U matrix results in an unsymmetrical $\mathcal{F}$.

The necessity for scaling is indicated by earlier experience of obtaining force constant values by machine, which often leads to instability in the convergence cycle. The instability is due to invalidity in the assumption that the relationship between $\delta\lambda$ and δP is linear, except for

small changes in δP values. Three scaling factors were specified in decreasing order of size, e.g. 1, 0.5, 0.1. These were then used to modify each δP set, in turn, until the lowest value was used and the frequency fit obtained was an improvement on the previous fit (in RMS deviation).

A flowchart is given in Figure 10B, showing the programme logic. The set-up of the data is illustrated for the example $Pt(PF_3)_4$ in Appendix 1, for the A_1 block of frequencies.

As stated earlier, the UBG1 programme had to be tested, with its modifications and on the new computer, to see if its performance matched that of the "old" programme. The best documented example (99) which was suitable for such a test was provided by a 9-parameter force-field study of the molecule SF_5Cl.

This example was rather a complex one, as it involved G matrices for 4 symmetry species of SF_5Cl, and used 5 SVFF constants and 4 Urey Bradley force constants for the 11 vibrational frequencies. The G, F and Y matrices were set up according to (99). Gratitude is expressed to Dr.M.J.Bruton for consultation and discussion of the setting up procedure and 'modus operandi' of his programme UBG1. After much correction of paper-tape errors a working programme

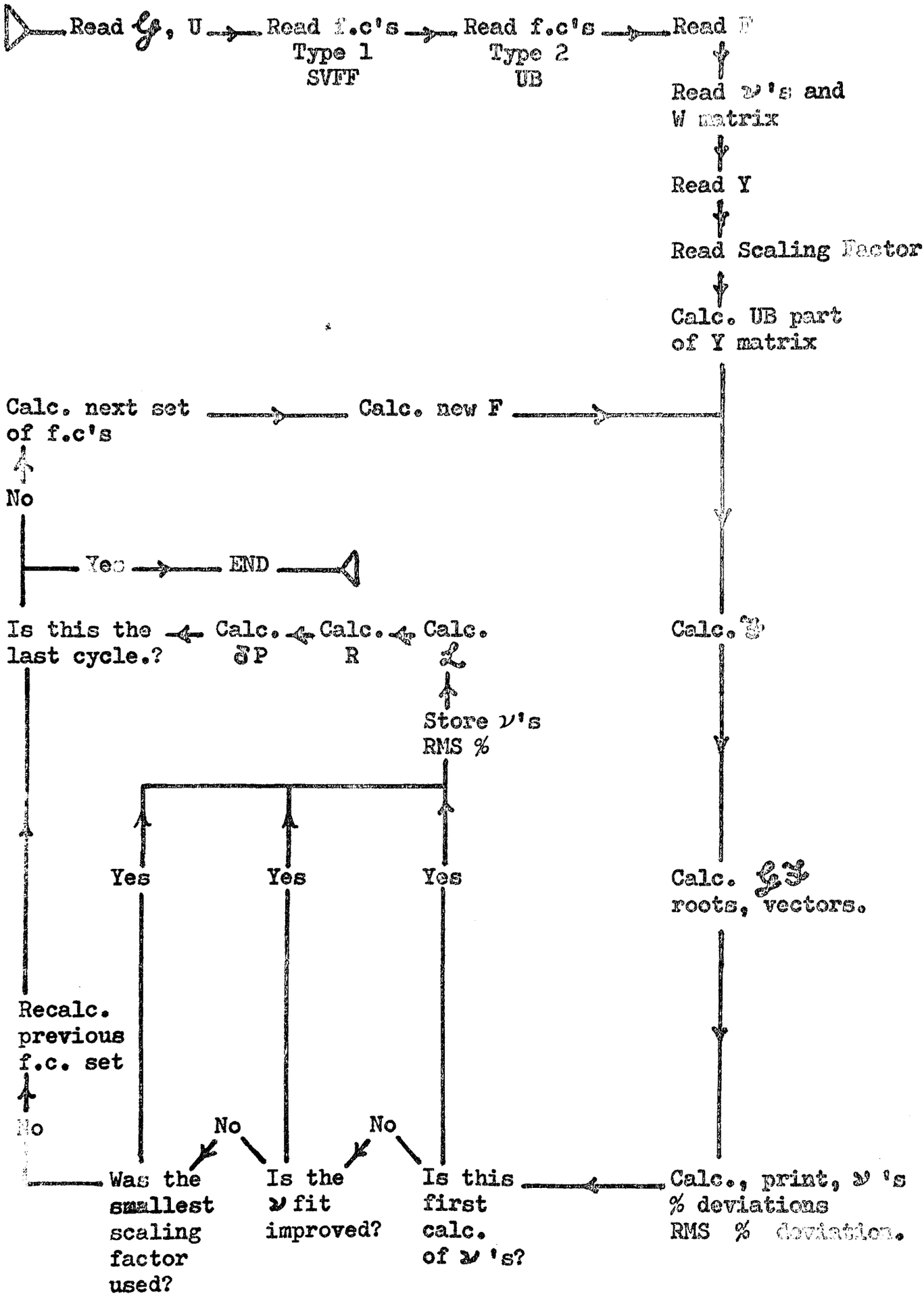


Figure 10 B. Flowchart, UBG 1 Programme Logic.

was obtained, which for SF_5Cl gave the 'best fit' frequency set in Table 10C. Bruton's results are given for comparison; to all intents and purposes the two are identical and confirms the reproducibility of the new programme.

10(4) Application of UBG1 to $M(PF_3)_4$ molecules

Before applying the UBG1 Programme to $Ni(PCl_3)_4$ it was essential to investigate $Ni(PF_3)_4$ in a similar manner, for comparison purposes. Some slight difference was observed between the force constants calculated using UBG1 and those calculated using the simple procedures of Chapter 7. Because of this, the molecule $Pt(PF_3)_4$ was also re-examined with UBG1.

The force-field selected was a diagonal 3-parameter field, as in Chapter 7. The $\mathcal{G}$, U and F matrices were constructed as indicated previously. Only the A_1 block of frequencies was considered. Scaling factors were 0.5, 0.1, and 0.05, and the number of programme cycles or modifications was 20. A typical data-tape containing this information, as exemplified by $Pt(PF_3)_4$, is given in Appendix 1.

The results were obtained after some 4 minutes of computer time per molecule. In Table 10D are given the

TABLE 10C

Test on the UBG1 Programme

SF_5Cl 9-parameter force-field

Modification 12

Scaling Factor 0.5

Present Work "KDF9"		M.J.Bruton (99) "Mercury"	
ν (cm^{-1})	% deviation	ν (cm^{-1})	% deviation
856.20	0.26	856.20	0.26
715.00	1.71	715.04	1.71
593.75	-1.37	593.70	-1.38
403.31	-0.17	403.31	-0.17
610.06	-2.23	610.04	-2.24
398.07	0.52	398.09	0.53
503.99	-0.00	504.00	0.00
917.91	1.09	917.91	1.09
577.52	-0.08	577.53	-0.08
444.46	0.56	444.47	0.56
267.55	-0.91	267.55	-0.91
RMS deviation	1.065%	RMS deviation	1.065%

TABLE 10D

$Ni(PF_3)_4$ and $Pt(PF_3)_4$

Results from UBG1

Molecule	Initial force constant set (Z units)	Final f.c.set Z units	Final f.c.set 10^5 dynes/cm	No.of mods.	Calc.ν's (cm^{-1})	% deviation $\frac{\nu_{obs}-\nu_{calc.}}{\nu_{obs}}$ %	RMS % deviation
$Ni(PF_3)_4$	13.5131	13.1247	7.7311	17	954	0.00	0.00
	1.2205	0.9073	0.5344		534	0.00	
	3.3452	4.6351	2.7303		195	0.00	
$Pt(PF_3)_4$	13.1267	12.9943	7.6543	17	958	0.00	0.00
	0.9090	0.7742	0.4560		546	0.00	
	4.6247	6.9008	4.0649		213	0.00	

best-fit force constant set, the frequencies corresponding to this, and the RMS% deviation, for both molecules. An exact frequency fit between observed and calculated ν's is given for both molecules; although the final force constant sets are slightly different to the results in Chapter 7, due to the more sophisticated calculation and convergence procedures in the UBG1 programme, the conclusions of Chapter 7 are in no way affected by this. The largest difference is in the k_{Pt-P}, which is increased from 3.8 to 4.0 x 10^5 dynes/cm. The convergence is rapid, as is shown by the graph (Figure 10C) showing the RMS% discrepancy at every modification for $Pt(PF_3)_4$.

10(5) Application of UBG1 to $Ni(PCl_3)_4$

It will be remembered from 10(1) that the force-field was "ill-conditioned" for convergence to the observed frequency values of $Ni(PCl_3)_4$. A data-tape was constructed for this molecule after the fashion of Appendix 1. The scaling constants chosen were 0.5, 0.1 and 0.05. The calculation of the λ-values from the initial force constant set progressed normally, but the programme <u>failed</u> to obtain a set of frequencies from the newly modified force constants. The actual result was:

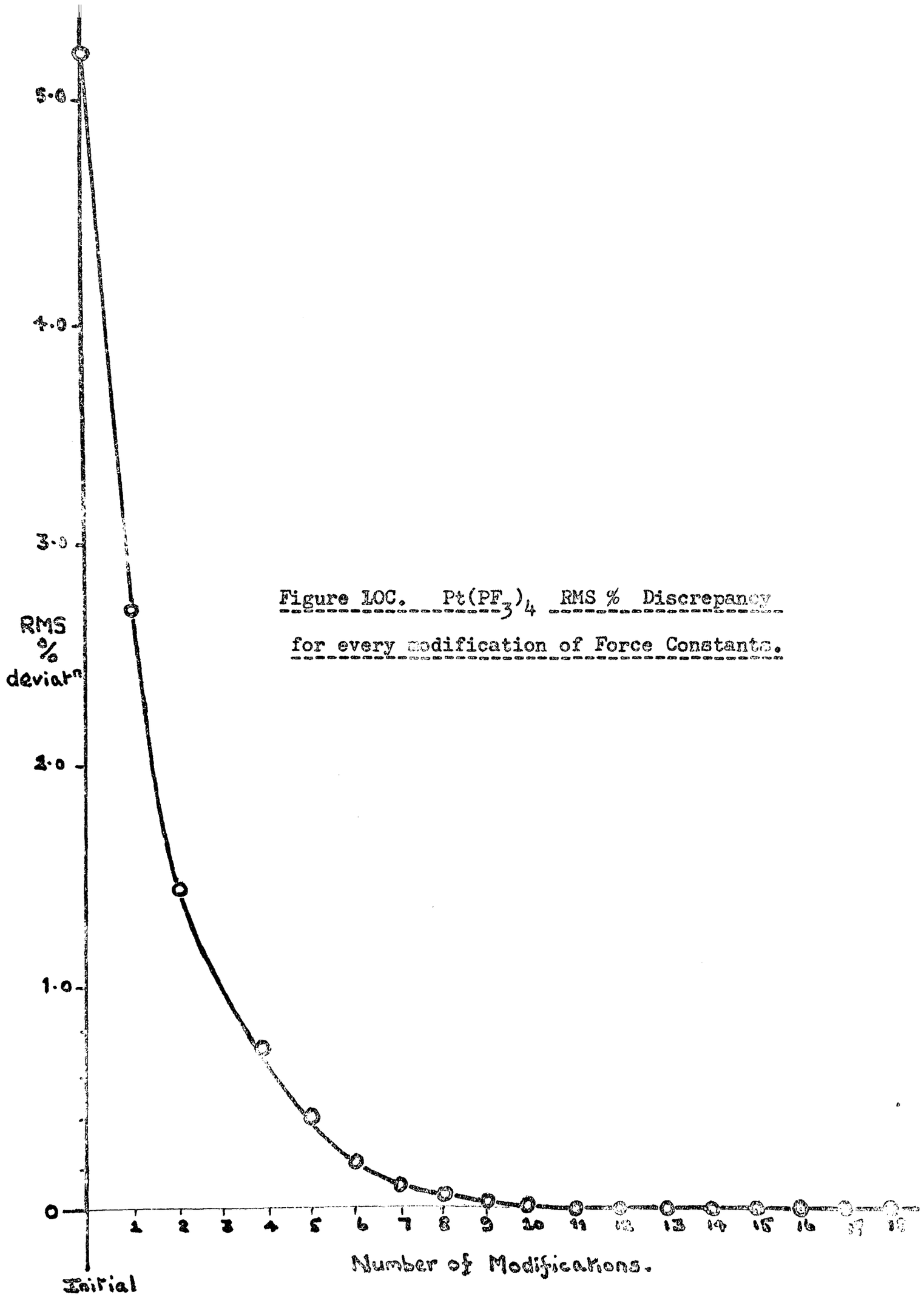


Figure LOC. $Pt(PF_3)_4$ RMS % Discrepancy for every modification of Force Constants.

		ν	%
Force constant set	3.9056	giving 554.51	7.05
	0.5672	300.84	-2.96
	4.1211	129.77	-3.87
		RMS deviation	4.95%

Scaling Factor 0.5

This failure of the programme is mysterious; a post-mortem revealed that the square root of a negative number was attempted, causing break-down of the logic. The programme baulked at the scaling factor of 0.5, which must thus be conferring too large a "jump" on the δ P value. If the force-field description is ill-conditioned, then even moderately small changes in δ P could result in a vastly different set of $\delta\lambda$ values.

The remedy in such a case is obviously to converge more slowly upon the λ-values, by taking smaller 'steps' of δ P in a modification of the initial force constant set. Different scaling factors were then employed and the results were as follows:

Scaling Factor Set			No.of modifications	Final RMS%
0.5	0.1	0.05	None	4.95
0.1	0.05	0.01	2	4.92
0.01	0.005	0.001	10	4.92

In Table 10E the convergence results are summarised (a) for the scaling factors of 0.1, 0.05, 0.01 (b) for the scaling factors of 0.01, 0.005, 0.001.

Even with as low a scaling factor as 0.001, the "best fit" is attained with an RMS deviation of 4.92% which is hardly better than the results obtained at higher scaling factors. Table 10E provides an excellent example of the working of the programme: if the RMS deviation of the calculated ν's from the modified is greater than that obtained with the previous set, a re-calculation is made with the next lowest scaling factor, and so on until the lowest scaling factor has been used.

Although all this work with smaller scaling factors has improved the result of the simpler process by very little only, one very interesting fact to emerge is the sensitivity of the nickel-phosphorus λ-value (or frequency) and force constant to very small changes in the force constant set. In the close neighbourhood of the "best fit" at an RMS deviation of $\sim$ 4.92% there are several sets (albeit similar) of force constants giving a similar RMS deviation in frequency fit. There are some 6 of these sets in all:

TABLE 10E

Convergence in $Ni(PCl_3)_4$

(a) Scaling Factors 0.1, 0.05, 0.01

Scaling Factor	F.C.set	ν set	% dev.	RMS %	Modif.
	3.9056	554.51	7.05		
	0.5672	300.84	-2.96		
	4.1211	129.77	-3.87	4.946	Initial
0.10	3.6273	555.56	7.25		
	0.9144	302.49	-2.42		
	1.8990	107.00	-20.74	12.763	1
0.05	3.7665	553.87	6.93		
	0.7408	301.64	-2.70		
	3.0100	124.28	-7.94	6.279	
0.01	3.8778	554.20	6.99		
	0.6019	300.95	-2.92		
	3.8989	129.59	-4.01	4.946	
0.10	4.2273	553.89	6.93		
	0.3086	302.50	-2.42		
	5.4553	114.07	-15.50	9.902	2
0.05	4.0525	553.26	6.81		
	0.4553	301.48	-2.75		
	4.6771	126.18	-6.53	5.673	
0.01	3.9127	553.88	6.93		
	0.5726	301.04	-2.89		
	4.0545	129.51	-4.07	4.929	

PROGRAMME FAILS

(b) Scaling Factors .01, 0.005, .001

Scaling Factor	F.C.set	ν set	% dev.	RMS %	Modif.
	3.9056	554.51	7.05		
	0.5672	300.84	-2.96		
	4.1211	129.77	-3.87	4.946	Initial
0.01	See (a)				1
0.01	See (a)				2
	.	.	.	.	.
	.	.	.	.	.
	.	.	.	.	.
	.	.	.	.	.
0.01	4.1996	555.24	7.19		
	0.3155	302.44	-2.44		
	5.4921	115.09	-14.74	9.575	9
0.005	4.0607	553.52	6.86		
	0.4478	301.55	-2.73		
	4.7280	125.86	-6.77	5.783	
0.001	3.9495	553.03	6.76		
	0.5536	301.32	-2.80		
	4.1167	128.99	-4.45	4.946	
0.01	3.9327	552.71	6.70		
	0.5760	301.42	-2.77		
	3.9684	128.95	-4.48	4.921	10

PROGRAMME FAILS

TABLE 10F

Force Constants of $Ni(PCl_3)_4$ and PCl_3

$Ni(PCl_3)_4$ Present work Mean			PCl_3 (92) Lorenzelli	PCl_3 (5) Herzberg	
Z units	10^5 dynes/cm				
		k_{P-Cl} str.	2.05	2.12	x 10^5 dynes/cm
3.9281	2.3138	k_{P-X} str.			
0.5758	0.3392	k_{PX_3} def.	k_{PCl_3} def. 0.43	0.32	
3.9827	2.3460	k_{Ni-P} str.			

	3.9299	3.9217	3.9327
	0.5714	0.5800	0.5760
	4.0158	3.9639	3.9684
RMS%	4.922	4.921	4.921
	3.9127	3.9065	3.9055
	0.5726	0.5794	0.5924
	4.0545	4.0128	3.9013
RMS%	4.929	4.926	4.929

The mean of the three upper sets was taken - giving a mean RMS deviation of 4.921%, and is given in Table 10F, together with the force constants of PCl_3 for comparison. The discrepancy between the results of Lorenzelli (92) and Herzberg (5) can be accounted for by the interaction constants considered in the former case.

10(6) Bonding in $Ni(PCl_3)_4$

Very little can be said in the way of a detailed discussion of the bonding in $Ni(PCl_3)_4$ considering the extent of mixing of the a_1 modes, shown by the vectors in 10(1). The P-Cl stretch is considerably 'impure', and this mode incorporates much Ni-P stretching. One is, thus,

not justified in making any conclusions as to whether the P-Cl bond has been strengthened or weakened on being bound to a nickel atom. Qualitatively, as deduced in Chapter 7, one might expect that the phosphorus-chlorine bond would be subjected to two opposing effects,

(a) a strengthening of the bond. Donation of the lone pair leaves the P atom with a formal positive charge. The Cl atoms should thus move nearer to the phosphorus, but not to so great an extent as in PF_3, since chlorine is less electronegative than fluorine.

(b) a bond-weakening. π-donation from the nickel to the phosphorus reduces the positive charge on the P atom which then repels the chlorine.

Contributions of the $P{=}Cl^+$ type are more favoured for chlorine than the analogous contribution in the PF_3 case, and this, too, would tend to strengthen the P-Cl bond.

The nickel-phosphorus stretching mode, ν_3, by comparison is quite pure, and the force constant is 87% of the corresponding force constant in $Ni(PF_3)_4$. Now PCl_3 is a better σ-donor than PF_3, but would be much worse as a π-acceptor. Thus, graphically we can illustrate this difference and its effect on the Ni-P bond as follows,

(I) $Ni \underset{\sigma}{\overset{\pi}{\rightleftarrows}} PF_3$ $\qquad$ $Ni \underset{\sigma}{\overset{\pi}{\rightleftarrows}} PCl_3$ (II)

A possible explanation for the decrease in k_{Ni-P} would be that, although the σ-bond is stronger for (II) compared with (I), the π-function is much weaker. Since the net result is a weakening of the k_{Ni-P}, one must conclude that the π-back donation is of great importance in these $Ni(PX_3)_4$ compounds (and outweighs the difference in σ-donation between PCl_3 and PF_3).

This is an interesting conclusion and it is unfortunate that it cannot be tested by comparison of the k_{P-X} stretching force constant (which is impure in the case of the PCl_3 compound).

A similar investigation on $Ni(PBr_3)_4$ using the UBGl Programme gave only slight improvement on the simple calculation, but the final RMS% deviation is still 10.77%, after 8 modifications with a scaling factor of .01, .005, and .001:

Initial set of f.c.'s	1.8000	0.3000	2.5000
RMS% deviation	11.01%		
Final set	1.7782	0.3719	2.0478
RMS% deviation	10.77%		

The same frequency fit is given in each case. No conclusions can be made concerning bonding in this molecule since

the mixing between the modes is so extensive that not one mode is identifiably pure.

CHAPTER 11

Chapter 11

TETRAKISTRIMETHYLPHOSPHINE-NICKEL° AND -PLATINUM°

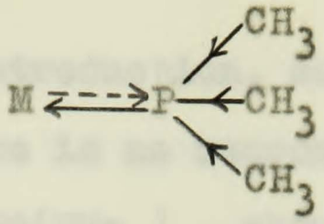
$Ni(PMe_3)_4$ AND $Pt(PMe_3)_4$

11(1) Introduction

Although the partially-substituted compounds $Ni(CO)_x(PMe_3)_{4-x}$ $x = 1 \rightarrow 3$, have been characterised and studied (34,38), the compound $Ni(PMe)_4$ cannot be obtained by reacting PMe_3 with nickel carbonyl. The tetrakistriethylphosphine analogue was isolated by Wilke (101) from the reaction of four moles of triethylphosphine with bis-π-allyl nickel, a zerovalent nickel compound. The compound $Ni(P\emptyset_3)_4$, $\emptyset$ = phenyl, is also known (66) as an unstable, air-sensitive red solid.

There is no reported literature on the analogous $Ni(PMe_3)_4$; trimethylphosphine is not favoured (66) as a ligand in organometallic work on account of its spontaneous inflammability in air and high volatility at room temperatures. For spectroscopic studies, however, PMe_3 is preferred to the higher organophosphines because of its relatively simple vibrational spectrum.

It would be of interest to attempt a synthesis of $Ni(PMe_3)_4$ in the present work. The diagram below illustrates a PMe_3 molecule bound to a metal atom M:



The inductive effect of the methyl groups makes the phosphorus atom rather more 'negative' than it would be in the case of halogen substituents. The phosphorus atom now has an increased donor-capacity, as is shown by the series below:

$F_3B.PMe_3$	>	$F_3B.PCl_3$	>	$F_3B.PF_3$
Stable		Decomposes 6°C		Not known
Forms immediately				
(61)		(102)		(61)

The tendency to form an adduct decreases from left to right of the series.

Although the increased power of donation in PMe_3 relative to, say, PF_3 would result in a stronger σ-bond between the metal and phosphorus atoms, the 'negative' phosphorus will decrease the extent of back-donation. It would be extremely interesting, therefore, to compare the vibrational spectra of the $-PMe_3$ and $-PF_3$ compounds and to examine the effect of this reversal of inductive effect in the ligand on the metal-phosphorus bond.

Although the introduction, so far, has been concerned with $Ni(PMe_3)_4$, there is no reason why the corresponding platinum compound, $Pt(PMe_3)_4$, should not exist. The compound $Pt(P\emptyset_3)_4$, $\emptyset$ = phenyl, is known (103,104), and is a yellow solid that is air-stable for only a few hours.

11(2) Preparation of the ligand, PMe_3

The preparation of trimethylphosphine has been described by Mann and Wells (105), who reacted phosphorus trichloride with methyl magnesium iodide under cooled conditions. The extent of the cooling was not specified, but such information is important, since, if the reaction is performed at room temperature a green slime is produced (106). The PMe_3 is prepared under a nitrogen atmosphere, since it is spontaneously inflammable in air, and the phosphine isolated as the air-stable adduct with silver iodide. In the present work the following procedure was adopted; experience of the preparation having been obtained during an earlier spectroscopic investigation of PMe_3 (107).

45 g. of fine magnesium turnings were placed in a two-litre, three-necked flask fitted with a reflux condenser, tap-funnel, and a motor-driven stirrer incorporating a nitrogen inlet. The apparatus was purged

with dry, O_2-free nitrogen and the reaction commenced by adding a few ml. of a 1:1 methyl iodide-diethyl ether solution to the magnesium. At regular intervals a solution of 90 ml. (210 g.) of methyl iodide in 450 ml. ether was added slowly. Frequent cooling of the reaction vessel in ice-water was necessary to prevent overheating. At the end of the reaction a small amount of magnesium remained; it is imperative that, although excess Grignard reagent is required for the subsequent reaction with PCl_3, there should be no methyl iodide present as this would diminish the yield of PMe_3 by forming the quaternary phosphonium iodide.

The reaction flask was now cooled in an acetone-CO_2 bath to -40°C, and whilst stirring rapidly a solution of 28 ml. (46 g.) PCl_3 in 150 ml. diethyl ether was added dropwise from the tap-funnel. The contents of the flask became bright orange in colour. Local excess of PCl_3 was avoided by stirring, so minimising the formation of the complex $2PMe_3.PCl_3$ which removes phosphorus trichloride from the reaction sphere (108). After completion of the addition of PCl_3, the flask was maintained at -40°C for ½ hour, and then was allowed to stand at room temperature for one hour to complete the reaction. The reflux condenser was now set for distillation, the receiver being another 2-litre, three-necked flask. In the receiver was placed a concentrated

solution of silver iodide (120 g.) in potassium iodide (200 g.) in 200 ml. water. The end of the condenser was fitted with a delivery tube, leading the nitrogen stream through the silver iodide-potassium iodide solution.

The temperature of the reaction flask was slowly raised to 230°C and maintained at this temperature for two hours. The trimethylphosphine was slowly liberated by thermal decomposition of the complexes in the reaction flask, and carried over in the nitrogen stream into the receiver. A white solid, an AgI-PMe_3 adduct, was formed. The receiver was left to stand overnight, and the white solid filtered off and dried over phosphorus pentoxide.

The yield from two such preparations was 90 g. of the dry adduct, which subsequently gave 22 g. of PMe_3, 46% of the theoretical yield. Long and Sackmann (109,110) have studied the preparations of Group V trimethyls and report that the best yield obtainable for trimethylphosphine under the above conditions was less than 50%. Lowering of yield is caused by hydrolysis, cleavage of the P-C bond in alkaline or acid conditions, and oxidation of the PMe_3 formed (111).

The silver iodide adduct of trimethylphosphine is stable to air at room temperature but smells strongly of PMe_3. The generation of trimethylphosphine from the adduct was accomplished using the apparatus of Figure 11A. Owing to

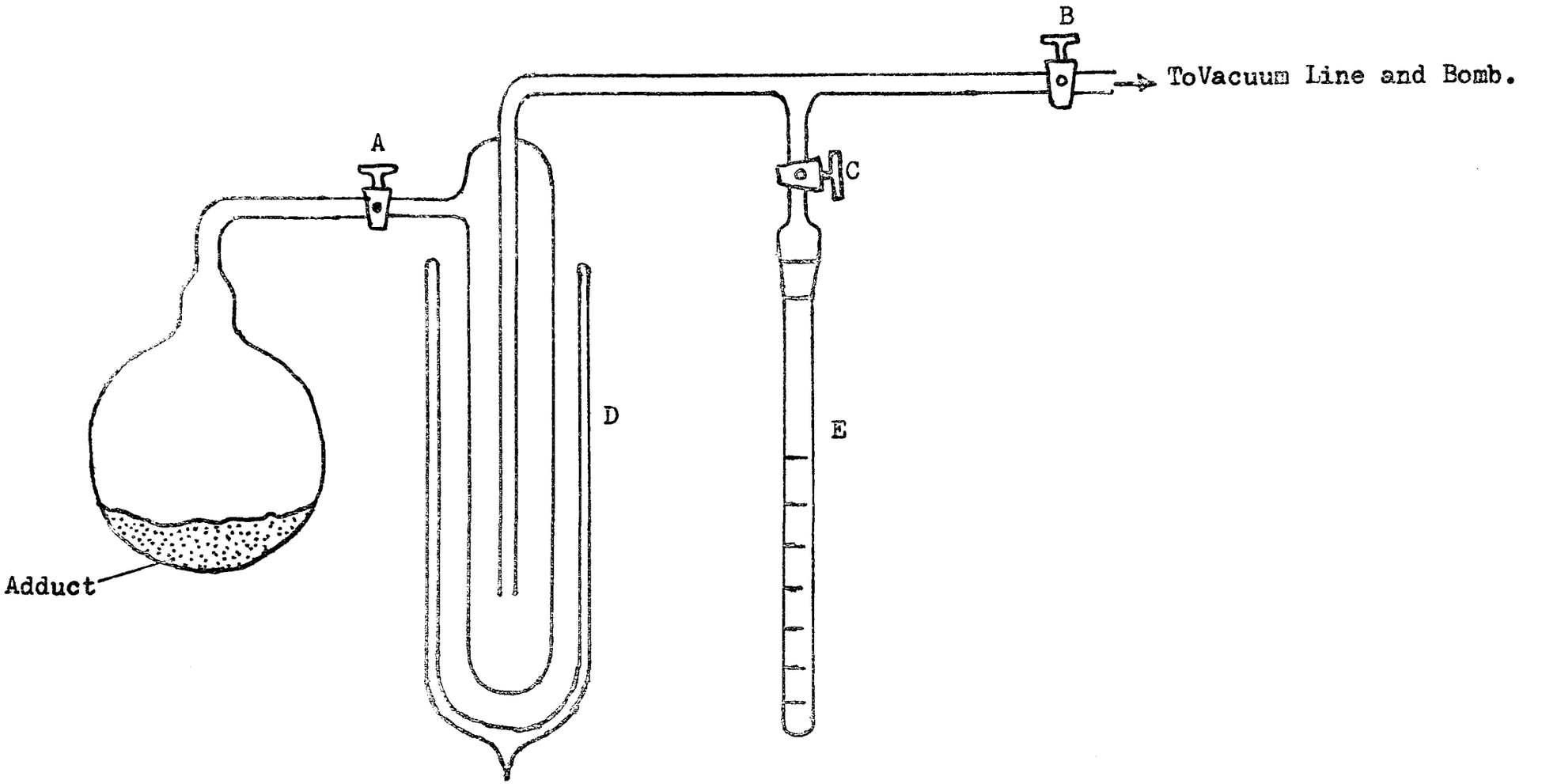


Figure 11A. Generation of PMe_3 from the Silver Iodide Adduct.

the spontaneous inflammability of the phosphine, the isolation of liquid PMe_3 was performed in an evacuated system. The heated vapours of the phosphine are especially likely to inflame with oxygen; hence the great care taken in the preparation of PMe_3 from the Grignard complexes, where ether was present to add to the explosion hazard.

In Figure 11A, the whole apparatus was evacuated and trap D cooled in liquid nitrogen. With taps B, C closed and A open, the adduct was heated with a coal-gas flame. The phosphine was liberated and condensed as a white solid in D. On heating, the adduct became yellow in colour and finally deep orange as the last of the PMe_3 was removed. Tap A was closed, C opened, and the liquid nitrogen bath transferred from trap D to the graduated tube E. The phosphine condensed in E, and by weighing a known volume the density of liquid PMe_3 was determined (8.0 ml. liquid phosphine weighed 6.4 g., giving a density of 0.80 gm./ml.). In this way a known weight of trimethylphosphine could be collected from the adduct, and condensed in the bomb, which was attached to the vacuum line beyond tap B, precisely as in the preparations involving PF_3.

11(3) Preparation of the $M(PMe_3)_4$ compounds (M is Ni,Pt)

The procedure is exactly analogous to that used in the preparation of the $M(PF_3)_4$ compounds, namely, a reductive phosphorylation at high pressures of PMe_3.

$$\underset{129}{NiCl_2} + \underset{304}{4PMe_3} + \underset{127}{2Cu} \longrightarrow \underset{363}{Ni(PMe_3)_4} + 2CuCl$$

The anhydrous metal halide was intimately mixed with a 100% excess of copper dust over the stoichiometric quantity. The bomb charge consisted of,

0.7 g. $NiCl_2$ 1.3 g. Cu dust, 6.4 g. PMe_3.

This quantity of phosphine gave a pressure of 170 atmospheres at 100°C.

Attempts to recover the excess phosphine after reaction in the usual manner revealed the interesting result that more PMe_3 than expected had been consumed. It is thought that the reason for this must be that the cuprous chloride formed in the reaction forms the adduct $[CuCl.PMe_3]_4$, which is well known (111). For every 1 gm. of CuCl formed in the reaction, 0.8 g. PMe_3 will be complexed in this way, amounting to some 20% wastage of ligand.

Since $Ni(PMe_3)_4$ was not previously reported, its physical properties were not known. After removal of the excess

phosphine, no volatile reaction product was evident. Opening of the bomb confirmed that the reaction product was a solid. During this process, exposure of the crude solids to the atmosphere resulted in visible decomposition and a smoke of $POMe_3$ was produced. After a short time, or on contact with filter paper, the solids burst into flame and decrepitated, giving clouds of smoke.

The extraction of any reaction product, such as $Ni(PMe_3)_4$, from the crude solids can thus only be attempted under anaerobic conditions. In subsequent preparations the bomb was detached from the vacuum line under nitrogen, and opened in a nitrogen-filled, dry glove-box. The caked solids from the bomb were ground and extracted with dry, de-gassed hexane.

After filtration and repeating the extraction a few times a clear red solution, and a greyish-white solid were obtained. The solution, amounting to 200 ml., was placed in a 500 ml. flask and transferred from the glove-box to the vacuum line. The hexane was removed under rotary-pump vacuum and condensed in two liquid-nitrogen traps, leaving a pink solid in the flask. This pink solid was collected and bottled in the glove-box. Some of the solid was tested qualitatively. The solid was air-stable for the period of the tests (10 minutes), and had a very strong PMe_3 odour. A green solution was given

with concentrated nitric acid, giving positive results for nickel and phosphorus tests.

A precisely similar preparation, using $PtCl_2$ instead of $NiCl_2$, yielded a pale-yellow solid which was markedly less stable in air than the nickel compound.

11(4) Characterisation of $Ni(PMe_3)_4$ and $Pt(PMe_3)_4$

Aside from the tetrakis-compounds, a likely product from the reaction of MCl_2 (M = Ni,Pt) with PMe_3 might be $MCl_2(PMe_3)_2$. These complexes, of the divalent metals, are well-known (112-115), and from colour considerations are unlikely to be the solids isolated above. $(Et_3P)_2NiCl_2$ is deep purple in colour, and $(PMe_3)_2PtBr_2$ is white. Qualitative tests on the reaction products suspected of being $M(PMe_3)_4$, showed that chlorine was absent.

Analyses for nickel and platinum were performed by the standard methods reported earlier. Carbon and hydrogen analyses were obtained and the results were:

	pink solid			pale yellow solid		
	Ni	C	H	Pt	C	H
Found %	15.99	38.22	9.65	38.81	27.30	7.10
Calc.for $M(PMe_3)_4$	16.17	39.69	10.00	39.08	28.84	7.27

The C,H analyses were too low in both cases, but this is not surprising in view of the high vapour pressure of phosphine above the solids. The analyst reported great difficulty in the weighing of milligram quantities of the solids, due to the phosphine being liberated continuously.

The solutions of the solids in benzene or hexane are fairly stable; the nickel compound gave a deep blood-red solution in benzene (0.5M) and the platinum compound gave a yellow solution (0.1M) which was much less stable than that of the nickel compound. The benzene solution was injected into an n.m.r. tube in the glove-box. The n.m.r. spectrum, obtained by B.E.Mann Esq. on a JEOL 100 Mc instrument, consisted of a single resonance at 8.96 τ indicates that all the hydrogen atoms are equivalent, lending support to the proposed structure of $Ni(PMe_3)_4$. With T_d symmetry for the molecule of $Ni(PMe_3)_4$ all 36 H atoms would be equivalent symmetrically.

11(5) Vibrational spectra of $Ni(PMe_3)_4$ and $Pt(PMe_3)_4$

A configuration for $Ni(PMe_3)_4$ which possesses all the symmetry elements of the T_d point group is shown in Figure 11B. The molecule contains 53 atoms, and application of group theory gives the following species for the vibrations,

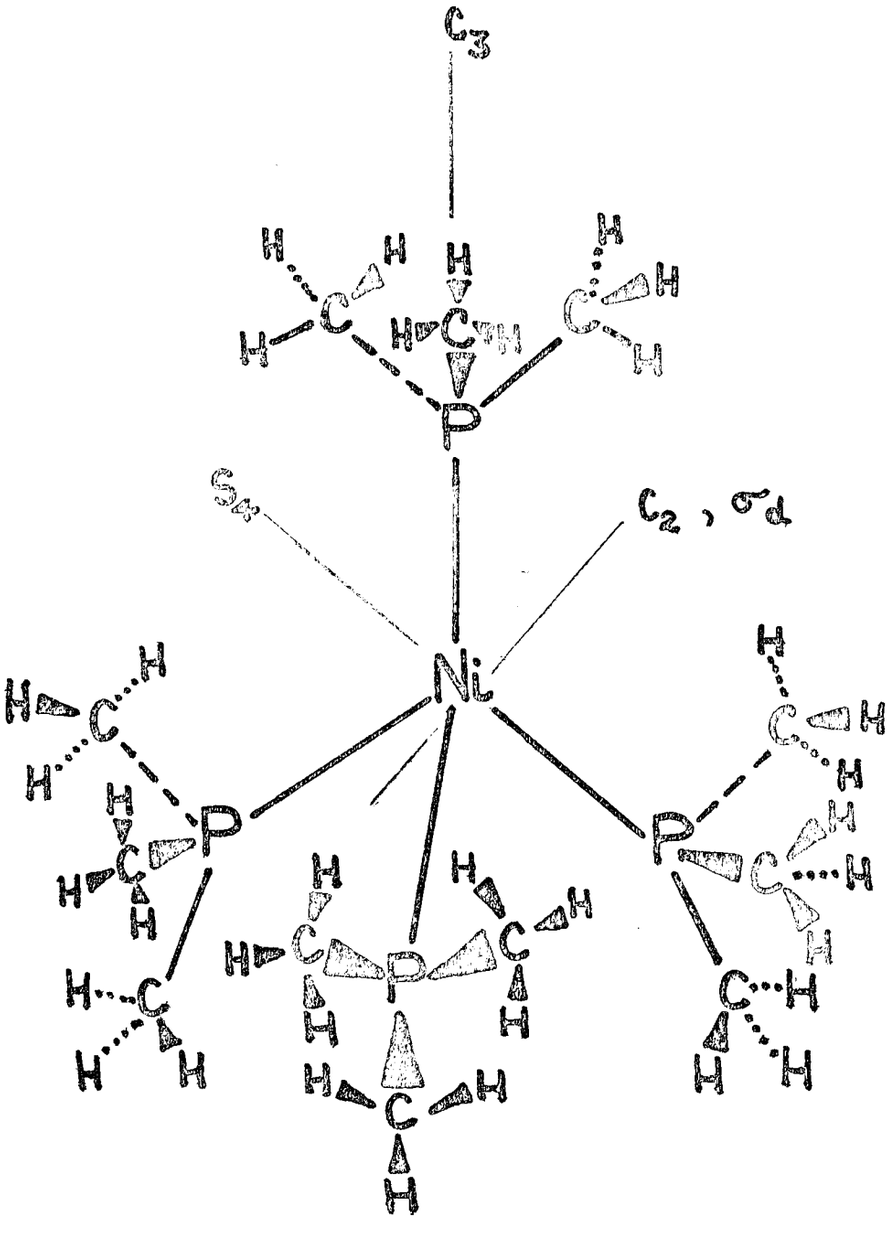


Figure 11B. Tetrakistrimethylphosphinenickel.

$$\Gamma = 8A_1 + 5A_2 + 13E + 17F_1 + 21F_2$$

Raman: $8A_1 + 13E + 21F_2$

Infra-red: $21F_2$

There should be 8 polarised features in the Raman spectrum, and 21 coincidences between Raman and infra-red, for assignment of the molecule to the point group T_d.

For both compounds the infra-red spectrum was obtained with nujol mulls. Hexachlorobutadiene mulls (hcbd) were used to study the C-H deformation and stretching regions obscured in the nujol mulls. The hcbd mulls were rather unstable, as a result, it is thought, of the solubility of the $M(PMe_3)_4$ compounds in the chlorinated mulling agent. This instability was also manifest in solutions of $Ni(PMe_3)_4$ in carbon tetrachloride, a yellowish-green solid, nickel chloride, being deposited from the red solution within one minute of the solution being made. The mulls of the platinum compound were rather more sensitive to the heating effects in the infra-red beam than were the mulls of the nickel compound; decomposition to platinum occurred within 10 minutes.

Insufficient supplies of the platinum compound could be isolated at any one time to enable the Raman spectrum of the solid to be investigated. Unlike the nickel compound

which was stable for weeks in a sealed tube under an atmosphere of nitrogen, the platinum compound was stable for a matter of hours only under identical conditions. No Raman spectrum was attempted for solutions of the platinum compound in hydrocarbons, since these solutions were unstable.

The Raman spectrum of the nickel compound in the solid state was obtained by M.J.Gall, Esq., Southampton, using a Cary Laser RamanSpectrometer with Ne 6328 Å as the exciting line. The spectrum was not particularly good in quality, but the P-C modes and Ni-P stretching modes were easily identifiable. Some decomposition occurred whilst the solid was in the laser beam. The spectrum is shown in Figure 11D.

The nickel compound gave very stable solutions in benzene and hexane, with no tendency towards the turbidity phenomenon noticed for $Ni(PCl_3)_4$. The solutions were, however, very highly coloured and syrupy at higher concentrations (0.5 → 1.0 M). To determine the feasibility of exciting the Raman spectrum with the Helium Source, the visible absorption spectrum was obtained (Figure 11C). The concentration of the test solution was 0.036M in benzene solution, and, like all other operations involving the nickel compound, this solution was made up in the nitrogen-filled glove-box. The optimum concentration of the solution for

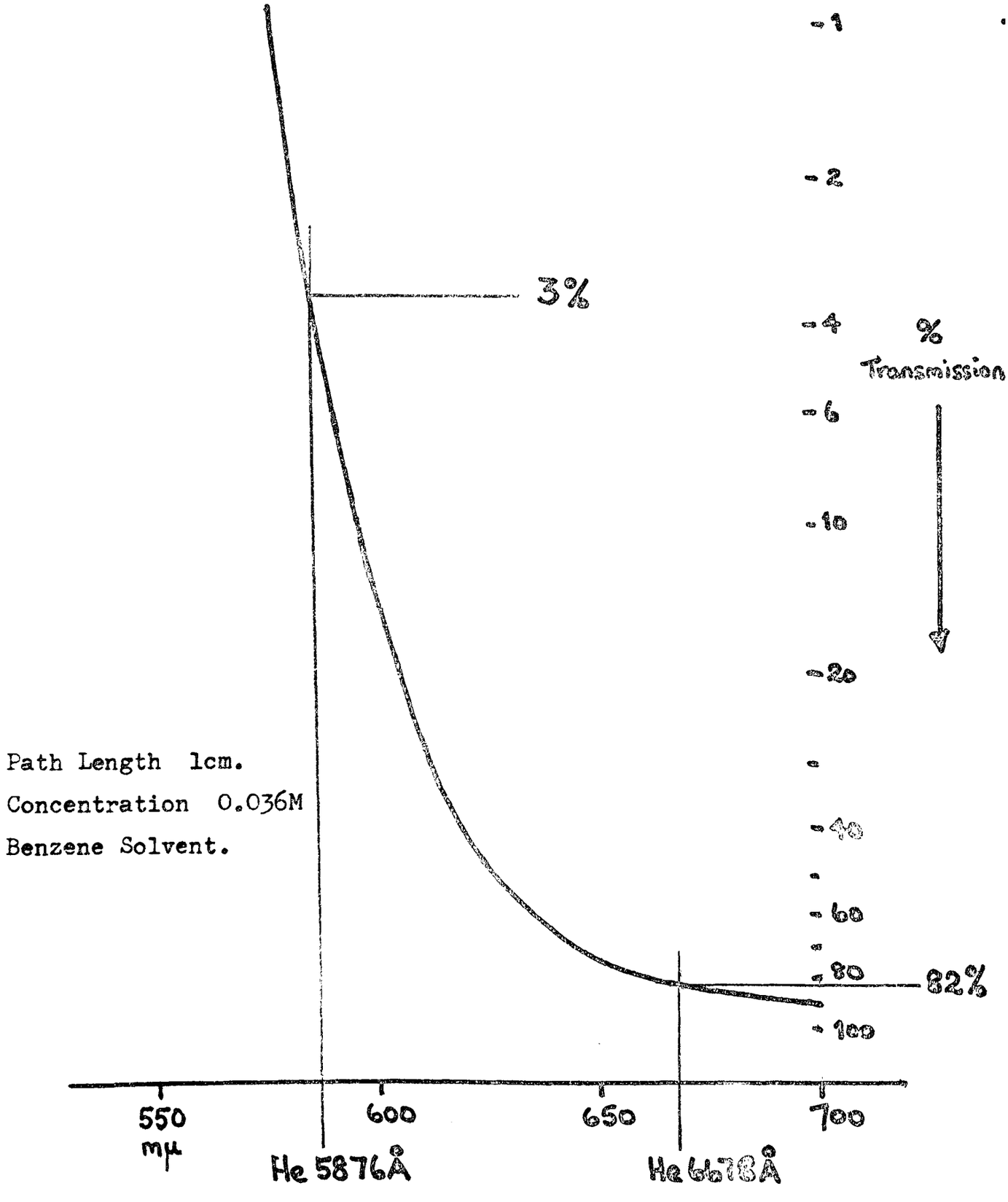


Figure 11C. Visible Absorption of $Ni(PMe_3)_4$.

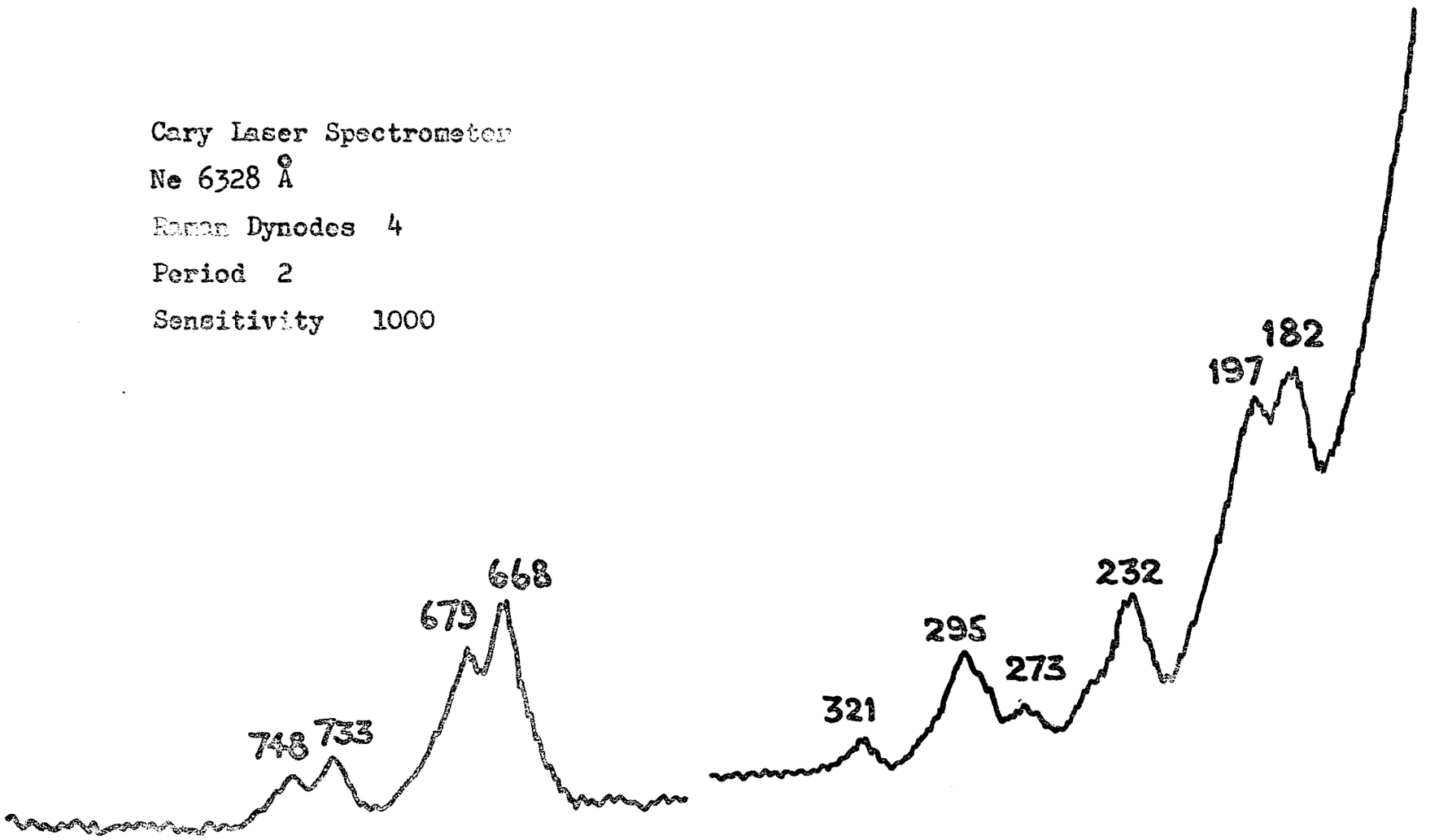


Figure 11D. The Raman Spectrum of $Ni(PMe_3)_4$ solid.

excitation with the red line, He 6678 Å, was calculated (using the Creighton formula) to be 0.07 M, i.e. 0.25 g. solid per 10 ml. benzene. This concentration is rather low for the excitation of Raman spectra in the red, but attempts were made to obtain Raman spectra from benzene solutions which were 0.15M and 0.07M in $Ni(PMe_3)_4$.

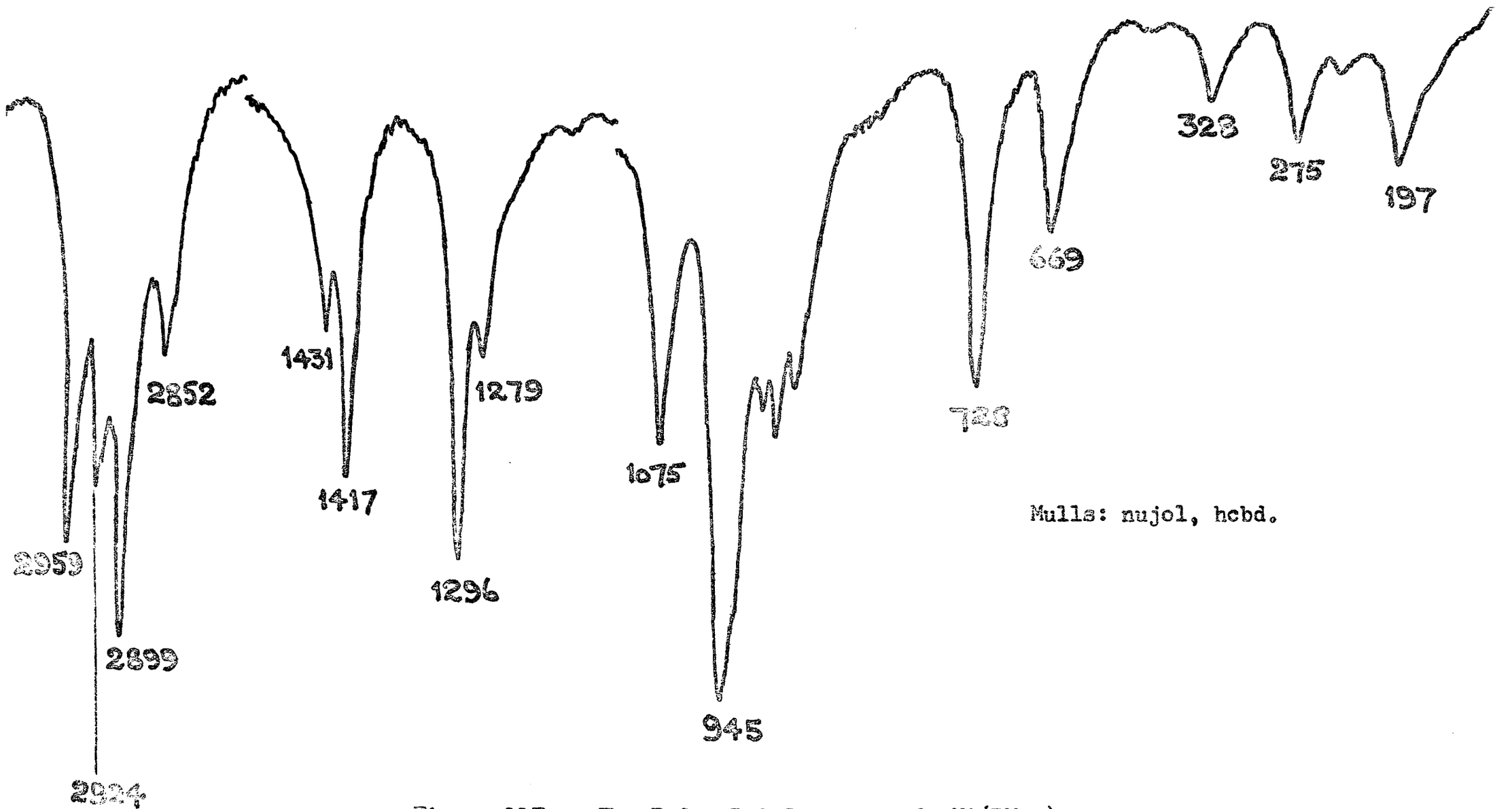
The solutions were investigated at the temperature of the Helium Source (uncooled). Spectra of mediocre quality were obtained, being very weak, and exposures of up to 3 hours at slit widths of 100 μ and 150 μ were made. At these longer exposures, the halation of the plate in the neighbourhood of the exciting line introduced a darkening of the background which made observation of the weak features difficult. The weak features observed in the solutions, and the bands obtained from the solid, are listed in Table 11A. In the case of the solution investigation, the higher features ascribed to P-C stretching were not observed due to fall-off in sensitivity of the Oa-F plates in this region.

The infra-red spectrum of the nickel compound is illustrated in Figure 11E, and an assignment given in Table 11B. Assignments of the Raman and infra-red spectra are assisted by reference to the vibrational spectra of trimethylphosphine (107,117,118), and $POMe_3$ (116). The

TABLE 11A

Raman spectrum of $Ni(PMe_3)_4$

Solid Ne 6328 Å	Assignment	0.07M solution in benzene He 6678 Å
182 m 197 m	ν NiP a_1, f_2	187 w
232 m	δ PC_3 and ρ PC_3 a_1, f_2, e	225 vw
255 w,sh		246 vw
273 mw		268 vw
295 m		
321 w		
668 m	ν P-C a_1, f_2, e	
679 mw,sh		
733 mw		
748 mw		



Mulls: nujol, hcbd.

Figure 11E. The Infra-Red Spectrum of $Ni(PMe_3)_4$.

TABLE 11B

Infra-red assignment of $Ni(PMe_3)_4$

F_2-species

Assignment	ν	cm^{-1}	ir, R PMe_3 (21,22)	ir, R $POMe_3$ (20)
ν_{C-H} asym.	ν_1	2959 s	2970	2999
	ν_2	2924 ms	2920	
ν_{C-H} sym.	ν_3	2899 s	2850	2923
	ν_4	2852 m		
δ_{CH_3} asym.	ν_5	1431 m, sh	1430	1437
	ν_6	1417 s	1417	1420
δ_{CH_3} sym.	ν_7	1296 s	1310	1340
	ν_8	1279 ms, sh	1298	1292
ρ_{CH_3}	ν_9	1075 s	1067	
	ν_{10}	945 vs	960	937
	ν_{11}	880 mw	947	
	ν_{12}	865 m		872
	ν_{13}	848 mw		
ν P-C asym.	ν_{14}	728 vs	717	756
ν P-C sym.	ν_{15}	669 ms	652	671
δPC_3 sym.	ν_{16}	328 m	*263	**256
δPC_3 asym.	ν_{17}	275 m	*305	**311
ρPC_3	ν_{18}	250 mw		
ν Ni-P asym.	ν_{19}	197 ms		
τ Me	ν_{20}	(228 w)		275
δNiP_4	ν_{21}	-		

* Incorrect assignment of the deformations (see text)

**

early published work on the assignment of the PC_3 deformation frequencies in these molecules was shown to be erroneous when polarisation measurements in the Raman spectra were made (107,119). A partial comparison assignment of the a_1, e, and f_2-species skeletal modes is made in Table 11C.

For the platinum compound, far less data are available since only the infra-red spectrum could be obtained. The latter proved more difficult to obtain than for the nickel analogue owing to the instability of the platinum compound in the infra-red beam. The general features of the spectrum are similar to those obtained for the nickel compound, and are assigned in Table 11D.

11(6) Discussion

Previous spectroscopic work on zerovalent metal-trimethylphosphine complexes was carried out by Bigorgne et al.(34,37,38). In this work, the authors were mainly concerned with observations on the C-O stretching frequencies of partially-substituted nickel and molybdenum carbonyls. For only one case, that of $Ni[P(OMe)_3]_4$, was the nickel-phosphorus stretching frequency quoted, being 178 cm^{-1} for the a_1-mode in the Raman spectrum. In the present work, with reference to the $Ni(PMe_3)_4$, it is seen that the symmetric P-C stretch has increased in frequency relative to

TABLE 11C

Assignment of skeletal frequencies of $Ni(PMe_3)_4$

Mode	Species	Raman solid	I.R. solid
ν C-H asym.	a_1	-	inactive
ν C-H sym.	a_1	-	"
δ CH_3 asym.	a_1	-	"
δ CH_3 sym.	a_1	-	"
ρ CH_3	a_1	-	"
ν PC sym.	a_1	679	
δ PC_3 sym.	a_1	295	"
ν Ni-P sym.	a_1	182	"
ν P-C asym.	e	748	inactive
δ PC_3 asym.	e	(255,232)	"
ρ PC_3	e	(255,232)	"
δ NiP_4	e	-	"
ν P-C asym.	f_2	733	728
ν P-C sym.	f_2	668	669
δ PC_3 sym.	f_2	321	328
δ PC_3 asym.	f_2	273	275
ρ PC_3 }	f_2	255	250
τ Me }		232	228
ν Ni-P asym.	f_2	197	197
δ NiP_4	f_2	-	-

TABLE 11D

Assignment of $Pt(PMe_3)_4$ (infra-red only)

F_2-species

Mode	$Pt(PMe_3)_4$
ν C-H asym.	2965 m,bd
ν C-H sym.	2906 ms
	2854 mw
δ CH_3 asym.	1407 s, bd
δ CH_3 sym.	1303 sh
	1282 s
ρ CH_3	940 s
ν P-C asym.	739 m, bd
ν P-C sym.	667 m
δ PC_3 sym.	314 mw
δ PC_3 asym.	276 m
ρ PC_3	-
ν Pt-P asym.	189 mw
δ PtP_4	-

$Ni[P(OMe)_3]_4$, and now was found at 182 cm^{-1}. This would normally indicate that the phosphorus-carbon bond is slightly stronger in the former. In addition, a comparison with $Ni(PF_3)_4$ reveals that, despite the lighter mass of the methyl group relative to fluorine, the a_1-species nickel-phosphorus stretch in $Ni(PMe_3)_4$ is some 15 cm^{-1} lower than in the fluoro-case. A force-constant calculation will later be carried out on the skeletal a_1-modes of $Ni(PMe_3)_4$.

Although the evidence for the pink solid being $Ni(PMe_3)_4$ is favourable, the platinum analogue is less well-characterised. The similar analyses and infra-red spectrum to those of the nickel compound seem to indicate that the compound might fairly be termed $Pt(PMe_3)_4$. No conclusions may be drawn about the bonding in this platinum compound, since the Raman spectrum, and the vital a_1-modes, could not be obtained. A comparison of the infra-red spectra of both compounds, however, reveals a similarity in the frequencies of f_2-class modes - and there is no reason why the a_1-class modes in the case of $Pt(PMe_3)_4$ should be vastly different from those observed in the Raman spectrum of the nickel analogue.

11(7) Extension of Procedure

A further extension of the preparative method, which involved the use of PCl_3 as a ligand in the reductive phosphorylation, was applied in the attempted synthesis of $Pt(PCl_3)_4$. Essentially similar procedures were used, as in the experiments involving trimethylphosphine, but even with pressures of 250 atmospheres of PCl_3 at 120°C in the presence of $PtCl_2/Cu$, only very small quantities of an extremely-unstable yellow solid could be isolated. An infra-red spectrum of the solid in the form of a nujol mull showed two strong features assignable to P-Cl stretching modes.

536 s
518 s
} ν P-Cl ?

The solid was very unstable to heat and other regions of the spectrum were observed, with this and other samples, without success.

11(8) Force Constant Calculation

In the absence of vibrational data concerning the methyl group vibrations in the Raman spectrum of $Ni(PMe_3)_4$, the skeletal vibrations only were considered. The a_1-modes are now,

P-C symmetric stretch

PC_3 symmetric deformation

Ni-P symmetric stretch.

The methyl groups were considered (120) as point masses of 15.0 a.m.u. The G, $\mathcal{F}$ matrices are exactly analogous to those derived for the $M(PF_3)_4$ molecules. A diagonal force-field was assumed for the purposes of the calculation.

In Table 11E, the previous force-constant work on the free ligand, PMe_3, is given. The earlier work is unreliable because of an error in the original vibrational assignment by Rosenbaum (118) which was discovered only recently (107,119). Using the results of earlier work carried out by the present author (107) and also by Bigorgne (119), reasonable initial force-constant values were obtained for the P-C stretching and PC_3 deformation modes.

As was expected, on account of the similarity between the molecules of $Ni(PMe_3)_4$ and $Ni(PCl_3)_4$ as regards their skeletal vibrations, perfect convergence onto the observed frequency-values was not attained in the force-constant calculation. Owing to the 'mixing' of the a_1-species modes it was found impossible to converge on the observed set of frequencies completely. The ν_2 mode, a P-C deformation, was particularly 'soft' in this respect; whereas quite good

TABLE 11E

Force Constants of PMe_3

Author	Ref.	Assumptions made	Force Constants (10^5 dynes cm^{-1}) k_{P-C} stretch	k_{PC_3} def.
Rosenbaum	118	Wrong assignment; Me = 15	2.78	0.214
Sheline	120	Wrong assignment; Me= 15	2.93	0.240
Siebert	121	C-H factored off, 5 x 5 $\mathcal{G}_{A1}$ Wrong assignment	2.99	0.252
Long	122	Wrong assignment; Me = 15 SVFF, UBFF	3.028	0.271
Edwards	107	Me = 15	3.00	0.20
	107	Complete A_1 calculation	2.81	0.51
Bigorgne	119	Me = 15	2.84	0.320

agreement between the observed and calculated frequency-values of ν_1 and ν_3 could be obtained, ν_2 could not be approached. A similar phenomenon as that which was experienced in the case of $Ni(PCl_3)_4$ was again encountered, namely, the refinement of a previous force-constant set resulted in divergence rather than convergence onto the observed set of frequencies. In Table 11F is given a list of force-constant sets which illustrate this point. The extent of 'mixing' is indicated by a comparison of force constant sets 2 and 3 in Table 11F, where, keeping k_1 and k_2 constant, change in the Ni-P force constant k_3 resulted in a large change in the frequencies of <u>all three</u> a_1 modes but very little change in ν_3 was observed. This is contrary to the basic assumption of the SVFF, that a force constant k_i steers it s own frequency value ν_i and has but little effect on $\nu_j,k....$

In view of this 'mixing', as for $Ni(PCl_3)_4$, little <u>detailed</u> conclusion can be derived from the force-constants obtained in the so-called 'best-fit' in Table 11F. It seems however, that the k_{P-C} stretching force constant of $Ni(PMe_3)_4$ derived above lies in the region of 5.4 (units of z). This could well be a significant increase over the similar stretching force constant of PMe_3, which is 4.76 (units of z)

TABLE 11F

Force-constants of $Ni(PMe_3)_4$

Set	Force Constants (z units)			Calculated ν's cm^{-1}			Observed ν's cm^{-1}			RMS deviation
1	5.136	0.242	3.721	657	371	150	679	295	182	18.0%
2	5.4829	0.1532	5.5152	686	402	132				26.3%
3	5.4829	0.1532	3.721	673	349	130				19.6%
'Best fit' on ν_1 and ν_3	5.430	0.420	4.113	678	427	184				26.2%

or circa 2.8 dynes cm^{-1}. Such an increase in k_{P-C} for the molecule of $Ni(PMe_3)_4$ would be expected from the previous considerations [11(1)] of σ-bonding between the nickel and the phosphorus atoms. The value of the Ni-P stretching force constant, seems to be similar to that observed for the $Ni(PCl_3)_4$ molecule i.e. smaller than in the PF_3 analogue: which attractively supports the conclusion that, despite the increase in σ-donor capacity of the PMe_3 and PCl_3 ligands relative to PF_3, the decrease in π-accepting ability over the same series results in a <u>weaker</u> metal-phosphorus bond.

CHAPTER 12

Chapter 12

TRICHLOROSTIBINE-TRISCARBONMONOXIDE NICKEL

$Ni(CO)_3SbCl_3$

12(1) General Introduction and Preparation

Although the tetrakistrihalogenophosphine compounds of nickel are well characterised, no such compounds of nickel exist for the corresponding antimony series. Reaction between nickel carbonyl and antimony trichloride proceeds readily to the monosubstitution stage only (33). Bigorgne (35) has found that $SbEt_3$, $Sb\emptyset_3$, $BiEt_3$, $Bi\emptyset_3$, also give mono-substituted products of nickel carbonyl, and the di-substituted reaction product $Ni(CO)_2(SbEt_3)(SbClEt_2)$ has been isolated.

In the arsenic series, the halogens AsF_3, $AsCl_3$ and AsI_3 all react with nickel carbonyl to produce coloured products which were too unstable to be isolated (34), although some substituted compounds have been isolated from the reaction with molybdenum carbonyl (34). Stable products of nickel carbonyl and organo-arsines such as $AsEt_3$, $As(OMe)_3$ and $As\emptyset_3$, have, however, been identified. The mono-substituted carbonyl was formed at 0°C, but at 60°C the di-derivative was obtained (34).

The phosphorus series of substitution products is well known for halophosphines (39) and also for the organophosphines and -phosphites (36,38). Bigorgne has studied the vibrational spectra of the latter complexes, with especial reference to the carbonyl stretching region; the conclusion seems to be that the π-bonding in these compounds containing PF_3 or PR_3 (R = organic moiety) is very feeble. No vibrational data have yet been reported for any antimony-substituted nickel carbonyl, and in the present work the compound $Ni(CO)_3SbCl_3$ was investigated. The preparation has been described by Wilkinson (33), and in the present work the following procedure was adopted:

Nickel carbonyl (4.0 ml., density 1.32 g./ml.) was reacted with excess $SbCl_3$ (> 7 g.) in cyclohexane solution at room temperature.

$$Ni(CO)_4 + SbCl_3 \longrightarrow Ni(CO)_3SbCl_3 + CO$$

The usual precautions were taken in the handling of nickel carbonyl, and the cyclohexane solvent was dried over sodium. The antimony trichloride (provided through the courtesy of I.A.Steer, Esq.) had been vacuum sublimed to remove water. Antimony trichloride is not very soluble in cyclohexane so rather large volumes of solvent (circa 400 ml.) were required. A pale buff precipitate of the

substitution compound was obtained after allowing the reaction solution to stand for a few hours. This was filtered off, washed with cyclohexane and pumped dry. Yields were rather low (20-30% of theoretical).

Qualitative tests on the precipitate dissolved in nitric acid showed the presence of Cl, Ni, Sb. A Lassaigne test (fusion with $(NH_4)_2SO_4$ and sodium) indicated that carbon was present. A quantitative analysis for nickel, chlorine and antimony was carried out; the solid was dissolved in nitric acid and the nickel, chlorine determined by the usual means. The antimony was determined by dissolving the compound in concentrated hydrochloric acid, diluting, and titrating with chloramine-T (itself standardised with tartar emetic).

	Found %	Calc.for $Ni(CO)_3SbCl_3$
Nickel	15.96	15.83
Antimony	33.2	32.83
Chlorine	28.4	28.69

The compound is an amorphous powder, insoluble in hydrocarbon or halogenated solvents. Carbon disulphide reacts, giving black residues and liberating carbon monoxide. Decomposition occurs on heating and on standing for prolonged

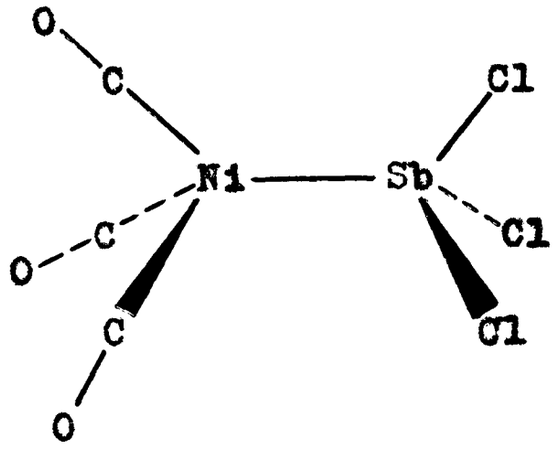
periods in the atmosphere. It was, thus, found to be impossible to recrystallise the compound from any solvent with which it did not react.

12(2) Vibrational Spectra of $Ni(CO)_3SbCl_3$

In Figure 12A the molecule is represented in an 'eclipsed' configuration of C_{3v} symmetry. Other structures of lower symmetry can be envisaged, such as the 'gauche' or staggered configuration. The activity of the vibrations for the point group C_{3v} was deduced from the character table and is given in Figure 12A. It is seen that 16 vibrations should be active in both the infra-red and the Raman spectrum.

Because of the insolubility/reactivity of the compound it was necessary to obtain vibrational spectra in the solid state. Raman spectra were excited with the mercury 4358 Å, 5461 Å lines, and infra-red spectra were obtained with nujol mulls. The frequencies, together with an approximate description of the vibrational modes involved, are given in Table 12A. Two low-frequency features in the Raman spectrum were obtained by M.J.Gall, Esq., on the Cary Laser instrument at Southampton.

The assignment was made by analogy with the vibrational spectra of nickel carbonyl (37,38,88,123,124) and antimony trichloride (93,125). Since no polarisation measurements



Point Group: C_{3v}

$$\Gamma = 7A_1 + 2A_2 + 9E$$

Activity: Raman $7A_1 + 9E$
Infra-red $7A_1 + 9E$
} Coincident in both

Inactive in both: $2A_2$

Figure 12A. Activity of vibrations of $Ni(CO)_3SbCl_3$

TABLE 12A

Assignment of $Ni(CO)_3SbCl_3$

Species	ν	Description of mode	Raman (solid)	Infra-red (solid)
A_1	ν_1	C-O symmetric stretch	-	2073 m
	ν_2	Ni-C-O symmetric def.	480 mw	472 w
	ν_3	Ni-C symmetric stretch	409 ms	404 mw,bd
	ν_4	Sb-Cl symmetric stretch	376 m	377 mw,sh
	ν_5	Ni-Sb stretch	232 m	227 ms
	ν_6	$SbCl_3$ symmetric def.	171 w	175 mw
	ν_7	NiC_3 symmetric def.	*74 mw	-
A_2	ν_8	Ni-C-O rock	inactive	inactive
	ν_9	Ni-C-O torsion		
E	ν_{10}	C-O asymmetric stretch	n.o.-	1997 m
	ν_{11}	Ni-C-O asym.def.	424 mw	422 w,sh
	ν_{12}	Ni-C asym.stretch	(376m)	(377 mw,sh)
	ν_{13}	Sb-Cl asym.stretch	351 m	354 ms
	ν_{14}	$SbCl_3$ asym.def.	156 mw	145 mw
	ν_{15}	NiC_3 asym.def.	*53 w	-
	ν_{16}	$SbCl_3$ rock	-	-
	ν_{17}	Ni-C-O rock	-	? 272 w
	ν_{18}	NiC_3 rock	-	-

- = not observed
sh = shoulder
bd = broad
* Cary He/Ne Laser

were possible the assignment of the a_1 modes with any certainty is difficult. In Figure 12B the correlation diagram for $Ni(CO)_4$, $SbCl_3$, and $Ni(CO)_3SbCl_3$ is shown. Of some assistance in the assignment was the work of Bigorgne (35) on $Ni(CO)_3SbR_3$, R = organic radical; more useful, though indirectly, was Bouquet's work (34) on $Ni(CO)_3AsEt_3$, since a complete vibrational spectrum was reported. In Table 12B the vibrational data for $Ni(CO)_3SbCl_3$ and related compounds are listed for comparison.

12(3) Discussion of the Assignment

Reference to Figure 12B and Table 12B indicates that, although the assignment is mainly straightforward, there are a few interesting features. Perhaps the most obvious inconsistency in the correlation diagram lies in the Ni-C stretching region. Two frequencies were observed, at 376 cm^{-1} and 409 cm^{-1}, in the spectrum of $Ni(CO)_3SbCl_3$ which were assigned to the symmetric and asymmetric Ni-C stretching vibrations. In his assignment of the related molecule, $Ni(CO)_3AsEt_3$, Bigorgne (34) assigned these nickel-carbon stretches in reverse order compared with their assignment in nickel carbonyl, the polarised (a_1) frequency becoming the upper of the two features in the spectrum of the arsenic compound. In the absence of polarisation data, a similar situation has been presumed to exist for the

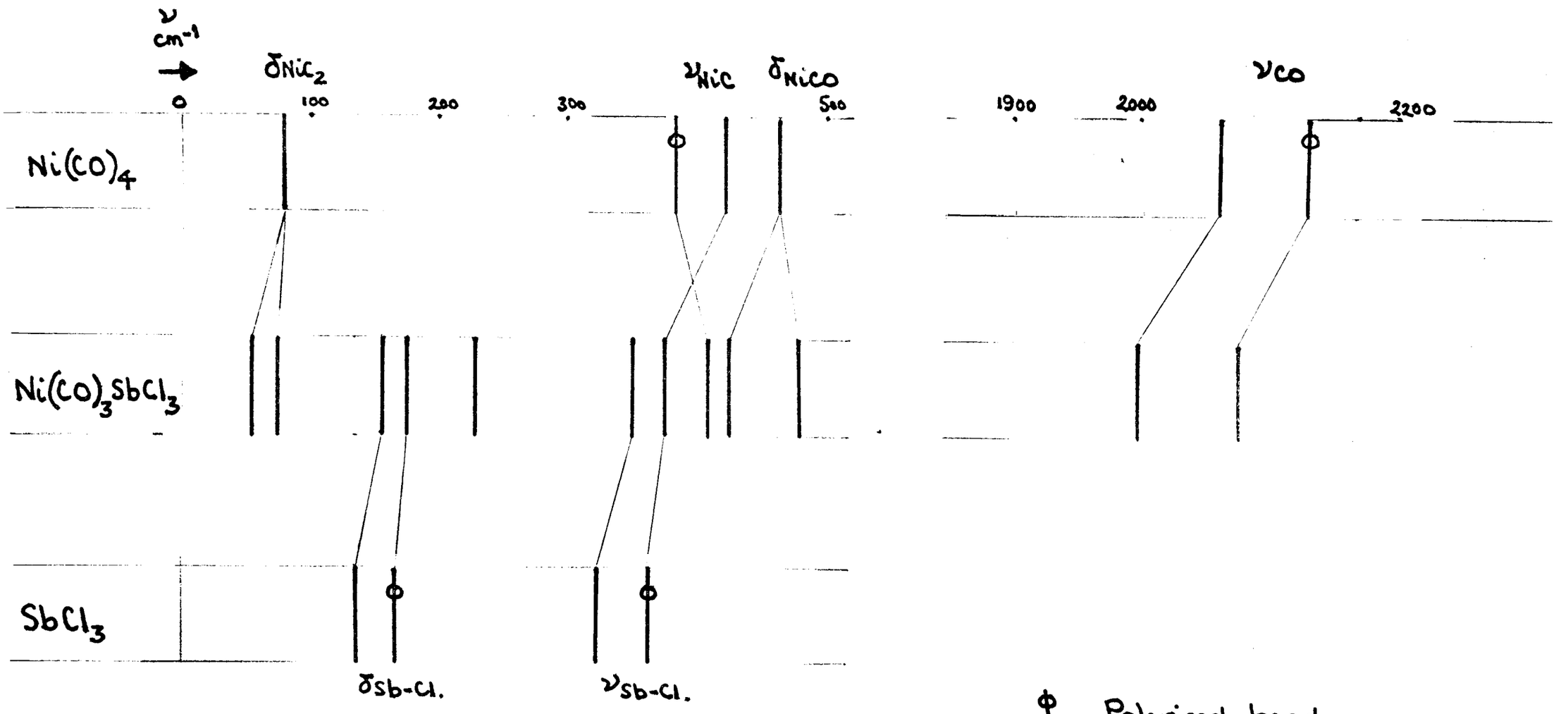


Figure 12B. Correlation Diagram for $Ni(CO)_3SbCl_3$.

TABLE 12B

$Ni(CO)_3SbCl_3$ and related compounds

Description of mode	$Ni(CO)_3SbCl_3$ (Present work)	$Ni(CO)_3SbEt_3$ (35)	$Ni(CO)_3SbClEt_2$ (35)	$Ni(CO)_3PCl_3$ (38)	$Ni(CO)_3AsEt_3$ (34)	$Ni(CO)_4$ (38)	$SbCl_3$ (125)
ν C=O sym	2073	2067	2082	2103	2066	2127	
ν C=O asym	1997	1996	2009	2043	1988	2057	
ν Ni–Sb	227	-	-				
ν Ni–As					207		
ν Ni–C sym	409	-	-	-	421	383	
ν Ni–C asym	376	-	-	-	373	422	
δ Ni–C–O	424 480	-	-	-	429 486	462	
δ NiC_3 sym	74	-	-	-	110		
δ NiC_3 asym	53	-	-	-	70	79	
ν Sb–Cl sym	376		-				360
ν Sb–Cl asym	351		-				320
δ $SbCl_3$ sym	171		-				164
δ $SbCl_3$ asym	156		-				134

$Ni(CO)_3SbCl_3$ studied in the present work.

The absence of polarisation data also means that some of the other a_1 assignments are tentative; for example, the assignment of the a_1- and e-deformations, δ Ni-C-O.

An interesting feature is the medium-intensity band at 376 cm^{-1} in the Raman spectrum (377 cm^{-1} in the infra-red). Since there are two distinct vibrations which are expected to appear in this region of the spectrum, there is no alternative but to assign both, namely ν_4 and ν_{12}, to this feature. Again, polarisation data would be of assistance. The remaining antimony-chlorine vibrations seem to be reasonably assigned on a comparison with $SbCl_3$ itself. The two low-frequency bands, at 74 cm^{-1} and 53 cm^{-1}, are also weak points in the assignment. Such frequency-values, although reasonable for ν_7 and ν_{15} the nickel-carbon deformations, could well be due to lattice-vibrations.

The remaining feature to be discussed is the band at 227 cm^{-1} in the infra-red (232 cm^{-1} in the Raman spectrum). In $Ni(PCl_3)_4$, it was seen earlier in the present work that the Ni-P stretching vibration (a_1) occurred at 135 cm^{-1}. Bouquet et al (34) assigned the nickel-arsenic stretch in $Ni(CO)_3AsEt_3$ to a strong, polarised feature at 207 cm^{-1}. There are no published data on the Ni-P stretching frequency

of monosubstituted nickel carbonyl phosphine compounds. Bigorgne was interested only in the C=O stretching region of monosubstituted nickel carbonyl antimony compounds. The tentative assignment of the nickel-antimony stretch in the present work to the band at 227 cm^{-1} (infra-red) is, therefore, unique, as there is no other feature in this region of the spectrum.

The fact that the nickel-antimony stretch is <u>higher</u> in frequency than the nickel-arsenic stretch might seem rather perplexing. A possible explanation for this would be the increased donor-capacity of the Sb atom relative to As, which would result in a stronger nickel-Group V metal σ-bond.

12(4) Conclusions

When antimony trichloride is substituted into nickel carbonyl, donation of the lone pair from the antimony to the nickel atom results in a formal negative charge on the nickel which may be relieved in either of two ways:

(a) Back-donation into vacant d-orbitals of the antimony, and thence into the Sb-Cl bonds

or

(b) Back-donation into the carbon monoxide ligands.

There has been much discussion on the bonding in partially-substituted zerovalent metal carbonyls. Cotton

et al.(126,127) have considered the force constants of metal-carbon and carbonyl stretching in substituted phosphine hexacarbonyls; concluding that the carbonyl stretching force constant should decrease if a carbon monoxide group were to be replaced by other ligands which make less demand for metal $d\pi$ electrons. Miller (114) made a similar study of carbonyl-phosphine 'competition' in substituted carbonyls and concluded that back-donation effects were small, and that the observed force-constant changes could be explained in terms of the σ-donor capacity of the phosphine ligands.

From the assignment of $Ni(CO)_3SbCl_3$ proposed in this work, it may be concluded that:

(i) The molecule is very similar, as regards the vibrational spectrum, to $Ni(CO)_3AsEt_3$ in its relationship to nickel carbonyl and the free ligand.

(ii) The a_1-species C-O stretching frequency has decreased relative to its value in nickel carbonyl.

(iii) The Sb-Cl a_1-species stretching frequency has increased relative to the free ligand.

Owing to the tentative nature of the assignment of the a_1-species modes, attendant on the absence of polarisation data, it was felt unjustifiable to pursue a force-constant study on the a_1-species vibrations. Briefly, however, it

may be concluded that the following seems to pertain:

(i) The C-O a_1-species stretching force constant has decreased relative to nickel carbonyl. This would happen if the electronic donation from antimony was dispersed by the nickel over the three carbonyl ligands. This incurs some increase in the degree of π-bonding between nickel and carbon.

(ii) The antimony atom retains a formal positive charge after donation of its lone pair to the nickel atom. The electronegative chlorine atoms may now 'move closer' to the antimony, shortening the bond length and increasing the Sb-Cl force constant.

CHAPTER 13

Chapter 13

TETRAHALO-COMPLEXES OF TRANSITION METALS

13(1) Introduction

Divalent metals of the first transition series do not form the tetrahalo-complexes, MX_4^{2-}, fully in aqueous solution. In non-aqueous solvents these compounds are fully formed, and solid salts $Y_2^{I}M^{II}X_4$ have been isolated in the presence of excess X^-. This method was employed by Gill and Nyholm (128), and by Gill and Taylor (129), to investigate the ultra-violet spectra of $R_2M^{II}X_4$ compounds, where R is Et_4N^+, ϕ_3MeAs^+ and M = Mn, Fe, Co, Ni, Cu, or Zn. A similar investigation was carried out by Cotton et al (130).

Group theory gives the four normal modes of a five-atomic MX_4 molecule of point group T_d as:

$$\Gamma = A_1 + E + 2F_2$$

In Chapter 1, such a molecule was discussed, and it was deduced that all the vibrations will be Raman-active, but only those of species F_2 would be active in the infra-red. The infra-red spectra of MX_4^{n-} complexes (n = 1,2) have been examined by Sabatini (131), Clark (132,133) and Adams(134).

Raman studies on such complexes in aqueous solution were carried out by Delwaulle (135) and Davidson (136) for ZnX_4^{2-}, and by Woodward (137) for $FeCl_4^-$ in ether. Ware (28) investigated the complexes in non-aqueous solvents and obtained complete data for MnI_4^{2-}, although attempts at obtaining the Raman spectra of $MnCl_4^{2-}$, $CoCl_4^{2-}$, $NiCl_4^{2-}$ and NiI_4^{2-} were unsuccessful. Davidson (26) obtained the Raman spectrum of $MnBr_4^{2-}$, but investigations of $MnCl_4^{2-}$, $CoCl_4^{2-}$, $CoBr_4^{2-}$ proved unsuccessful.

The present work reports an investigation of the MX_4^{n-} ions above, concerning which previous workers had failed to obtain the Raman spectra.

13(2) Preparation

All the compounds studied in this work were prepared in the standard manner (128,129), which is summarised below.

The chloro compounds $MnCl_4^{2-}$ and $CoCl_4^{2-}$ were prepared as Et_3NH^+ salts as follows; stoichiometric quantities of the alkyl ammonium halide and the metal halide, not necessarily anhydrous, were dissolved in the minimum quantities of hot absolute ethanol or isopropanol. A typical preparation of $(Et_3NH)_2MnCl_4$ involved the addition of 2 g. of $MnCl_2.4H_2O$ to 2.7 g. of Et_3NHCl in 10 ml. hot isopropanol. On cooling to room temperature, the yellow solution deposited pale greenish-

yellow leaflets of the complex salt, which were filtered off and recrystallised from isopropanol.

For Raman work, the triethylammonium cation is preferred to tetraethylammonium since the solubility of the R_2MX_4 salt in organic solvents is far greater for the former. Previous infra-red work, however, involved the use of the Et_4N^+ cation in the complexes, so the tetraethylammonium complexes were also prepared. The $(Et_4N)_2MCl_4$ complexes were insoluble in the hot ethanol or isopropanol and were precipitated from hot solution; recrystallisation from methanol-ethanol solution was effected.

Similar techniques applied to the synthesis of the bromo-compounds. Since triethylammonium bromide is not sufficiently soluble in organic solvents such as $CHCl_3$ to give the excess of bromide ion necessary to suppress solvolysis in the Raman solutions, the bromo-compounds were prepared as the Bu_4N^+ compounds. The preparation was analogous to that used for the chloro-complexes, except that the bromo-compounds, being very soluble in cold alcohol, were precipitated from the reaction mixture with benzene. To obtain good crystals, benzene was added to the hot alcoholic reaction solution until a precipitate just formed. When the mixture cooled a good yield of the complex was

obtained. The Et_4N^+ compounds were also prepared.

The iodo-species were readily prepared as tetrabutylammonium salts from the reaction mixture containing 100% excess alkyl ammonium halide. Precipitation with benzene and washing of the crystals with ethyl acetate (to remove iodine) gave the complex $(Bu_4N)_2MI_4$. The crystals are rather unstable and discolour slowly on keeping, but storage in a sealed tube in a dark cupboard arrested this discolouration process. Alternatively, glacial acetic acid may be used as the reaction solvent(129).

The nickel complexes were shown to be less easily formed (28) than their manganese or cobalt analogues. Although the tetraethylammonium compounds can be made in a similar fashion, a modification had to be made for the Bu_4N^+ salts. This involved the refluxing of, say, 1.3 g. anhydrous $NiCl_2$ with 10 g. Bu_4NCl in 20 ml. of methyl cyanide. A blue solution was given and pale blue crystals of $(Bu_4N)_2NiCl_4$ were obtained by the addition of benzene.

The preparation of $Fe^{III}Cl_4^-$ was carried out using $FeCl_3$(anhydrous) in an analogous way, for Me_4N^+, Et_4N^+ and Bu_4N^+ cations. For the preparation of $RFe^{III}Br_4$, however, equimolar quantities of $FeBr_2$, RBr (where R was Et_4N^+ or

Bu_4N^+) and liquid Br_2 were dissolved in absolute ethanol. The solution was heated and allowed to stand overnight. The bromine oxidises Fe^{II} to Fe^{III}, and crude $RFeBr_4$ crystallised out. This was recrystallised from absolute ethanol, containing the appropriate alkyl ammonium halide. The main interest in these Fe^{III} complexes centred on the fact that they are isoelectronic with the Mn^{II} tetrahalo-compounds.

A modification was also necessary for the isolation of a sample of R_2NiI_4. This ion is not formed in iso-propanol and is only obtained in methyl cyanide with difficulty. $(Bu_4N)_2NiI_4$ was prepared by refluxing a suspension of NiI_2 and Bu_4NI in ethyl acetate. The rose-carmine crystals which separated were filtered, washed with ether and dried.

13(3) Characterisation of the compounds

Complexes of the type under investigation have been well characterised by previous workers. Quantitative analyses were performed, and the results for the compounds of importance are given in Table 13A. The C, H, N analyses were carried out by the laboratory analyst; the halogen and, in some cases the metal, was determined by the author.

TABLE 13A

Analytical data for R_2MX_4

Compound		%C	H	N	X= halogen	M
$(Et_3NH)_2MnCl_4$	calc.	35.93	8.04	6.98	35.35	13.70
	found	35.82	8.26	6.93	35.87	13.59
$(Bu_4N)_2MnBr_4$	calc.	44.70	8.44	3.26	37.20	6.40
	found	44.53	8.43	3.28	37.54	6.32
$(Et_4N)_2MnBr_4$	calc.	30.3	6.35	4.4	50.3	
	found	30.72	6.17	4.39	50.56	
$(Bu_4N)_2MnI_4$	calc.	36.67	6.93	2.68		
	found	36.41	6.84	2.73		
$(Et_3NH)_2CoCl_4$	calc.	35.58	7.96	6.91	35.00	14.55
	found	35.65	8.12	7.22	35.41	14.23
$(Bu_4N)_2CoBr_4$	calc.	44.49	8.40	3.25	37.03	6.83
	found	44.77	8.46	3.29	36.98	6.77
$(Bu_4N)_2CoI_4$	calc.	36.53	6.90	2.67		
	found	36.75	7.00	2.71		
$(Bu_4N)_2NiCl_4$	calc.	56.06	10.59	4.09		8.57
	found	55.97	10.66	4.15		8.49
$(Bu_4N)_2NiBr_4$	calc.				37.04	6.80
	found				37.26	6.75
$(Bu_4N)_2NiI_4$	calc.				48.30	5.58
	found				48.72	5.49
Bu_4NFeBr_4	calc.	31.09	5.87	2.27	51.74	
	found	31.18	5.89	2.26	51.89	

The absorption spectra of the complexes in the visible region serve as a characterisation of the compounds prepared in the present work when compared with the published spectra (128,130). The absorption curves are essential, too, for determining the feasibility of attempting Raman work and for the calculation of the optimum concentrations of the solutions under investigation. The absorption spectra were investigated using a 1 cm. thickness of solution, the reference beam containing pure solvent only. The absorption spectra were analogous to those quoted in the literature. Details of the transmission of each solution at certain wavelengths, and the optimum concentration at the best wavelength for Raman excitation, are given in Table 13B. In all cases, especially for the bromo- and iodo-compounds, the test solution was made $\sim$ 0.5 M to 1.0M in alkyl ammonium halide.

The visible ultra-violet spectra agreed with the previous work reported in the literature - for the manganese compounds (130,138,139), cobalt and nickel(128).

13(4) Raman Spectroscopy

Reference to Table 13B shows the most favourable conditions for the excitation of Raman spectra of the compounds under investigation as regards choice of exciting

TABLE 13B

Transmission of MX_4^{n-} solutions

Complex	Conc. of test solution	Cell Path (cm)	Solvent	Colour		$C_{opt.}$	Raman λ's (Transmission %)			
				Solid	Solution		4358	5461	5876	6678Å
$(Et_3NH)_2MnCl_4$	1.5M	1.0	MeCN	p.gr.-yellow	p.yellow	5.1M	45	95	96	
$(Bu_4N)_2MnBr_4$	0.4	1.0	CH_2Cl_2	gr.-yellow	yellow	1.6		81	87	
$(Bu_4N)_2MnI_4$	0.05	1.0	MeCN	yellow	yellow	.05	17	85	91	100
$(Et_3NH)_2CoCl_4$	0.5	1.0	MeCN	blue	blue	0.9	50			
$(Bu_4N)_2CoBr_4$	0.05	1.0	MeCN	p.blue	p.blue	0.04	73	68		
$(Bu_4N)_2CoI_4$	0.05	1.0	MeCN	green	green	0.01		19	29	
$(Bu_4N)_2NiCl_4$	0.1	1.0	MeCN	p.blue	blue	0.8	95	20		
$(Bu_4N)_2NiBr_4$	0.2	1.0	MeCN	blue	blue	0.09	56			
$(Bu_4N)_2NiI_4$	0.05	1.0	MeCN	red	brown	0.01			10	24
Bu_4NFeBr_4	0.2	0.1	MeCN	brown	red	0.01			47	74

gr. = green, p. = pale

line and the optimum concentration at that wavelength. There has been little previous Raman work on relevant MX_4^{n-} compounds, and this amounts to:

(i) $FeCl_4^-$, complete vibrational assignment by Woodward and Taylor (137),

(ii) MnI_4^{2-}, partial assignment by Ware (28),

(iii) $MnBr_4^{2-}$, complete assignment by Davidson (136).

An unsuccessful attempt at obtaining the Raman spectrum of $FeBr_4^-$ by Creighton, and of $MnCl_4^{2-}$ by Ware (28), was followed by an investigation of $MnCl_4^{2-}$ by Davidson. In the latter work, a very weak feature at $\sim$ 250 cm^{-1} was assigned to ν_1, the symmetric Mn-Cl stretching frequency. In the present work the Raman spectrum of $MnCl_4^{2-}$ was investigated successfully, completing the vibrational data for the manganese series of compounds. The Raman investigations of the present work are summarised below:

Manganese compounds

The pale-yellow $MnCl_4^{2-}$ was investigated as a 1.5M solution in methyl cyanide using Hg 5461 Å. A rather weak, possibly medium,-intensity feature at 249 cm^{-1}, polarised, was observed. Although no other bands were observed, it seems reasonable to assign this feature to the ν_1 vibration of $MnCl_4^{2-}$, which is by far the strongest

Raman-active mode for molecules of tetrahedral symmetry. The spectrum, which is typical of the kind of Raman spectrum obtained for the molecules investigated in this work, is reproduced in Figure 13A.

No results could be obtained from work on the solid using Hg 5461 Å. However, very useful confirmatory evidence was provided by laser excitation of $R_2^{II}MnCl_4$, where R = Et_3NH, Et_4N, Bu_4N. Also, Clarke (140) has observed a polarised band at 255 cm^{-1} in a melt (500°C) of stoichiometry 2 KCl : $MnCl_2$.

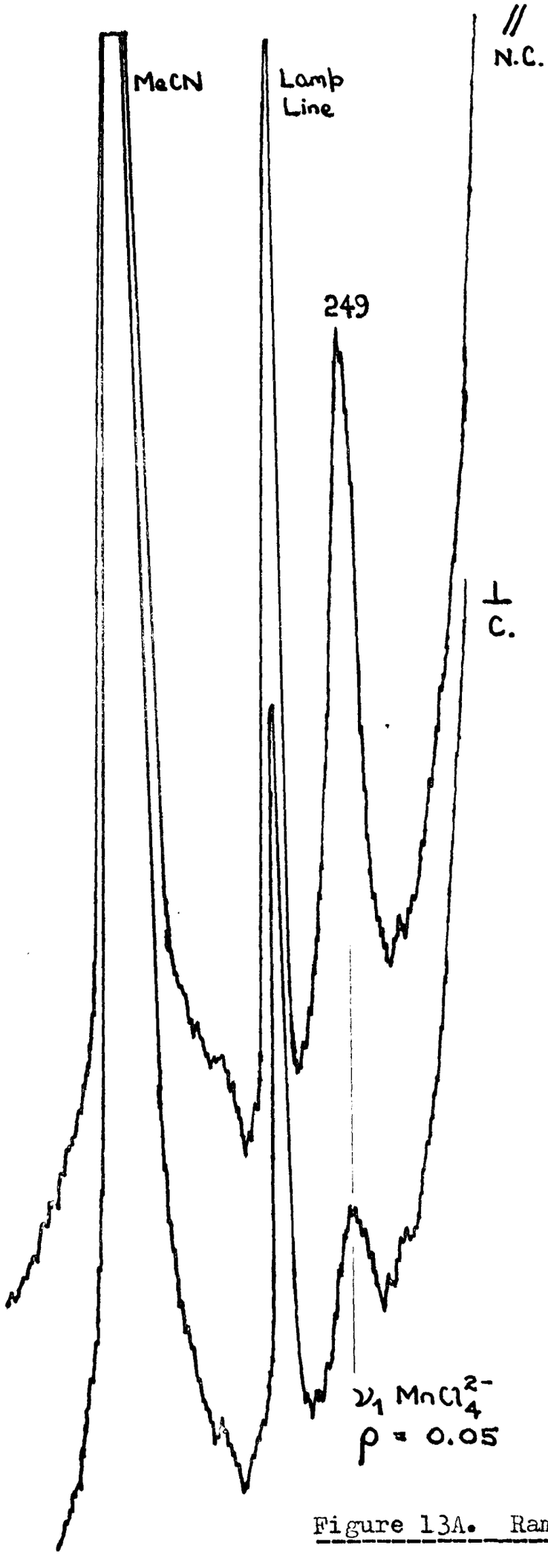
For the bromo-compound, as stated above, Davidson has obtained a complete assignment, with ν_1 at 195 cm^{-1}, using He 5876 Å. Laser excitation of the solid $(Bu_4N)_2MnBr_4$ showed the presence of a feature at $\sim$ 195 cm^{-1}.

The iodo-species was investigated by Ware (28) who found ν_1 (at 116 cm^{-1}), ν_2 and ν_4. Laser studies on the Et_4N^+ and Bu_4N^+ solids confirm this by the presence of a strong band at $\sim$ 108 cm^{-1}.

The Raman results are tabulated in Table 13C.

Tetrabromoferrate^{III}

All attempts to excite Raman spectra from weak solutions of $FeBr_4^-$ failed using He 6678 Å. This was only to be expected in view of the extremely low value of the optimum concentration. Exposures of up to 4 hours on He 6678 Å,



Hg 5461A
Single Slits
Sensitivity 3000
MeCN solution
(1.5M in $MnCl_4^{2-}$)
Period 15
Raman Dynodes 3

Figure 13A. Raman Spectrum of $MnCl_4^{2-}$.

TABLE 13C

Raman spectra of MnX_4^{2-}

Complex	Cation	State	Conc$^{n.}$	Exciting line	Assigned ν_1 (cm^{-1})
$MnCl_4^{2-}$	Et_3NH^+	solution	1.5 M in MeCN	Hg 5461 Å	249, w, pol.
	[a] Et_3NH^+	solid		Ne 6328 Å	256, w
	[a] Et_4N^+	solid		Ne 6328 Å	259, w
	[a] Bu_4N^+	solid		Ne 6328 Å	251, w
	[b] K^+	melt	$2KCl/MnCl_2$	Ne 6328 Å	255, pol.
$MnBr_4^{2-}$	[c] Bu_4N^+	solution	0.3M in $CHCl_3$	He 5876 Å	195, ms, pol.
	[a] Bu_4N^+	solid		Ne 6328 Å	195 m
MnI_4^{2-}	[d] Bu_4N^+	solution	0.2M in CH_2Cl_2	He 5876, 6678 Å	116 s
	[a] Et_4N^+	solid		Ne 6328 Å	108s
	[a] Bu_4N^+	solid		Ne 6328 Å	107 s

a M.J.Gall, private communication

b J.H.R.Clarke (140)

c G.Davidson (136)

d M.J.Ware (28)

with slits 100 μ, gave no discernible solute features. Laser excitation with Ne 6328 Å, however, produced Raman spectra from both solid and solution states, with Et_4N^+ and Bu_4N^+ cations. The data are tabulated in Table 13D, and a comparison is made with the available data for $FeCl_4^-$.

Cobalt and nickel compounds

Apart from the iodides, which are green and pink respectively, the cobalt and nickel compounds give blue solutions which do not readily lend themselves for excitation using Hg 4358 Å. Despite the low optimum concentrations, however, polarised weak features were observed for the chloro-complexes (and therefore assigned to ν_1 in each case). Absorption by the deep blue bromo-solutions invalidated any observation of Raman scattering. The helium-neon laser failed to excite a Raman spectrum for the chloro- and bromo-complexes, but investigations on the iodo-complexes were successful.

The results are summarised in Table 13E.

13(5) Infra-red spectroscopy

The infra-red spectra of the tetrahalo-complexes were obtained with nujol mulls in the 33-800 cm^{-1} region, using polythene and caesium iodide plates. The frequency-values

TABLE 13D

Raman spectrum of $FeBr_4^-$

Cation	State	Exciting line	Features and assignment
[a] Bu_4N^+	solution (0.5M in MeCN)	Ne 6328 Å	202 vs, pol. ν_1 303 mw, depol. ν_3
[a] Bu_4N^+	solid	"	78 ms ν_2 ? 114 m ν_4 200 s ν_1 303 w ν_3
[a] Et_4N^+	solid	"	114 m ν_4 200 s ν_1

Correlation with $FeCl_4^-$

	$FeBr_4^-$ Raman		$FeCl_4^-$ Raman	
	solution (a)	solid (a)	solution (137)	solid (a)
ν_1	202	200	330	333
ν_2	-	78	106	111
ν_3	303	303	385	387
ν_4	-	114	133	-

a. M.J.Gall, private communication

TABLE 13E

Raman spectra of CoX_4^{2-} and NiX_4^{2-}

Complex	Cation	State	Exciting line	ν_1
$CoCl_4^{2-}$	Et_3NH^+	Solution (0.5M in MeCN)	Hg 4358 Å	269 vw, ? pol.
$NiCl_4^{2-}$	Bu_4N^+	Solution (0.6M in MeCN)	"	264 w, pol.
[a] CoI_4^{2-}	Bu_4N^+	Solid	Ne 6328 Å	118 mw
[a] NiI_4^{2-}	Bu_4N^+	Solid	Ne 6328 Å	105 mw

a M.J.Gall, private communication.

of the infra-red active fundamentals, ν_3 and ν_4, are given in Tables 13F,G for the present work and for previous investigations. Although the general agreement of frequency-values is seen to be good, a splitting of the ν_3 feature was often observed in the present work which was not reported in earlier investigations. In the latter, comment on the broadness and intensity of this infra-red stretching feature was often made, and the observation of such a splitting in the present work can probably be ascribed to better instrumentation and resolution.

The splitting of ν_3 into two strong features is explicable if the symmetry of the MX_4^{n-} ion is lowered from T_d to C_{3v} through solid-state interaction. Each F_2-species infra-red active mode on the T_d model would thus give two infra-red active modes, $1A_1 + 1E$, on the C_{3v} model. Sabatini and Sacconi also assigned (131) such a splitting to solid-state interactions. In the present work, the similar expected splitting of the ν_4 vibration was <u>never</u> observed, possibly because the splitting in such a mode might be expected to be smaller than in ν_3.

If the molecular symmetry in the solid state is lowered from T_d to C_{3v}, the previously inactive ν_1 vibration, the metal-halogen symmetric stretch, now becomes active in the

TABLE 13F

Infra-red fundamentals of MnX_4^{n-} and $FeBr_4^-$

Compound	Cation		Present Work	Sabatini (131)	Clark (132)	Adams (134)
$MnCl_4^{2-}$	Bu_4N^+	ν_3	287, 275vs			
		ν_4	120 s			
	Et_3NH^+	ν_3	301,278 vs			
		ν_4	120 s			
	Et_4N^+	ν_3	288, 277 vs	284 s	282 s	281
		ν_4	118 s	118 m	-	-
$MnBr_4^{2-}$	Bu_4N^+	ν_3	221, 209 vs			
		ν_4	89 s			
	Et_4N^+	ν_3	223, 218 vs	221 s	216 s	221, 210
		ν_4	89 ms	85 ms	-	-
MnI_4^{2-}	Bu_4N^+	ν_3	188 vs			
		ν_4	58 ms			
	Et_4N^+	ν_3	193, 188 vs			
		ν_4	56 s			
	$n\text{-}Pr_4N^+$	ν_3		185 s		
		ν_4		-		
$FeBr_4^-$	Bu_4N^+	ν_3	295 vs			
		ν_4	96 ms			
	Et_4N^+	ν_3	295 vs		290 s	289
		ν_4	97 ms		-	-

TABLE 13G

Infra-red fundamentals of CoX_4^{2-} and NiX_4^{2-}

Compound	Cation		Present Work	Sabatini (131)	Clark (132)	Adams (134)
$CoCl_4^{2-}$	Et_3NH^+	ν_3	311, 291 vs			
		ν_4	135 s			
	Et_4N^+	ν_3		297 s	300, 281 s	295
		ν_4		130 m	-	-
$CoBr_4^{2-}$	Bu_4N^+	ν_3	231, 222 vs			
		ν_4	96 m			
	Et_4N^+	ν_3		231 s	227 s	233, 228
		ν_4		91 m	-	-
CoI_4^{2-}	Bu_4N^+	ν_3	197 vs			
		ν_4	56 m			
	Et_4N^+	ν_3	202, 194 vs			
		ν_4	56 m			
$NiCl_4^{2-}$	Bu_4N^+	ν_3	294, 280 vs			
		ν_4	119 s			
	Et_4N^+	ν_3		289 s	285 s, bd	283
		ν_4		112 m	-	-
$NiBr_4^{2-}$	Bu_4N^+	ν_3	228 vs			
		ν_4	81 m			
	Et_4N^+	ν_3		231, 224 s	224 s, bd	
		ν_4		83 m	-	
NiI_4^{2-}	Bu_4N^+	ν_3	191			
		ν_4	-			

infra-red. In all the investigations, no trace of such a ν_1 vibration could be observed in the infra-red (and likewise for the symmetric deformation ν_2). The reason for this must be the low intensity of these features, combined with the fact that both lie in difficult regions for observation of very weak features; ν_1 would lie on the low-frequency side of the very intense, broad ν_3, whereas ν_2 lies in the far infra-red, normally less than 100 cm^{-1} in frequency.

The infra-red activity of the overtones and combination bands of MX_4^{n-} species provides a means of checking on the Raman assignment of the ν_1 vibrations. It was deduced for XY_4 molecules in Chapter 1 that binary and ternary combinations of ν_1 and ν_2 with ν_3 and ν_4 are infra-red active. Although the assignment of combination bands in the infra-red is rarely unique, the concept has been much neglected in application to the MX_4^{n-} species.

In the present work, combination bands in the infra-red spectra of MX_4^{n-} species were tentatively assigned and values of ν_1 and ν_2 were deduced. Although the chloro-compounds, as thick mulls, gave reasonably strong combination features, the intensity of such bands decreased rapidly on going to the bromo-complexes, and the features became very weak in the MI_4^{2-} spectra. In Figures 13B,C the actual

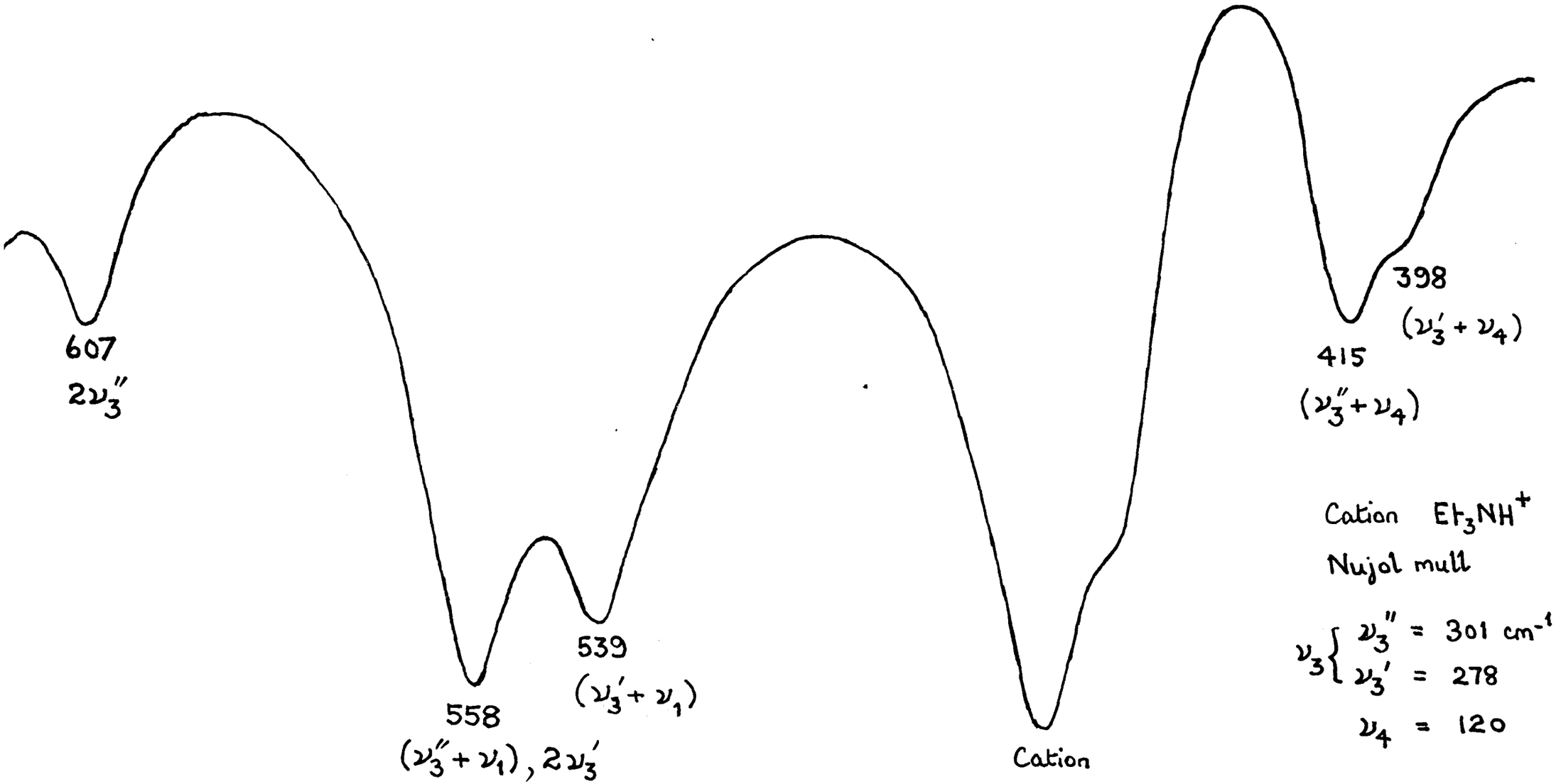
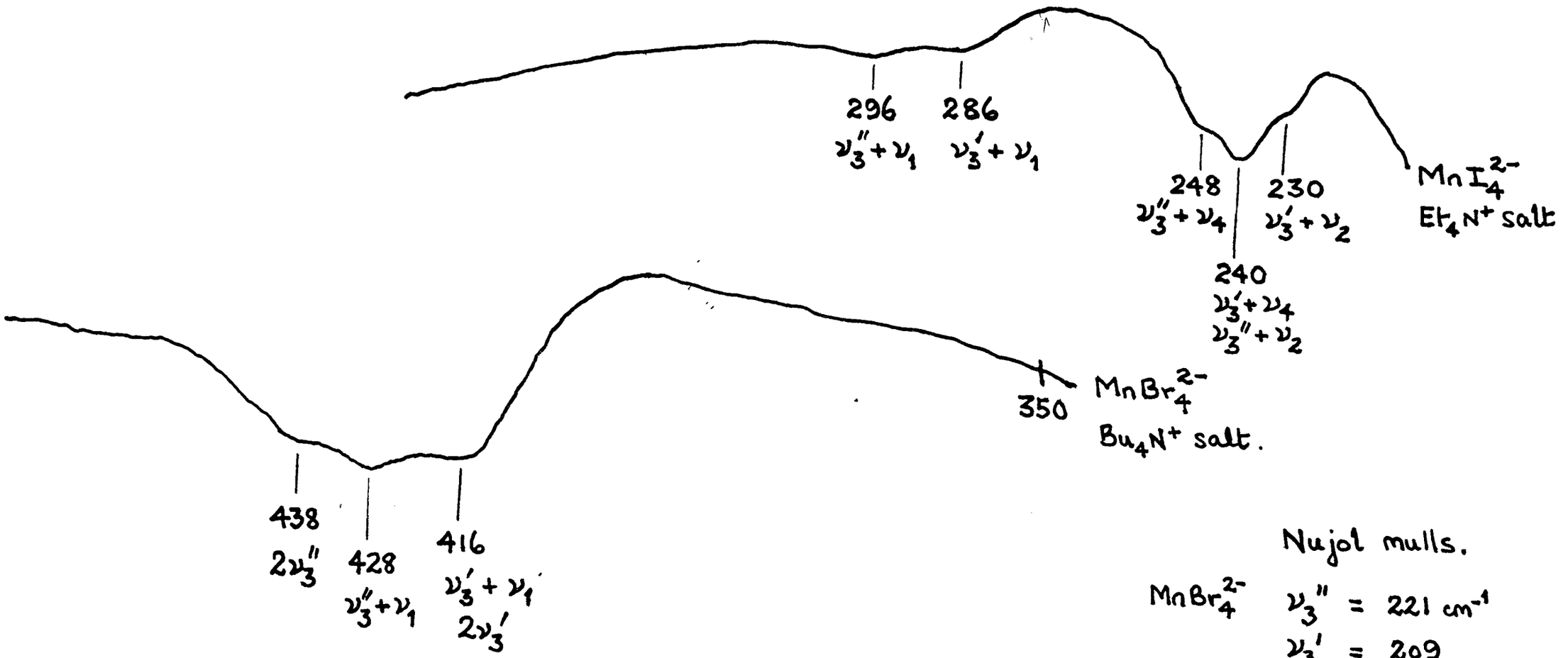


Figure 13B. Combination Bands in $MnCl_4^{2-}$.



Nujol mulls.

$MnBr_4^{2-}$	ν_3''	=	221 cm^{-1}
	ν_3'	=	209
	ν_4	=	89
MnI_4^{2-}	ν_3''	=	193
	ν_3'	=	188
	ν_4	=	56.

Figure 13C. Combination Bands in $MnBr_4^{2-}$, MnI_4^{2-}.

intensities of the combination features for the manganese series of compounds are depicted. The results are given in Tables 13H, I, J, in which the combination features are tentatively assigned and the calculated ν_1 and ν_2 frequency values are compared with the observed Raman data. To assist in the latter, the FeX_4^- compounds were also considered.

It is seen that the calculated ν_1 values (and those of ν_2 when available) are reasonably close to the observed ν_1's. This, for the number of compounds investigated, is a vindication of the concept of using combination bands to predict the ν_1 frequencies of tetrahedral molecules from the infra-red spectra.

13(6) Force Constants of MX_4^{2-} species

Because the A_1 and E species contain but one vibrational mode, the calculation of the force constants for the a_1-stretch and e-deformation is trivial. Utilisation of the F_2-species modes (two in number) makes it possible to evaluate some interaction constants. The force constant for symmetric stretching, k_1, is given by,

$$k_1 = \lambda_1 m_Y = 5.8894 \times 10^{-2} \nu_1^2 M_Y \text{ dynes . cm}^{-1}$$

TABLE 13H

Overtones and Combination bands of MnX_4^{2-}

Complex	Cation	ν_3	ν_4	Band (cm^{-1})	Assignment	Mean Calc. ν_1 (cm^{-1})	Mean Calc. ν_2 (cm^{-1})	Raman ν_1 (cm^{-1})	Raman ν_2 (cm^{-1})
$MnCl_4^{2-}$	Et_3NH^+	301,278	120	207 vw	$\nu_4 + \nu_2$		87		n.o.
				240 w	$2\nu_4$				
				398 mw, 415 mw	$\nu_3 + \nu_4$				
				539 m, 558 m	$\nu_3 + \nu_1$	259		249	
	Et_4N^+	288,277	118	205 vw	$\nu_4 + \nu_2$		87		
				392 w, 403 w	$\nu_3 + \nu_4$				
				530 mw, 539 mw	$\nu_3 + \nu_1$	252			
$MnBr_4^{2-}$	Bu_4N^+	221,209	89	280 w	$\nu_1 + \nu_4$	191		195	
					$\nu_2 + \nu_3$		65		65
				311 w, 322 w	$\nu_3 + \nu_4$				
				416 w	$\nu_3 + \nu_1$	207			
				428 w, 438 w	$2\nu_3$				
MnI_4^{2-}	Et_4N^+	193,188	56	230 vw, 240 vw	$\nu_3 + \nu_2$		44		46
				248 vw	$\nu_3 + \nu_4$				
				286 vw, 296 vw	$\nu_3 + \nu_1$	101		116	

TABLE 13I

Overtones and combination bands at CoX_4^{2-} and NiX_4^{2-}

Complex	Cation	ν_3	ν_4	Band (cm^{-1})	Assignment	Mean Calc. ν_1 (cm^{-1})	ν_2	Raman ν_1 (cm^{-1})	ν_2
$CoCl_4^{2-}$	Et_3NH^+	311, 291	135	414 mw 450 mw	$\nu_3 + \nu_4$				
				536 mw 556 mw	$\nu_3 + \nu_1$	245		269?	n.o.
$CoBr_4^{2-}$	Bu_4N^+	231, 222	96	315 w 330 w	$\nu_3 + \nu_4$				
				360 w 386 w	$\nu_3 + \nu_1$	146		n.o.	n.o.
CoI_4^{2-}	Et_4N^+	202, 194	56	301 vw 310 vw	$\nu_3 + \nu_1$	108		118	
$NiCl_4^{2-}$	Bu_4N^+	294, 280	119	360 w 382 w	$\nu_3 + \nu_2$		84		n.o.
				529 mw 548 mw	$\nu_3 + \nu_1$	252		264	
$NiBr_4^{2-}$	Bu_4N^+	228	81	280 w	$\nu_3 + \nu_2$		52	n.o.	n.o.
				358 w	$\nu_3 + \nu_1$	130			
NiI_4^{2-}	Et_4N^+	191	-	282 vw	$\nu_3 + \nu_1$	91		105	n.o.

TABLE 13J

Overtones and combination bands of FeX_4^-

Complex	Cation	ν_3	ν_4	Band (cm^{-1})	Assignment	Calc. ν_1	Mean Calc ν_2	Raman ν_1	Raman ν_2
$FeCl_4^-$	Et_4N^+	388,375	136	467 mw	$\nu_1 + \nu_4$	331		330	
				495 w	$\nu_3 + \nu_2$		107		106
				705 m }	$\nu_3 + \nu_1$	331			
				719 m }					
$FeBr_4^-$	Bu_4N^+	295	96	375 w	$\nu_3 + \nu_2$		80		78
				388 w	$\nu_3 + \nu_4$				
				496 w	$\nu_3 + \nu_1$	201		200	

where ν_1 is the metal-halogen stretching frequency (a_1) and M_Y is the atomic weight of the halogen. A plot of k_1 versus halogen for the manganese compounds under study in the present work yielded the graph of Figure 13D. The interesting conclusion that was inferred from the graph was that there was an anomaly in the force-constant trend for MnX_4^{2-}. For all other known MX_4 species there is a "dog-leg" shape in the force-constant trend for the halogen series,

i.e. k_1 chloro- > k_1 bromo- > k_1 iodo- species.

It may be inferred, then, that the manganese-bromine bond is stronger than the manganese-chlorine bond for the MnX_4^{2-} species.

A communication was published (141) embodying the $MnCl_4^{2-}$ results of the present work, Davidson's $MnBr_4^{2-}$ results, and the work of Ware on MnI_4^{2-}. No explanation of the anomaly could be suggested, but it was felt that a more detailed consideration of the force constant calculation was merited to evaluate the interaction constants.

Müller (142) and Pistorius (143) have performed calculations on XY_4 tetrahedral molecules, but it was decided to derive the $\mathcal{G}$ and $\mathfrak{F}$ matrices in the present work from first principles. The 10 x 10 G matrix was reduced to the final, factored form using the following symmetry coordinates:

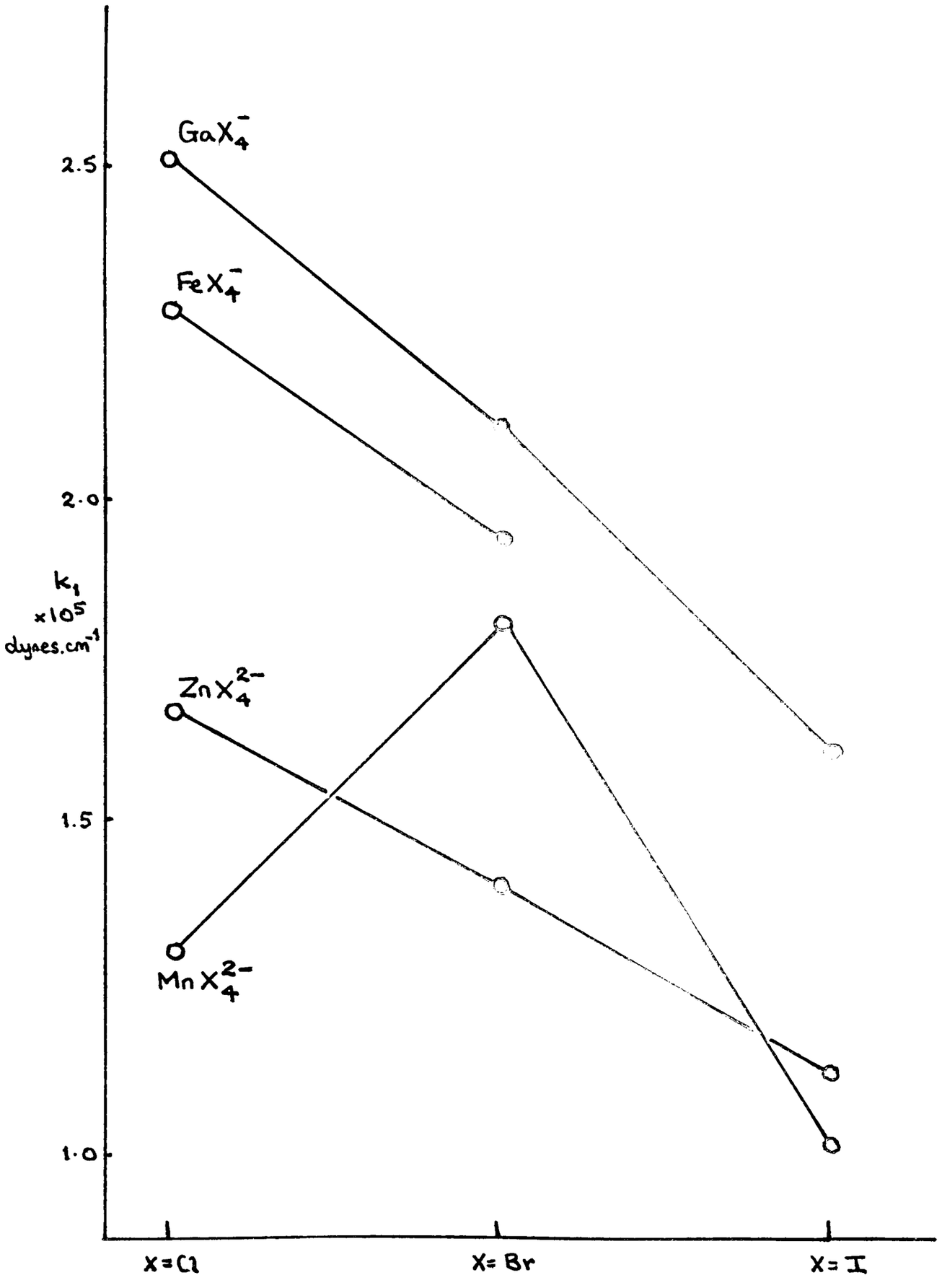


Figure 13D. Force Constants of MX_4 Species.

A_1 species $S_1 = \frac{\Delta}{2}(R_1 + R_2 + R_3 + R_4)$

redundant $\rightarrow S_2 = \frac{\Delta R}{\sqrt{6}}(\alpha_{12} + \alpha_{13} + \alpha_{14} + \alpha_{23} + \alpha_{24} + \alpha_{34})$

E species $S_3 = \frac{\Delta R}{\sqrt{12}}(2\alpha_{12} - \alpha_{13} - \alpha_{14} - \alpha_{23} - \alpha_{24} + 2\alpha_{34})$

F_2 species $S_4 = \frac{\Delta}{2}(R_1 + R_2 - R_3 - R_4)$

$S_5 = \frac{\Delta R}{\sqrt{2}}(\alpha_{12} - \alpha_{34})$

The completed $\mathcal{G}$ and $\mathcal{F}$ matrices are shown in Table 13K. Detailed calculations were carried out for the manganese, zinc and iron(III) series. Assuming a SVFF diagonal field for the F_2-species calculation, k_3 and k_4 were estimated. k_{RR} could now be evaluated, and when the k_2 value (from ν_2) was substituted into the F_2 block calculation a value of $k_{R\alpha}$ could be obtained.

The results of such calculations are given in Table 13L, and an abnormally high k_{RR} interaction constant for $MnBr_4^{2-}$ was indicated.

13(7) Sequel

Whilst an explanation for the anomalous behaviour of manganese was being sought, a communication was received from Dr.D.M.L.Goodgame of Imperial College, London, who had been engaged in a similar investigation of MnX_4^{2-} species.

TABLE 13K

$\mathcal{G}$ and $\mathcal{F}$ matrices for MX_4 (tetrahedral)

$\mathcal{G}$	A_1	E	F_2	species
	μ_X			
		μ_X		
			$(\mu_X + 4/3\,\mu_M)$	$-4/3\,\mu_M$
				$(2\mu_X + 16\mu_M/3)$

$\mathcal{F}$				
	$k_R + 3k_{RR}$			
		$k_\alpha + k_{\alpha\alpha'} - 2k_{\alpha\alpha}$		
			$k_R - k_{RR}$	$(k_{R\alpha} - k_{R\alpha'})\sqrt{2}$
				$k_\alpha - k_{\alpha\alpha'}$

$k_1 = k_R + 3k_{RR}$

$k_2 = k_\alpha$ neglecting $k_{\alpha\alpha'}$

$k_3 = k_R - 3k_{RR}$

$k_4 = k_\alpha$ neglecting $k_{\alpha\alpha'}$

$k_{34} \cong \sqrt{2}.\ k_{R\alpha}$

TABLE 13L

Interaction Constants for MX_4^{n-}

Species	k_1 from ν_1	k_2 from ν_2	k_3	k_4	Calc. ν_2 from k_4 cm^{-1}	obs. ν_2 cm^{-1}	k_{RR}	k_R
$MnCl_4^{2-}$	1.30	0.05	0.87	0.07	98	[87]	0.11	0.98
$MnBr_4^{2-}$	1.79	0.07	0.77	0.05	56	65	0.26	1.03
MnI_4^{2-}	1.01	0.05	0.59	0.03	34	46	0.10	0.70
$ZnCl_4^{2-}$	1.66	0.05	0.96	0.07	98	82	0.18	1.14
$ZnBr_4^{2-}$	1.39	0.06	0.74	0.05	58	61	0.16	0.90
ZnI_4^{2-}	1.11	0.05	0.56	0.04	38	44	0.14	0.70
$FeCl_4^{-}$	2.27	0.08	1.64	0.08	109	106	0.16	1.80
$FeBr_4^{-}$	1.92	0.10	1.35	0.07	64	78	0.14	1.49
*$MnBr_4^{2-}$ (revised)	1.15	0.07	0.77	0.05			0.09	0.87

All k's in dynes cm^{-1}

[ ] not observed directly, calc. from combinations

The outcome was a dispute over the ν_1 symmetric stretching frequency of $MnBr_4^{2-}$.

A re-investigation of $MnBr_4^{2-}$ with the Oxford Helium Source failed to confirm Davidson's earlier results under identical instrumental and exposure conditions. It was at first thought that Davidson and Goodgame had been observing different species, but the ultraviolet spectrum in both cases was characteristic of $MnBr_4^{2-}$.

When the original plates of Davidson became available the source of error was revealed. Firstly, there seemed to have been an error in the estimation of the intensities of the features attributed to $MnBr_4^{2-}$, and the 195 cm^{-1} band supposedly of medium-strong intensity was weak only. Other features were even weaker, and nothing was observed in the 150-160 cm^{-1} region wherein the Goodgame value of ν_1 lay. Also, contrary to the claims of Davidson (136), no polarisation measurements had been made.

Further experiment, both on the Helium Source and on the Cary Laser instrument (M.J.Gall), indicated that the Raman lines supposedly due to $MnBr_4^{2-}$ might possibly originate from the Bu_4NBr present in solution. In MnX_4^{2-} work it is common to dissolve excess of quaternary ammonium halide in the solutions to suppress solvolysis; Davidson used a 3:1

molar ratio of Bu_4NBr to $(Bu_4N)_2MnBr_4$. A re-investigation of the solid $MnBr_4^{2-}$ and solution by M.J.Gall seems to confirm the conclusions of Goodgame:

	Present work		Goodgame (144)	
Assignment	solid Bu_4N^+	solution	solid Et_4N^+	solution in $MeNO_2$
? ν_1	157 cm^{-1}	158, pol.	157 cm^{-1}	156 cm^{-1}
cation	182), 197) bd			
cation	230			
	Et_4N^+			
? ν_1	159 cm^{-1}			
	184), 196) bd			
cation	231			

In the earlier work, a feature at $\sim$ 160 cm^{-1} had been observed for the $MnBr_4^{2-}$ solids with the laser instrument; no data could at that time be obtained from solution studies, so this feature was assigned to a lattice vibration.

If one accepts this revised ν_1 for $MnBr_4^{2-}$, the anomalous behaviour of the MnX_4^{2-} force constants disappears - the force constant calculations were repeated for the revised assignment and the summarised data are included at the foot of Table 13L.

All is not straightforward, even with the revised ν_1 assignment for $MnBr_4^{2-}$, since we are now faced with yet another anomaly, namely, that of the combination bands in the infra-red spectrum of $MnBr_4^{2-}$. There are no features that may be assigned to ($\nu_3 + \nu_1$) for a ν_1 value of 158 cm^{-1}. Also, the features previously assigned to ($\nu_3 + \nu_1$) are unassignable with the newly adopted Goodgame value for ν_1. It was mentioned earlier that combination bands ($\nu_3 + \nu_1$) afforded reasonable values of ν_1, where ν_1 was already well characterised in the Raman spectrum (e.g. as in the FeX_4^- series). The combinations give reasonable ν_1 values for chloro- and iodo-compounds of manganese, yet fail in the case of the bromo-compound. This is inexplicable and provides the only documented case of the breakdown of the combination band concept; as such, therefore, the newly proposed ν_1 for $MnBr_4^{2-}$, providing no recognisable combination bands in the infra-red spectrum, should be viewed with suspicion.

The whole situation remains unsatisfactory and whichever ν_1 is accepted, there is an anomaly to be considered. Supporting the present infra-red work is the work of Clark (132) on $(Et_4N)_2MnBr_4$- the same combination feature, ($\nu_3 + \nu_1$), yielded a value of ν_1 of 199 cm^{-1}, compared with 207 cm^{-1} in the present work!

Appendix 1

Data for $Pt(PF_3)_4$, Programme UBG 1

```
1  No.of G blocks
3  Order of G block
0.063391  -0.043036  -0.018636
-0.043036   0.277408   0.074543  G A1
-0.018636   0.074543   0.032277

3  40    U matrix 3 rows, 40 columns
1  0.28868  2  0.28868  3  0.28868  4  0.28868  5  0.28868
6  0.28868  7  0.28868  8  0.28868  9  0.28868  10  0.28868
11 0.28868  12 0.28868
END
13  0.20412  14  0.20412  15  0.20412  16  0.20412  17  0.20412
18  0.20412  19  0.20412  20  0.20412  21  0.20412  22  0.20412
23  0.20412  24  0.20412  25 -0.20412  26 -0.20412  27 -0.20412
28 -0.20412  29 -0.20412  30 -0.20412  31 -0.20412  32 -0.20412
33 -0.20412  34 -0.20412  35 -0.20412  36 -0.20412
END
37  0.50000  38  0.50000  39  0.50000  40  0.50000
END

3    No.of SVFF force constants
13.1267  0.9090  4.6247  Values of initial set
```

F matrix

12 1 1 2 2 3 3 4 4 5 5 6 6 7 7 8 8 9 9
10 10 11 11 12 12
24 13 13 14 14 15 15 16 16 17 17 18 18 19 19
20 20 21 21 22 22 23 23 24 24 25 25 26 26
27 27 28 28 29 29 30 30 31 31 32 32 33 33
34 34 35 35 36 36
4 37 37 38 38 39 39 40 40

0 No. of Urey Bradley force constants

958
546
213 Frequencies, arranged in descending order

1.18725
11.2521
485.828 W matrix

1 1 END Y matrix

END

END

2 1 END

END

3 1 END

0.5 0.1 0.05 Scaling factors

20 Number of modifications

→

? ?

REFERENCES

References

Key to Abbreviations

Naturwiss.	Naturwissenschaften
J.C.P.	Journal of Chemical Physics
J.Opt.Soc.Amer.	Journal of the Optical Society of America
Ann.de Phys.	Annales de Physique
Spect.Acta	Spectrochimica Acta
Phys.Rev.	Physical Review
Anal.Chem.	Analytical Chemistry
J.A.C.S.	Journal of the American Chemical Society
J.C.S.	Journal of the Chemical Society
Bull.Soc.Chim. France	Bulletin Societie de Chimie France
J.Inorg.Nucl.Chem.	Journal of Inorganic and Nuclear Chemistry
Compt.Rendu	Comptes Rendu
Z.Naturforsch	Zeitschrift für Naturforschung
Z.Physik	Zeitschrift für Physik
Inorg.Chem.	Inorganic Chemistry
Chem.Comm.	Chemical Communications
J.Mol.Spec.	Journal of Molecular Spectroscopy
Proc.Roy.Soc.	Proceedings of the Royal Society
Proc.Phys.Soc.	Proceedings of the Physical Society
Trans.Far.Soc.	Transactions of the Faraday Society
Z.A.A.C.	Zeitschrift für Anorganische und Allgemeine Chemie

1. C.V.Raman and U.Krishnan, Nature, 121, 501, (1928).

2. A.Smekal, Naturwiss., 11,873, (1923).

3. G.Placzek, "The Rayleigh and Raman Scattering" in "Handbuch der Radiologie", Marx, Acad.Verlag, Leipzig (1934).

4. E.B.Wilson, J.C.Decius and P.C.Cross, "Molecular Vibrations", McGraw-Hill, (1955).

5. G.Herzberg, "Infra-Red and Raman Spectra", Van Nostrand, (1945).

6. F.A.Cotton, "Chemical Applications of Group Theory", Interscience, (1963).

7. E.B.Wilson, J.C.P., 7, 1042, (1939).
ibid., 9, 76, (1941).

8. L.A.Woodward in "Raman Spectroscopy, Theory and Practice", ed.Szymanski, Plenum, (1967).

9. J.R.Nielsen, J.Opt.Soc.Amer., 20, 701, (1930).

10. R.A.Sawyer, "Experimental Spectroscopy", Dover, (1963).

11. S.Walker and H.Straw, "Spectroscopy", Vol.II, Chapman and Hall, (1967).

12. J.H.R.Clarke, D.Phil.Thesis, Oxford, 1966.

13. V.S.Ellis, D.Phil.Thesis, Oxford, 1967.

14. D.H.Rank and R.E.Kagarise, J.Opt.Soc.Amer., 40, 89, (1950).

15. J.Cabannes, Ann.de Phys., 18, 285, (1932).

16. J.Cabannes and R.Roussett, Ann.de Phys., 19, 229, (1933).

17. J.Koningstein in ref.8.

18. A.W.Vŭgel-Hogler, Acta Phys.Austriaca, 1, 323, (1948).

19. F.A.Cotton and W.Horrocks, Spect.Acta, 17, 134, (1961).

20. M.J.Gall, private communication, Southampton.

21. H.Stammreich, Phys.Rev., 78, 79, (1950).

22. H.Stammreich, Spect.Acta, 8, 41, (1956).

23. H.Stammreich and R.Forneris, Spect.Acta, 17, 775, (1961).

24. H.Stammreich, R.Forneris and Y.Tavares, ibid., 17, 1173, (1961).

25. D.Rendell, D.Phil.Thesis, Oxford, 1960.

26. M.J.Ware, Part II Thesis, Oxford, 1962.

27. H.Stammreich and R.Forneris, J.Chem.Phys., 22, 1624, (1955).

28. M.J.Ware, D.Phil.Thesis, Oxford, 1965.

29. J.A.Creighton, D.Phil.Thesis, Oxford, 1961.

30. H.Stammreich, Spect.Acta, 16, 363, (1960).
ibid. 17, 661, 1961.

31. E.R.Lippincott and R.D.Fisher, Anal.Chem., 26, 435, (1954).
E.R.Lippincott, J.P.Sibilia and R.D.Fisher, J.Opt.Soc.Amer., 49, 83, (1959).

32. J.W.Irvine and G.Wilkinson, Science, 113, 742, (1951).

33. G.Wilkinson, J.A.C.S., 73, 5501, (1951).

34. G.Bouquet and M.Bigorgne, Bull.Soc.Chim.France, 433, (1962).

35. D.Benlian and M.Bigorgne, ibid., 1583, (1963).

36. M.Bigorgne, J.Inorg.Nucl.Chem., 26, 107, (1964).

37. M.Bigorgne, Compt.rendu, 250, 3484, (1960).

38. M.Bigorgne, Bull.Soc.Chim.France, 1986, (1960).

39. L.S.Meriwether and M.L.Fiene, J.A.C.S., 81, 4200, (1959).

40. R.Schmutzler, "Phosphorus-Fluorine Chemistry", p.150-, in Adv.in Chem.Series 37, 'Reactions of Coordinated Ligands'.

41. Th.Kruck and A.Prasch, Z.Naturforsch., 19b, 669, (1964).

42. G.Wilkinson, J.A.C.S., 73, 5503, (1951).

43. L.A.Woodward and J.R.Hall, Nature, 181, 831, (1958).
Spect.Acta, 16, 654, (1960).

44. F.Seel, K.Ballreich, and R.Schmutzler, Chem.Berichte, 94.1, 1173, (1961).

45. Th.Kruck and K.Baur, Chem.Berichte, 98, 3070, (1965).

46. Th.Kruck, Z.Naturforsch., 19b, 165, (1964).

47. R.W.Parry and T.C.Bissot, J.A.C.S., 78, 1524, (1956).

48. J.Chatt, Nature, 165, 637, (1950).

49. Th.Kruck, Angewandte Chemie (Int.Ed.), 6, 53, (1967).

50. J.Chatt, J.C.S., 3061, (1951).

51. G.Booth, Adv.in Inorganic and Radiochem., 6, 1, (1964).

52. L.M.Venanzi, 'σ vs π bonds in phosphine complexes', Chem.in Brit., 4.4., 162, (1968).

53. A.Pidcock, R.E.Richards, L.M.Venanzi, J.C.S.(A), 707,(1966).

54. R.S.Nyholm and M.L.Tobe, Adv.in Inorganic and Radiochem., 5, 23, (1963).

55. L.Tisza, Z.Physik, 82, 48, (1933).

56. D.M.Yost and T.F.Anderson, J.C.P., 2, 624, (1934).

57. H.S.Gutowsky and A.D.Liehr, J.C.P., 20, 1652, (1952).

58. M.K.Wilson and S.R.Polo, J.C.P., 20, 1716, (1952).

59. J.H.Meal and S.R.Polo, J.C.P., 24, 1126, (1956).

60. M.L.Delwaulle and F.Francois, Compt.Rendu, 222, 550, (1946).

61. J.Chatt and A.A.Williams, J.C.S., 3061, (1951).

62. Th.Kruck, Chem.Berichte, 97, 2018, (1964).

63. R.J.Clark and E.O.Brimm, Inorg.Chem., 4, 651, (1965).

64. J.F.Nixon and M.D.Sexton, Inorg.Nucl.Chem.Letts., 4, 275, (1968).
J.F.Nixon, Chem.Comm., 34, (1966).

65. Th.Kruck and K.Baur, Z.Naturforsch., 21b, 489, (1966).

66. M.L.H.Green, Oxford, private communication.

67. R.J.Clark, J.Inorg.Chem., 3, 1395, (1964).

68. R.J.Clark and P.I.Hoberman, J.Inorg.Chem., 4, 1771, (1965).

69. Th.Kruck and A.Prasch, Angewandte Chemie, 76, 892, (1964).

70. Th.Kruck, A.Prasch, W.Lang and K.Baur, ibid., 77, 706, (1965).

71. Th.Kruck and K.Baur, Angewandte Chemie (Int.Ed.), 4, 521, (1965).

72. Th.Kruck, Köln, private communication.

73. Dodd and Robinson, "Experimental Inorganic Chemistry".

74. Inorganic Syntheses, V, p.208, VIII, p.232.

75. M.J.Ware and C.Holloway, private communication.

76. J.Aldous and J.M.Mills, Spect.Acta, 18, 1073, (1962).

77. J.C.Decius, J.C.P., 16, 1025, (1948).

78. K.Shimizu and H.Murata, Bull.Chem.Soc.Japan, 30, 487,(1957).

79. K.Shimizu and H.Murata, J.Mol.Spec., 5, 44, (1960).

80. D.A.Long, A.H.S.Matterson and L.A.Woodward, Proc.Roy.Soc., A, 224, 33, (1954).

81. K.Venkateswarlu and S.Sundaram, Proc.Phys.Soc.London, A69, 180, (1956).

82. A.M.Mirri, F.Scappini, and P.G.Favero, Spect.Acta, 21, 965, (1965).

83. E.G.Claeys and G.P.van der Kelen, Spect.Acta, 22, 2095, (1966).

84. G.W.Bethke and M.K.Wilson, J.C.P., 26, 1118, (1957).

85. R.C.Taylor, J.C.P., 26, 1131, (1957).

86. T.L.Cottrell, "Strengths of Chemical Bonds", Butterworths S.P., London, 1954, p.276.

87. W.Gordy, H.Ring and A.B.Burg, Phys.Rev., 78, 512, (1950).

88. B.L.Crawford and P.C.Cross, J.C.P., 6, 525, (1938).

89. G.Wilkinson, Z.Naturforsch., 9b, 446, (1954).

90. F.Basolo and R.G.Pearson, Adv.in Inorg.and Radiochemistry, 3, 68, (1961).

91. Inorganic Syntheses, V, p.201.

92. V.Lorenzelli, Compt.Rendu, 252, 3219, (1961).

93. P.W.Davies and R.A.Oetjen, J.Mol.Spec., 2, 253, (1958).

94. J.R.Neilsen and N.E.Ward, J.C.P., 10, 81, (1942).

95. D.M.Yost and J.Sherbourne, J.C.P., 2, 125, (1934).

96. J.R.Hall, D.Phil.Thesis, Oxford, 1958.

97. R.A.McAlpine and B.Soule - Prescott and Johnson's "Quahitative Chem.Analysis", Van Nostrand, 1933.

98. H.Stammreich, R.Forneris and Y.Tavares, J.C.P., 25, 580, (1956).

99. M.J.Bruton, D.Phil.Thesis, Oxford, 1964.

100. M.J.Bruton and L.A.Woodward, Spect.Acta, 23A, 175, (1967).

101. G.Wilke and B.Bogdanovic, Angewandte Chemie, 73, 756, (1961)

102. P.Baumgarten and H.Bruns, Chem.Berichte, 80, 517, (1947).

103. J.Chatt, J.Inorg.Nuclear Chem. 8, 517, 1958.

104. L.Malatesta and C.Cariello, ibid., 562, (1958) J.C.S., 2323, (1958).

105. F.G.Mann and A.F.Wells, J.C.S., 708, (1938).

106. L.M.Venanzi, private communication.

107. H.G.M.Edwards, B.Sc.Thesis, Oxford, (1966).

108. R.R.Holmes and E.F.Bertaut, J.A.C.S., 80, 2980, (1958).

109. L.H.Long and J.F.Sackmann, Trans.Far.Soc., 50, 1177,(1954).

110. L.H.Long and J.Sackmann, Research Correspondence, Suppl. to Research 8, S23, (1955).

111. J.R.van Wazer, "Phosphorus and its Compounds", Volume I, Interscience, N.Y. (1958).

112. P.L.Goggin and R.J.Goodfellow, J.C.S.(A), 1462, (1966).

113. P.M.Boorman and A.J.Carty, Inorg.and Nucl.Chem.Letters, 4, 101, (1968).

114. J.R.Miller, Adv.in Inorganic and Radiochem., 4, 133,(1962).

115. G.E.Coates and C.Parkin, J.C.S., 421, (1963).

116. L.W.Daasch and D.C.Smith, J.C.P., 19, 22 (1951).

117. M.Halmann, Spect.Acta, 16, 407, (1960).

118. E.J.Rosenbaum, D.J.Rubin and C.R.Sandberg, J.C.P., 8, 366, (1940).

119. G.Bouquet and M.Bigorgne, Spect.Acta, 23A, 1231, (1967).

120. R.K.Sheline, J.C.P., 18, 602, (1950).

121. H.Siebert, Z.A.A.C., 273, 161, (1953).

122. D.A.Long and R.B.Gravenor, Spect.Acta, 19, 961, (1963).

123. L.H.Jones, J.C.P., 28, 1215, (1958).
J.Mol.Spec., 5, 133 (1960).

124. B.L.Crawford and W.Horwitz, J.C.P., 16, 147, (1948).

125. J.K.Wilmshurst, J.Mol.Spec., 5, 343, (1960).

126. F.A. Cotton and C.S.Kraihanzel, J.A.C.S., 84, 4432,(1962).

127. F.A.Cotton, Inorganic Chem., 3, 702, (1964).

128. N.S.Gill and R.S.Nyholm, J. .S., 3997, (1959).

129. N.S.Gill and F.B.Taylor, Inorganic Syntheses IX, 136.

130. F.A.Cotton, D.M.L.Goodgame and M.Goodgame, J.A.C.S., 84, 167, (1962).

131. A.Sabatini and L.Sacconi, J.A.C.S., 86, 17, (1964).

132. R.J.H.Clark and T.M.Dunn, J.C.S., 1198, (1963).

133. R.J.H.Clark, Spect.Acta, 21, 955, (1965).

134. D.M.Adams, J.Chatt, J.M.Davidson and J.Gerratt, J.C.S., 2189, (1963).

135. M.L.Delwaulle, Compt.Rendu, 240, 2132, (1955).

136. G.Davidson, D.Phil.Thesis, Oxford, 1967.

137. L.A.Woodward and M.J.Taylor, J.C.S., 4473, (1960).

138. C.J.Jørgensen, Acta Chem.Scand., 11, 53, (1957).

139. C.A.Furlani, J.Inorg.and Nucl.Chem., 19, 51, (1961).

140. J.H.R.Clarke, private communication.

141. H.G.M.Edwards, M.J.Ware and L.A.Woodward, Chemical Communications, 1968, p.540.

142. A.Müller and A.Fadini, Spect.Acta, 22, 1523, (1966).

143. C.W.F.T.Pistorius, J.C.P., 28, 514, (1958).

144. D.M.L.Goodgame, London, private communication.